GROUNDWATER RECHARGE, FLOW AND DISCHARGE IN A LARGE CRYSTALLINE WATERSHED

by

Thomas Philip Gleeson

A thesis submitted to the Department of Civil Engineering

in conformity with the requirements for

the degree of Doctor of Philosophy

Queen's University

Kingston, Ontario, Canada

July, 2009

Your file Votre référence
ISBN: 978-0-494-65317-3
Our file Notre référence
ISBN: 978-0-494-65317-3

This thesis is dedicated to my parents.

Abstract

The objective of this thesis is to constrain the fundamental hydrogeological processes of a large crystalline fractured rock watershed in the Canadian Shield. The fundamental hydrogeological processes of groundwater recharge, flow and discharge are examined individually as well as holistically using a revised conceptual model. The study area is the topographically-subdued Tay River watershed in eastern Ontario where a thin veneer of soil overlies Precambrian crystalline rocks and Paleozoic sediments. Spatial scales from local-scale (100s m^2 to 1 km^2) to watershed-scale (>100 km^2) are examined. Recharge processes are defined using hydrogeological characterization, numerical simulation and isotopic, thermal and hydraulic responses to a snowmelt event. Soil thickness and bedrock transmissivity are highly heterogeneous at the local scale. Cold, δ^2H depleted snowmelt locally recharged the bedrock aquifer to depths of at least 20 m within two days. This rapid recharge process is localized to areas where the soil is very thin whereas slow recharge is likely widespread. The impact of lineaments on groundwater flow at the watershed-scale is examined using geomatic analysis, hydrogeological characterization, numerical simulation and fracture mapping. Lineaments are interpreted as structural features because the two principal lineament sets are oriented parallel to fracture and fault orientations. The fractured bedrock underlying lineaments generally consists of poorly connected zones of reduced permeability suggesting lineament can be barriers to recharge and flow in this setting. Natural conservative, radioactive, and thermal tracers are integrated with streamflow measurements and a steady-state advective model to delimit the discharge locations and quantify the discharge flux to lakes, wetlands, creeks and the Tay River. The groundwater discharge rate to most surface water bodies is low. Groundwater discharge is distributed across the watershed rather than localized around lineaments or zones of exposed brittle fractures. In the revised conceptual model, recharge is considered two separate processes, groundwater flow is compartmentalized and the discharge flux

is considerably lower than porous media watersheds. This thesis provides a better understanding of fundamental hydrogeological processes in a large crystalline fractured rock watershed which impacts the sustainability of water resources and ecology.

Co-Authorship

Tom Gleeson is the primary author on this thesis and all the enclosed documents. Chapters 2 to 4 were written as independent manuscripts in which the co-authors provided intellectual supervision and editorial comment, except where noted below. Chapter 2 is submitted to the Journal of Hydrology and is co-authored by Dr. Kent Novakowski and Dr. Kurt Kyser. Chapter 3 is published by Geological Society of America Bulletin and is co-authored by Dr. Kent Novakowski. Chapter 4 is in press with Water Resources Research and is co-authored by Dr. Kent Novakowski, Dr. Peter Cook and Dr. Kurt Kyser. Dr. Peter Cook provided the original ideas and collaboration for the steady-state advective model discussed in Chapter 4 as well as writing part of the text describing the model.

Acknowledgements

First, I would like to thank my supervisor Kent Novakowski for his support, mentoring and openness to discussion. Kent's 'sure, let's try it' attitude encouraged me to attempt many new ideas, some of which appear in this thesis, and others which are best left forgotten. I hope to carry forth this excitement and engagement with fundamental and applied research.

My research greatly benefited from interactions with fellow students and other colleagues as well as the collegial atmosphere at Queen's. Discussions and connections with graduate students Dan Baston, John Kozuskanich, Jana Levison, Titia Praamsma, Morgan Schauerte, Ant West, Mike West and others were integral. I also appreciated the warm response from and research discussions with researchers in the Department of Civil Engineering and other departments (Laurent Godin, Rob Harrap, Kurt Kyser and Vicki Remenda). The isotope analysis would not have been possible without the guidance of Kerry Klassen. Summer research associates Matt Herod and Richard Zavitz were excellent help in the field. Matt Herod single-handedly completed the field work that is summarized in Appendices 2 and 3. Other colleagues helped in a myriad of ways from solving nitty-gritty modeling or field equipment problems to inspiring discussions of large-scale hydrogeology. These colleagues include Dragan Andjelkovic, Jonathan Caine, Peter Cook, Sandy Cruden, Derek Lane-Smith, Patrick Larson, Andrew Manning, Rob McLaren and Young-Jin Park. Finally, reviews by Victor Bense, Fred Day-Lewis, Ken Raven and other anonymous reviewers greatly improved manuscript versions of Chapters 2 to 4. I look forward to more discussion and collaboration within these friendly networks.

Scholarships from Natural Science and Engineering Research Council, the province of Ontario and Queen's University are acknowledged. The research was funded by the Ontario Research and

Development Fund, Natural Science and Engineering Research Council of Canada, Ontario Ministry of Natural Resources, the Ontario Ministry of the Environment and Rideau Valley Conservation Authority. John Miller is thanked for the access to the hay field, and residents of the Tay River watershed, including the Friends of the Tay are thanked for their interest and support.

Finally, but as a roaring round of applause I would like to thank my family, friends and partner Emilie for the years of support, encouragement all round good heartedness. You make it possible and worthwhile.

Table of Contents

List of Figures

List of Tables

Chapter 1
Introduction

Fractured rock settings are complex hydrogeological systems that are essential for water resources and contaminant disposal around the world [*Edet, et al.*, 1998; *Magowe and Carr*, 1999; *Flint, et al.*, 2001; *Berkowitz*, 2002; *Caine and Tomusiak*, 2003; *Sener, et al.*, 2005; *Shaban, et al.*, 2006]. Research on fractured rock hydrogeology has historically focused on local-scale problems, driven by mining, nuclear waste or contaminated site concerns [*Berkowitz*, 2002; *Neuman*, 2005]. Increasingly hydrogeologists realize that examining groundwater systems at large scales and integrated with surface water and biological systems is essential for managing and protecting water resources and ecosystems [*Sophocleous*, 1992; *Danielopol, et al.*, 2003; *Danielopol, et al.*, 2004]. Understanding the sustainability of fractured rock aquifers at watershed scales is critical as areas underlain by fractured rock host burgeoning populations and large-scale industrial water modifications (*e.g.* water bottling or mine dewatering). Few previous studies have examined fractured rock hydrogeology at a large scale [*Stephenson, et al.*, 1992; *Desbarats and Bachu*, 1994; *NRC*, 1996; *Tiedeman, et al.*, 1998; *Flint, et al.*, 2001; *Rayne, et al.*, 2001; *Shapiro*, 2001; *Kennedy and Woodbury*, 2002; *Cook*, 2003; *Mayo, et al.*, 2003; *Sykes, et al.*, 2003; *Nastev, et al.*, 2004; *Follin, et al.*, 2005; *Wellman and Poeter*, 2006; *Ahmed, et al.*, 2007; *Denny, et al.*, 2007; *Krásný and Sharp*, 2007]. Watersheds, the fundamental landscape unit of hydrology [*Winter*, 2001], are the ideal scale to determine water budgets, assuming no underflow. However, studies that holistically examine how hydrogeological processes affect fractured rock watersheds are rare [*Rosenberry and Winter*, 1993]. Water resource managers in jurisdictions around the world, including the province of Ontario, are developing water budgets for watersheds that often assume fractured rock watersheds function as porous media watersheds or assume fluxes or parameters that are more appropriate for porous media. The objective of this thesis is to constrain the fundamental hydrogeological processes of a large crystalline fractured rock watershed in the Canadian Shield in order to enable sustainable groundwater management.

Fractured rock watersheds in the Canadian Shield were first examined in detail by the nuclear industry starting in the 1970's [*Farvolden, et al.*, 1988]. Deep drilling and characterization programs as well as research at or near the surface indicated that permeability decreased with depth in the bedrock and that significant, shallowly-dipping structures were common [*Davison and Kozak*, 1988]. Modern groundwater (recharged since 1950) was found ubiquitously in shallow (<100 m), relatively permeable bedrock aquifers [*Stephenson, et al.*, 1992; *Gascoyne, et al.*, 1993; *Kotzer, et al.*, 1998; *Gascoyne*, 2004]. The shallow bedrock was interpreted to function largely as porous media aquifers with water tables near the surface with groundwater recharging in topographic highs and discharging in topographically lower surface water features. The processes and fluxes of groundwater recharge and discharge remained largely uncertain.

Groundwater conditions as well as the connection between groundwater and surface water have also been examined at a number of small, experimental watersheds underlain by crystalline fractured rock and variable soil thickness in the Canadian Shield and elsewhere [*Rosenberry and Winter*, 1993; *Peters, et al.*, 1995; *Devito, et al.*, 1996; *Branfireun and Roulet*, 1998; *Gburek and Folmar*, 1999b; *Buttle, et al.*, 2001; *Spence and Woo*, 2003; *Buttle, et al.*, 2004; *Peters, et al.*, 2006; *Manning and Caine*, 2007]. Previous studies in the Canadian Shield focused on runoff and streamflow generation, surface water storage and surface-subsurface connectivity and emphasized the importance of the distribution of soil thickness. Groundwater discharge is limited where soil is minimal and perennial streams only develop in drainage areas >0.25-0.5 km^2 [*Buttle, et al.*, 2004; *Steedman, et al.*, 2004]. Previous studies in other crystalline watersheds document discrete fractures at the local scale although larger scales are generally considered to function as equivalent porous media [*Tiedeman, et al.*, 1998; *Manning and Caine*, 2007]. One of the purposes of this thesis is to examine a large crystalline watershed which is a more common scale for water resource management.

The fundamental hydrogeological processes of a watershed are groundwater recharge, flow and discharge [*Winter*, 2001]. Figure 1.1A illustrates a conceptual model for a watershed underlain by a homogeneous, isotropic porous media aquifer [*Tóth*, 1962; *Freeze and Witherspoon*, 1967]. Recharge areas are much larger than discharge areas. Recharge, flow and discharge are slow, inexorable and relatively predictable. Groundwater and surface water bodies are strongly connected in discharge areas [*Winter*, 1999; *Alley, et al.*, 2002]. Figure 1.1B illustrates a watershed underlain by crystalline fractured rock with variable fracture density and variable soil thickness as is typical in the Canadian Shield. This aquifer system is highly anisotropic and heterogeneous, the water table is near the surface and surface water bodies are common. A zone of high fracture density may manifest at the surface as an observable linear feature or lineament. Fundamental unanswered questions about this type of watershed include:

1) How does groundwater recharge the fractured rock aquifer?
2) How do lineaments affect groundwater flow in the fractured rock aquifer?
3) How does groundwater discharge to surface water bodies from the fractured rock aquifer?

Answering these questions is the primary contribution of this thesis which is structured to follow a groundwater flow line from recharge processes (Chapter 2) to flow processes (Chapter 3) and finally discharge processes (Chapter 4). Additional contributions of this thesis include developing a revised conceptual model of fractured rock watersheds and discussing results within the context of sustainable groundwater resources (Chapter 5).

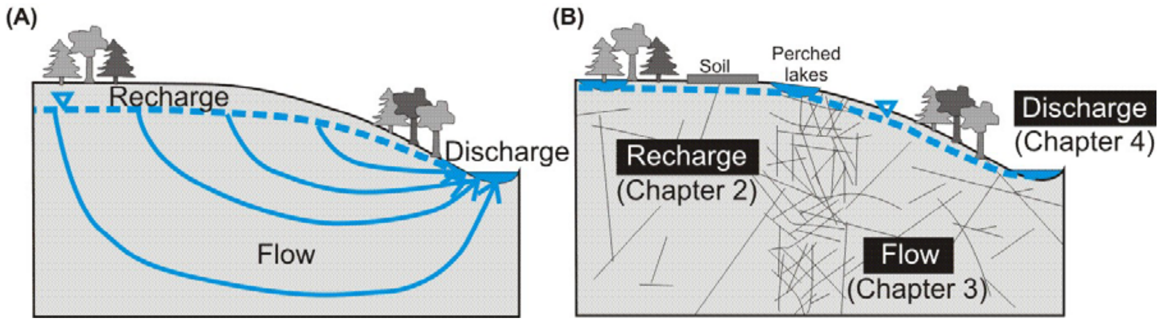

Figure 1.1 Conceptual model of a watershed underlain by (A) a porous media aquifer and (B) a fractured rock aquifer.

The thesis focuses on the ~900 km^2 Tay River watershed in eastern Ontario (Figure 1.2A). In this topographically subdued watershed, a thin veneer of soil overlies the Precambrian Grenville Province and the Paleozoic Nepean sandstone [*Easton*, 1992; *Kettles*, 1992]. Groundwater is primarily derived from shallow residential wells drilled into bedrock [*Golder Associates Ltd.*, 2003]. Chapters 2 to 4 each focus on a different 'study area' within the watershed (Figure 1.2B) as well as a different hydrogeological process (Figure 1.1B). Chapter 2 focuses on local-scale recharge processes (in a hay field and surrounding area) since it is often necessary to better constrain local-scale processes before attempting to upscale. Chapter 3 examines groundwater flow around lineaments in the central part of the watershed. Chapter 4 documents groundwater discharge to surface water bodies throughout the watershed. Because Chapters 2 to 4 focus of different areas, spatially and thematically, previous studies and relevant literature are introduced in the pertinent chapters.

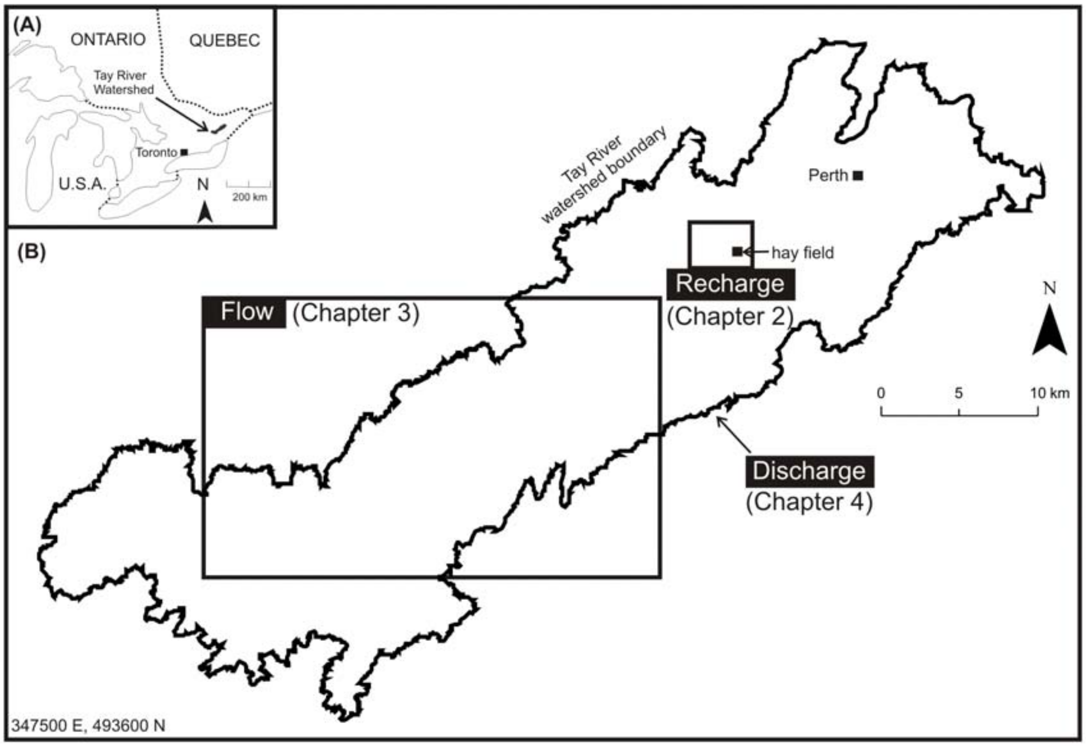

Figure 1.2 (A) The Tay River watershed in eastern Ontario. (B) The study areas examined in Chapters 2 to 4 are highlighted.

Scale and scaling is a relevant issue to this thesis as in much of hydrology [*Neuman*, 1987; *Allison and Peck*, 1989; *Neuman*, 1990; *Blöschl and Sivapalan*, 1995; *Bergstrom and Graham*, 1998; *Hsieh*, 1998; *Schulze-Makuch, et al.*, 1999; *Bonnet, et al.*, 2001]. A representative elementary area (REA) has been proposed for watersheds [*Wood, et al.*, 1988; *Woods, et al.*, 1995; *Sanford, et al.*, 2007] based on the continuum theory of representative elementary volumes [*Bear*, 1972]. The concept of representative elementary area provides a useful theoretical framework for analyzing the vertical fluxes (recharge or discharge) at different scales (Figure 1.3). The measured or simulated vector areal fluxes (q, units L/T) at a certain point in time are represented. At local scales in fractured rock settings (*i.e.* hay field on Figure 1.3) hydrogeological fluxes are highly heterogeneous [*Novakowski, et al.*, 2006] however for areas greater than a representative elementary area the flux is relatively constant [*Sanford, et al.*, 2007]. Proposing the REA concept for fluxes assumes that hydraulic conductivity and gradient are also represented by a REA since flux is a product of hydraulic conductivity and gradient. The scaling of hydraulic conductivity in fractured rock is uncertain [*Neuman*, 1987; *Clauser*, 1992; *Hsieh*, 1998; *Shapiro*, 2001; *Love, et al.*, 2007]. Hydraulic gradients in fractured rock settings can be represented as a continuum at large scales but the continuum scale can vary within individual aquifers [*Wellman and Poeter*, 2005; *Wellman and Poeter*, 2006]. Key questions at different scales for each flux (recharge, flow and discharge) are also shown on Figure 1.3.

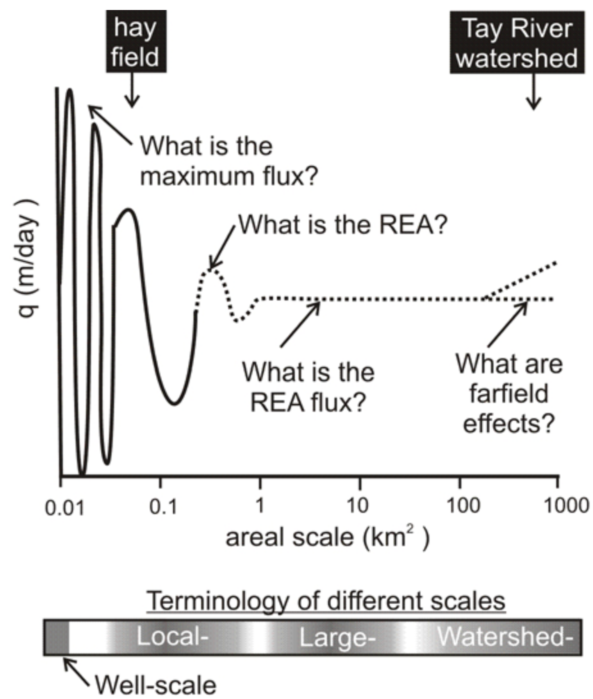

Figure 1.3 The representative elementary area (REA) concept for watersheds. The area of the hay field and the Tay River watershed as well as the terminology of different scales are shown for reference.

Scale is also pragmatically important since watershed-scale studies should make watershed-scale measurements [*Blöschl and Sivapalan*, 1995; *Yeh, et al.*, 2008] but most hydrogeological data are point values that represent a small area or volume of the aquifer or watershed. This thesis attempts to use or derive methods for making large-scale measurements but was not successful at this in all cases. For example, Chapter 2 focuses on local-scale recharge processes that are poorly understood rather than trying to upscale or constrain recharge at a larger scale. Applying formalized scaling theory [*Neuman*, 1990; *Blöschl and Sivapalan*, 1995] is difficult using the data derived in Chapters 2 to 4. Therefore Chapter 5 concludes by qualitatively discussing different fluxes at multiple scales. For clarity throughout this thesis, 'watershed-scale' refers to the scale of the Tay River watershed (>100 km^2). 'Local-scale' refers to the scale of a single site such as the hay field or a small surface water body (100s m^2 to 1 km^2) and 'large-scale' refers to an intermediate scale between watershed-scale and local-scale. 'Well-scale' refers to the area around a single well (10s to 100s m^2). Figure 1.3 illustrates this terminology of different spatial scales.

The sustainability of groundwater in fractured bedrock aquifers is critical to many communities and ecosystems across Canada. The definition of sustainability depends upon the context and approach [*Redclift*, 1987]. This thesis focuses on groundwater sustainability by considering groundwater a *resource*. Maintaining the quality and quantity of both groundwater and surface water are integral to sustainable groundwater resources [*Sophocleous*, 2000; *Bredehoeft*, 2002]. Alternatively, groundwater can be considered within a broader sustainable development framework integrating economic, environmental and social analysis [*Hiscock, et al.*, 2002] but this approach will not be applied in this thesis. Historically, sustainable groundwater resources were often simplistically defined as the recharge rate using the safe yield concept [*Sophocleous*, 2000; *Bredehoeft*, 2002]. However, withdrawing the 'safe yield' induces recharge and/or decreases discharge which can result in lower water tables, dried up surface water bodies, ecological impacts and reversed groundwater flow directions [*Sophocleous*, 1997; *Sophocleous*, 2000; *Alley and Leake*, 2004]. *Theis* [1940] referred to the sum of induced recharge and decreased discharge as 'capture'.

A more comprehensive model of groundwater resource sustainability should include at least the following two aspects. First, sustainability should be evaluated assuming that groundwater and surface water are holistically connected through recharge and discharge processes and the concept of capture [*Bredehoeft*, 2002]. *Sophocleous* [2000] suggests evaluating sustainability by identifying the transition from groundwater storage depletion to induced recharge from surface water bodies. This sustainability criterion necessitates knowledge of groundwater storage and groundwater-surface water interactions at the watershed scale. Alternatively, watershed-scale recharge and discharge fluxes can be compared. This more rudimentary sustainability criterion does not necessitate knowledge of groundwater storage at the watershed scale and will be applied in Chapter 5. Second, an examination of groundwater resource sustainability must include groundwater quality. Groundwater quality is dependent on recharge processes which govern the potential for surface contamination as well as the mean residence time of the aquifer. Longer mean residence times result in more significant water rock interactions which can degrade water quality. Therefore, understanding and quantifying recharge and discharge processes are critical to evaluating the sustainability of groundwater resources.

Chapter 2

Groundwater recharge: extremely rapid and localized

2.1 Introduction

Recharge is a critical parameter for understanding, modeling and protecting groundwater systems from overexploitation and contamination [*Lerner, et al.*, 1990; *Lerner*, 1997; *Scanlon, et al.*, 2002]. In porous media aquifers located in humid climates, recharge is relatively homogeneous at local scales and typically quantified on the scale of months or years [*Allison*, 1988; *Solomon, et al.*, 1993; *Healy and Cook*, 2002; *Scanlon, et al.*, 2002]. In northern porous media aquifers snowmelt recharge can be a rapid flux, localized by topographic depressions, that is significant in the annual water budget [*Hayashi, et al.*, 2003; *French and Binley*, 2004]. Recharge rates and patterns in fractured rock have been previously examined using groundwater ages, stable isotopes, numerical simulations and water table responses [*Cook, et al.*, 1996; *Lee, et al.*, 1999; *Abbott, et al.*, 2000; *Zanini, et al.*, 2000; *Cook and Robinson*, 2002; *Bockgard, et al.*, 2004; *Cook, et al.*, 2005; *Surrette*, 2006; *Praamsma, et al.*, 2009b]. Local-scale recharge studies in fractured rock are complicated by preferential fracture flow paths, unknown vertical connections, matrix diffusion, uncertain specific yield and unpredictable hydraulic responses [*Aeschbach-Hertig, et al.*, 1998; *Gburek and Folmar*, 1999a; *Cook and Robinson*, 2002; *Scanlon, et al.*, 2002].

Water tables rising rapidly and significantly during and after precipitation events have been observed at scattered fractured rock sites [*Gburek and Folmar*, 1999a; *Rodhe and Bockgard*, 2006; *Heppner, et al.*, 2007; *Milloy*, 2007; *Praamsma, et al.*, 2009b]. Multiple-meter water table rises within hours of rain events have been documented in fractured sedimentary rocks overlain by 0.5-

1.5 m of silty loam at a small research site in Pennsylvania [*Gburek and Folmar*, 1999a; *Risser, et al.*, 2005; *Heppner, et al.*, 2007]. Large water-table rises can reflect actual recharge (mass transfer across the water table) in an aquifer with low specific yield or be primarily a hydraulic response, possibly magnified by air entrapment during rapid recharge [*Gburek and Folmar*, 1999a; *Weeks*, 2002]. Without a precipitation tracer it is difficult to determine if a water table rise is entirely attributable to actual recharge or is primarily a hydraulic response with little actual recharge. At a crystalline rock site in Sweden overlain by thicker soils (10 m of till), the bedrock water table responds to precipitation but the rise is less then a meter [*Rodhe and Bockgard*, 2006]. *Rodhe and Bockgard* [2006] interpret the water-table rise as primarily a hydraulic response to a weight increase in saturated soil during precipitation with a minor amount of actual recharge to the bedrock aquifer. Therefore previous studies suggest soil thickness may affect the recharge mechanism and rate in fractured rock aquifers. The heterogeneity of recharge patterns could not be evaluated at either of these sites due to the homogeneity of soil thickness, the limited study area and the small number of wells [*Gburek and Folmar*, 1999a; *Rodhe and Bockgard*, 2006].

The objective of this chapter is evaluating the spatial and temporal variability of recharge in a fractured crystalline aquifer overlain by variable thickness of soil. Hydrogeological and geophysical field work characterizes the bedrock aquifer and overlying soils. Detailed water table, groundwater temperature, groundwater δ^2H and meteorological data revealed the rate and localization of recharge during the 2007 snowmelt freshet. This well constrained recharge event was then numerically simulated to determine the physical hydrogeological variables that govern the recharge processes in this setting. The primary contribution of this chapter is characterizing the complexity and importance of recharge processes in a common hydrogeological setting.

2.2 Site description

This chapter focuses on the central part of the Tay River watershed in rural Eastern Ontario, Canada (Figure 2.1). Elevations range from 150 to 190 m above sea level. The humid climate is characterized by an average annual precipitation of 0.95 m which is distributed relatively uniformly through out the year (30 years of data from Environment Canada Station 6104027 in Kemptville, ON augmented with 3 years of an onsite weather station). Typically 20 % of the annual precipitation falls as snow. During winter 2006-7, the mean daily temperature was below $0^{o}C$ for 2.5 months ending in a rapid freshet event, described below.

In this topographically subdued catchment, a veneer of soil overlies two fractured rock aquifers: the Precambrian crystalline rock and the Paleozoic Nepean sandstone [*Easton*, 1992; *Kettles*, 1992]. The Precambrian crystalline rocks are part of the Grenville Province of the Canadian Shield, and are a fracture-controlled aquifer with low permeability, storativity and primary porosity. Near the surface the most significant fractures in crystalline rocks are typically sub-horizontal sheeting fractures [*Holzhausen*, 1989; *Sukhija, et al.*, 2006]. The geometric mean transmissivity from a provincial compilation of water well data (n = 7875) is 4.8 x 10^{-5} m^2/s [*Singer, et al.*, 2003]. The overlying Nepean Sandstone occurs as an isolated sedimentary outlier at higher elevations, and are more permeable with a geometric mean transmissivity (n = 7418) of 2.3 x 10^{-4} m^2/s [*Singer, et al.*, 2003]. Groundwater is primarily derived from shallow residential wells drilled into bedrock [*Golder Associates Ltd.*, 2003]. This chapter examines data from both the crystalline and sandstone aquifers. The veneer or blanket of soil is a sandy or silty diamicton [*Kettles*, 1992]. Bedrock transmissivity and soil composition, hydraulic conductivity and thickness are examined in more detailed during this chapter.

Previous hydrogeological studies focused on a hay field adjacent to the Tay River [*Milloy*, 2007; *Novakowski, et al.*, 2007b; *Levison and Novakowski*, 2009; *Praamsma, et al.*, 2009b]. A network of eleven bedrock monitoring wells with multi-level completions were constructed (TW1-11 in Figure 2.1). A rain-gauge and climate stations were also installed. These studies indicated that discharge to the Tay River may be insignificant, that recharge can be localized and that the annual recharge rate may be very low. Predicting the location and quantifying the fluxes of recharge features remained elusive. In this chapter, the well network is expanded to encompass ~10 km^2 in the central part of the watershed (Figure 2.1B).

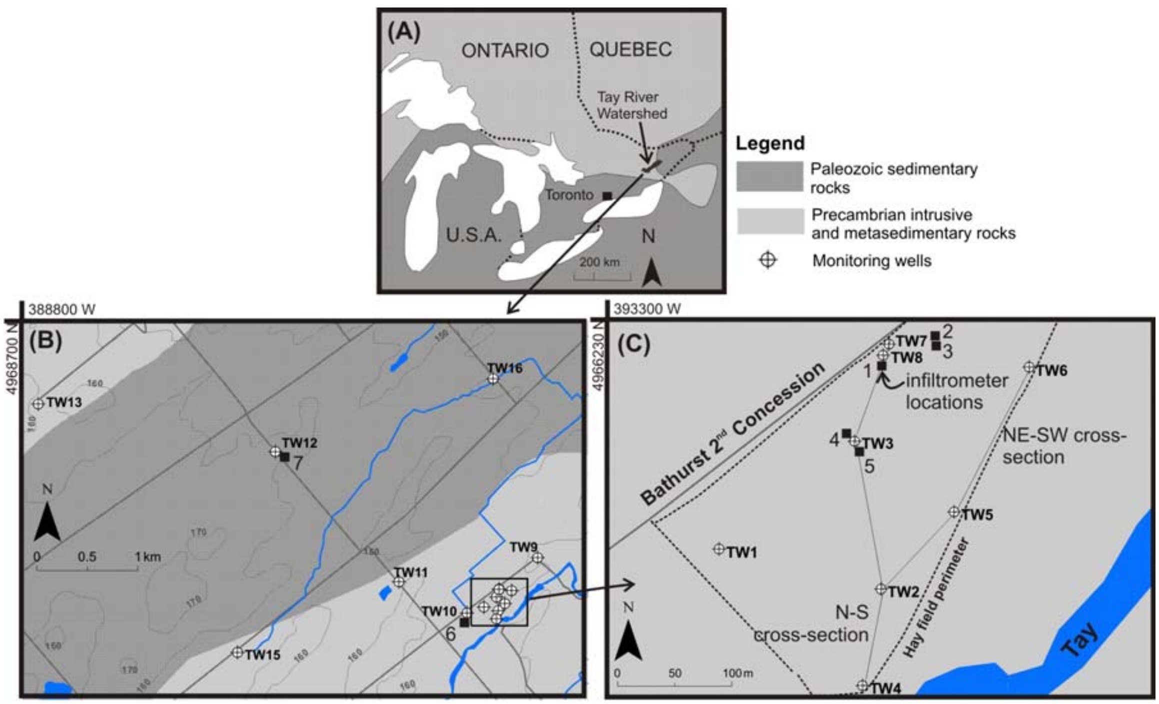

Figure 2.1 (A) Location of Tay River watershed in Eastern Ontario at the contact between Precambrian crystalline rocks (light grey) and overlying Paleozoic sedimentary rocks (dark grey). (B) Study area for this chapter showing topography in meters above sea level and the location of monitoring wells (white circles with crosses) and infiltrometer experiments (black squares). (C) Hay field well cluster (TW1-8) and infiltrometer locations (1-5). The location of cross-sections in Figure 2.2 also highlighted.

2.3 Field methods

In 2006-2007, four additional 0.152 m diameter bedrock wells were drilled in the study area (TW12, 13, 15 and 16 on Figure 2.1) resulting in an expanded network of 15 wells, completed for a total of 38 piezometers. Each bedrock well is completed with two 0.051 m diameter PVC piezometers separated by >3 m of bentonite and an open, uncased section, herein referred to as the shallow piezometer. The top of the shallow piezometers were grouted and cased to 0.5 m above ground surface and open 0.5-1 m below the soil-bedrock interface, resulting in a network capable of monitoring conditions immediately below the soil-bedrock interface. The bottom of the deep piezometers range from 31-56 m below ground surface. Shallow, mid and deep piezometers for each well are referred to as S, M and D respectively (*e.g.* TW12S, TW12M and TW12D). Drilling chips sampled from discrete depths were used to identify rock type and were tested for the presence of carbonate using dilute hydrochloric acid. All wells were characterized using a down hole camera and via hydraulic testing with 1.77 m test intervals isolated by straddle packers. Slug tests were completed in each interval using 5 L of water and analyzed using the *Hvorslev* [1951] method. The approximate range of transmissivities that can be tested using this apparatus is 1×10^{-3} m^2/s to 1×10^{-8} m^2/s. Each piezometer was developed until groundwater was not turbid by pumping for 1-2 hours. Note that TW8 and TW14 are not included in this chapter because they were drilled for other purposes [Chapter 3; *Cooke*, 2007]. Additionally, TW2 and TW1S could not be sampled during this chapter because TW2 is not permeable enough to quickly produce aquifer water during cold, winter sampling conditions and TW1S was dry at the time of the snowmelt event.

Soil characteristics were mapped by air-photo interpretation, well drilling, seismic refraction, hand-augering, driving a steel rod to refusal and infiltrometer experiments. Soil thickness and composition was mapped over the entire 10 km^2 study area. First, the location and spatial extent of bedrock outcrop in the study area were analyzed on 1:15 000 scale air photos. Second, a steel rod was driven to refusal at the soil-bedrock interface using a posthole driver along 60 m long transects. The steel rod was useful for detailed mapping of the soil-bedrock interface up to depths of 1.4 m but at greater depths removing the steel rod by hand was impossible. Along the same transects soil samples were collected from discrete 0.1 m depth intervals using a hand-auger and described. At two locations outside the hay field (Figure 2.1B), bulk saturated hydraulic conductivity was estimated from double-ring infiltrometer experiments [*Sharma, et al.*, 1980; *Bouwer*, 1986; *Reynolds*, 1993; *Lai and Ren*, 2007]. Bulk saturated hydraulic conductivity was calculated assuming steady-state infiltration conditions were established after 60 minutes of infiltration, following *Sharma et al.* [1980]. For each infiltration experiment, a hydraulic conductivity value using data from both the inner and outer ring are calculated and compared.

In the hay field, seismic refraction confirmed the soil thickness and additional infiltrometer experiments estimated the soil hydraulic conductivity. The depth of soil was identified using seismic refraction with a Geometrics ES-2401 apparatus and the SIPwin interpretation program. Geophones were spaced 2-3 m apart in nine 50-75 m arrays traversing the hay field. Nine pulses of seismic energy were emitted from a buffalo gun for each array, resulting in overlapping data and robust interpretations. Intersecting and perpendicular arrays were terminated near wells with a known depth of bedrock. Five infiltration experiments (Figure 2.1C) estimated bulk, vertical saturated hydraulic conductivity within the hay field.

Previous studies indicated that recharge events are often characterized by large rises in hydraulic head and that the snowmelt can result in measurable groundwater isotopic excursions [*Milloy*, 2007; *Novakowski, et al.*, 2007b; *Praamsma, et al.*, 2009b]. Therefore a field experiment was designed to observe the groundwater isotopic value, hydraulic head and temperature in the network of shallow piezometers completed just below the soil-bedrock interface during the 2007 snowmelt freshet. During the winter of 2007 the mean daily temperature was below 0^{o}C for 2.5 months and then warmed to 5-10 ^{o}C which caused the snow to melt rapidly over a ~24 hour period during March 13, 2007. During the snowmelt, no other associated precipitation occurred and no significant overland ponding or flow was observed. Snow depth was measured on March 3, 2007 at each monitoring well in the hayfield and along transects between monitoring wells.

Dedicated pressure and temperature data loggers were installed in five shallow piezometers (TW3S, TW4S, TW6S, TW9S, TW12S) and a deeper piezometer (TW3D). Data was logged on 15 minute intervals. Pressure data was corrected for barometric fluctuations using the results from the onsite meteorological station and verified with weekly manual water level measurements. The pressure transducers and temperature loggers used are considered accurate to 0.005 m and 0.1^{o}C, respectively.

Groundwater and snow samples were collected monthly during the winter of 2007 and more frequently during and after the March 13, 2007 snowmelt freshet event. Groundwater samples were collected from the shallow piezometers (n=12) using dedicated hand or submersible pumps after purging 1-3 well volumes and stored in high-density polyethylene bottles. Snow samples were collected from different locations and different snow layers to examine isotopic heterogeneity in the snow pack. The ^{2}H stable isotopic analyses were completed at the Queen's Facility for Isotope Research using a Finnegan MAT 252 mass spectrometer. Isotope values are expressed in δ units (‰, parts per mil) relative to Vienna Standard Mean Ocean Water (VSMOW) with an analytical error of approximately ±1‰.

2.4 Field results

2.4.1 Bedrock transmissivity and soil thickness

Most of the wells are drilled and completed in the Precambrian crystalline rock (Figure 2.1). The remainder of the wells (TW12 and TW16) are drilled and completed in the Paleozoic Nepean sandstone and Precambrian crystalline rock. Bedrock transmissivity, calculated at ~2 m scale, for the four new bedrock wells (TW12, 13, 15 and 16) are compiled with the ten previous wells in the hay field and surrounding area (Figure 2.2; Appendix A). Transmissivity is highly heterogeneous ranging from 1 x 10^{-3} m^2/s to 1 x 10^{-8} m^2/s, which is approximately the entire range of transmissivity values observable with the slug test apparatus. The transmissivity variation is interpreted to result from high transmissivity discrete fractures or fracture zones that are embedded in a low transmissivity matrix. Figure 2.3 illustrates the mean logarithmic transmissivity at ~5 m scale that was calculated by averaging the logarithmic transmissivity values measured in each 5 m depth interval for all wells (n=25-40 for each 5 m depth interval; Table A.1). The standard deviation is constant with depth but the mean logarithmic transmissivity is greater at shallow depths (<10 m) than a deeper depths, suggesting the shallow depths are characterized by larger aperture fractures or higher fracture densities.

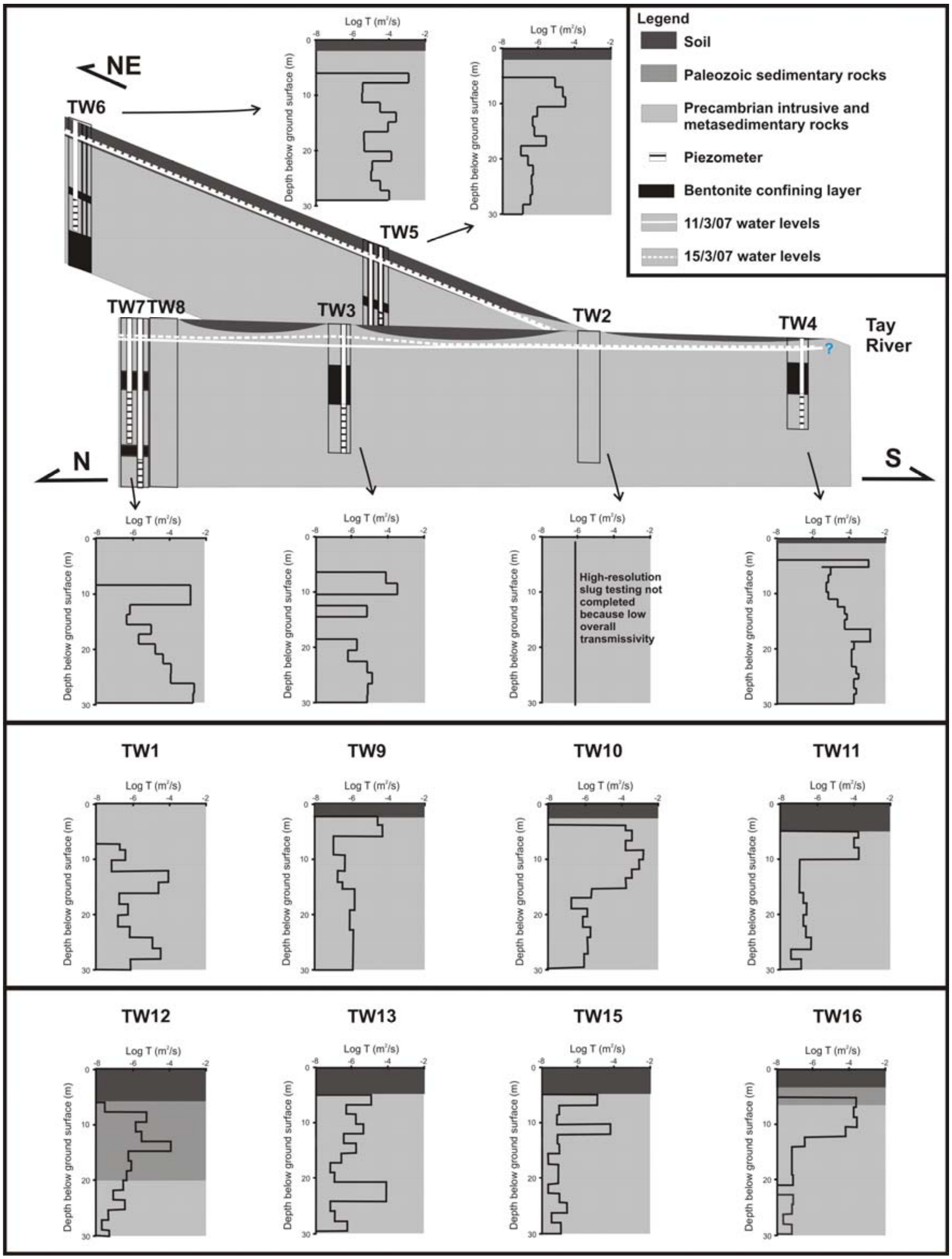

Figure 2.2 Vertically-exaggerated cross-sections through the hay field showing soil depth, bedrock geology, and logarithmic transmissivity from high-resolution slug testing. Water

levels measured before and after the 2007 freshet event are interpolated between wells. Cross-sections and wells are located on Figure 2.1. All data shown to a depth of 30 m regardless of total well depth. Data compiled from *Milloy* [2007], *Praamsma et al* [2009], *Levison and Novakowski* [2009] and Appendix A.

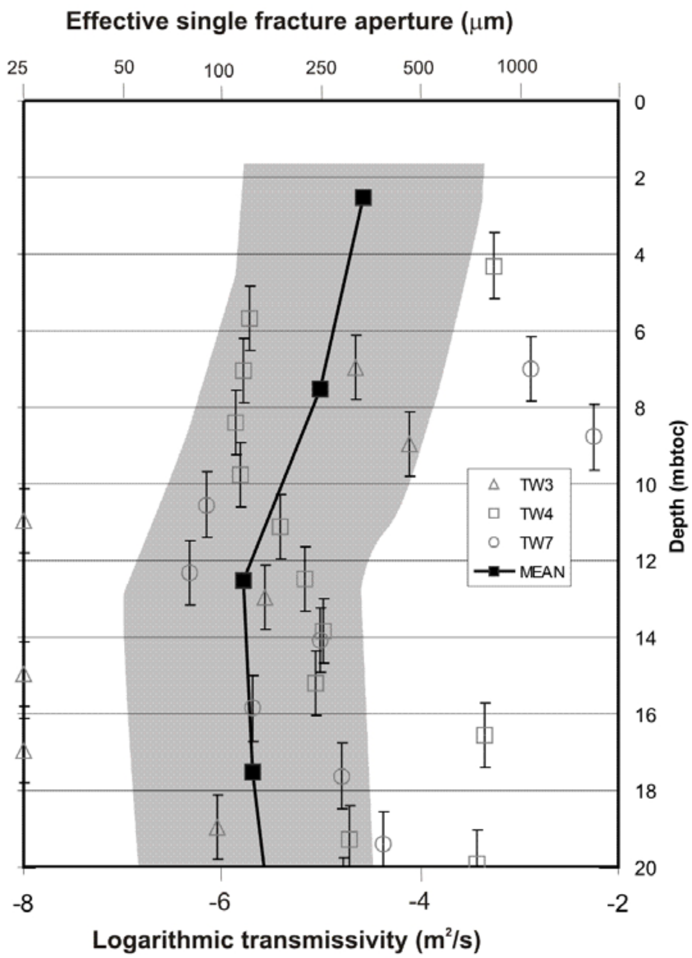

Figure 2.3 Mean logarithmic transmissivity at the scale of 5 m with standard deviation (2σ) shown in grey for all the wells. Data from selected wells also shown with vertical error bar indicating location of slug test interval. Effective single fracture aperture, calculated from transmissivity data, also shown.

The depth of soil in the vast majority of the study area is greater than 0.5 m thick and much of the area is underlain by soils thicker than 1.0 m (Figure 2.4A; Appendix B). Bedrock outcrops and areas with very thin soil are highly localized (<1% of area). Scattered outcrops and thin soils around the hay field well cluster enable examination of the role of soil thickness in recharge processes but they are not representative of the majority of the study area. Most of the soils are silty sands locally with minor gravel that are interpreted as glacial tills [*Kettles*, 1992]. The gravel cobbles are normally locally derived Nepean sandstone or Precambrian lithologies. In low-lying areas clay loam is common which is interpreted as glaciolacustrine deposits [*Kettles*, 1992]. Two infiltrometer experiments outside the hay field in the study area resulted in a range of hydraulic conductivities of 5.4 x 10^{-6} to 5.8 x 10^{-6} m/s (Appendix C). This range of hydraulic conductivity is consistent with a soil composition of silty sand at the infiltrometer locations [Figure 2.4; *Freeze and Cherry*, 1979].

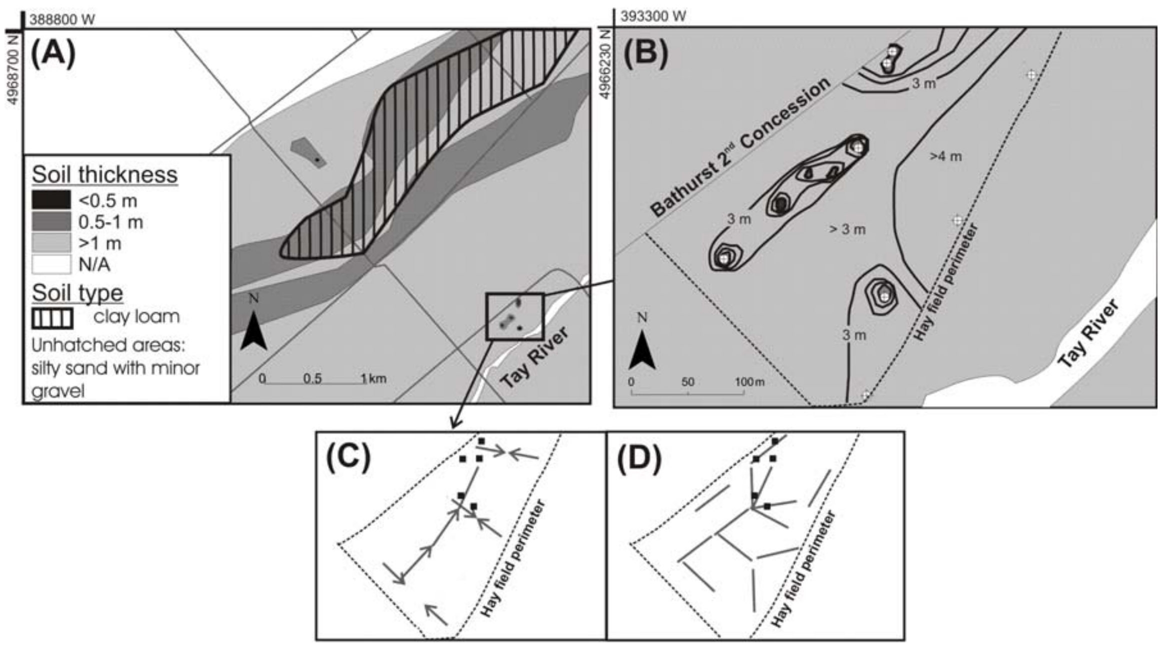

Figure 2.4 (A) Soil thickness and type in the study area from air photo analysis, driving a steel rod and hand augering. Note that the soil is silty sand with minor gravel unless marked by the hatch. (B) Soil thickness underlying the hay field interpreted from a synthesis of seismic refraction, well drilling and steel rod driving. Bedrock outcrops shown in dark grey and the contour interval on both maps is 0.5 m. Location of (C) seismic arrays and (D) traverses of hand-driven steel rod are also shown along with infiltrometer locations with black squares.

The depth of soil in the hay field is highly heterogeneous (Figure 2.4B; Appendix B). Small bedrock outcrops are scattered throughout the field but up to 4.3 m of soil was encountered during well drilling (Table 2.1). The depth of soil between wells was easily identified using seismic refraction because the seismic velocity of the soil and bedrock were 300-500 m/s and >2000 m/s, respectively. The interpreted soil-bedrock interface was verified where arrays intersected other arrays, where arrays terminated near wells with a known depth of soil, and by hand-driving steel rods. The interpreted soil-bedrock interface was accurate to <0.5 m in all cases. The soil composition in the hay field is silty sand. Five infiltrometer experiments in the hay field resulted in a range of hydraulic conductivities of 4.8×10^{-7} to 3.6×10^{-6} m/s (Stations 1-5 in Table 2.2; Appendix C). The geometric mean of all the infiltrometer experiments is 2.1×10^{-6} m/s and 2.4×10^{-6} m/s for the inner and outer ring, respectively. This range of bulk hydraulic conductivity is consistent with a soil composition of silty sand at the infiltrometer locations [Figure 4; *Freeze and Cherry*, 1979].

Table 2.1 Well depth and depth of soil from drilling records

Well	Well depth below ground surface (m)	Depth of soil (m)
TW1S	1.8 - 3.6	0
TW2	1.8 - 31.5	0
TW3S	2.1 - 8.4	0
TW3D	19.2 - 31	0
TW4S	2.1 - 3.9	<2
TW5S	4.8 - 13.7	4.3
TW6S	4.8 - 16.7	4
TW7S	1.2 - 12.8	0
TW9S	2.4 - 6.7	2
TW10S	2.7 - 15.4	2.1
TW11S	4.8 - 13.9	4.1
TW12S	5.1 – 8.0	5.6
TW13S	4.3 - 6.3	0.7
TW15S	4.5 - 7.5	5.2
TW16S	4.5 - 7.8	2.4

Table 2.2 Bulk hydraulic conductivity of soil from double-ring infiltrometer experiments

Station	K (m/s)	
	Inner ring	Outer ring
1	2.7E-06	2.8E-06
2	1.2E-06	1.4E-06
3	1.1E-06	4.8E-07
4	7.1E-07	2.5E-06
5	2.1E-06	3.6E-06
6	5.8E-06	5.8E-06
7	5.4E-06	5.4E-06
Geometric mean	2.1E-06	2.4E-06

2.4.2 Snowmelt freshet

Snowmelt is a valuable tracer because it has a distinct thermal and isotopic signature that is naturally applied simultaneously and evenly to the entire ground surface. The snow pack was a ~0.1 m thick before the snowmelt, which equates to 0.01-0.05 m of snow water equivalent [*Lehr, et al.*, 2005]. Snow sampled from different layers and different locations in the hay field on March 3, 2007 had δ^2H isotopic values of -116 to -130 ‰ VSMOW. The isotopic value of snow samples from the top, middle and bottom of the snow pack collected on March 3, 2007 indicated that isotopic layering was insignificant. Snowmelt isotopic values must be inferred from the snow isotopic values because snowmelt samples were not collected directly from snow lysimeters. The isotopic fractionation between snow and snowmelt is variable but depends on the time of contact between snow and water and the isotopic layering in the snow pack [*Clark and Fritz*, 1997; *Rodhe*, 1998]. Theoretically the difference between the isotopic values of the snow and snowmelt decreases with increasing melt intensity because the time of contact between snow and water decrease [*Rodhe*, 1998]. Since the snowmelt was intense the snowmelt isotopic value, like the snow δ^2H value, should be significantly lower than the groundwater. The groundwater isotopic value, temperature, and depth to water were stable for three months before the snowmelt at approximately -70 to -75‰ δ^2H VSMOW, 7^oC, and 4-5 m below ground surface, respectively (Figure 2.5).

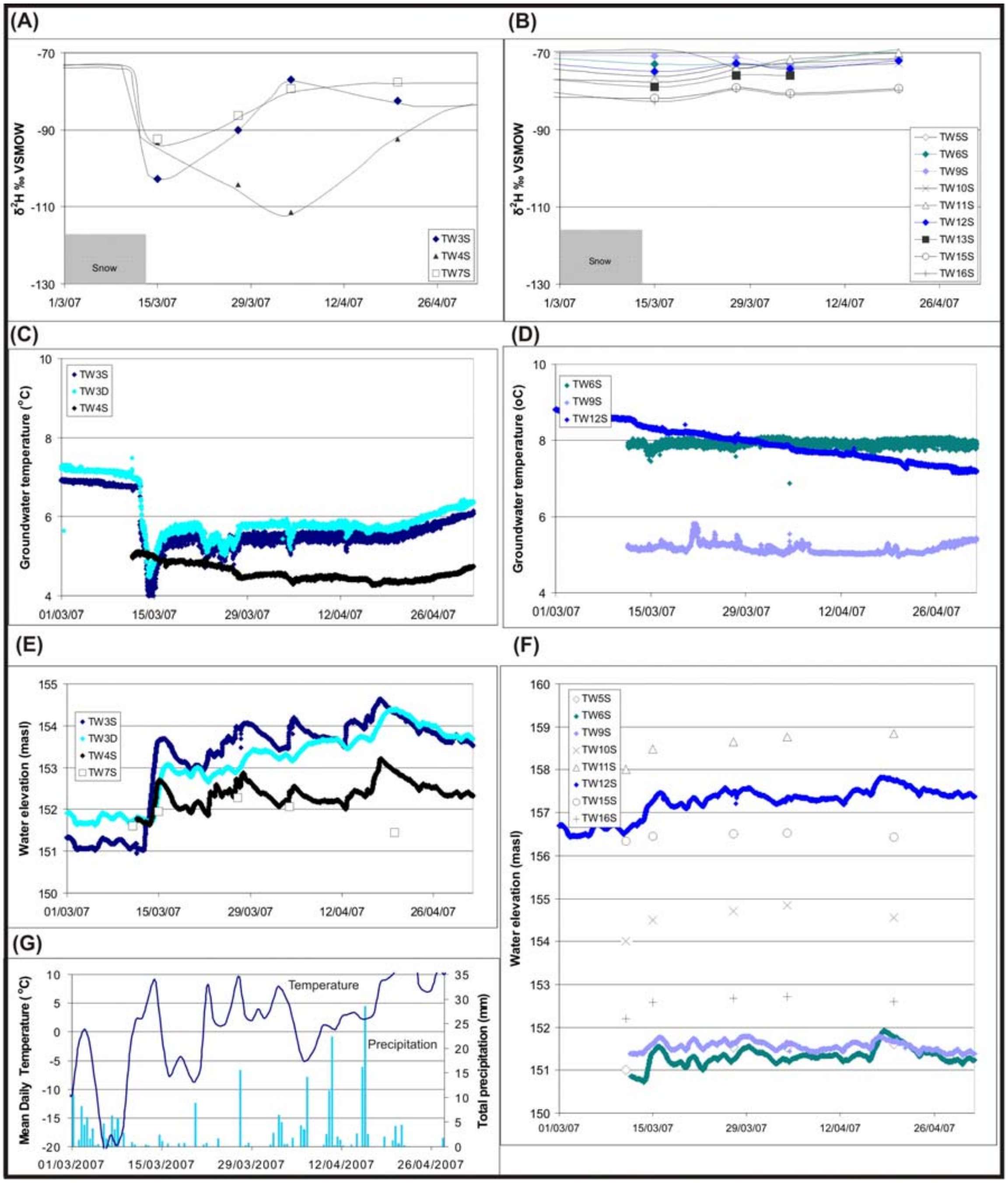

Figure 2.5 Groundwater freshet response in isotopic value (A&B), temperature (C&D), and hydraulic head (E&F). All data is from shallow bedrock piezometers except TW3D. Meteorological data (G) indicate that the freshet was associated with temperatures above 0^{o}C and insignificant precipitation. Data from TW1S, TW2 and TW8 were not collected because the wells were dry or inaccessible as discussed in text. Point symbols of isotopic values and water elevations represent the sampling dates. Monthly data from winter 2007

were -70 to -80‰ δ^2H VSMOW for all wells. Since isotope values were constant during the winter, the winter isotopic value is extrapolated to the start of the rapid recharge event.

During and after the snowmelt, the hydraulic head increased and the groundwater temperature decreased rapidly in a minority of the shallow piezometers (Figure 2.5). For example, the hydraulic head in TW3S increased by 2.7 m and the groundwater temperature decreased by 2.7^{o}C over a ~36 hour period. The first isotopic samples after the snowmelt were collected on March 15, 2007 and the same piezometers that had rapid and significant hydraulic and thermal excursions also had marked isotopic excursions. For example, TW3S, TW4S and TW7S piezometers had isotopic excursions of 20-30‰ δ^2H (Table 2.3). This significant response indicates that cold, δ^2H depleted snowmelt rapidly recharged the groundwater system, causing rapid rises in hydraulic head. The similar response in TW3S and TW3D, both thermally and hydraulically, suggests these two wells are vertically connected by a fracture network that extends continuously to a depth of at least 20 m. Thermal, isotopic and hydraulic head data also indicate the shallow groundwater system quite rapidly returned to ambient conditions after the snowmelt pulse (Figure 2.5). Isotopically the groundwater system recovered in 3-4 weeks. Thermally and hydraulically, the piezometers rapidly recovered back to a new thermal or hydraulic normal in less than one week.

However, the majority of the wells responded with a hydraulic head rise of less than 0.75 m, no thermal excursion, and an undetectable or minor (4-7‰ δ^2H) isotopic excursion (Figure 2.5). This muted response suggests these piezometers may be affected by snowmelt recharge but with different mechanisms than the other piezometers.

Table 2.3 Groundwater δ^2H values before and after the 2007 snowmelt freshet

$10^3\delta^2H$	TW3S	TW4S	TW5S	TW6S	TW7S	TW9S	TW10S	TW11S	TW12S	TW13S	TW15S	TW16S
7/2/07	-72	-67	-	-70	-70	-71	-72	-76	-71	-75	-78	-78
15/3/07	-103	-93	-78	-73	-92	-71	-76	-69	-75	-79	-82	-83
27/3/07	-90	-104	-74	-73	-86	-71	-73	-74	-73	-76	-79	-79
4/4/07	-77	-111	-73	-73	-79	-73	-74	-72	-74	-76	-80	-81
20/4/07	-83	-92	-72	-69	-78	-72	-73	-70	-72	-	-79	-80
2/8/07	-72	-	-73	-73	-77	-72	-72	-70	-72	-75	-78	-79

The piezometers that are interpreted as rapidly recharging, all have little or no overlying soil and higher transmissivity zones at the soil-bedrock interface (Figures 2.2 and 2.3). The piezometers with a muted response to the snowmelt event all have >2 m overlying soil and/or are characterized as having lower transmissivity zones. Even within the group of wells that are interpreted as rapidly recharging, TW4S responded slightly differently from TW3S and TW7S. TW4S did not have a marked thermal excursion, the isotopic excursion was delayed, and had a lesser hydraulic head increase. TW4S has a higher transmissivity zone at the soil-bedrock interface. However, TW4S was drilled through minimal (<2 m) of soil unlike TW3S and TW7S. Therefore, the depth of overlying soil and whether there are hydraulically significant fractures at the soil-bedrock interface are considered the two critical controls of the rapidly recharge process during the 2007 snowmelt.

2.5 Simulating the snowmelt freshet event

2.5.1 Conceptual approach

Numerical simulations are used to evaluate the factors that govern localized recharge, in a fractured crystalline rock setting with limited or no soil. The 2007 freshet event is simulated because the hydraulic and isotopic response are well constrained. A model domain is designed to represent a cross-sectional slice through the hay field (Figure 2.6). The modeling goal is to better constrain the processes controlling localized recharge, rather than attempting to model the exact fracture network, aperture distribution, topography and soil characteristics of the hay field site. Therefore a cross-sectional domain rather than a 3-D domain is used due to computational burden and the lack of well-resolved 3-D fracture networks. A base case scenario is developed from field-based parameters and then a one-at-a-time sensitivity analysis is completed [*Daniel*, 1973; *Saltelli, et al.*, 2000]. In the base case, freshet snowmelt is conceptualized as recharging the fractured rock with no overlying soil. In the sensitivity analysis, the importance of the depth and hydraulic conductivity of overlying soil is examined. Throughout the design and implementation of the base case and sensitivity analysis, the number of variables is parsimoniously minimized to enable better understanding of the physical processes [*Hill*, 2006; *Hill and Tiedeman*, 2007].

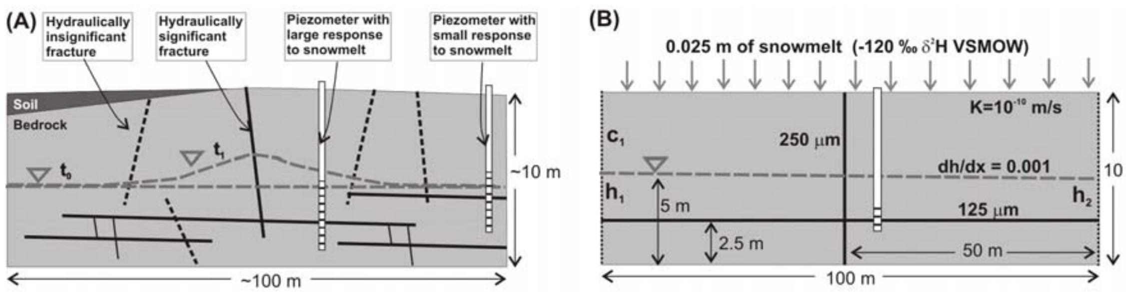

Figure 2.6 (A) Conceptual model of localized snowmelt recharge with the water table before (t_0) and after (t_1) snowmelt shown schematically. Fractures can be hydraulically insignificant if they lack connectivity or are sealed. (B) Numerical implementation showing fracture network, observation location and boundary conditions: snowmelt and two constant head boundaries ($h_1$and h_2). Both cross-sections are vertically-exaggerated.

The fracture network is conceptualized based on geological and hydrogeological observations at the hay field and the surrounding area and in other sites underlain by crystalline rock. Groundwater flow and transport is considered to be fracture controlled because matrix hydraulic conductivity (Figure 2.2) and porosity is very low, as has been found at other sites underlain by crystalline rock [*Hsieh and Shapiro*, 1996; *Karasaki, et al.*, 2000]. Fracture mapping in the surrounding areas (Chapter 3) suggests fracture patterns are dominated by sub-horizontal ‘sheeting’ fractures and sub-vertical to vertical fractures. High-resolution slug testing suggests the bedrock near to the surface can have fracture features with an equivalent single fracture aperture ranging from 100 μm to 800 μm (Figure 2.3). However, the groundwater gradient, pumping test results and the hydraulic response to the freshet all suggest that large aperture fractures or fracture zones are not persistent across the site.

In fracture-dominated systems, the magnitude and consistency of groundwater gradients are a useful indicator of fracture connectivity [*Novakowski, et al.*, 2006]. The groundwater gradient is relatively homogeneous, and approximately equivalent to the topographic gradient, suggesting that connectivity is limited at the local scale and that no large aperture fractures extend across the whole site [*Levison and Novakowski*, 2009]. In addition, interference drawdown between wells (~100 m spacing) was not observed during open-hole pumping tests (8-24 hour duration) conducted before wells were completed as nested piezometers [*Praamsma, et al.*, 2009b]. The hydraulic response to freshet snowmelt and other precipitation events is also not constant across the site. In other field areas underlain by crystalline rock, sheeting fractures commonly control the shallow hydrogeological regime and can persist on scales of tens to hundreds of meters [*Sukhija, et al.*, 2006]. Detailed hydrogeological observations from a similar crystalline setting at Mirror Lake, New Hampshire indicated that thin nearly horizontal fracture zones extend laterally a distance of 20-50 m and are embedded in a network of less transmissive fractures [*Hsieh and Shapiro*, 1996; *Hsieh*, 1998; *Day-Lewis, et al.*, 2000]. Therefore conceptually, horizontal groundwater flow is controlled by the persistence, connectivity and aperture distribution of sub-horizontal fractures or fracture zones which likely extend tens of meters [Figure 2.6; *Praamsma, et al.*, 2009b]. Vertical groundwater flow is controlled by the spacing and aperture of the sub-vertical fractures or fracture zones as well as the thickness and hydraulic conductivity of the soil.

Additional complications to our conceptual model are that snowmelt recharge can be localized by topographic undulations and/or macropores and limited by frozen soil conditions [*Lerner, et al.*, 1990; *Hayashi, et al.*, 2003; *French and Binley*, 2004; *Cey, et al.*, 2006]. No topographic undulations are included in the model, which is a simplification consistent with the lack of observed overland flow during the freshet event. Similarly, soil macropores are not included because soil fracturing was not observed in pits in the hay field [*Levison and Novakowski*, 2007] and the double-ring infiltrometer estimates the bulk *in situ* vertical hydraulic conductivity which includes any potential macropores. Frozen soil conditions are not included because the water table is meters below the shallow soil-bedrock interface. Additionally, frozen soils are effectively impermeable [*Hayashi, et al.*, 2003] so simulations with low soil hydraulic conductivity are comparable. Future simulations could include the influence of topographic undulations, macropore development and frozen soil on recharge processes.

2.5.2 Numerical methods and parameter values

The base case fracture domain is simplified to a single horizontal fracture and single vertical fracture, in order to be parsimonious in the model domain that is limited to the shallow subsurface (Appendix D). Since large aperture fractures are locally observed at wells yet do not likely persist across the site, the horizontal fracture could either be conceptualized as a large-aperture fracture bound by or embedded in lower-aperture fractures or a fracture with a constant and smaller aperture. Preliminary simulations indicate that similar hydraulic and isotopic responses can result from these different distributions of horizontal fracture aperture. For example, the hydraulic and tracer response of a 250 μm fracture bounded by a 50 μm fracture is very similar to the response observed in a fracture with a constant aperture of 125 μm. Therefore the constant and smaller horizontal fracture aperture of 125 μm is simulated because this reduces the number of parameters (*i.e.* length and aperture of both small and large aperture fractures).

A single vertical fracture is assigned the mean effective single fracture aperture (250 μm) for shallow depths (Figure 2.6). A single vertical fracture may seem sparse but I am examining hydraulically open fractures that rapidly recharge. Other sub-vertical or vertical fractures may be present in the system but are not hydraulically significant due to fracture sealing or abundant soil. In the sensitivity analysis the impact of additional vertical fractures that are hydraulically significant is examined. The horizontal and vertical fractures are further assumed to be parallel plates without variable apertures.

The high-resolution numerical simulations were completed using *HydroGeoSphere*, a finite-element, fully-integrated subsurface and surface flow model derived from the original subsurface model of *Therrien and Sudicky* [1996]. *HydroGeoSphere* was used because it is a robust simulator of variably saturated conditions and surface water – groundwater interactions in both porous and discretely-fractured media [*Cey, et al.*, 2006; *Li, et al.*, 2008]. A modified form of the Richards' equation described transient subsurface flow in variably saturated media and areal surface flow was represented in the diffusion-wave approximation of the Saint Venant equation [*Therrien, et al.*, 2006]. The model uses a common node approach to couple surface and subsurface domains where a continuity of head is assumed between the two domains. Therefore the difference in hydraulic head between the surface and subsurface at a common node determined if water infiltrates. Details concerning the theory and numerical solution techniques used in *HydroGeoSphere* are given in *Therrien et al.* [2006].

The cross-sectional domain was 10 m deep, 100 m long with a unit-width representing a slice through the hay field (Figure 2.6B). The single vertical fracture was in the middle of the domain (y=50 m) and the single horizontal fracture was 7.5 m below ground surface. The length of the domain was chosen to minimize the effects of the boundary conditions in the part of the domain of interest (*i.e.* 10 m around vertical fracture). The grid was highly refined near fractures (~1 x 10^{-3} m nodal spacing) and graded away from fractures to a maximum of 0.5 m nodal spacing, resulting in a domain of approximately 155 000 nodes. As surface water nodes were coupled to fracture nodes through a common porous media node, the coupled nodes were assigned a porous media hydraulic conductivity (~1 x 10^{-5} m/s) equal to the vertical fracture transmissivity so that recharge was limited by the vertical fracture aperture rather than the hydraulic conductivity of the coupled node. The bedrock matrix hydraulic conductivity, storativity and porosity were respectively assigned 1 x 10^{-10} m/s, 1 x 10^{-6} and 1%. Overland flow parameters such as the Manning roughness coefficient (in x and y) and rill storage height were assigned 3.5 x 10^{-6} $m^{-1/3}s$ and 0.002 m, respectively. Additional flow parameters used in the simulation are listed in Table 2.4 and Appendix D. The isotopic composition and mixing of event water and pre-event water was simulated following *Cey et al.* [2006]. Transport parameters used for the conservative tracers are listed in Table 2.4 and Appendix D.

Initial flow and transport conditions throughout the domain were a depth to water of 5 m and an isotopic value of -80‰ δ^2H VSMOW, respectively, which is consistent with pre-freshet conditions. A 0.001 horizontal hydraulic gradient, typical of the hay field site and consistent with pre-freshet conditions, was applied by assigning constant head boundary conditions to the two ends of the cross-section. A boundary of constant concentration (-80‰ δ^2H VSMOW) was also applied at the upgradient end of the cross-section to ensure that inflowing water had the background isotopic value. *HydroGeoSphere* is not able to model the snowmelt process so the freshet event considered a 0.025 m thick pulse of melted water with an isotopic value of -120‰ δ^2H VSMOW applied to the top of the domain over a 24 hour period starting after day 1. Evapotranspiration was not included because it is considered minimal immediately following snowmelt [*Rodhe*, 1998]. Temperature is not included in the model because *HydroGeoSphere* can not simulate temperature in unsaturated systems. In addition, the density difference between the cold snowmelt and groundwater is assumed to be insignificant because the temperature difference is less than 8°C.

Table 2.4 Simulation input parameters

Parameter	Base case value	Source of value	Range simulated
Initial water table depth	5 m	Field data	2.5-7.5 m
Initial groundwater δ^2H value	80‰ VSMOW	Field data	-
Snow water equivalent depth	0.025 m	Field data	0.0125-0.0375 m
Horizontal gradient	0.001	Field data	0.005-0.015
Fractures			
Vertical fracture aperture	250 μm	Field data	25-375 μm
Number of vertical fractures	1	Assumption	1-3
Horizontal fracture aperture	125 μm	Assumption	62.5 - 187.5 μm
Brooks-Corey λ	2.5	Reitsma and Kueper 1994	1.25-3.75
Bedrock matrix			
Hydraulic conductivity	1×10^{-10} m/s	Assumption	-
Storativity	1×10^{-5}	Assumption	-
Porosity	1%	Assumption	-
Overburden			
Thickness	0 m	Field data	0-3 m
Hydraulic conductivity	n/a	Field data	2×10^{-6} to 5×10^{-8} m/s
Brooks-Corey λ	2.5	Assumption	-
Fluids			
Density	1000 kg/m3	Assumption	-
Viscosity	1.12×10^{-3} N·s/m^2	Assumption	-
Air-water interfacial tension	0.0718 N/m	Assumption	-
Solute transport			
Free solution diffusion coefficient	1.73×10^{-4} m^2/d		-
Longitudinal dispersivity	0.05 m	Assumption	-
Transverse dispersivity	0.005 m	Assumption	-
Overland flow			
Manning roughness coefficient	3.5×10^{-6} m$^{-1/3}$s	Therrien et al, 2006	7×10^{-6} to 1.8 x 10-6 m$^{-1/3}$s
Rill storage height	0.002 m	Therrien et al, 2006	0.001 - 0.004 m

Thirty-day transient simulations were executed with time-steps controlled by the Newton-Raphson iteration scheme for variably-saturated flow [*Therrien, et al.*, 2006]. The robustness of the flow solution was tested by separate simulations where the nodal density was doubled and time steps were refined by a factor of ten. The hydraulic head response and isotopic value were constant to ±0.005 m and ±0.1‰, respectively. Therefore the solution is considered insensitive to discretization and time step control. All hydraulic and tracer results for the simulations are examined at a point in the horizontal fracture 5 m from the vertical fracture, which represents a piezometer completed in a horizontal fracture near a vertical fracture (Figure 2.6). In all simulations, the hydraulic and isotopic response, as well as the volume of recharged water, is monitored.

A sensitivity analysis was completed by multiplying the input parameters of interest by 0.5 and 1.5 (Table 2.4). Additional simulations with low vertical fracture aperture (25, 50 and 67 μm) were completed. Finally, the importance of overlying soils were evaluated by first simulating 0.1 m thick soils of variable hydraulic conductivity (2×10^{-6} to 5×10^{-8} m/s) and secondly simulating soils of variable thickness (0.1-1 m) and variable hydraulic conductivity (1×10^{-5} m/s to 5×10^{-7} m/s). The measured geometric mean hydraulic conductivity (2×10^{-6} m/s) is within this range of simulated hydraulic conductivities. By adding soil of variable hydraulic conductivity and thickness, and varying other parameters in the sensitivity analysis, I am attempting to understand the characteristics that control recharge in both the rapidly recharging and the non-rapidly recharging wells. Although the hydraulic and isotopic response in various piezometers are used to define the important parameters that govern recharge in this setting, I am not attempting to perfectly match the response to this natural tracer test due to the potential for non-uniqueness in the multi-parameter ensemble.

2.5.3 Simulation results

The base case was designed to simulate the rapid freshet response observed in wells in the hay field (*e.g.* TW3S) using reasonable parameter values and boundary conditions. Note that the 24-hour freshet occurs during day 2 in the simulations, which is approximately equivalent to March 13, 2007. The base case simulation (Figure 2.7) using the *a priori* parameter estimations discussed above, is a reasonably good fit of field observations at TW3S (Figure 2.5). During the simulated 24 hour snowmelt period, there is a ~2.5 m increase in hydraulic head and a ~30‰ decrease in δ^2H at the observation point (5 m from the vertical fracture). After the snowmelt period, the hydraulic head rapidly recovers (within 2 days) and the isotope values return to pre-event values within two weeks. Therefore, the base case simulation seems to be a reasonable approximation of the physical system that leads to the rapid recharge. During the simulation, only 2% of the applied snowmelt recharges the bedrock system; the remainder runs off through the critical depth boundary. This recharge flux is consistent with the low recharge flux calculated using the water table fluctuation method for wells in the hay field [*Milloy*, 2007; *Novakowski, et al.*, 2007b]. The significant simulated run off is different from the lack of observed overland flow. In the hay field outcrops are smaller (<5 m in length) and more isolated than the base case simulation (100 m length of exposed bedrock). Therefore in the hay field, the snowmelt runoff likely enters nearby soils and is drained from the area by installed 'tile drains'. The tile drains are installed in the hay field explicitly to artificially increase interflow and drain saturated soils. An important implication of the small simulated recharge volumes is that only a small volume of snowmelt is necessary to result in the significant observed hydraulic and isotopic responses.

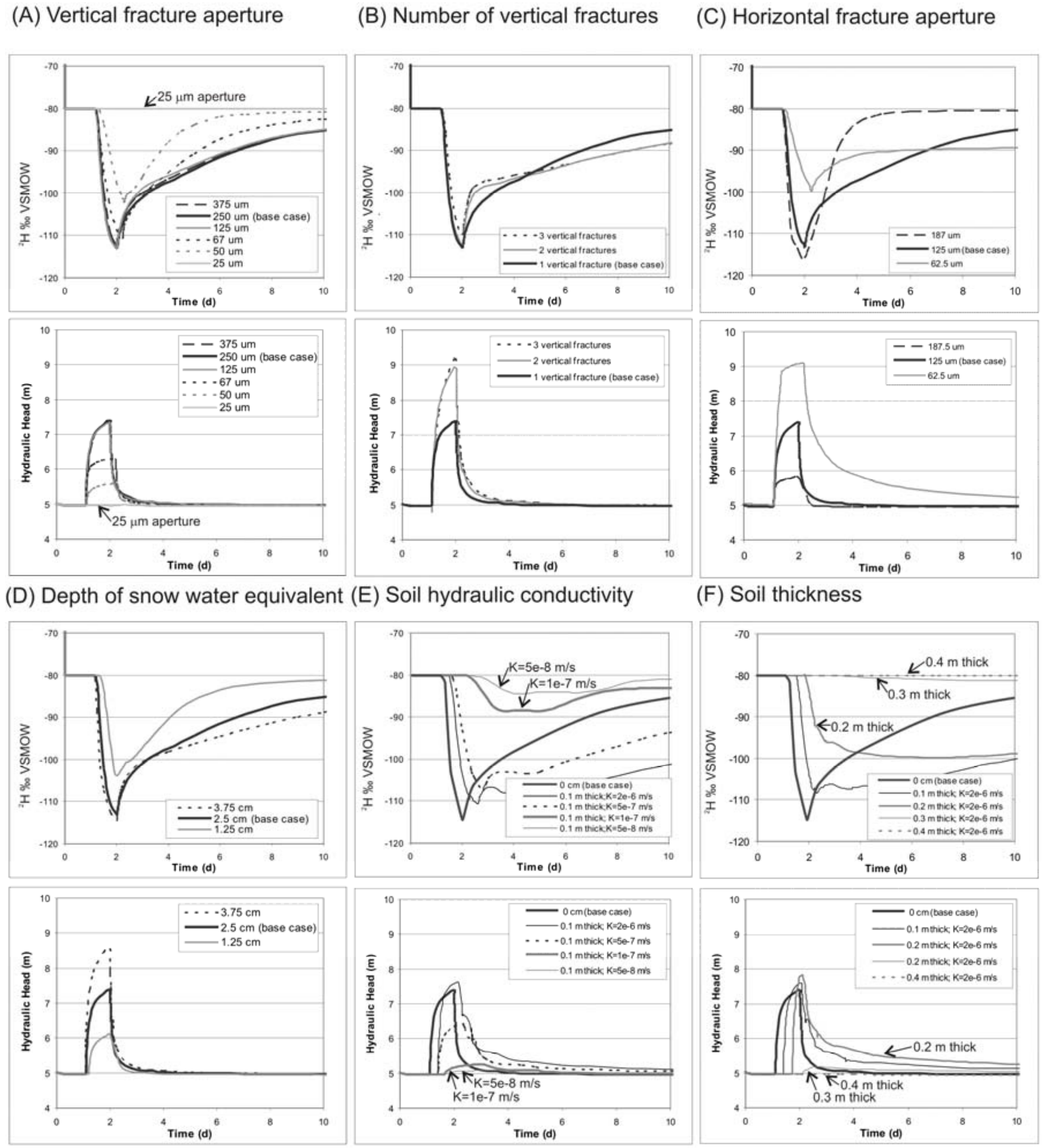

Figure 2.7 Simulation results of the sensitivity to (A) vertical fracture aperture, (B) number of vertical fractures, (C) horizontal fracture aperture, (D) depth of snow water equivalent, (E) soil hydraulic conductivity and (F) soil thickness. Snowmelt was applied for 24 hours during day 1 of the simulations. Compare to field results in Figure 2.5.

The vertical fracture aperture and number of vertical fractures govern the vertical transmissivity of the bedrock system and were thus expected to be important recharge controls. Multiplying the vertical fracture aperture of the base case (250 μm) by 0.5 and 1.5 does not affect the flow or transport solution significantly (Figure 2.7A). Therefore the vertical fracture aperture was further decreased to 67 μm, 50 μm and 25 μm in subsequent simulations to determine the lower limit of vertical fracture aperture that could lead to rapid recharge. The simulation with a single vertical fracture having an aperture of 67 μm was still not significantly different than the base case simulation. However, the simulations with 50 μm and 25 μm vertical apertures significantly reduced hydraulic head rise, and snowmelt recharge.

Increasing the number of vertical fractures increased the head rise but did not significantly change the rate of snowmelt recharge (Figure 2.7B). The actual recharge flux to the bedrock aquifer increased moderately from 2% to 3% of the applied snowmelt for the simulation with three vertical fractures. The isotopic signature of this moderate increase in recharge is not obvious because the groundwater at the observation point is close to the snowmelt value following the recharge. This underscores the importance of using multiple data types (*i.e.* hydraulic and isotopic) to constrain recharge events.

The head rise and snowmelt recharge is sensitive to the horizontal fracture aperture (Figure 2.7C) because constant head boundary conditions are more or less significant for larger or smaller horizontal apertures, respectively. As discussed above, the length of the domain (100 m) was chosen to minimize the effects of the boundary conditions. However this is only valid for the horizontal fracture aperture simulated in the base case (125 μm). For larger horizontal fractures, the domain size would have to be increased so the central part of the domain would only be minimally impacted by the boundary conditions. This underscores the importance of lateral connectivity in these sparsely fractured domains and the importance of testing the robustness of the flow and transport solution using various domains and boundary conditions [*Hill and Tiedeman*, 2007].

The depth of snow water equivalent during the snowmelt period is also an important parameter controlling the hydraulic head rise and recharge flux (Figure 2.7D). Increasing the depth of snow water equivalent by 1.5 times led to a 3.5 m hydraulic head rise. Conversely, decreasing the snow water equivalent by 0.5 times led to a hydraulic head rise of 1 m and a slightly dampened recharge rate and flux.

The soil thickness and hydraulic conductivity are expected to be important controls in dampening or retarding the snowmelt response. First, a 0.1 m thick layer of soil with variable hydraulic conductivity (2×10^{-6} to 5×10^{-8} m/s) was simulated (Figure 2.7E). The hydraulic head and snowmelt recharge is very sensitive to this range of hydraulic conductivity of the soil, even for this thin soil veneer. For example, minimal recharge is simulated for a 0.1 m thick soil with a hydraulic conductivity of 5×10^{-8} m/s. The sensitivity to hydraulic conductivity is expected to increase with increasing soil thickness. Second, soils of variable thickness (0.1 - 1 m) with a range of hydraulic conductivity of 1×10^{-5} m/s to 5×10^{-7} m/s were simulated. Simulations with the geometric mean of measured hydraulic conductivities (2×10^{-6} m/s) are shown in Figure 2.7F as an example. With thin soils (<0.2 m) both the minimum in isotopic values and recovery (hydraulically and isotopically) are delayed and dampened. Increasing soil thickness delays and attenuates the snowmelt response because the soils both impede and store snowmelt, unlike bedrock at the surface that has higher runoff. Thicker soils (>0.4 m) result in effectively no rapid recharge, for all the simulated soil hydraulic conductivities, as is obvious both hydraulically and isotopically (Figure 2.7F).

Figure 2.8 illustrates sensitivity to additional parameters. The horizontal gradient was halved and increased by 1.5 times which is the approximate range of field conditions. Changing the horizontal gradient does not affect the hydraulic response or the initial isotopic response to snowmelt recharge (Figure 2.8A). However, the isotopic recovery following the snowmelt incursion is more rapid with a higher horizontal gradient which is consistent with a more rapid flushing of the system with surrounding pre-event water. Modifying the depth of the water table does not change the rate or magnitude of the isotopic or hydraulic response (Figure 2.8 8B). The hydraulic response for each simulation are offset by the higher or lower initial water table levels that are controlled by the constant head boundaries at either end of the domain. Therefore the depth of water table does not govern the rate or magnitude of the rapid recharge process.

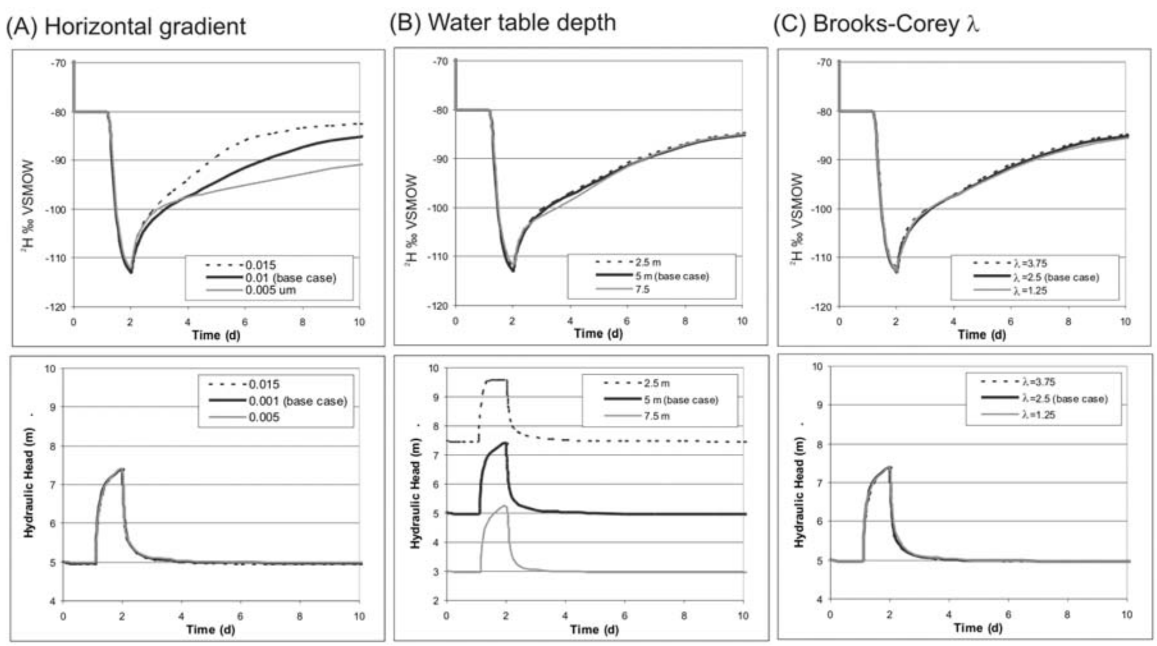

Figure 2.8 Simulation results of the sensitivity to (A) horizontal gradient, (B) water table depth and (C) Brooks Corey λ. Snowmelt was applied for 24 hours during day 1 of the simulations. Compare to field results in Figure 2.5.

Finally, the values of important variables for variably-saturated flow and overland flow were halved and increased by 1.5 times. The Brooks-Corey λ is an empirical pore size distribution index that controls the pressure-saturation relations in variably saturated conditions [*Brooks and Corey*, 1964]. The simulated λ range of 1.25 to 3.75 is consistent with the range derived theoretically and from laboratory experiments in single fractures of variable aperture [*Brooks and Corey*, 1964; *Reitsma and Kueper*, 1994]. The isotopic and hydraulic response was not sensitive to the Brooks-Corey λ value (Figure 2.8C). The lack of sensitivity to both water table depth and λ is likely because the subsurface reached near saturated conditions rapidly and suggests this system is not governed by the variably-saturated parameters. If vertical flow is initiated, the snowmelt response is rapid and significant both isotopically and hydraulically. The system is similarly not sensitive to the Manning overland friction coefficient or rill height (not shown), which indicates that the rapid response is controlled by subsurface parameters rather than surface parameters.

In summary, the base case scenario that was based on *a priori* parameter estimations is a reasonable representation of the physical system governing rapid recharge. The rapid recharge response is most sensitive to the thickness and hydraulic conductivity of overlying soil. The number and aperture of vertical fractures is less significant. Only a small volume of snowmelt is necessary to result in the significant observed hydraulic and isotopic responses.

2.6 Discussion

The hydraulic, isotopic, and thermal data indicate that cold, δ^2H depleted snowmelt rapidly recharged a fractured crystalline aquifer with thin soils. The snowmelt recharge event began on the first day with a mean daily temperature above 0^oC in the spring of 2007, locally causing a multiple-meter hydraulic head rise. Within two days, a minority of monitoring wells had a multiple-meter rise in water table, a ~25‰ decrease in δ^2H value and a 3.5^{o}C decrease in temperature (Figure 2.5). Detailed temperature and pressure data is not available for all wells due to the limited number of data loggers. Additionally temperature is not a conservative tracer due to the bedrock thermal conductivity. Therefore the interpretation of actual recharge flux focuses on the stable isotope results but is also supported by the temperature and water table data. The wells with a multiple-meter rise in water table recovered hydraulically (to a higher water table level) within one week and the isotopic value returned to approximately pre-event values within two weeks. The piezometers affected by rapid recharge were primarily shallow but also occurred in deeper intervals (below 20 m depth in TW3D). Subsequent artificial tracers tests have confirmed that TW3D is connected to the ground surface [*Praamsma, et al.*, 2009a]. Instrumentation and sampling of other deeper wells was not part of this chapter.

Recharge is often quantified and discussed as an annual flux [*e.g. Scanlon, et al.*, 2002] although previous snowmelt recharge studies in porous media settings document rapid recharge occurring over days [*Hayashi, et al.*, 2003; *French and Binley*, 2004]. Field results and numerical simulations suggest the 2007 snowmelt event was extremely rapid, occurring over hours. These observations are consistent with the interpretation of rapid recharge at a research site in Pennsylvania based on hydraulic data [*Gburek and Folmar*, 1999a; *Risser, et al.*, 2005; *Heppner, et al.*, 2007].

However, hydraulic, isotopic, and thermal data also indicate that most wells do not rapidly recharge. During the freshet event most wells maintained near constant groundwater δ^2H values and temperatures indicating that cold, δ^2H depleted snowmelt is not rapidly recharging these wells (Figure 2.5). However the barometrically-corrected water table in these wells rose consistently by

0.6 - 0.75 m during the freshet event, suggesting that these wells did respond hydraulically to the recharge event. Muted water table rises due to surface–loading have been documented at a crystalline rock site in Sweden overlain by 10 m of till [*Rodhe and Bockgard*, 2006]. *Rodhe and Bockgard* [2006] interpret the water-table rise as primarily a hydraulic response to a weight increase in saturated soil during precipitation with a minor amount (2-3% of precipitation) of actual recharge to the bedrock aquifer. The rate and magnitude (less then a meter) of the water table rise is identical to the wells in which thicker soils were encountered in this study. The synchronicity and consistency of the water table rises across the 10 km^2 study area suggests the wells in this study may similarly respond to surface-loading of the sediments by the snowmelt. Therefore the areas with wells that do not rapidly recharge are likely being slowly and inexorably recharged implying that two separate recharge processes, one slow and the other rapid, may be occurring simultaneously in this study area.

Field and numerical modeling results are integrated to determine the variables that govern the spatial distribution of rapid recharge. There is no correlation between pre-event depth to water table and the distribution of rapid recharge. The limited number of wells that rapidly recharge all have thin or no overlying soil and a higher than average bedrock transmissivity data immediately below the soil-bedrock interface (Table 2.1, Figures 2.3 & 2.4). For example, TW3 and TW7 are located on outcrops with shallow high transmissivity zones. TW4 which was drilled through thin soils (<2 m) had a more muted or delayed isotopic, thermal and hydraulic response to the freshet (Figure 2.5) than the wells drilled directly into outcrops. All the wells that did not respond rapidly to the freshet event are drilled through thicker soil (2 – 5.6 m).

The results of the numerical simulations support the field-observations that soil conditions govern the rapid recharge process. The thickness and hydraulic conductivity of overlying soil are critical parameters in governing the response. Using the geometric mean of measured soil hydraulic conductivity (2×10^{-6} m/s) the bedrock aquifer only responds to the freshet snowmelt with a soil thickness of <0.4 m (Figure 2.7). Yet most of the field is underlain by soils that are thicker than 0.4 m (Figure 2.4). Therefore, both field results and numerical simulations indicate rapid recharge is localized at the bedrock outcrops, or the outcrop fringes and other areas with a thin soil veneer. Exposed outcrop occupies only 0.3 % and <0.1 % of the area in the hay field and study area, respectively. Therefore the pulses of rapid recharge are likely extremely localized in this study area but may be more ubiquitous in other areas with a discontinuous veneer of soil. Spatial heterogeneity and localization of recharge may not have been documented at other humid, fractured rock study areas due to the limited number of wells and/or small study area [*Gburek and Folmar*, 1999a; *Rodhe and Bockgard*, 2006; *Heppner, et al.*, 2007]..

The presence of a steep to vertical fracture is also critical (Figure 2.6). But simulations suggest that the aperture of the vertical fracture is less significant, since a vertical fracture aperture of 50 μm allows significant snowmelt recharge (Figure 2.7). The mean transmissivity of the shallow bedrock is $10^{-4.6}$ m^2/s or a single effective fracture aperture of 260 μm. Therefore the shallow depths have total transmissivity (vertical plus horizontal) many times larger than the vertical transmissivity necessary to transmit rapid recharge, especially since bedrock groundwater flow in this setting is governed by the cubic law (*e.g.* the flux through a 260 μm fracture is 140 times larger than the flux through a 50 μm fracture under a unit gradient). This suggests that fractures with a sufficiently large fracture aperture to allow rapid recharge are likely common in the shallow bedrock, underscoring the importance of soil thickness in governing the spatial distribution of rapid recharge.

Although not explicitly simulated during this research, the field results contribute to our understanding of the importance of air entrapment in fractured rock recharge in humid settings. The rapid and large water table rises suggest that air entrapment (*i.e.* the Liesse effect) is possibly occurring although it is unlikely because the Liesse effect is only documented in very well-sorted soils with a small range of intergrain throat openings [*Weeks*, 2002]. Natural fractured rock displays a wide range of fracture apertures in a single fracture [*Konzuk and Kueper*, 2004] which results in fingering of the air-water interface. However, it is difficult to determine if the water table rise is entirely attributable to actual recharge or is magnified by air entrapment processes in previous studies due to the lack of precipitation tracer. By integrating multiple tracers (temperature and δ^2H) I unequivocally observe that the rapid and significant water table rises are due to snowmelt recharge and not air entrapment. Additionally, this phenomena was successfully simulated using reasonable field parameters. The simulations indicate that a small amount of snowmelt recharge can result in a large hydraulic response, due to the low specific yield of fractured crystalline rock [*Gburek and Folmar*, 1999a].

Ongoing research in the Tay River watershed supports the interpretation of rapid and localized recharge in this hydrogeomorphic setting. Long-term water level monitoring reveals that rapid and significant water table fluctuations are locally common but that these result in minimal actual recharge [*Milloy*, 2007; *Novakowski, et al.*, 2007b]. Stable isotope data indicate seasonal, recharge-related isotopic excursions that are highly heterogeneous both with depth and location [*Praamsma, et al.*, 2009b]. Artificial recharge tracer experiments reveal that water ponded at the surface can rapidly travel into bedrock piezometers [*Levison and Novakowski*, 2007; *Praamsma, et al.*, 2009a].

2.7 Conclusions and implications

Salient conclusions from this chapter include:

1) Rapid recharge is a direct, but localized and transient, connection between the hydrosphere and the shallow geosphere. Event-scale recharge to fractured rock aquifers is localized due to subsurface hydrogeological conditions, specifically the distribution of overlying soils and vertical bedrock fractures. This localization is different than topographically-driven, snowmelt recharge localization documented in porous media aquifers [*Hayashi, et al.*, 2003; *French and Binley*, 2004] and harder to characterize and predict because the governing controls are below the surface.
2) The two distinct hydraulic, thermal and isotopic responses observed in wells suggest two different recharge mechanisms are occurring simultaneously in the study area. One is rapid and localized and the other is slow and widespread. Assessing the recharge rate and contribution of each of these mechanisms to groundwater budgets is an important question for future research.
3) Stable isotopes (*e.g.* δ^2H) are robust indicators of actual recharge mass flux during snowmelt because they are conservative and applied to the entire surface area evenly. Water table and temperature are important supportive evidence of recharge processes but can be difficult to interpret due to the low specific yield and high thermal conductivity of bedrock, respectively.
4) Integrating hydrogeological characterization, numerical simulations and a detailed multi-tracer natural experiment result in an enriched understanding recharge to fractured rock aquifers.

The similarity of the results from this study area and others [*Heppner, et al.*, 2007] suggest rapid recharge is a real physical process that I expect to be common in humid fractured rock settings with thin soil cover. This hydrogeomorphic setting is common in Canada, the northeastern United States and northern Europe. Therefore this chapter has broad implications for groundwater management and protection, as well as our understanding of recharge processes. Fundamentally, recharge rates in this setting are highly heterogeneous, both spatially and temporally. But as a first order approximation, soil thickness mapping could be used to identify areas of potential rapid recharge if the bedrock fractures are either ubiquitous or have an unknown and unpredictable distribution.

Calculating recharge rates and protecting groundwater from contamination is essential for groundwater management. Calculating recharge rates in this setting, where two very different recharge rates and mechanisms are simultaneously occurring at the local scale, may be difficult. For example, a single observation well in the study area could significantly over- or under-estimate recharge rates. Rapid recharge pathways also imply that any surface contaminants have little or no time to be remediated in the vadose zone. Therefore point and non-point source pollution is an important concern for groundwater protection in these settings [*Levison and Novakowski*, 2009; *Praamsma, et al.*, 2009a]. Recharge is typically quantified and simulated on the scale of years [*Cook and Robinson*, 2002; *Bockgard, et al.*, 2004; *Cook, et al.*, 2005], but in humid fractured rock settings with shallow soils, this type of conceptual model may not be appropriate if rapid pulses of precipitation can locally reach greater than 20 m depth within days.

Chapter 3
Groundwater flow: lineaments as watershed-scale hydraulic barriers

3.1 Introduction

Identifying and characterizing structures that control watershed-scale groundwater flow is essential for both groundwater management and understanding fluid flow in bedrock aquifers [*Ferrill, et al.*, 2004; *Seaton and Burbey*, 2005; *Denny, et al.*, 2007]. Lineaments are extensive linear surface features and the surface expression of fracture zones, faults or geological contacts [*O'Leary, et al.*, 1976; *Prost*, 1994; *Jackson*, 1997; *Singhal and Gupta*, 1999]. Lineament identification is standard practice in fractured rock hydrogeology, though also controversial and periodically questioned by hydrogeologists and structural geologists [*Wise*, 1982]. This chapter presents a necessary and rigorous examination of the hydrology of lineaments, within the context of the current understanding of fault hydrology. Lineament identification is defensible when multiple observers use multiple image types, classify lineaments by significance, and cull observations that do not meet reproducibility criteria [*Mabee, et al.*, 1994; *Sander, et al.*, 1997; *Singhal and Gupta*, 1999; *Tam, et al.*, 2004]. Lineament identification is a useful hydrogeological tool when lineaments are identified with a defensible and reproducible method and analyzed with supplementary geomatic, geologic and hydrogeological data within a well-documented structural geology framework.

Early studies suggested that lineaments are associated with higher well yields although the number of studied wells were small [*Lattman and Parizek*, 1964; *Lattman and Matzke*, 1971; *Siddiqui and Parizek*, 1971]. Consulting hydrogeologists and researchers often continue to assume that lineaments are fractured recharge and flow conduits with high groundwater potential [*e.g. Krishnamurthy, et al.*, 2000; *Sener, et al.*, 2005; *Shaban, et al.*, 2006]. However, lineaments do not correlate with well yields or only lineaments of certain characteristics correlate to well yields but these correlations are not consistent across different geological, topographic and geomorphic settings [*Waters, et al.*, 1990; *Gustafsson*, 1994; *Mabee, et al.*, 1994; *Sander, et al.*, 1997; *Edet, et al.*, 1998; *Mabee*, 1999; *Magowe and Carr*, 1999; *Mabee, et al.*, 2002; *Moore, et al.*, 2002; *Solomon and Quiel*, 2006; *Sander*, 2007]. Therefore the assumption that lineaments are fractured conduits is not consistent with much of the well yield data around lineaments.

To the best knowledge of the author, lineaments have not previously been examined using recent models of fault architecture and permeability. Fault zones are conceptualized as fault cores and flanking damage zones that cross-cut an undeformed protolith [*Caine, et al.*, 1996]. Permeability is typically reduced in fault cores due to brecciation, cataclasis, and clay-rich gouge zones [*Evans*, 1988; *Goddard and Evans*, 1995; *Caine and Forster*, 1999]. In crystalline rocks, the permeability of the damage zone is often higher than the protolith due to fracture networks that can be infilled by mineral precipitation during or after deformation, reducing permeability [*Evans, et al.*, 1997; *Rawling, et al.*, 2001]. The fault core and surrounding damage zone result in an anisotropic permeability structure that is a hydraulic conduit, barrier, or conduit-barrier system depending on the fault zone architecture and direction of flow examined [*Forster and Evans*, 1991; *Caine and Forster*, 1999; *Caine and Tomusiak*, 2003; *Bense and Person*, 2006]. The permeability, width and anisotropy of a damage zone and fault core can be extremely heterogeneous along strike [*Evans and Chester*, 1995; *Caine and Forster*, 1999; *Fairley and Hinds*, 2004; *Minor and Hudson*, 2006] and vary during deformation [*Chester, et al.*, 1993]. For watershed-scale groundwater flow, high permeability structures are recharge and flow conduits that can increase subsurface connectivity [*Mayer and Sharp*, 1998; *Flint, et al.*, 2002; *Denny, et al.*, 2007]; low permeability barriers restrict recharge and flow and can compartmentalize flow systems [*Marler and Ge*, 2003; *Seaton and Burbey*, 2005]; and conduit-barriers can have complex behavior such as compartmentalizing lateral flow while allowing significant vertical flow or recharge [*Ferrill, et al.*, 2004; *Bense and Person*, 2006]. The complexity of permeability patterns in field-based, fault architecture models suggests the assumption that lineaments are fractured conduits may be too simplistic.

In this chapter, a preliminary inspection of a watershed underlain by granitic and gneissic terrain of the Canadian Shield suggests that lineaments are associated with linear lakeshores and perennial wetland complexes. The perennial nature of the surface water bodies suggests water infiltration is limited rather than enhanced in lineament areas possibly due to subsurface permeability. The objective of this chapter is to determine if lineaments are structurally controlled, hydraulic barriers to groundwater recharge and flow in this geological setting. Lineaments are identified using a defensible, remote sensing method and analyzed using supplementary geomatic data. Mapping fracture patterns constrains the structural geometry of lineaments. The relationship between surface water and groundwater is characterized in detail at a representative lineament. Finally, a synthetic domain representing a typical lineament is simulated to reveal the significance of hydraulic conductivity and fracture aperture in the observed surface water and groundwater systems. This chapter is an important example of applying remote sensing and geomatics to a complex hydrogeological problem, as has been called for in recent reviews [*Becker*, 2006; *Brunner, et al.*, 2007]. Since lineaments are surface expressions of subsurface phenomenon and common on the earth's surface, examining lineaments using rigorous and defensible methods from multiple disciplines may aid the study of other hydrogeological and geologic problems.

3.2 Regional geology and hydrogeology

The ~900 km^2 Tay River watershed is located in rural eastern Ontario, Canada (Figure 3.1). The watershed is characterized by an undulating upland area underlain by Precambrian rocks and a topographically subdued downstream area underlain by Paleozoic sedimentary rocks. This chapter is focused on the bedrock geology and hydrogeology of the Precambrian terrain. The Precambrian units are upper greenschist to granulite metamorphic grade metasediments and metavolcanics with associated intrusive rocks of the Frontenac and Sharbot Lake Terranes of the Grenville Province [*Culotta, et al.*, 1990; *Easton*, 1992]. Metasedimentary and metavolcanic rocks are strongly foliated and consist of marble, dolomite, siliciclastic and quartzofeldspathic gneiss, and felsic to intermediate metavolcanics. Weakly to strongly foliated intrusive rocks comprise granodiorite, granite, diorite, syenite, migmatite and minor mafic intrusive rocks (gabbro, anorthosite, and norite). Flat lying Paleozoic sandstone, dolomite and dolomitic limestone locally overlie Precambrian units. Complex ductile fabric orientations are locally common in Precambrian units but the predominant structural and metamorphic grain is consistently striking northeast [*Wilson*, 1961; *Davidson and Ketchum*, 1993; *Easton*, 2001].

The Ottawa-Bonnechere graben is a Tertiary northwest-trending normal fault system that defines significant topographic features north of the study area [*Kay*, 1942]). The graben is considered a Neoproterozoic failed arm of a triple junction which was repeatedly reactivated by Phanerozoic tectonism [*Kumarapeli*, 1978; *Kumarapeli*, 1981; *Rimando and Benn*, 2005]. The southern half of the graben is characterized by north-facing topographic breaks with down-thrown north side hanging walls. Joint orientations in the regions surrounding the faults are predominantly parallel to fault orientations, which is consistent with joint development during normal faulting. Although the Tay River watershed is south of the area mapped by Kay [1942], the southernmost fault of the Ottawa-

Bonnechere graben is interpreted to extend through the central Tay River watershed [Kay, 1942 Plate 6].

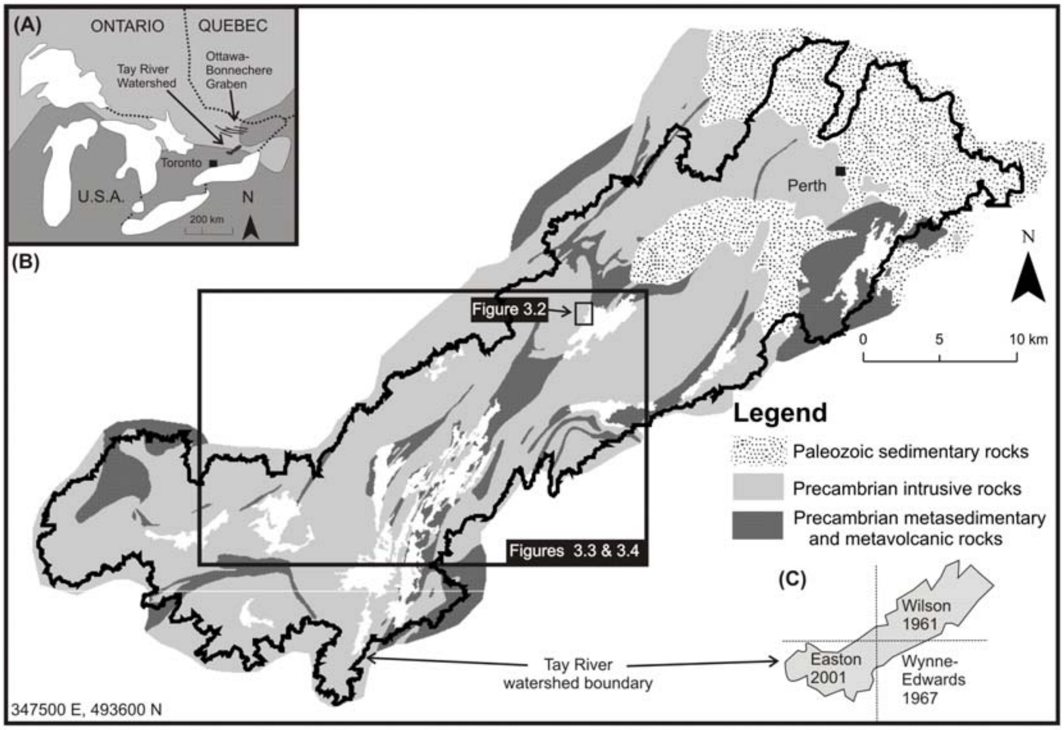

Figure 3.1 (A) Tay River watershed study location in Ontario. light grey are Precambrian rocks; and dark grey are Paleozoic rocks; Ottawa-Bonnechere graben shown for reference. (B) Simplified geological map of the Tay River watershed derived from existing Geological Survey of Canada and Ontario Geological Survey maps. Individual rock types are grouped together into hydrogeologically significant units. (C) Index of map sources for geological compilation (Wilson, 1961; Wynne-Edwards, 1967; Easton 2001a; and Easton 2001b).

The surficial geology of the study area is a thin (<1m) and discontinuous till veneer with littoral or organic deposits adjacent to surface water bodies [*Kettles*, 1992]. The discontinuous till veneer rarely masks the structure of the underlying bedrock. The course-grained littoral and organic deposits are limited in extent and thickness (1-5 m). Glacial striae and drumlins indicate that the predominant ice flow direction was south-southwestward [*Kettles*, 1992]. Surficial mapping and residential water well records indicate that unconsolidated materials do not provide significant groundwater potential and are therefore not the focus of this study.

Bedrock geological mapping conducted by the Geological Survey of Canada and Ontario Geological Survey was compiled and simplified into hydraulically significant lithologic groups in Figure 3.1, following *Caine and Tomusiak* [2003]. Individual rock units were reclassified under the assumption that rock types with similar geologic history and response to brittle deformation should exhibit similar hydrogeological properties at the watershed scale [*Caine and Tomusiak*, 2003]. The hydrogeological consistency of the amalgamated rock groups was evaluated using the specific capacity of residential water wells [*MOE*, 2006]. Specific capacity was derived from drawdown data during one hour pumping tests conducted after well completion [*Freeze and Cherry*, 1979]. Null (*i.e.* no drawdown during pumping) and spurious (*i.e.* drawdown greater than depth of well) specific capacity values were removed from the database. Wells completed in metasedimentary and metavolcanic rocks (n = 383) and intrusive rocks (n = 749) have a mean specific capacity of 2.3×10^{-5} $m^3/s/m$ and 3.0×10^{-5} $m^3/s/m$, respectively. For comparison, wells completed in sedimentary rocks (n = 357) have a mean specific capacity of 7.3×10^{-5} $m^3/s/m$. The similarity of specific capacity in Precambrian units suggests that they have similar hydrogeological characteristics at the watershed scale [*Singer, et al.*, 2003].

Regional groundwater flow in the Tay River watershed is towards the northeast, parallel to the Tay River, with an approximate groundwater gradient of 0.001 [*Golder Associates Ltd.*, 2003]. At a local scale groundwater-surface water interactions and recharge processes have been examined at a site far from mapped lineaments [*Praamsma*, 2006; *Milloy*, 2007]. Hydraulic testing coupled with hydraulic head measurements revealed that recharge is limited to ~1% of precipitation [*Milloy*, 2007]. No attempt to predict the location of recharge features or understand the role of lineaments was undertaken in these studies.

The areas underlain by Precambrian rocks are characterized by subdued (<200 m) yet heterogeneous and hummocky topography with complex surface water patterns due to the glacial history. The Tay River watershed consists of over 3000 permanent surface water features. The size and type of surface water features vary from >10 km^2 lakes to <100 m^2 vernal ponds. Linear lakeshores and wetland complexes are commonly persistent over kilometers. Extremely high surface water gradients between adjacent surface water features suggest poor subsurface connectivity. The numerous lakes and wetlands in the Tay River watershed are important and characteristic hydrographic features in the watershed like other areas of the Canadian Shield [*Farvolden, et al.*, 1988].

3.3 Methods

This chapter examines two scales. At the watershed scale, geological, remote sensing, and water well data was integrated into a geomatic database to identify and analyze lineaments. At a local scale, a lineament that is representative in length, orientation, topography, surface water gradient and specific capacity was characterized using hydrogeological and numerical modeling tools.

3.3.1 Geomatics

In this chapter, lineaments are defined as linear tonal and/or topographic features with a minimum length of 500 m. The methodology of lineament identification generally followed *Mabee et al.* [1994] and is summarized in the Appendix E. The potential hydraulic importance of lineaments was explored using the culled specific capacity data base for residential water wells, described above [*MOE*, 2006].

For the analysis, only wells completed in Precambrian units (n = 1132) were used. The culled database was interpolated using kriging and an inverse weighted distance function. Interpolation using the two methods was compared visually and qualitatively using raster mathematics to recognize any systematic trends due to the interpolation method. The interpolated values were then visually compared to the distribution of identified lineaments.

Hydraulic barriers typically have hydraulic head discontinuities or high hydraulic gradients oblique to the structure [*Bense and Person*, 2006]. The relative paucity of high quality hydraulic head measurements near lineaments in the study area precludes an analysis of groundwater gradients. However, in a well connected surface water-groundwater system, surface water features are also manifestations of the water table [*Fredrick, et al.*, 2007]. Therefore, if lineaments are permeable features with high connectivity, the surface water gradients around lineaments are expected to be low. Surface water gradients were mapped by manually compiling DEM surface elevations for all permanent water bodies. The potential gradient between adjacent surface water bodies was mapped by first creating a triangulated irregular network of interpolated elevations between surface water features.

Twenty lineaments representing the various geological and physiographic settings and lineament orientations were verified by field ground-truth during spring, summer and fall, 2006 to ensure that surface water features are perennial. The physiographic expression, wetland classification and nearby outcrops (see next section) were inspected during field work.

3.3.2 Fracture mapping

Lineaments in topographically subdued areas are typically wet, low-lying areas with little exposed outcrop which challenges structural analysis [*Isachsen*, 1976; *Spitzer*, 1981; *Wise, et al.*, 1985]. Therefore fractures were measured and characterized at 17 outcrops both adjacent to and in between mapped lineaments. Outcrops with two near-orthogonal faces were preferred to avoid orientation bias [*La Pointe and Hudson*, 1985]. Observations typically include fracture orientation, length, and termination style (abutting, blind or through-going). The orientation and type of foliation were also recorded. A 180 m scanline (TG06-07 on Figure 3.2) was completed on an unusually well exposed outcrop adjacent to the lineament described in detail below, herein called the 'Christie Lake lineament.' Fracture measurements from the scanline were corrected for orientation bias using the *Terzaghi* [1964b] method. Fracture and foliation measurements from other outcrops were not corrected for orientation bias because the outcrops do not have a systematic trend.

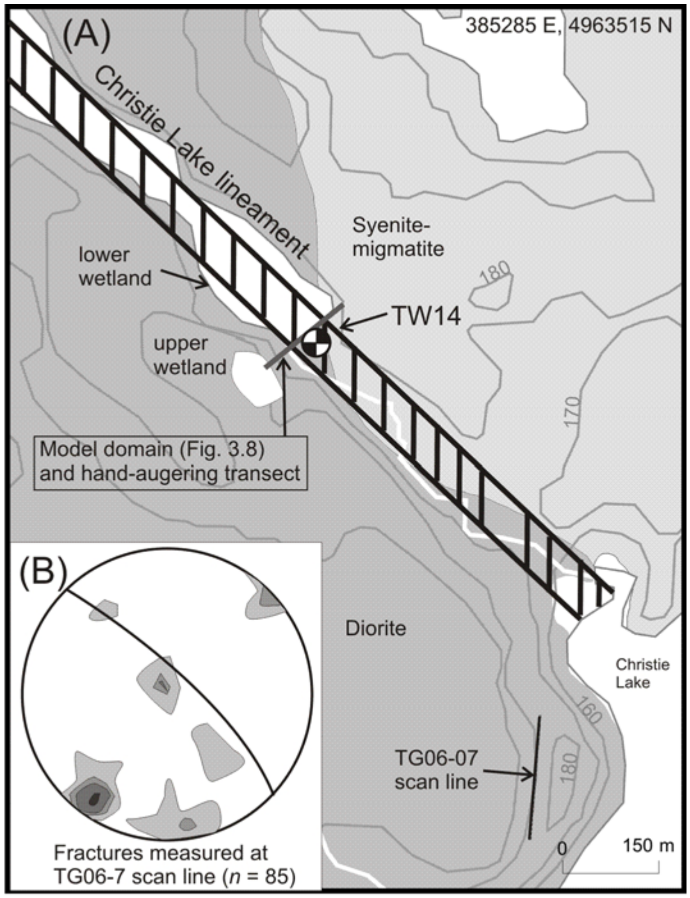

Figure 3.2 (A) Christie Lake study site with bedrock geology from *Wilson* [1961]. The 'Christie Lake' lineament, originally mapped as a fault truncating units to the northwest, is shown as 100m wide zone oriented 310^o bisecting a linear wetland complex. Borehole TW14 is located in the center of the lineament. The location of cross-sectional model domain and hand-augering transect described in the text is also shown. (B) Equal area, lower hemisphere stereonet projection of poles to fractures measured at the nearby TG06-07 scanline, plotted with 2 sigma uncertainty. The mean orientation (305/80) of fractures is also plotted for comparison to the lineament orientation.

3.3.3 Hydrogeological characterization

The 3 km long northwest trending 'Christie Lake lineament' bisects a wetland complex, herein called 'Lower wetland', and is mapped as a fault of unknown displacement that truncates units to the northwest [Figure 1.2; *Wilson*, 1961]. The lineament is a topographic break where elevation increases to the southwest. A number of wetlands are found in the upland area to the southwest including the swamp herein called 'Upper wetland' (Figure 3.2). The Christie Lake lineament was characterized in detail because it is representative of lineaments in the study area in length, orientation, and physiography.

A monitoring well (TW14; 0.152 m diameter) was drilled in the middle of the lineament to a depth of 44 m below ground surface. Drilling chips sampled from discrete depths were tested for the presence of carbonate using dilute hydrochloric acid to determine the vein mineralogy. Well TW14 was characterized using a down hole camera and via hydraulic testing with 1.77 m test intervals isolated by straddle packers. Slug tests were completed in each interval using 5 L of water and analyzed using the *Horslev* [1951] method as described in *Butler* [1998]. Measured transmissivities were converted to hydraulic conductivities and single fracture effective apertures for each interval [*Novakowski, et al.*, 2007a]. Two slotted 0.051 m diameter multilevel piezometers set in #2 sand were installed in the transmissive zones of TW14 and separated by >3 m of bentonite. The upper portion of the well was left open resulting in three discrete piezometer intervals (TW14S, TW14M and TW14D). Each piezometer was developed until groundwater was not turbid by pumping for 1-2 hours. Pressure transducers were installed in the upper and lower piezometer and the adjacent Lower wetland. Hydraulic head data was recorded on 15 minute intervals for three months to constrain possible hydraulic connections between surface water features and the subsurface intervals.

Ten shallow boreholes were drilled until refusal using a hand-auger along a 20 m transect perpendicular to the lineament to evaluate the properties of the unconsolidated material in the Lower wetland. Intact core was removed from the hand auger and logged at 0.1 m intervals using the Unified Soil Classification System [*American Society for Testing and Materials*, 2007].

3.3.4 Numerical simulations of surface water-groundwater interactions

HydroGeoSphere, a finite-element, coupled groundwater and surface water model was used to explore local-scale interactions between surface water and groundwater in this fractured rock terrain [*Therrien and Sudicky*, 1996; *Therrien, et al.*, 2006]. *HydroGeoSphere* was used because it is a reliable simulator of variably saturated conditions and surface water – groundwater interactions, which has been proven accurate for a variety of geologic settings and spatial and temporal scales [*Cey, et al.*, 2006; *Li, et al.*, 2008]. A synthetic cross-sectional domain was built that is physically consistent to both the Christie Lake lineament site and other lineaments in the study area (Appendix D). The topographic gradient (0.4) was based on a detailed WAAS-corrected GPS topographic survey of the area surrounding these two perennial wetland areas (cross section located on Figure 3.2). The model domain was a 100 x 50 x 1 m cross-section discretized into 39,000 nodes with 0.5 m spacing at the bottom grading finer towards the surface where the main head and flux dynamics occur. No flow boundaries were applied along the lateral and bottom boundaries of the domain to enable examination of surface-groundwater interactions without additional complicating influences [*Panday and Huyakorn*, 2004]. The robustness of the flow solution was tested using more discretized grids. Transient simulations were run until steady-state conditions are derived (1-30 years in model time) with a maximum allowable water balance error of 1% of inflow. The domain was simulated using both equivalent porous media and discrete fracture network approaches to constrain possible bulk hydraulic conductivity values or fracture apertures, respectively. For the equivalent porous media approach, it was assumed that the hydraulic conductivity tensor is isotropic and homogenous. For the discrete fracture domain, an orthogonal fracture network was implemented because of observed fracture patterns (see Results). The assigned values of hydraulic conductivity and fracture aperture are discussed below because they are derived from hydraulic testing results. Since surface and subsurface flow is explicitly coupled in *HydroGeoSphere*, rainfall either directly ran off through a critical depth boundary (exiting the domain at the lowest topographic point), ponded in the topographic depressions, or infiltrated. The rainfall pathway was dependent on subsurface permeability (bulk hydraulic conductivity and fracture aperture) as well as overland flow and evapotranspiration parameters. Overland flow and evapotranspiration parameters were derived from *Randall* [2005] who simulated a similar geologic and physiographic setting. A long-term mean annual rainfall of 0.9 m/year was applied to the surficial nodes [*Golder Associates Ltd.*, 2003]. Simulations were completed with and without evapotranspiration to evaluate the importance of this parameter.

Depth of water in the upper wetland is considered the primary fitting parameter because, in the absence of a dense network of monitoring wells, it is the most sensitive and hydraulically significant parameter to changes in hydraulic conductivity and fracture aperture. The maximum depth of water in the Upper wetland is 2 m in the model domain. At greater depths overland flow towards the lower swamp is initiated. Numerical simulations indicate that the depth of water in the Upper wetland is reproducible to 0.1 m. This modeling exercise is considered a useful numerical experiment for testing conceptual models of groundwater-surface water interactions, because numerous subsurface targets are not available for calibration and verification.

Table 3.1 Numerical model input parameters.

Parameter	Value	Unit	Reference
Evapotranspiration			
Evaporation	0.5	m/year	[*Golder Associates Ltd.*, 2003]
Maximum rooting depth	2.0	m	[*Canadell, et al.*, 1996]
Leaf area index	4	-	[*Scurlock, et al.*, 2001]
Wilting point	0.06	-	[*Schroeder, et al.*, 1997]
Field capacity	0.15	-	[*Schroeder, et al.*, 1997]
Overland flow			
Manning roughness coefficient	0.006	-	[*Randall*, 2005]
Rill storage height	0.0001	m	[*Randall*, 2005; *Therrien, et al.*, 2006]

3.4 Results

3.4.1 Lineament identification and analysis

A greater number of lineaments were repeatedly observed using the Landsat imagery (111) than with the DEM (78). The lineament data is compiled in Appendix E. Landsat-derived lineaments have a unidirectional northeast orientation, with linear directional mean of 042^{o} (Figure 3.3A). This trend is coincident with lineaments derived from a different Landsat image by an independent study [*Andjelkovic and Cruden*, 1998] indicating that lineament detection is a robust and reproducible technique if completed systematically (Figure 3.3). DEM-derived lineaments have a bidirectional northeast and northwest orientation, with linear directional means of 033^{o} and 312^{o}, respectively (Figure 3.3B). For both DEM and Landsat medium, selected lineaments were also observed in aerial photographs and targeted ground truthing. Every observed lineament was related to a surface water feature (*i.e.* a linear lakeshore, wetland complex or river reach). Field observations indicate that the wetlands associated with lineaments were perennial rather than vernal. Although Landsat highlights tonal differences and the DEM highlights topographic differences, the same lineaments were often detected on both DEM and Landsat. The shared lineaments typically also share characteristics (scale detected and linearity), suggesting that lineaments in this study are tonal-topographic features. Therefore both data types are considered useful, but as discussed below, lineament detection using DEM data may be more valuable in identifying structural discontinuities in a topographically subdued landscape.

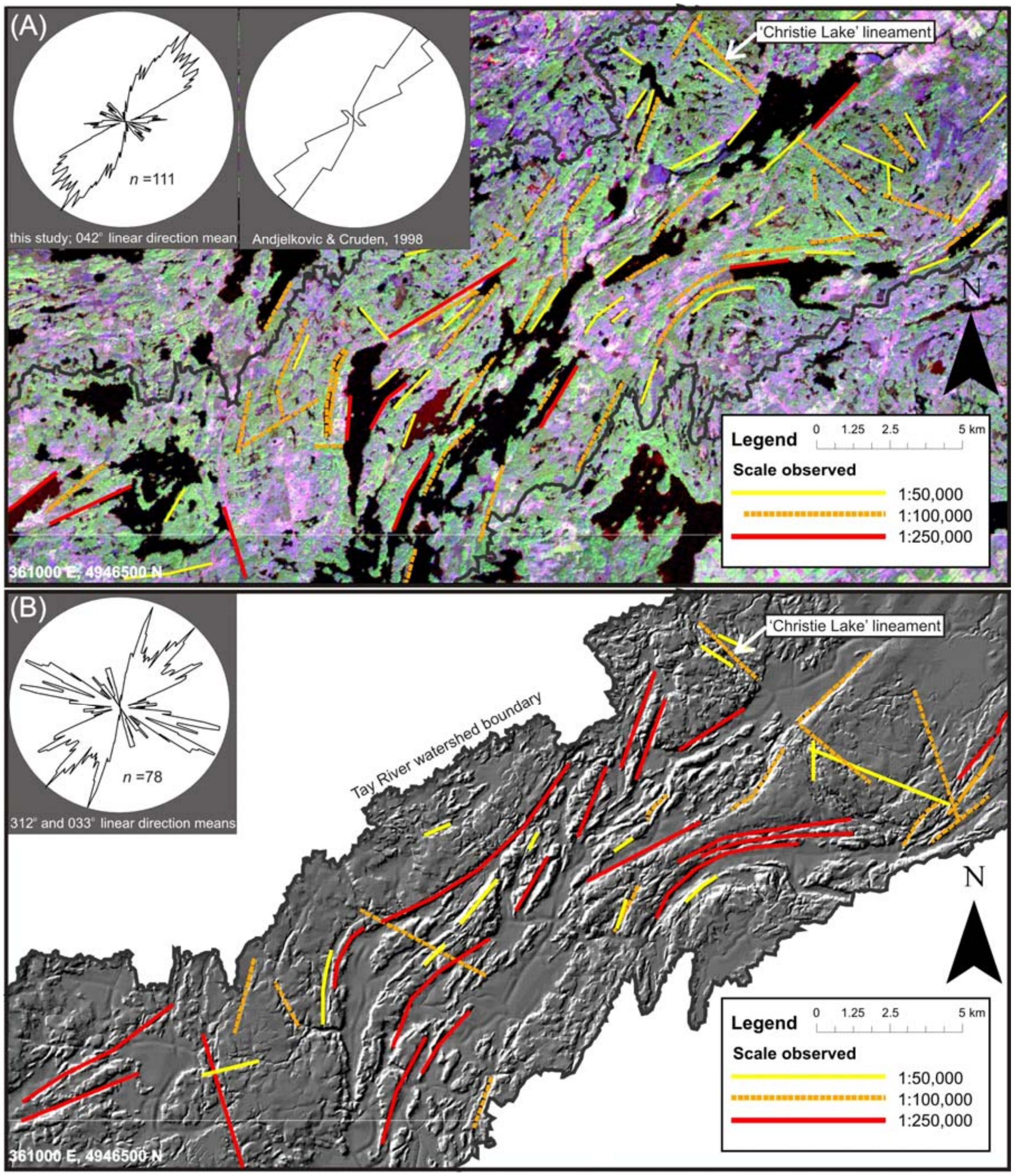

Figure 3.3 Lineament distributions on (A) Landsat false color composite (bands 754) and (B) hillshade enhanced digital elevation model (DEM). Both at scale 1:100,000 with lineaments shown by scale of identification. Rose diagrams with 10^{o} bin spacing are inset in each image. Also inset is a rose diagram of lineaments identified by *Andjelkovic and Cruden* [1998] using Landsat imagery of the Frontenac terrane. The rose diagrams indicate the consistency of identification between different observers and images.

The specific capacity database was analyzed to examine permeability trends in lineaments areas. The database was interpolated using kriging and inverse weighted distance functions. For kriging, a spherical variogram model was chosen based on visual best fit with a resultant range and sill of 800 m and 350 $(L/min/m)^2$, respectively (Appendix E). No systematic differences were observed when the results for the two interpolation methods were compared visually and qualitatively using raster mathematics. Figure 3.4A illustrates the interpolation using inverse weighted method and the distribution of DEM-derived lineaments. The specific capacity of residential wells completed in Precambrian rock is not higher near lineaments at a watershed scale. Detailed spatial analysis indicates that there is no correlation between specific capacity and distance from lineaments (Table 3.2).

Table 3.2 Specific capacity of water wells at various distances from DEM derived lineaments

Distance from Lineament (m)	Number of wells	Specific Capacity (L/min/m)
25	11	1.4 ± 2.5
50	23	1.2 ± 2.3
100	124	1.7 ± 5.8
250	179	1.7 ± 5.6
All wells in watershed	1132	2.36 ± 7.8

Figure 3.4B depicts the potential gradient between adjacent surface water features and the location of DEM-derived lineaments not associated with lakeshores. Lineaments associated with lakeshores are not included because the gradient at a lake shore is zero by definition. Generally, lineaments are coincident with higher potential surface water gradients. If lineaments are well connected, high permeability features, the surface water and groundwater gradients would be relatively low. The correlation of lineaments with high potential surface water gradients and lower specific capacity indicates that lineaments are less permeable features that may be regional hydraulic barriers.

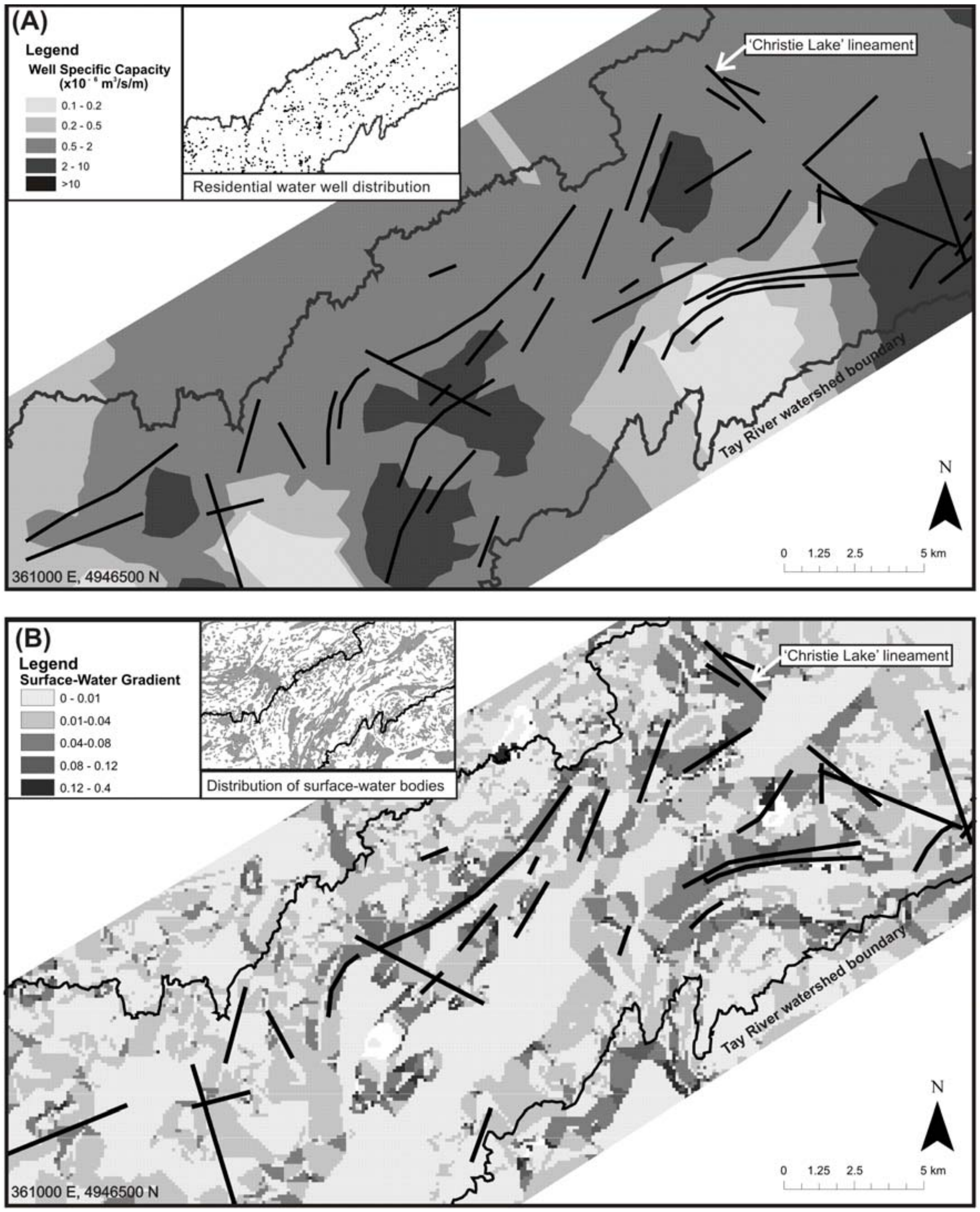

Figure 3.4 Lineament distribution compared to supplementary geomatic data. (A) DEM-derived lineament distribution compared to residential water well specific capacity. (B) Non-lakeshore DEM-derived lineaments compared to interpolated surface water gradients. Lakeshore lineaments are excluded because the surface water gradient is zero at lakeshores. Inset are the source data distribution of residential wells (MOE, 2006) and surface water bodies.

3.4.2 Fracture mapping

At a watershed scale, three fracture sets were generally observed (Figure 3.5A). The structural data is compiled in Appendix F. The most prominent is the steep to vertical northwest striking set (306/83 mean orientation calculated as the great circle normal to highest concentration of fracture poles), which are typically through-going and greater than 5 m in length. The northwest set parallels the fracture set related to the Ottawa-Bonnechere graben, interpreted to have developed during normal faulting [*Kay*, 1942]. The second fracture set is steep northeast striking (039/79 mean orientation) and is typically through-going or abutting and less than 5 m in length. The northeast set parallels the metamorphic foliation that dips moderately to steeply and strikes north-northeast across the watershed (Figure 3.5B). The foliation is defined by well developed schistose and gneissic fabric in metamorphic rocks and poorly to moderately developed in plutonic rocks. The least statistically prominent fracture set in outcrop is a shallowly dipping fracture set that is interpreted as sheeting fractures, common in crystalline terrains [*Sukhija, et al.*, 2006; *Novakowski, et al.*, 2007a]. At the Christie Lake outcrop, the only significant fracture set observed is the steep to vertical northwest set (Figure 3.2B).

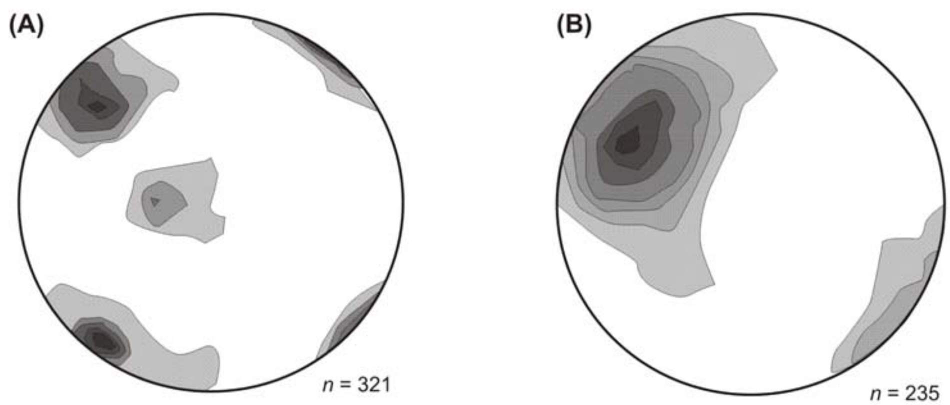

Figure 3.5 Lower hemisphere equal area stereonets of the poles to (A) fracture and (B) metamorphic foliation measurements from the Tay River watershed. Plotted with 2σ.

3.4.3 Hydrogeological characterization

Subsurface observations from TW14, at the center of the Christie Lake lineament, indicate the presence of both hydraulically significant and insignificant fractures. Qualitative down hole camera observations show pervasive highly angular brecciation and white vein in-filling (Figure 3.6), which is consistent with previous geological mapping suggesting this lineament is a fault [*Wilson*, 1961]. Brecciation and vein-filling are not in any consistent orientation. Chip samples tested with dilute hydrochloric acid indicate that the both carbonate and non-carbonate veins are present. Down hole camera observations also reveal the presence of discrete shallow fractures accentuated by spalling during drilling. The transmissivity distribution indicates discrete hydraulically significant zones are embedded in generally low permeability rock (Figure 3.6). The low permeability zones indicate that the pervasive brecciation is not consistently transmissive. Instead, the hydraulically significant zones correlate with the spalled discrete, shallowly dipping fractures (Figure 3.6). Therefore, the hydraulically significant zones in this well are assumed to be due to shallowly dipping fracture features, possibly sheeting fractures. The hydraulic conductivity of the shallowly dipping fracture zones are 10^{-3} m/s to 10^{-5} m/s. The effective single fracture aperture of these fractured zones is 270-540 μm. The lowest hydraulic conductivity intervals (10^{-7} m/s to $2x10^{-8}$ m/s) are interpreted as the matrix transmissivity, which includes the pervasive infilled veins. Although the matrix may contain numerous small fractures, the extremely limited permeability of these contributes little to the flow system in the fracture network.

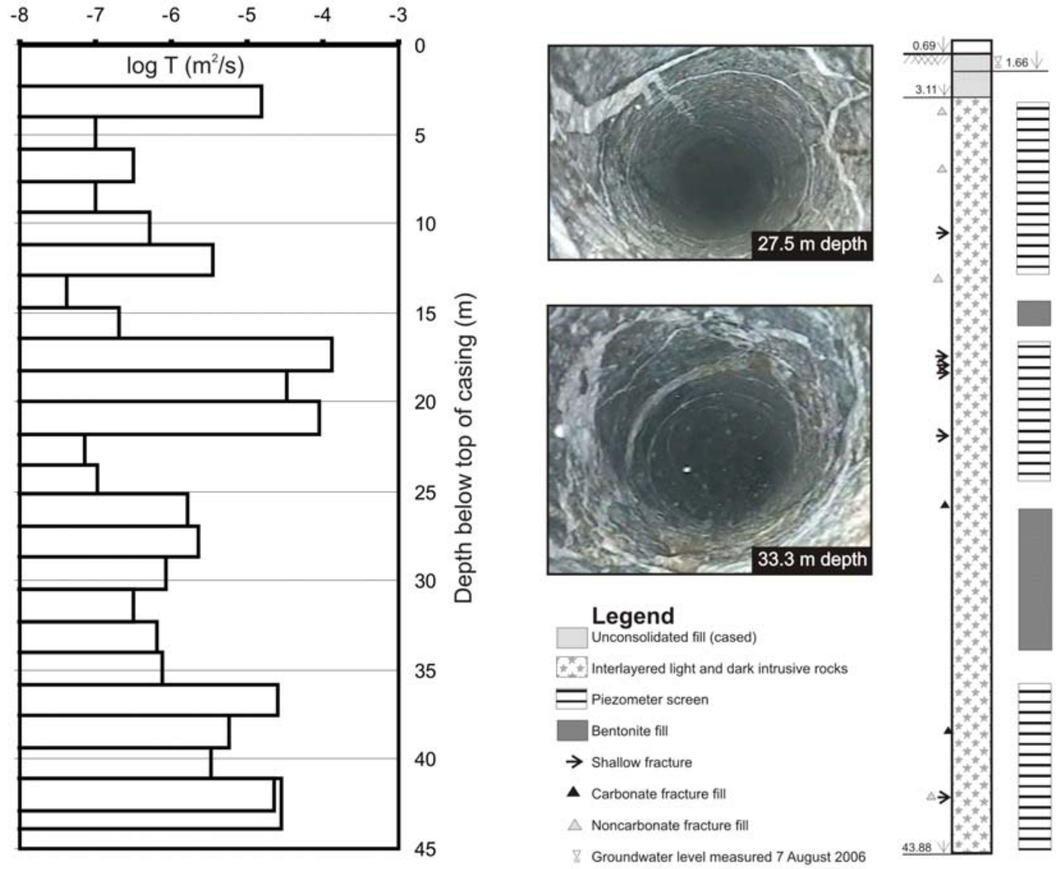

Figure 3.6 Subsurface data from TW14 borehole drilled in the Christie Lake lineament. Images from down hole camera (borehole diameter is 0.152 m) reveal brecciation and fracture infilling. The presence of carbonate and non-carbonate veins (from chip samples) and horizontal and vertical fractures (from down hole video logging) is noted. Hydraulic testing of 1.77 m test sections is analyzed using the *Horslev* [1951] method. High transmissivity zones correlate with horizontal fractures observed during video logging. The well was completed with three discrete piezometers (TW14S, TW14M, TW14D) in fractured, transmissive zones.

Since TW14 is located in a topographic depression with nearby surface water features at higher elevations, an upward vertical gradient in the well is expected. However, hydraulic head measurements recorded in the piezometers (TW14S, TW14M, and TW14D) indicate that there is effectively no vertical gradient (< 0.001) in the well (Figure 3.7). The lack of vertical gradient is not due to a short circuit in the well annulus because the well completions were tested and shown to be independent. Water levels in the Lower wetland trend with hydraulic head measurements in the shallow and deep piezometers albeit slightly dampened by the larger storage capacity of the Lower wetland. This indicates that the swamp and all levels of the well are connected by steeply dipping bedrock fractures. The lack of vertical gradient and correlation in water levels between the Lower wetland and piezometers indicates that the subsurface system is connected to the Lower wetland but not connected to the Upper wetland. The hydraulic testing and water levels also indicate the presence of both shallowly and steeply dipping fractures in the vicinity of TW14. Hydraulic testing results indicate that the shallow fractures are hydraulically significant but this does not imply a hydraulic significance for the steeply dipping fractures. The hydraulic significance of steeply-dipping fractures is explored in the numerical modeling, described below.

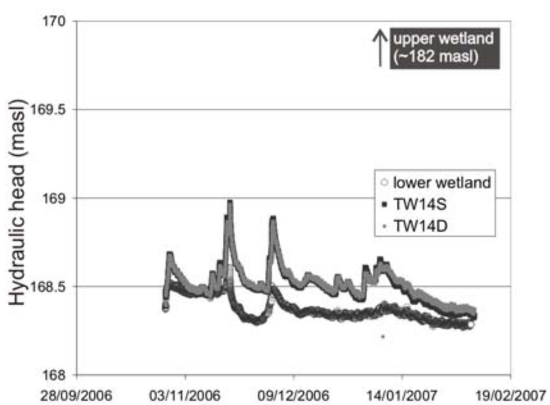

Figure 3.7 Hydraulic head data from TW14 and the adjacent Lower wetland that suggest that surface water and groundwater are connected at the Christie Lake lineament.

The ten boreholes hand-augured in the Lower wetland in a transect perpendicular to the Christie Lake lineament reveal mainly coarse grained clastics and organics with localized fine grained material. Each hole was drilled until refusal which was typically 0.5-2 m depth below ground. The 1.66 m depth of unconsolidated material drilled at TW14 suggests the depth of refusal is near or at the bedrock interface. The coarse grained clastics consisted of sand and gravel intermixed with modern organic material, consistent with watershed-scale descriptions of modern littoral unconsolidated material [*Kettles*, 1992]. A 10 cm thick layer of clay was found in one borehole but has an extent of less than 1 m^2. The predominance of coarse grained material indicates that there is no extensive low hydraulic conductivity soil limiting infiltration at the Christie Lake lineament.

3.4.4 Numerical simulations of surface water-groundwater interactions

The model domain is conceptualized in Figure 3.8A with topography based on a WAAS-corrected GPS topographic survey of the Christie Lake lineament and subsurface data derived from TW14 hydraulic testing, down hole camera observations and head measurements. The topographic gradient is also consistent with other lineaments in the study area (Figure 3.5A). The high topographic gradient and the lack of upward vertical gradient in TW14, suggest that subsurface connectivity is low between the surface water features. Hydraulic testing data and head data, as well as the fracture sets in the adjacent TG06-07 scanline, indicate the presence of discrete steep and shallow fractures. Unconsolidated material was not considered in the model because the hand-augured boreholes suggest it does not limit infiltration.

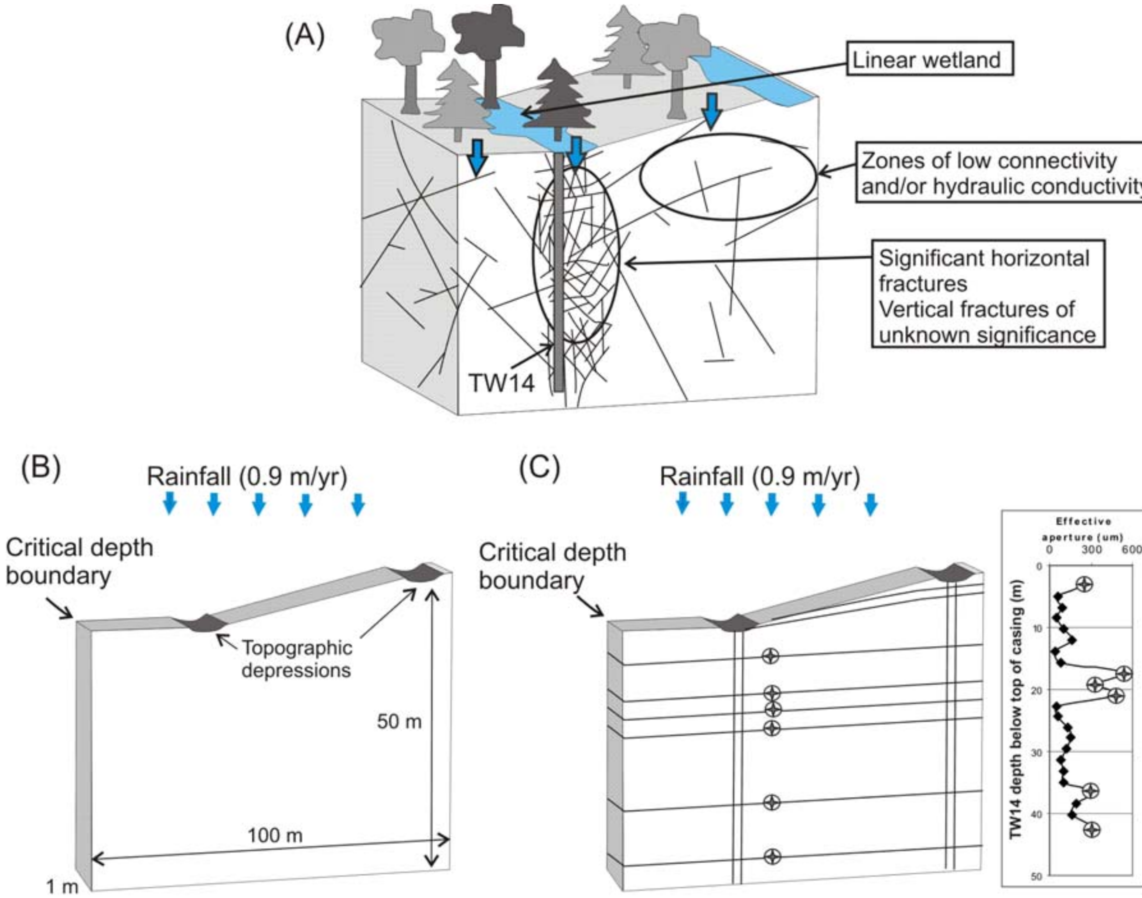

Figure 3.8 Lineament cross-sectional domain from conceptual model (A) to numerical implementation using an equivalent porous media approach (B) and a discrete fracture network approach (C). Topographic depressions are 2 m deep. The horizontal aperture distribution in the discrete fracture model are derived directly from hydraulic testing of TW14, as described in the text.

Although the hydrogeological characterization of the Christie Lake site clearly indicates the presence of discrete fractures, a preliminary cross-sectional domain was simulated using a porous media approach to constrain the bulk hydraulic conductivity of the system (Figure 3.8B). The total transmissivity of TW14 was used as a starting point and hydraulic conductivity varied, using depth of water in the Upper wetland as the fitting parameter. The depth of the water in the Upper wetland is very sensitive to bulk hydraulic conductivity (Figure 3.9A). A range of hydraulic conductivities of less than a half order of magnitude ($1.5x10^{-7}$ to $8x10^{-8}$ m/s) differentiates dry and overflowing conditions in the Upper wetland. The hydraulic conductivities that maintain water in the Upper wetland are consistent with measurements interpreted to be the unfractured rock matrix (10^{-7} m/s to $2x10^{-8}$m/s), suggesting the area between the two wetlands is largely unfractured. The depth of water in the Upper wetland was reproducible to 0.1 m indicating that the domain is numerically stable and that the depth of water is a useful fitting parameter. The depth of water in the Upper wetland was insensitive to evapotranspiration (Figure 3.9A).

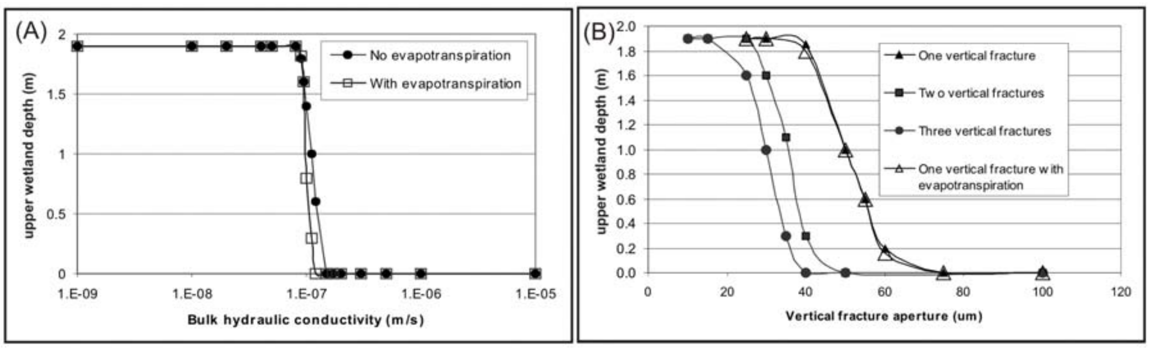

Figure 3.9 Numerical model results for lineament cross-sectional domain. Depth of water in the Upper wetland with varying bulk hydraulic conductivity using an equivalent porous media approach (A) and vertical fracture aperture using a discrete fracture network approach (B). A very limited range of hydraulic conductivities or fracture apertures maintain the depth of water in the Upper wetland without overflowing it, suggesting that subsurface permeability controls the distribution of perennial surface water features. The similarity of results incorporating evapotranspiration indicates that evapotranspiration is not an important control on the depth of water in surface water bodies.

Subsurface conceptualization and implementation of the discrete fracture network domain was based on hydraulic testing data from TW14 and fracture patterns from TG06-7 (Figure 3.2A). An orthogonal fracture network was implemented because vertical and shallowly dipping fractures are observed. Matrix hydraulic conductivity was assigned as the lowest value from hydraulic testing ($2x10^{-8}$ m/s), which is consistent with equivalent porous media model results. Horizontal fracture aperture was assigned directly from hydraulic testing data by calculating a single fracture effective aperture for each interval (Figure 3.8C). The aperture calculation assumes a single fracture is responsible for the measured transmissivity (Figure 3.6) of each test interval [*Novakowski, et al.*, 2007a]. Down hole camera data indicates that this was a reasonable assumption because singular fractures can be related to the transmissive zones identified by hydraulic testing. Vertical fractures were assigned to the subsurface below the wetland areas to explore the role of vertical fracture aperture in maintaining a perennial wetland complex with high intervening gradients. The number of vertical fractures underlying each wetland was also varied because the number of vertical fractures is unknown. The depth of the water in the Upper wetland is also very sensitive to vertical fracture aperture, with an aperture range of 20 μm differentiating dry and overflowing conditions (Figure 3.9B). The maximum vertical fracture aperture that can sustain water in the upper swamp is 60 μm, which is a hydraulically insignificant fracture aperture. Similar to the porous media approach, the depth of water in the Upper wetland during discrete fracture network modeling is reproducible and insensitive to evapotranspiration (Figure 3.9B). The results from the porous media and discrete fracture network both indicate that low hydraulic conductivity and/or low connectivity are necessary to maintain nearby surface water bodies with a high intervening gradient.

3.5 Discussion

Figure 3.10 summarizes previous and refined conceptual models for the relationship between lineaments and groundwater flow. In general, lineaments are considered surface expressions of fracture zones, faults or other subsurface discontinuities [*O'Leary, et al.*, 1976; *Wise, et al.*, 1985; *Singhal and Gupta*, 1999]. Recent studies have been based on the *a priori* assumption that lineaments are recharge zones with high groundwater potential, which implies high permeability [Fig. 10A; *Krishnamurthy, et al.*, 2000; *Sener, et al.*, 2005; *Shaban, et al.*, 2006]. I propose that lineaments in this study area, and possibly other geological settings, are surface expressions of structural features with diminished permeability due to structural and/or fluid flow processes (Figure 3.10B).

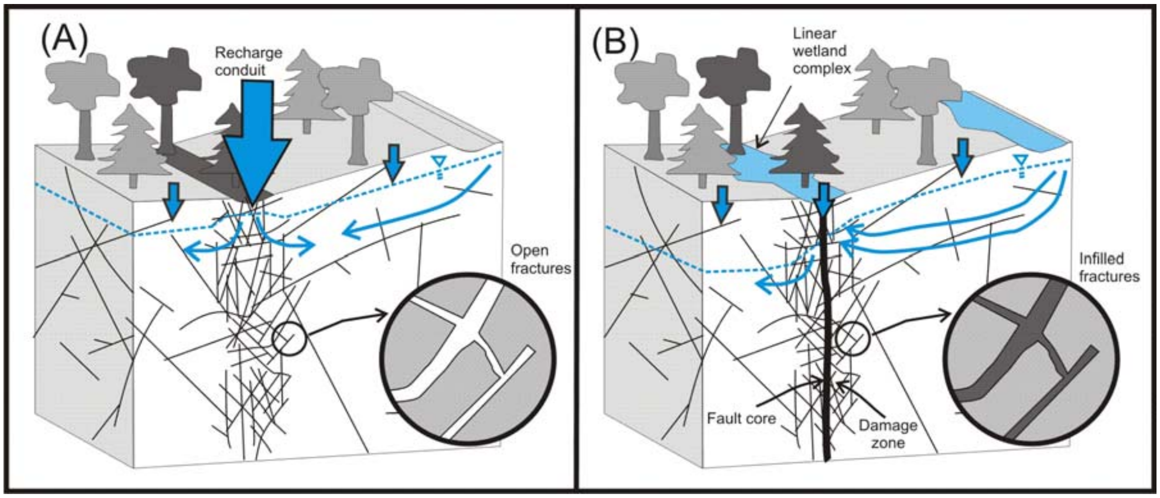

Figure 3.10 An idealized cross-sectional domain of showing (A) previous and (B) new conceptual models of the relationship between lineaments and groundwater. The surface expression of the lineament is a topographic depression and a tonal difference, highlighted here by the dark trees. Below the surface, lineaments are generally considered to zones of intense fractures and joints. Approximate flow lines are shown but true flow paths would depend on the connectivity and aperture distribution of the fracture network. Recent recharge studies have assumed lineaments have a higher groundwater potential due to the intense fracturing. Contrary to previous studies, lineaments in this chapter are surface water features with low permeability and/or connectivity due to structural and/or fluid flow processes.

A myriad of structural and tectonic processes have been proposed for the origin of lineaments [*Wise, et al.*, 1985]. The different structural processes can be categorized simplistically into those with displacement (faults) and those without displacement. Defining a kinematic and dynamic structural model for the development of lineaments in this study area is impossible due to the poor exposure of lineaments. Instead, fracture patterns and geologic data are compiled to define possible structural styles of lineaments. The coincidence of fracture orientations and lineament orientations both at a watershed scale and at the Christie Lake study area suggests lineaments are structurally controlled (Figures 3.2, 3.3 & 3.5). The predominant lineament set trends northeast with a linear direction mean orientation of 042^{o} (Landsat) or 033^{o} (DEM). The northeast trending lineament set parallels the steep northeast striking fracture set (Figure 3.5A) and the regional structural grain defined in outcrop by schistose and gneissic foliation (Figure 3.5B). The northeast trending fracture and lineament set is not consistent with any recognized regional brittle fault structures. The major northeast striking structures are ductile shear zones [*Easton*, 1992; *Davidson and Ketchum*, 1993]. The northeastern lineaments are likely a result of minimal displacement in zones of joints developed parallel to the well developed metamorphic grain [*Andjelkovic and Cruden*, 1998]. An alternative explanation is that the northeast trending lineament set may be due to glacial landforms since the southwest-northeast is the direction of glacial advance and retreat [*Kettles*, 1992]. However, the northeastern lineaments are not likely of glacial origin because the discontinuous till veneer rarely masks the structure of the underlying bedrock [*Kettles*, 1992].

The secondary northwest trending lineament set with a linear directional mean of 312^{o} is observed in the DEM data but not in Landsat imagery in this chapter or a previous study [*Andjelkovic and Cruden*, 1998]. The northwest trending lineament set parallels the vertical northwest striking fracture set (Figure 3.5A). The Christie Lake lineament is part of this lineament set, and is interpreted as a fault based on the subsurface brecciation (Figure 3.6), the linear topographic break (Figure 3.2), and the mapped unit truncation to the northwest [*Wilson*, 1961]. Permeability reduction at the Christie Lake lineament is discussed below. The north-facing topographic break, the northwest lineament trend and vertical northwest striking fracture set suggest that the faulted Christie Lake lineament is part of the Ottawa-Bonnechere graben system [*Kumarapeli*, 1978; *Rimando and Benn*, 2005]. Northwest trending lineaments in eastern Ontario, which decrease in frequency away from the center of the graben, have been previously interpreted as part of the Ottawa-Bonnechere graben [*Spitzer*, 1981]. The interpretation of the Christie Lake lineament as a fault associated with the Ottawa-Bonnechere graben suggests that other northwest trending lineaments may also be associated with faults. Northwest trending lineaments were not observed in Landsat imagery suggesting that digital elevation models (or other topographic remote imagery) may be more useful for identifying faults at a watershed scale than tonal remote imagery, especially in topographically subdued terrain [*Nyborg, et al.*, 2007].

Previous studies document limited or inconsistent correlation between well yields and lineaments, suggesting the permeability underlying lineaments is variable [*Waters, et al.*, 1990; *Gustafsson*, 1994; *Mabee, et al.*, 1994; *Sander, et al.*, 1997; *Edet, et al.*, 1998; *Mabee*, 1999; *Magowe and Carr*, 1999; *Moore, et al.*, 2002]. Similarly, permeable zones with high inflow in bedrock tunnels do not correlate consistently with the location of lineaments [*Banks, et al.*, 1992; *Mabee, et al.*, 2002]. The lack of correlation can be attributed to the presence of shallow dipping sheeting fractures that are not detected during lineament analysis [*Mabee, et al.*, 2002] or the presence of fault cores [*Banks, et al.*, 1992]. Well yields in this study area are actually lower in areas near lineaments (Table 3.2). Lower well yields in conjunction with high surface water gradient (Figure 3.4B) suggest lineaments in this study are potential hydraulic barriers with low to moderate permeability and connectivity. The similarity in orientation, length, topography (Figure 3.3B), surface water gradient (Figure 3.4B) and specific capacity (Figure 3.4A) of the Christie Lake site to other areas in this study suggest that the Christie Lake lineament is a representative lineament. Therefore the conclusions based on the hydrogeological characterization and numerical experiments have implications for other lineaments. Subsurface permeability of the Christie Lake lineament is controlled by discrete shallow and steep fractures. Numerical modeling indicates that the steep fractures must have small apertures to maintain adjacent surface water features with high intervening gradients. Therefore, lineaments in this study area are likely zones where limited or diminished fracture aperture, density or connectivity results in low permeability barriers to flow.

The reduction of permeability is likely the result of fault core development and/or mineral deposition during or after faulting. Permeability is reduced in fault cores due to brecciation, cataclasis, the development of clay-rich gouge zones, and other processes reviewed by *Caine et al.* [1996]. Low permeability, clay rich fault features have been observed directly below lineaments in a bedrock tunnel through Precambrian granite [*Banks, et al.*, 1992]. Numerous drilling records near lineaments in the study area record ‘granite’ overlying ‘clay’ which is consistent with the fault core development in a crystalline setting. The reduced permeability of the Christie Lake lineament, which is interpreted as a fault, may be due to fault core development, even though fault core was not observed in TW14. TW14 is interpreted to have drilled through the damage zone of the Christie Lake lineament-fault based on the pervasive brecciation and vein-infilling. The location of the potential fault core, the size of the damage zone and other fault architecture characteristics [*Caine, et al.*, 1996] cannot be quantified due the lack of exposed lineament outcrop. Permeability can also be reduced by syn- or post-deformation fluids infilling fractures by depositing dissolved constituents [*Evans and Chester*, 1995; *Goddard and Evans*, 1995]. Pervasive fracture infilling is evidenced in down hole video camera data from TW14. Chips samples recovered during drilling suggest that that both carbonate and non-carbonate minerals are infilling fractures. The infilled brecciation suggests that the examined area of the Christie Lake lineament-fault was previously a fluid conduit but that fault and fluid flow process together led to permeability reduction. Therefore, the reduction of permeability associated with lineaments in the study area is probably a result of fault characteristics common in crystalline settings: clay-rich fault cores and damage zones that are heavily fractured and vein-infilled.

Reduced fault zone permeability can compartmentalize regional groundwater flow [*Ferrill, et al.*, 2004]. High surface water gradients (Figure 3.4A), hung wetland complexes upgradient of the Christie Lake lineament and other lineaments, numerical modeling results (Figure 3.9) and the subsurface conceptual model (Figure 3.10B) suggest lineaments in this study area are barriers that are compartmentalizing flow. Detailed fault studies in other regions suggest that fault architecture is extremely complex and heterogeneous [*Evans and Chester*, 1995; *Caine and Forster*, 1999; *Fairley and Hinds*, 2004; *Minor and Hudson*, 2006] so the permeability reduction may or may not be persistent along strike over kilometers. Numerical modeling and field examples discussed by *Bense and Person* [2006] indicate that faults with large hydraulic head discontinuities can be conduit-barrier systems with significant preferential flow parallel to the fault, rather than pure hydraulic barriers. However, the pervasive fracture infilling observed in TW14, measured low hydraulic conductivity in the damage zone, and ubiquitous surface water bodies along lineaments suggest significant preferential flow and recharge along the Christie Lake lineament and other lineaments is not likely.

3.6 Conclusions and implications

Lineaments as geological structures that could impact regional flow systems in a low gradient crystalline bedrock aquifer in the Canadian Shield were investigated. I identified and characterized watershed-scale low permeability zones by integrating diverse geomatic, geological and hydrogeological data sets and numerical simulations. Salient conclusions for lineaments in this study area include:

(1) Lineaments are structural features, either fault zones or fracture zones with limited displacement.

(2) The fractured bedrock underlying lineaments are generally poorly connected, low permeability zones due to fault zone and/or fluid flow processes.

(3) Permeability reduction results in lineament areas being recharge and flow barriers that compartmentalize lateral flow systems.

(4) Faulted lineaments can be more effectively identified by topographic data (*e.g.* DEM) than by tonal imagery (*e.g.* Landsat).

Although lineaments have been controversial in the geological and hydrogeological literature, this chapter shows that lineaments are important and useful if identified with a defensible method and analyzed with supplementary geomatic, geologic and hydrogeological data within a well-documented structural geology framework. Interpreting lineaments as watershed-scale low permeability zones in this study area may affect recharge estimates and contaminant disposal practices in crystalline settings. Recharge estimates are critical for determining groundwater sustainability in water resource management. Recharge in crystalline bedrock aquifers is considered very limited [*Rodhe and Bockgard*, 2006; *Milloy*, 2007]. Recent studies applying remote sensing and geospatial analysis have been based on the *a priori* assumption that lineaments are recharge zones [*Krishnamurthy, et al.*, 2000; *Sener, et al.*, 2005; *Shaban, et al.*, 2006]. However, if lineaments are low permeability structures, the recharge potential of lineaments may be quite limited, and thus assuming lineaments are recharge zones would be misleading in this study area. Various northern countries plan to dispose nuclear waste in saturated crystalline repositories. Quantifying the permeability of lineaments and other geological structures is a significant concern when modeling the time of travel for nuclide transport to the biosphere.

This chapter shows that diverse datasets and geologically realistic models of lineament permeability are necessary to unravel patterns of fluid flow in the brittle uppermost crust (<100 m depth). The relationship between permeability and fault architecture was originally documented at the local scale [*Evans and Chester*, 1995; *Caine, et al.*, 1996; *Evans, et al.*, 1997; *Schulz and Evans*, 2000; *Rawling, et al.*, 2001]. Results from this chapter support other recent studies suggesting that brittle structures control regional groundwater flow in bedrock aquifers and that fault architecture models are a useful framework for examining the permeability of regional structures [*Ferrill, et al.*, 2004; *Seaton and*

Burbey, 2005; *Bense and Person*, 2006; *Denny, et al.*, 2007]. Although the study area is located in a Precambrian shield where deformation is ancient and polyphased, fault architecture and permeability studies suggest these results may be applicable to other areas with different protoliths or where deformation is more recent and less complex [*Evans*, 1988; *Caine, et al.*, 1996; *Caine and Forster*, 1999; *Rawling, et al.*, 2001].

Chapter 4
Groundwater discharge: diffuse and limited

4.1 Introduction

Quantifying the rate and pattern of groundwater discharge to surface water bodies is vital for developing watershed budgets, constraining recharge rates, and protecting the ecological integrity of lake and river ecosystems [*Hayashi and Rosenberry*, 2002; *Sophocleous*, 2002]. In watersheds underlain by porous media aquifers, groundwater and surface water are understood as intricately coupled systems with complex local-scale hyporheic exchange patterns and larger-scale gaining or losing stream sections [*Winter*, 1999; *Alley, et al.*, 2002; *Sophocleous*, 2002]. Discharge in fractured rock watersheds has been examined previously [*Stephenson, et al.*, 1992; *Rosenberry and Winter*, 1993; *Thorne and Gascoyne*, 1993; *Oxtobee and Novakowski*, 2002; *Cook, et al.*, 2006; *Fan, et al.*, 2007; *Praamsma, et al.*, 2009b] but significant questions remain about the rate, localization and conceptualization of discharge at a watershed-scale. Additionally, groundwater and surface water may not be as intricately coupled due to the low permeability of fractured rock. Discharge and baseflow have been examined in fractured rock watersheds using methods developed in porous-media settings [*Mau and Winter*, 1997; *Risser, et al.*, 2005; *Risser, et al.*, 2009]. Other studies examine and conceptualize discharge at discrete features such as faults, fracture zones, bedding planes or lineaments [*Stephenson, et al.*, 1992; *Oxtobee and Novakowski*, 2002; *Fan, et al.*, 2007; *Praamsma, et al.*, 2009b].

Groundwater recharge, baseflow and other important watershed characteristics are often estimated from hydrograph separation [*Rorabaugh*, 1964; *Moore*, 1992; *Rutledge and Daniel*, 1994; *Mau and Winter*, 1997; *Neff, et al.*, 2005; *Risser, et al.*, 2005; *Risser, et al.*, 2009].

Hydrograph or baseflow methods are only applicable to gauged and unregulated watersheds with substantial groundwater discharge [*Fetter*, 2001]. Many medium to large rivers are, however, regulated by dams or other control structures [*Nilsson, et al.*, 2005] and groundwater discharge in some rivers may be insignificant compared to streamflow. New methods for evaluating groundwater discharge in watersheds affected by dams or where groundwater discharge is minimal are essential. New and refined methods could lead to better prediction of low flow conditions in gauged and ungauged watersheds and better characterization of groundwater-surface water interactions [*Kalbus, et al.*, 2006; *Soulsby and Tetzlaff*, 2008; *Tetzlaff and Soulsby*, 2008].

Natural tracers can provide important constraints on groundwater discharge rates and patterns. Radon (^{222}Rn) is a radioactive gas that is an excellent tracer of groundwater discharging to surface water bodies [*Rogers*, 1958; *Ellins, et al.*, 1990; *Genereux, et al.*, 1993; *Cook, et al.*, 2006; *Charette, et al.*, 2008; *Cook, et al.*, 2008; *Stellato, et al.*, 2008]. Radon accumulates in groundwater due to the radioactive decay of uranium and radium in aquifer materials and activities in groundwater are typically 1-2 orders of magnitude larger than surface water bodies, where radon is lost due to air-water exchange and radioactive decay. Temperature, specific conductance, major ions (*e.g.* chloride) and stable isotopes (δ^2H, δ^{18}O) can also be useful indicators of groundwater discharge to surface water bodies [*Lee*, 1985; *Harvey, et al.*, 1997; *Constantz*, 1998; *Becker, et al.*, 2004; *Conant*, 2004; *Cox, et al.*, 2007; *Lowry, et al.*, 2007]. Natural tracers have been previously used to estimate discharge rates and patterns but generally studies examine a single water body type (lake or river).

The objective of this chapter is to evaluate the patterns and rates of groundwater discharge in a large, regulated fractured rock watershed using novel and standard methods that are independent of baseflow recession. Natural conservative (δ^2H, $\delta^{18}O$, Cl, and specific conductance), radioactive (^{222}Rn), and thermal tracers are integrated with streamflow measurements and a steady-state advective model to delimit the discharge locations and quantify the discharge fluxes. Low gradient watersheds in crystalline fractured rock settings, such as the Canadian Shield, are often dominated by lakes and wetlands [*Farvolden, et al.*, 1988; *Burn, et al.*, 2008]. I examine multiple types of water bodies (lake, wetland, river and creek) using multiple methods for each water body type. This chapter focuses on a large watershed underlain by fractured bedrock although the methodology developed is transferable to any large watershed. Since the baseflow rate in this watershed is uncertain I use the term 'low flow' rather than 'baseflow' [*Smakhtin*, 2001; *Burn, et al.*, 2008]. Also for clarity 'discharge' refers to groundwater discharge whereas 'streamflow' refers to the rate of water flow in a creek or river.

4.2 Regional hydrology

The study area is located in rural eastern Ontario, Canada in the ~900 km^2 Tay River watershed (Figure 4.1A) which is much larger than most previous hydrologic studies in the Canadian Shield [*Peters, et al.*, 1995; *Devito, et al.*, 1996; *Branfireun and Roulet*, 1998; *Buttle, et al.*, 2001; *Spence and Woo*, 2003; *Buttle, et al.*, 2004]. Previous studies in small watersheds focused on runoff and streamflow generation, surface water storage and surface-subsurface connectivity and emphasize the importance of the distribution of soil thickness. Groundwater discharge is limited where soil is minimal and perennial streams only develop in drainage areas >0.25-0.5 km^2 [*Buttle, et al.*, 2004; *Steedman, et al.*, 2004]. Previous research in a 2 km section of the Tay River (around SW1 and SW2 on Figure 4.1B) indicated that discharge to this section of the river was limited and standard isotope storm hydrograph methods are not appropriate because the Tay River is dominated by surface water flow [*Praamsma, et al.*, 2009b].

The topography throughout the watershed is undulating with over 3000 mapped permanent surface water features. Three cold-bottomed lakes support trout populations and other lakes support warm water fish species. Four wetlands in the study area contain biodiversity that is designated provincially significant (Rideau Valley Conservation Authority, unpublished data). The humid climate is characterized by an average annual precipitation of 0.95 m (30 years of data from Environment Canada Station 6104027 in Kemptville, ON augmented with 3 years of onsite data). Precipitation is distributed relatively uniformly through out the year with typical summer precipitation of 0.08 to 0.1 m per month.

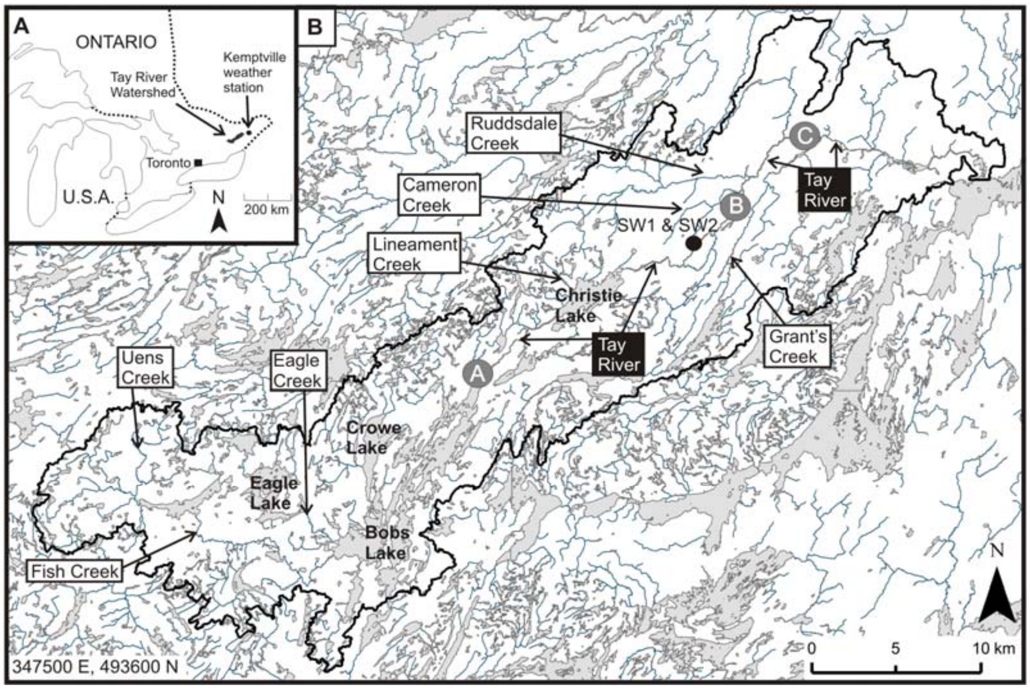

Figure 4.1 (A) Tay River watershed study area in Ontario. (B) The complex network of surface water features in the Tay River watershed. The watershed boundary is the black line. The creeks and large lakes as well as the surface water sampling locations (SW1 and SW2) from *Praamsma et al.* [2009] are shown for reference. The streamflow of the Tay River is measured at (A) the Bolingbroke Dam, (B) Bowes Road, and (C) the town of Perth. See Chapter 3 for the location of lineaments identified in Landsat and digital elevation model imagery.

Much of the watershed has minimal soil over Precambrian crystalline or flat-lying Paleozoic sedimentary units. The headwaters and upper Tay River watershed are underlain by crystalline rocks and have large lake and wetland areas with small interconnecting creeks such as Uens and Eagle Creek. The water bodies of the upper watershed all flow into Bobs Lake which is regulated by the Bolingbroke dam. The Tay River begins below the Bolingbroke dam and is divided herein into the upper and lower Tay River by Christie Lake. The lower Tay flows over exposed crystalline bedrock and sedimentary units. Other tributary creeks such as Grants and Ruddsdale flow over sedimentary units and flow into the lower Tay River. Two small, unnamed creeks examined in detail in this chapter are herein called 'Lineament Creek' and 'Cameron Creek' because they cross the Christie Lake lineament (Chapter 3) and Cameron Side Road, respectively.

The Tay River is typically 5-10 m wide and less than 1 m deep and gauged at the Bolingbroke dam, Bowes Road and the town of Perth (Figure 4.1B). The only significant surface water abstraction from the Tay River is by an industrial plant near Bowes Road that removes <0.5% of the streamflow. Elsewhere the sparse rural population predominantly uses groundwater supply. Examining the impact of water abstractions is outside of the scope of this research. Low-flow conditions for the Tay River typically occur in late July to early September [unpublished data from the Rideau Valley Conservation Authority] due to increased evapotranspiration. The surface water bodies typically have lower specific conductance (50-700 μs/cm) and warmer temperatures (15-25^{o}C) in the summer, relative to groundwater in the fractured bedrock aquifers that typically have a specific conductance and temperature of 500-1500 μs/cm and 8-12^{o}C, respectively.

4.3 Theory and methodology

4.3.1 Approach

Streamflow measurements are the most direct method for determining if rivers are gaining or losing along a reach but they are not as useful for constraining groundwater discharge to lakes and wetlands, due to larger uncertainties in other water budget terms such as evapotranspiration [*Winter*, 1981]. Therefore, streamflow measurements are integrated with chemical, isotopic and thermal tracers to delimit the groundwater discharge locations and quantify the groundwater discharge fluxes in lakes, wetlands, creeks and at various locations along the Tay River. Discharge is identified by exploiting the chemical, isotopic and thermal differences between groundwater and surface waters, which are accentuated in the low-flow summer months due to warmer temperatures and evaporation in the surface water bodies. Chloride, radon and streamflow data are used to quantify discharge rates. Stable isotope, specific conductance and thermal data are used to qualitatively evaluate discharge patterns due to uncertainty in fractionation factors and limited observation of specific conductivity and temperature anomalies.

Twenty-one representative lakes and wetlands were sampled for δ^2H, $\delta^{18}O$, Cl and specific conductance in May and August of 2006 and 2007 to evaluate the relative influence of evaporation and groundwater discharge. Groundwater plots close to the local meteoric water line [*Praamsma, et al.*, 2009b] whereas during the summer months open water bodies fractionate along a distinct isotopic trajectory with a slope of ~5 on the plot of δ^2H vs. $\delta^{18}O$ [*Gonfiantini*, 1986; *Clark and Fritz*, 1997]. Surface water features that are influenced by groundwater discharge would plot along a mixing line between evaporated rainfall and groundwater, although as the isotopic composition of groundwater would be expected to be similar to mean annual rainfall, this mixing line might be difficult to distinguish from the aforementioned evaporation line. Radon activities and chloride concentrations in groundwater are significantly greater than in surface water, and so elevated activities or concentrations of these tracers provide indications of groundwater discharge. Furthermore, because of the short half-life of radon and its propensity to be lost to the atmosphere, high activities of radon provide evidence of relatively recent groundwater discharge. In contrast, the residence time of chloride in lakes and wetlands can be much longer, and high chloride concentrations can also be due to evaporative enrichment. ^{222}Rn activities and Cl concentrations measured during one week in August 2008 are used to quantify groundwater discharge rates using a steady-state advective model described in Section 4.3.2.

Specific conductance, temperature and ^{222}Rn activities were continuously measured along a transect of the Tay River and Christie Lake. The Tay River was also sampled for δ^2H, δ^{18}O, Cl and specific conductance in May and August of 2006 and 2007 and this data is interpreted qualitatively. Additionally, streamflow rates for three gauging stations located on the Tay River are compared to determine if the Tay River is gaining with distance downstream. A number of creeks were sampled at multiple access points along their reach for δ^2H, δ^{18}O, Cl, specific conductance and ^{222}Rn to qualitatively identify groundwater discharge patterns. Streamflows were also manually measured at the multiple access points to determine if streamflow increases with distance downstream.

4.3.2 Steady-state advective model

A steady-state advective model is developed to estimate the rates of groundwater discharge and surface water inflow to lakes and wetlands in a large watershed (Figure 4.2). The steady-state model represents the flux of groundwater and surface water in the days before sampling due to the short half life of ^{222}Rn. Since the residence time of chloride is much greater than radon, the importance of the steady-state assumption for chloride is evaluated below in the uncertainty analysis. For steady-state conditions the water budget of a lake or wetland system can be expressed:

$$\frac{\partial V}{\partial t} = I_s + I_g + PA - EA - Q = 0 \qquad \textbf{Equation 1}$$

where V is the water volume (m^3), I_s is the surface water inflow rate (m^3/day), I_g is the groundwater discharge rate (m^3/day), Q is the combined surface water and groundwater outflow rate (m^3/day), P is the rate of direct precipitation to the water surface (m/day), E is the evaporation rate from the water surface (m/day), A is the surface water area (m^2) and t is time. Similarly, the conservative solute balance of a lake or wetland system can be expressed:

$$\frac{\partial cV}{\partial t} = I_s c_s + I_g c_g + PAc_p - kAc - Qc - \lambda Vc = 0 \qquad \textbf{Equation 2}$$

where k is the gas exchange velocity (m/day), λ is the radioactive decay constant (day^{-1}) and c, c_s, c_g and c_p are the solute concentration (mg/L) or activity (Bq/L) of the surface water, surface water inflow, groundwater discharge and precipitation, respectively. (1) and (2) can be combined and solved as:

$$c = \frac{I_s c_s + I_g c_g + PAc_p}{I_s + I_g - EA + PA + kA + \lambda V} \qquad \textbf{Equation 3}$$

Gas exchange and radioactive decay are negligible for a conservative ionic tracer, such as chloride. Therefore for chloride, (3) is simplified:

$$c_{Cl} = \frac{I_s c_{sCl} + I_g c_{gCl} + PAc_{pCl}}{I_s + I_g - EA + PA} \qquad \textbf{Equation 4}$$

Radon is an unreactive, radioactive gas with a negligible activity in the atmosphere and precipitation. The only source is radioactive decay of uranium and radium in aquifer materials and surface water inflow (c_s) if an upstream water body has significant radon activity. Therefore (3) can also be expressed as:

$$c_{Rn} = \frac{I_s c_{sRn} + I_g c_{gRn}}{I_s + I_g - EA + PA + kA + \lambda V} \qquad \textbf{Equation 5}$$

For this equation it is assumed that radium activities in the lake and the diffusive radon flux from the lake sediments are negligible, which will usually be the case. Using this assumption, a maximum groundwater discharge flux is calculated like other methods used in this chapter (see Section 5.1).

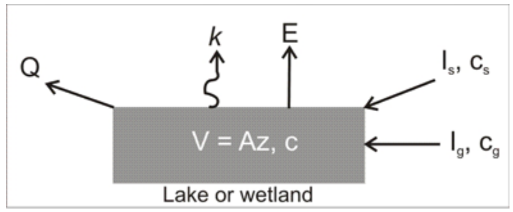

Figure 4.2 Steady-state advective model with the variables defined in the text.

Equations (4) and (5) can be simultaneously solved for I_g and I_s using measurements of c_{Cl}, c_{sCl}, c_{gCl}, c_{pCl}, c_{Rn}, c_{sRn}, c_{gRn}, A and V, estimates of P, E and k, and $\lambda = 0.18$ day^{-1}. Chloride concentrations in the surface water inflow (c_{sCl}) was assigned from measurements of the inflowing creek, the upstream lake if the inflowing creek was inaccessible or the concentration in precipitation ($c_{pCl} = 0.1$ mg/L) if as the lake or wetland does not have significant surface water inflow (*i.e.* headwater lake). Chloride precipitation values (c_{pCl}) are from a meteorological station 190 km north of the study area [*NATChem*, 2008]. For lakes and wetlands with radon activities below detection, the detection limit was used as the radon activity (c_{Rn}) for the steady-state advective model which provides a maximum rate of groundwater discharge (I_g). Groundwater radon activities (c_{gRn}) and chloride concentrations (c_{gCl}) were measured throughout the watershed but primarily near the hay field research site as discussed in Section 3.3. The surface area and volume of the lake or wetland is extracted from a provincial GIS database of surface water bodies or bathymetric surveys of the smaller water bodies and are considered <20% uncertain [*Winter*, 1981]. Monthly precipitation rate ($P = 0.002$ m/d) and lake evaporation rate ($E = 0.005$ m/d) was measured at a weather station ~50 km from the watershed (Figure 4.1A) are considered < 50% uncertain [*Winter*, 1981]. Lake evaporation is calculated using the observed daily values of pan evaporative water loss, the mean temperatures of the water in the pan and of the nearby air, and the total wind run over the pan. A gas exchange velocity of $k = 0.16$ m/d was calculated for a wetland in South Australia by *Cook et al.* [2008] using an injection of SF_6 tracers, and I have adopted this value for our model. This gas exchange velocity is also within the range of values derived for radon from other hydraulic settings [*Wanninkhof, et al.*, 1990; *Corbett, et al.*, 1997; *Kluge, et al.*, 2007] and is considered <20% uncertain . Using a similar model, *Cook et al.* [2008] showed that the solution for groundwater discharge (I_g) is much less sensitive to evaporation rate and gas exchange rate than to groundwater radon activity (c_{gRn}).

The steady-state model is considered a screening-level tool that is useful for analyzing synoptic chloride and radon data gathered from a large watershed. The model is appropriate for watershed-scale quantification of discharge (see Section 4.5.1) or constraining recharge patterns to focus detailed studies but would be inappropriate for analyzing data from a single water body [*Corbett, et al.*, 1997; *Kluge, et al.*, 2007; *Cook, et al.*, 2008] because of the inherent assumptions. The model accounts for differences in evaporation, gas exchange and radioactive decay in different surface water bodies using estimates of area and volume. Significant assumptions of the model are that 1) the chloride concentration and radon activity are at steady state in the surface water body; 2) the surface water body is well mixed (*i.e.* the collected surface water samples are representative) and 3) representative groundwater chloride concentrations and radon activities are available. The validity of the assumptions is discussed briefly here and evaluated more fully in a sensitivity analysis (Section 4.4.2) where each input parameter is varied over the expected range of potential uncertainty. Since radon has a very short half-life the primary concern with the steady-state assumption is chloride which has a longer residence time in lakes. Therefore, the appropriateness of the steady-state assumption is tested by examining the sensitivity of I_g to uncertainty in measured lake chloride concentrations.

Radon activities measured repeatedly in Christie Lake were consistent both spatially and temporally suggesting a representative activity was measured. But activities in other larger, deeper water bodies could be heterogeneous both vertically and horizontally due to thermal stratification and incomplete wind mixing, respectively [*Kluge, et al.*, 2007]. Radon activities in the lake documented by *Kluge et al.* [2007] were highest in the thermocline and lower in the epilimnion (due to gas exchange) and hypolimnion (due to limited groundwater water discharge at depth). In this chapter, the stratified lakes were sampled from the epilimnion where groundwater discharge is generally focused [*Winter*, 1978; *Kluge, et al.*, 2007]. In shallow wetlands mixing may also be limited [*Cook, et al.*, 2008]. Groundwater radon activities in crystalline aquifers are highly variable at the local scale [*Folger, et al.*, 1996; *Veeger and Ruderman*, 1998; *Wood, et al.*, 2004] suggesting it may be difficult to estimate activities in the vicinity of the water body. The sensitivity to the uncertainty of radon activities is evaluated in Section 4.4.2.

4.3.3 Field and laboratory methods

Field work was conducted with varying temporal resolution in the summers 2005, 2006, 2007 and 2008 during low flow conditions in late July – August. Sampling locations of the lakes, wetlands, creeks and along the Tay River are represented on Figure 4.3. One location at or near the outlet of each lake or wetland was sampled. The creeks and the Tay River were sampled near the middle way point of the reach. Multiple samples with depth or across the reach were not collected for the creeks or Tay River because they are generally very shallow (<0.5 m) and well mixed [*Praamsma, et al.*, 2009b].

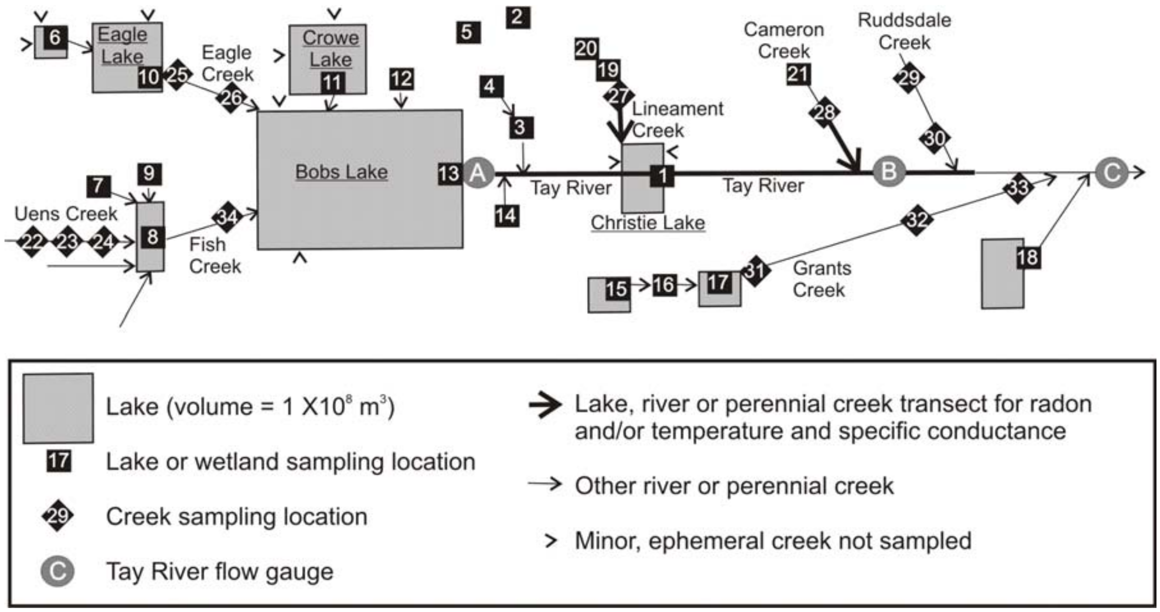

Figure 4.3 Schematic of surface water bodies sampled during the chapter. See Table 4.1 for the geographic name of each numbered sample location. The lakes and wetlands are scaled by volume. Water bodies that are smaller than the size of the label (~1x10^7 m^3) are only labeled. Both perennial and ephemeral creeks are shown. The Tay River is gauged at A) Bolingbroke dam, B) Bowes Road, and C) the town of Perth.

In terrestrial hydraulic systems, radon is typically discretely sampled and analyzed using liquid scintillation methods [*Rogers*, 1958; *Cook, et al.*, 2006; *Cook, et al.*, 2008]. Recently, continuous, real-time, *in situ* radon measurement developed by the oceanographic community [*Burnett, et al.*, 2001] have been used to measure radon activities in a lake [*Kluge, et al.*, 2007]. A commercial radon-in-air detector (RAD7) is outfitted with an air-water exchanger using the 'Rad-Aqua' methodology. Surface water is pumped continuously into the air-water exchanger and the activity of ^{222}Rn-in-air (which equilibrated with the surface water) is calculated by measurement of the α-emitting daughters ^{214}Po and ^{218}Po. Radon-in-water activities are calculated from radon-in-air activities using the temperature dependence of the air-water phase equilibrium of radon [*Burnett, et al.*, 2001]. Detection limits are the activities that can be counted with a precision of ±100% at the 95% confidence level [*EPA*, 2002]. Radon activities are measured over 10 minute intervals with a detection limit of 0.02 Bq/L. For the Tay River, the radon was measured continuously by canoeing slowly with the radon measuring apparatus. For individual lakes, wetlands and creeks three 10 minute intervals after the air and water equilibrated are integrated to lower detection limit to 0.01 Bq/L [*Kluge, et al.*, 2007]. Groundwater samples were collected from residential wells throughout the watershed and from 25 multi-level piezometers completed at 5-50 m below ground surface near SW1 and SW2 on Figure 4.1 [*Gleeson, et al.*, 2007; *Levison and Novakowski*, 2009; *Praamsma, et al.*, 2009b]. Groundwater samples were collected after purging for three well volumes and radon activity was analyzed using the Rad-H_20 methodology [*Kluge, et al.*, 2007] with a typical uncertainty of ±5%.

A temperature and specific conductance probe was manually dragged along the bottom of a 25 km long reach of the Tay River and four creeks [*Lee*, 1985; *Harvey, et al.*, 1997]. The probe is considered accurate to ±0.15^{o}C and ±1 μs/cm for temperature and specific conductance, respectively. The probe was directly inserted into open bedrock fractures or other potential discharge features in the middle of the reach as well as near the banks. During each transect temperature and specific conductance were logged at 1 second intervals for a total of more than 14500 individual temperature and specific conductance readings. Differential temperature and specific conductance values were calculated (daily mean minus individual value) and are reported below such that measurements from different days and locations are directly comparable. Potential groundwater discharge locations are identified by a brief negative temperature excursions and/or positive specific conductance excursions. During the transects the type of river bed (soil type or rock type) as well as the fracture density in the exposed bedrock river bottom was also mapped.

The streamflow of the Tay River was measured hourly and integrated into daily mean streamflow at the three gauging stations by the Rideau Valley Conservation Authority. Streamflow was also measured manually in monthly surveys and are considered accurate to ±5% for all levels of the rating curve by the National Water Research Institute of Canada. Streamflow measured at different locations along the Tay River are compared to determine if the Tay River is gaining or losing. Additionally, streamflow measurements using a pygmy Price AA flow meter in four creeks were made at multiple locations along their reach during low flow conditions following the *Hinton* [2005] method. Uncertainties accrue due to a number of factors including the number of verticals the cross-section is divided into, the length of measurement time and the flow velocity. Random and systematic uncertainties in the individual streamflow measurements were calculated to estimate potential error [*Hinton*, 2005].

The stable isotopic analyses were completed at the Queen's Facility for Isotope Research using Finnegan MAT 252 and ThermoFinnegan Delta Plus XP mass spectrometers for ^{2}H and ^{18}O, respectively. Isotope values are expressed in δ units (‰, parts per mil) relative to Vienna Standard Mean Ocean Water (VSMOW). Analytical error was approximately ±1‰ for ^{2}H and ±0.1‰ for ^{18}O. Surface waters were analyzed for major and minor elements using ion chromatography and inductively coupled plasma mass spectroscopy but only chloride concentrations are reported here.

4.4 Results

4.4.1 Stable isotopes and chloride

The lakes and wetlands of the Tay River watershed plot along a well-defined evaporative trajectory with an equation $\delta^2H = 4.7\delta^{18}O + 22.2x10^{-3}$ (Figure 4.4). The lakes and wetlands have a range of isotopic values (*i.e.* -4.2 to -9.5 ‰ $\delta^{18}O$ in August 2006) and a range of differences between spring and summer values of 0.3 to 2.4‰ $\delta^{18}O$. The differences between spring and summer isotopic values are a product of evaporative enrichment that increase isotopic values and/or groundwater discharge that causes a decrease in isotopic value as surface waters are mixed with isotopically depleted groundwater.

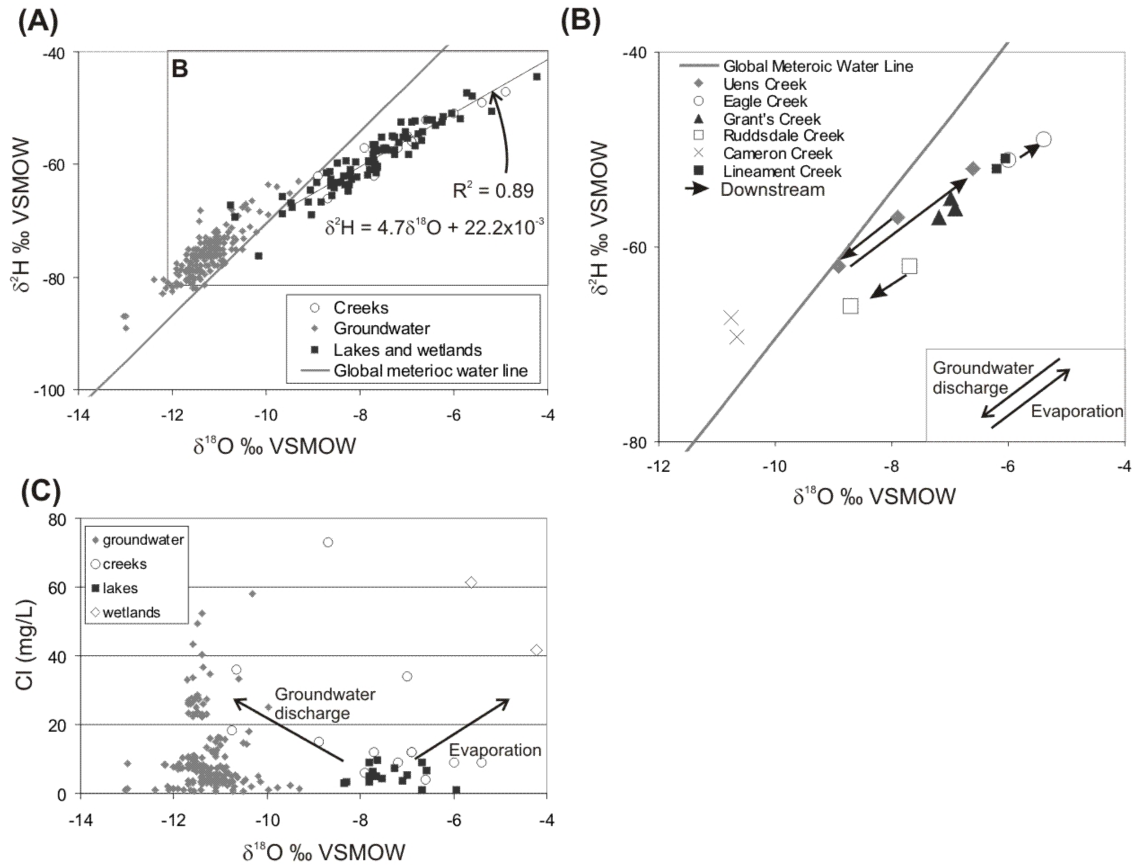

Figure 4.4 (A) Groundwater and surface water stable isotope data from the Tay River watershed. (B) low-flow stable isotope value along the different creeks, sampled on the same day. The laboratory uncertainty bars are equivalent to the size of the symbol. The arrows indicate sampling locations downstream from previous samples. Streams that are influenced by groundwater discharge or evaporation are differentiated by the direction of isotopic shift. (C) Chloride vs. δ^{18}O differentiates the influence of groundwater discharge or evaporation for lakes, wetlands and creeks. The trajectory of groundwater discharge and evaporation are approximate.

The creeks plot along an evaporative trend with a δ^2H/δ^{18}O slope of ~4.7 like the lakes and wetlands (Figure 4.4A). The relative influence of groundwater discharge versus evaporation can be directly evaluated using stable isotopes by sampling the creeks at multiple locations along their reach on the same day (Figure 4.4B). Cameron Creek plots directly in the groundwater field (Figure 4.4A, B) suggesting that the rate of groundwater discharge is high relative to the evaporation rate. The isotopic values of Ruddsdale Creek decrease with distance downstream, suggesting significant groundwater inflow within the sampled reach. Upper Uens Creek has a similar trend suggesting this headwater stream is groundwater dependent. However, lower Uens Creek and Eagle Creek have stagnant stretches and isotopic data suggests that evaporation is a more significant process in these systems (Figure 4.4B). Grants Creek and Lineament Creek do not show a significant downstream isotopic trend, suggesting that groundwater discharge and evaporative loss represent only a relatively small proportion of the streamflow on the sampled reach.

The influence of evaporation versus groundwater discharge for lakes and wetlands is also distinguishable when either stable isotope (δ^2H or $\delta^{18}O$) is plotted against chloride. Figure 4.4C illustrates $\delta^{18}O$ vs. chloride as an example. Chloride is a conservative ionic tracer that increases due to evaporation in surface waters or water-rock interactions in groundwater. A minority of shallow wetlands are significantly evaporated and a minority of creeks may be groundwater dependent (Figure 4.4C). However, most lakes and creeks are not significantly affected by either evaporation or groundwater discharge. Using stable isotopes in conjunction with chloride it is possible to qualitatively determine the relative influence of evaporation and groundwater discharge.

4.4.2 Radon and the steady-state advective model

The majority of the surface water bodies in the Tay River watershed have insignificant radon activities whereas groundwater activities are 2-3 orders of magnitude larger (Figure 4.5A). The median and upper quartile activities for lakes and wetlands are below detection at 0.01 Bq/L. Radon activities in Christie Lake were measured repeatedly over one week and in a transect across the lake (Figure 4.6). The activities varied within standard deviation both spatially and temporally suggesting the epilimnion of the lake is well mixed. For creeks the upper quartile is 0.05 Bq/L but the median is below detection like the lakes and wetlands. The largest value for the wetlands and creeks is the Cameron Creek headwater and reach, respectively (Figure 4.5A). Groundwater radon activities range from 9.8-112.1 Bq/L with a median value of 22.9 Bq/L.

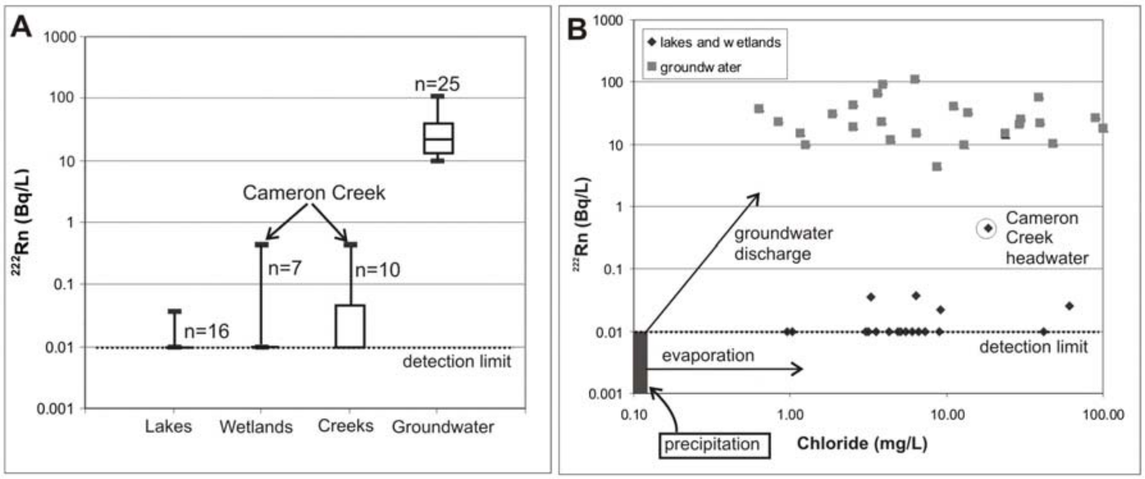

Figure 4.5 (A) Box-and-whisker plot of ^{222}Rn activities in lakes, wetlands, creeks and groundwater. The upper quartile of lakes and wetlands are below detection. The headwater of Cameron Creek is a wetland where the maximum value for all wetlands was detected. Groundwater activities are 1-2 orders of magnitude larger. (B) ^{222}Rn activities vs. chloride concentrations that are the primary input data for the steady-state advective model.

Radon activities in the Tay River are low, at or near the detection limit, and not correlated with lineament location or density of fractures in the exposed bedrock river bottom (Figure 4.6). Radon activities in the individual creeks support the stable isotope results (Table 4.1). Cameron Creek has the highest radon activity (0.444 ± 0.022 Bq/L) suggesting it is primarily groundwater discharge. Radon activities in Ruddsdale Creek increase downstream from 0.012 ± 0.002 to 0.041 ± 0.003 Bq/L and Uens Creek also has measurable radon activities of 0.052 ± 0.005 Bq/L, suggesting these creeks have a groundwater component. Eagle Creek, Lineament Creek and Grants Creek are all below detection for radon activities, consistent with stable isotopic results.

Table 4.1 Geochemical data and results of the steady-state advective model. Sample locations 1-21 are lakes and wetlands

Sample	Location	Mean depth (m)	Area (km^2)	Volume (1x10^6 m^3)	$10^3\delta^{18}O$ VSMOW	$10^3\delta^2H$ VSMOW	$10^3\delta^{18}O$ VSMOW	$10^3\delta^2H$ VSMOW	Cond. (μS/cm)	Cl (mg/L)	^{222}Rn (Bq/L)	±	I_g (m^3/day)	I_s (m^3/day)	I_g/V	I_g/I_s
					5/18/06		7/31/06		7/29-31/08							
1	Christie Lake	8.5	7	60	-8.2	-68	-7.6	-61	154	5	0.025	0.001	13065	321400	2.2E-04	4.1E-02
2	Unnamed wetland	1.2	0.1	0.1	-8.8	-73	-5.6	-54	386	61	<0.01	-	10	296	9.7E-05	3.3E-02
3	Davern Lake	15	0.5	8	-7.0	-64	-6.9	-58	259	5	<0.01	-	621	25498	8.3E-05	2.4E-02
4	Little Silver Lake	6	0.6	4	-8.3	-70	-7.7	-63	147	5	<0.01	-	325	2403	9.0E-05	1.4E-01
5	Unnamed wetland	1.3	0.1	0.1	-7.6	-66	-4.2	-50	215	42	<0.01	-	11	297	1.1E-04	3.8E-02
6	Leggat Lake	10	1.8	18	-5.9	-58	-5.7	-53	70	1	<0.01	-	1559	26611	8.7E-05	5.9E-02
7	Miller Lake	4	0.3	1.2	-8.6	-69	-7.3	-61	87	3	0.038	0.005	443	2048	3.7E-04	2.2E-01
8	Long Lake	11.5	3.4	39	-8.7	-67	-7.5	-63	116	3	0.036	0.005	11880	40765	3.0E-04	2.9E-01
9	Abbot Lake	2	0.1	0.2	-8.5	-66	-6.5	-58	140	4	0.022	0.006	51	461	2.6E-04	1.1E-01
10	Eagle Lake	15	6.4	96	-6.8	-58	-6.2	-58	134	7	<0.01	-	8018	29333	8.4E-05	2.7E-01
11	Crowe Lake	25	4.4	110	-8.1	-66	-7.7	-64	149	3	<0.01	-	9018	36353	8.2E-05	2.5E-01
12	Sucker Lake	2	0.3	0.6	-8.9	-69	-6.8	-61	164	1	<0.01	-	69	2291	1.1E-04	3.0E-02
13	Bob's Lake	20	29.5	590	-7.7	-65	-7.4	-63	145	4	<0.01	-	48730	560688	8.3E-05	8.7E-02
14	Farren Lake	8.3	1.7	14	-7.1	-59	-6.3	-59	156	9	<0.01	-	1225	5647	8.7E-05	2.2E-01
15	Big Crosby Lake	12	2.2	26	-8.1	-68	-7.7	-63	145	5	<0.01	-	2236	8974	8.5E-05	2.5E-01
16	Little Crosby Lake	9	0.6	5.4	-8.2	-69	-7.2	-62	147	6	<0.01	-	467	2291	8.6E-05	2.0E-01
17	Pike Lake	8.4	3.3	28	-7.7	-67	-7.7	-64	175	9	0.010	0.007	2387	35738	8.6E-05	6.7E-02
18	Otty Lake	9	6.7	60	-8.5	-70	-7.3	-61	229	7	<0.01	-	5210	24299	8.6E-05	2.1E-01
19	TW14 Lower wetland	1.5	0.01	0.02	-	-	-6.0	-57	-	-	-	-	-	-	-	-
20	TW14 Upper wetland	1.7	0.0001	0.0002	-	-	-7.0	-60	-	-	-	-	-	-	-	-
21	Cameron Creek headwater	1.1	0.0001	0.0001	-	-	-9.5	-73	403	18	0.451	0.022	0.61	0.03	6.1E-03	2.0E+01

Tay River		-	-	-	-8.2	-62	-7.2	-62	135	-	0.02-0.05	-
Creeks							7/31/07		7/29-31/08			
22	Uens Creek (upper)	-	-	-	-	-	-7.9	-57	281	4	0.052	0.005
23	Uens Creek (middle)	-	-	-	-	-	-8.9	-62	180	15	-	-
24	Uens Creek (lower)	-	-	-	-	-	-6.6	-52	181	6	-	-
25	Eagle Creek (upper)	-	-	-	-	-	-6.0	-51	144	9	<0.01	-
26	Eagle Creek (lower)	-	-	-	-	-	-5.4	-49	146	9	<0.01	-
27	Lineament Creek	-	-	-	-	-	-6.0	-51	125	-	<0.01	-
28	Cameron Creek	-	-	-	-	-	-11.5	-81	616	36	0.444	0.022
29	Ruddsdale Creek (upper)	-	-	-	-	-	-7.7	-62	382	12	0.012	0.002
30	Ruddsdale Creek (lower)	-	-	-	-	-	-8.7	-66	696	73	0.041	0.003
31	Grant's Creek (upper)	-	-	-	-	-	-7.2	-57	185	9	<0.01	-
32	Grant's Creek (middle)	-	-	-	-	-	-6.9	-56	198	12	<0.01	-
33	Grant's Creek (lower)	-	-	-	-	-	-7.0	-55	231	34	<0.01	-
34	Fish Creek	-	-	-	-	-	-	-	181	3	<0.01	-

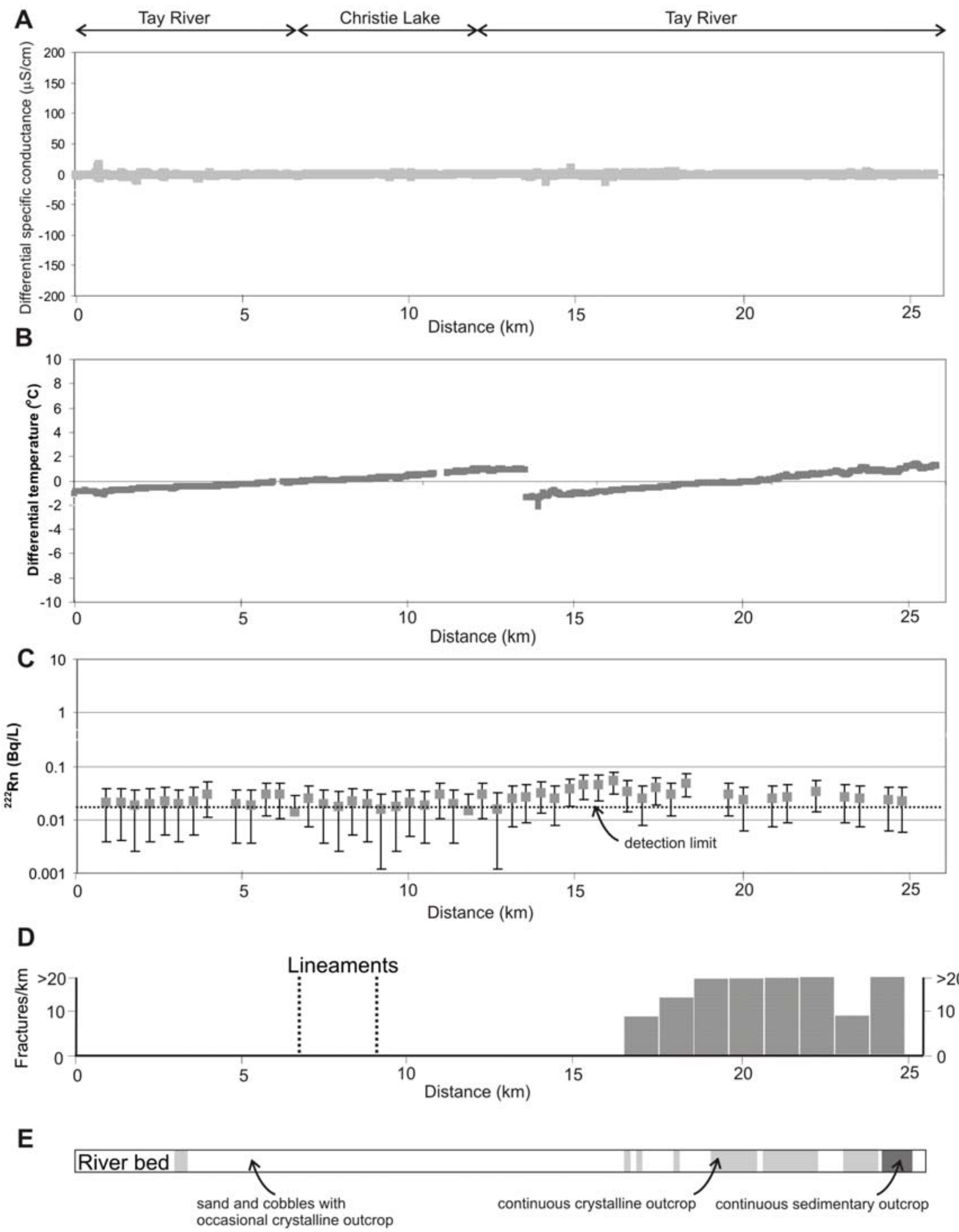

Figure 4.6 Specific conductance, temperature, ^{222}Rn, fracture density and river bed data from a 25 km long transect of the Tay River and Christie Lake. Groundwater discharge

is identified by high specific conductance, high ^{222}Rn activities and low temperature. Differential (A) specific conductance and (B) temperature is the difference between individual data points and the daily mean so that data from different days are comparable. Transects were completed over two days and the water temperatures fluctuate diurnally. The apparent offset in temperature around km 13 is due to the difference between morning and afternoon temperatures. (C) ^{222}Rn activities from the Tay River. (D) Fracture density, lineament location and (E) river bed type are plotted for reference.

Figure 4.5B compares radon activities and chloride concentrations. The headwater of Cameron Creek is an outlier between the groundwater and surface water populations. Estimates of groundwater discharge were made using the steady state advective model described in Section 4.3.2. Median groundwater values of 22.9 Bq/L and 10 mg/L were assumed for radon and chloride, respectively. Table 4.1 compiles lake area and volume as well as radon activities and chloride concentrations and the resulting estimates of surface water inflow (I_s) and groundwater discharge (I_g). Groundwater dependence is quantified by the ratio of groundwater discharge to volume of the wetland (I_g/V) and the ratio of groundwater to surface water inflow (I_g/I_s). Results indicate that all of the lakes and wetlands have low groundwater dependence, except the headwaters of Cameron Creek (Figure 4.7). The minimum, median and maximum ratio of I_g/I_s for individual lakes and wetlands are 2%, 14% and 29%, respectively. The groundwater/surface water inflow ratio for most lakes and wetlands is <20% suggesting that generally the Tay River watershed is not a groundwater dependent system.

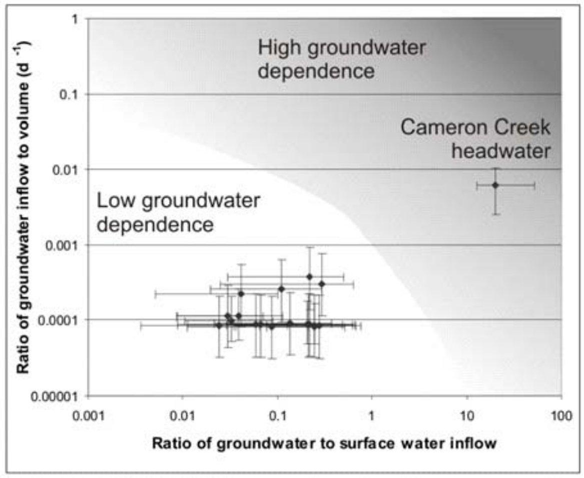

Figure 4.7 Results of the steady-state advective model indicate that most lakes and wetland are not dependent on groundwater except the headwaters of Cameron Creek. Error bars indicate range of values calculated using different groundwater ^{222}Rn activities.

The sensitivity of I_g/I_s and I_g/V ratios to a range of the groundwater ^{222}Rn activities (lower to upper quartile from the box-and-whisker plot in Figure 4.5A) was evaluated. This range is equivalent to an uncertainty of ±50% of the median groundwater ^{222}Rn activity. Figure 4.7 indicates that the uncertainty in groundwater ^{222}Rn activities does not affect the interpretation of groundwater dependence. Watershed-scale groundwater discharge (I_g) is most sensitive to groundwater radon activity (c_{gRn}), surface water radon activity (c_{Rn}), volume (V), and area (A) although volume and area are less uncertain than radon activities (Figure 4.8). Each parameter is varied over the expected range of potential uncertainty. Surface water radon activities were varied by ±50% which is the approximate range of heterogeneity documented in a thermally stratified lake [*Kluge, et al.*, 2007] and a shallow wetland with limited mixing [*Cook, et al.*, 2008]. Section 4.3.2 outlines the uncertainty for other parameters. Groundwater discharge is less sensitive to gas exchange velocity (k), evaporation (E) and chloride concentrations in groundwater (c_{gCl}) and surface water (c_{Cl}). The lack of sensitivity to surface water chloride concentration (c_{Cl}) suggests that model results are not highly sensitive to the steady state assumption (see Section 4.3.2). The sensitivity to groundwater (c_{gRn}) and surface water (c_{Rn}) radon activity suggests that the more important assumptions are a well mixed surface water body and a representative groundwater radon activities (see Section 4.5.2). Since the model is sensitive to radon activities, the sensitivity of watershed-scale groundwater discharge and surface water inflows to groundwater ^{222}Rn activities was evaluated in more detail (Table 4.2). The groundwater discharge (I_g) varies significantly but importantly, the ratio of groundwater discharge to surface water inflow (I_g/I_s) remains low and is relatively insensitive to groundwater radon activities suggesting the lakes and wetlands of the Tay River watershed are not groundwater dependent.

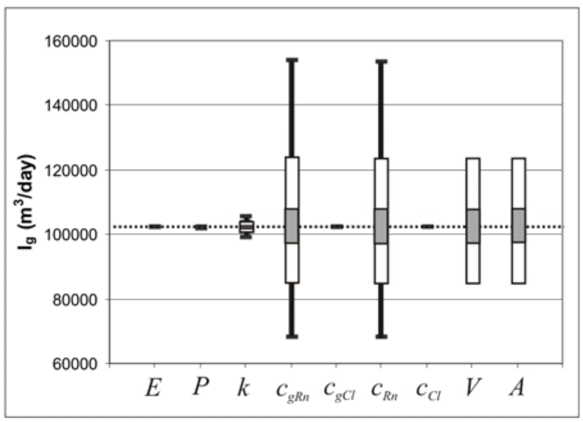

Figure 4.8 Sensitivity analysis of the total groundwater discharge for the sampled lakes using the advective, steady-state model. Each parameter is varied over the expected range of potential uncertainty. Grey and white rectangles depict ranges in I_g from ±5% and ±20% uncertainty in each parameter, respectively, while vertical lines represent ±50% uncertainty. The broken line represents the value of ~102,000 m^3/day estimated using the measured values from Table 4.1 as described in the text.

Table 4.2 Total groundwater discharge and surface water inflow rates for the 21 sampled lakes and wetlands from the steady-steady advective model with variable groundwater ^{222}Rn activities

C_{gRn}	I_g (m^3/d)	I_s (m^3/d)	I_g/I_s	I_g /V (d^{-1})
36 Bq/L (upper quartile)	64,157	805,441	0.08	0.00006
23 Bq/L (median)	102,305	1,118,595	0.09	0.00010
15 Bq/L (lower quartile)	156,717	1,177,372	0.13	0.00016

4.4.3 Temperature and specific conductance transects

Discrete groundwater discharge locations were mapped using high-resolution transects with a temperature and specific conductance probe of the Tay River and Christie Lake (Figure 4.6) as well as Lineament Creek and Cameron Creek (Figure 4.8). The transect in Figure 4.6 was completed over two days and the water temperatures fluctuate diurnally. The apparent offset in temperature around km 13 in Figure 4.6B is due to the difference between morning and afternoon temperatures. For the upper and lower Tay River and Christie Lake, no temperature and specific conductance anomalies were detected over a 25 km transect representing over 10,500 individual temperature and specific conductance measurements. Figure 4.6 also compiles type of river bed, lineaments that cross the river and fracture density in the exposed bedrock river bottom for the 25 km transect of the Tay River and Christie Lake. From the detailed transects of specific conductance, temperature and radon activities it is clear that discharge is not localized at lineaments or in zones of exposed, high-density fracturing.

Lineament and Cameron Creeks show larger temperature and specific conductance anomalies, likely due to their lower streamflow and smaller sizes (Figure 4.9). In Cameron Creek, a significant positive specific conductance anomaly and negative temperature anomaly was found near the beginning of the transect indicating localized groundwater discharge. The reach of Cameron Creek examined was downstream of the headwater reach of Cameron Creek which was not accessible. In Lineament Creek a positive specific conductance anomaly and negative temperature anomaly was not found.

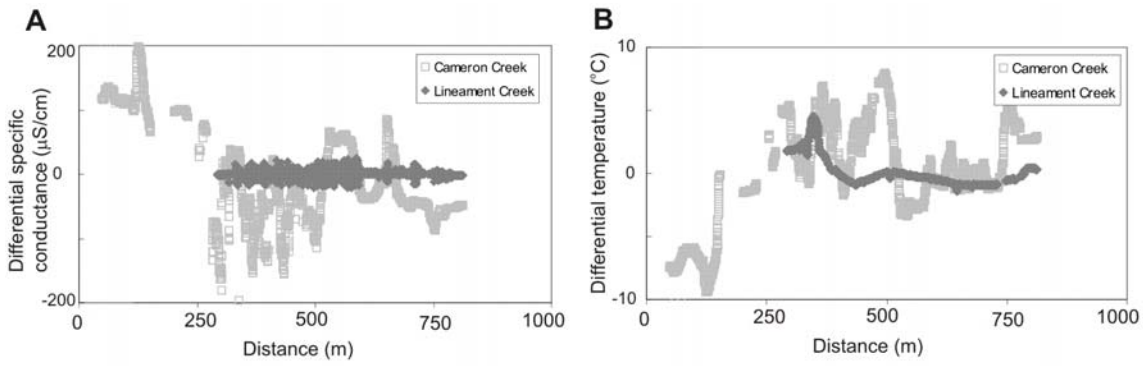

Figure 4.9 Transects of Cameron Creek and Lineament Creek showing (A) differential specific conductance and (B) differential temperature. Differential values are the mean of the whole transect minus the individual measurement. The upper part of Cameron Creek was not accessible.

4.4.4 Streamflow measurements

Streamflow from the three different stations along the Tay River (Figure 4.3) are compared to determine if the Tay River is gaining during low flow conditions in 2005 and 2006 (Figure 4.10). The furthest downstream station at the town of Perth is plotted with ±5% measurement uncertainty as error bars. This shows that during low flow conditions there is no measurable increase in streamflow downstream in the Tay River (Figure 4.10), even though minor tributary streams also contribute to the river streamflow (Figure 4.3).

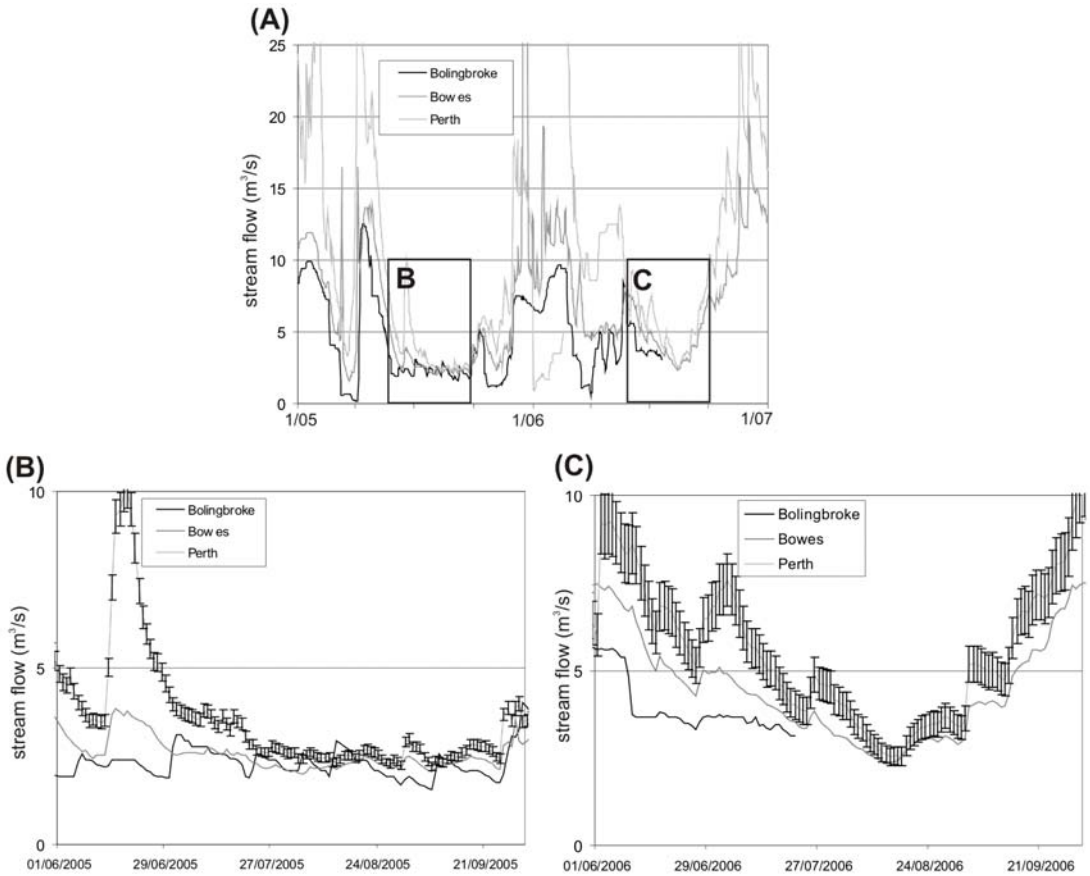

Figure 4.10 Tay River streamflow measured at three gauging stations by the Rideau Valley Conservation Authority. Error bars on Perth station is the measurement uncertainty (±5%) which indicate that during low-flow conditions, river streamflow does not increase downstream.

The total random and systematic uncertainty in the streamflow measurement of the four minor creeks was 26-48% due primarily to the low flow velocities that cause significant uncertainties in the rotations/minute of the flow meter (Appendix G). The downstream measurements are within the error uncertainty of the upstream measurement for all four streams (Figure 4.11). Groundwater discharge conditions are difficult to detect due to the large uncertainties in streamflow measurements.

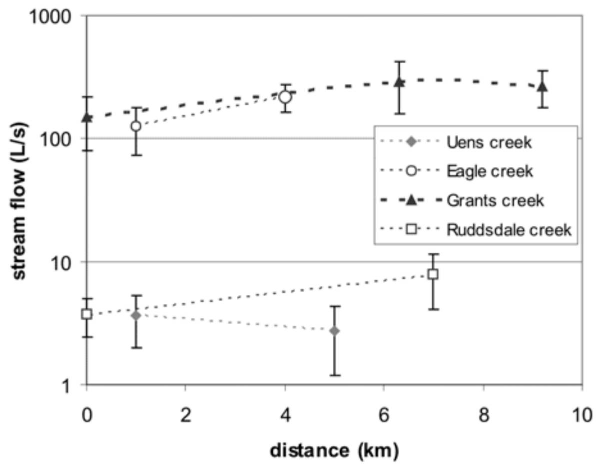

Figure 4.11 Low-flow streamflow measurement of minor creeks in the Tay River watershed in August 2007. The streamflow rate of Cameron Creek was too low to measure.

4.5 Discussion

4.5.1 Estimating groundwater discharge at the watershed scale

A maximal groundwater discharge estimate for the Tay River watershed during low flow conditions is calculated using a variety of methods to quantify discharge patterns and rates. Different methods were applied to the different types of surface water bodies and multiple methods were used for each type of water body to corroborate results from other methods. The total groundwater discharge at the watershed scale during low flow conditions is estimated by summing the approximate discharge from each component:

$$Q_{watershed} = Q_{lakes} + Q_{river} + Q_{creeks} \quad \textbf{Equation 6}$$

where Q is groundwater discharge (m^3/day) and $Q_{watershed}$, Q_{lakes}, Q_{river} and Q_{creeks} are the groundwater discharge to the total watershed, to the lakes and wetlands, to the Tay River, and to the creeks, respectively. Groundwater discharge via evapotranspiration is not quantified during this chapter. The groundwater discharge patterns and rates for each type of surface water body (lakes and wetlands, the Tay River and the creeks) are discussed in order to sum the total $Q_{watershed}$.

Multiple geochemical indicators (Figures 4.4 and 4.5) suggest that groundwater discharge to lakes and wetlands is systematically limited with the exception of the headwaters of Cameron Creek. Without a dense network of flow meters [*Lee*, 1977; *Taniguchi, et al.*, 2002] directly measuring distributed groundwater discharge in the lakes and wetlands is impossible. Qualitative analysis of the stable isotopes alone can not differentiate between the relative influence of evaporation and groundwater discharge in lakes and wetlands (Figure 4.4A). However, stable isotopes in conjunction with chloride concentrations reveal the patterns of groundwater discharge and the relative influence of evaporation and groundwater discharge but not used to quantify actual fluxes. The chemistry of most lakes and creeks are not significantly changed by either evaporation or groundwater discharge (Figure 4.4C). Low radon activities in surface water bodies and low I_g/I_s ratios (Table 4.1) support the interpretation of limited groundwater discharge to most lakes and wetlands. Additionally, the temperature and specific conductance transect in Christie Lake did not identify any significant thermo-chemical anomalies (Figure 4.6).

Results of the steady-state advective model suggest that the groundwater discharge to the 21 sampled lakes and wetlands is ~102,000 m^3/d (Table 4.2). The sampled lakes and wetlands represent 76 % of the lakes and wetlands in the Tay River watershed by volume. For the remainder of the lakes and wetlands an approximate discharge rate is calculated assuming a ratio of groundwater discharge to volume ratio of 0.0001 (Figure 4.7). The remainder of the lakes and wetlands therefore likely contribute ~31,000 m^3/d for a watershed total Q_{lakes} of ~133,000 m^3/d. It should be emphasized that the steady-state advective model is considered a screening-level tool that provides estimates of groundwater and surface water inflows. In many case these are maximal estimates because the radon activities were below detection. The assumptions discussed in Section 4.3.2 are also important caveats.

Daily flow measurements (Figure 4.10) and detailed transects of specific conductance, temperature and radon activities (Figure 4.6) all indicate that discharge to the Tay River in the 25 km reach examined in this study is not significant. Potential uncertainty in the flow measurements (±5%) indicate that Q_{river} is < 0.13 m^3/s or <11,000 m^3/d.

Discharge patterns to individual creeks evaluated using stable isotopes (Figure 4.4B) and radon activities (Table 4.1) are internally consistent. Cameron Creek has high radon activity and specific conductance as well as stable isotopic values suggesting it is primarily groundwater discharge. Radon activities and specific conductance in Ruddsdale Creek increase downstream concurrent with an isotopic shift indicating groundwater discharge. Uens Creek has measurable radon activities and an isotopic shift indicating groundwater discharge. Eagle Creek, Lineament Creek and Grants Creek are all below detection for radon activities, consistent with stable isotopic results. Temperature and specific conductance transects of Cameron Creek and Lineament Creek support these interpretations (Figure 4.9). Unfortunately, the significant uncertainty in streamflow measurements of the creeks (Figure 4.11) limits the usefulness of this data for quantifying groundwater discharge rates in the creeks. Instead, streamflow measurements can be used as the maximum potential groundwater discharge rate for the creeks that multiple geochemical indicators reveal groundwater discharge (Cameron Creek, <0.002 m^3/s streamflow; Uens Creek, 0.003 m^3/s; and Ruddsdale Creek, 0.008 m^3/s). Other creeks not examined in this study have insignificant streamflow compared to Q_{lakes} or Q_{river}. Therefore, the total Q_{creeks} is <0.013 m^3/s or <1,100 m^3/d.

The overall relationship of discharge rates to the different types of water bodies is therefore $Q_{lakes} > Q_{river} > Q_{creeks}$. Discharge to lakes and wetlands that is distributed over a very large surface area is therefore the most important for constraining $Q_{watershed}$. Individual estimates that are summed in the steady-state advective model are maximal values since many lakes were below detection limits for radon. But higher values are possible if lower groundwater radon activities are considered (Table 4.2 and Figure 4.8). The maximum groundwater discharge for the watershed ($Q_{watershed}$) is less than ~144,100 m^3/d, assuming the median groundwater radon activity for the steady-state advective model. The impact of this discharge rate is discussed in Section 4.5.3. The low-flow discharge rates and patterns in the Tay River watershed could be influenced by the higher surface water levels due to regulation structures such as the Bolingbroke dam. High water levels could lead to lower hydraulic gradients in the groundwater which would lower discharge. But since the water table is generally near the surface throughout the year, discharge is more likely controlled by bedrock permeability than hydraulic gradients.

4.5.2 Comparison to other groundwater discharge rates

Groundwater discharge rates in the Tay River watershed can be compared to other hydrologic settings by calculating an areal discharge flux (cm/d). The average areal discharge flux (total I_g divided by total lake and wetland area) for the 21 lakes and wetlands examined using the steady-state advective model is 0.15 cm/d. In other hydrologic settings, average areal discharge fluxes to lakes and wetlands have been estimated using radon to be 0.30-0.74 cm/d [*Corbett, et al.*, 1997], 0.36 cm/d [*Kluge, et al.*, 2007] and 0.22-0.39 cm/d [*Cook, et al.*, 2008]. In the topographically-subdued continental shelf of Louisiana, *McCoy et al.* [2007] recently documented low rates of submarine groundwater water discharge (0.01-0.14 cm/d) which were corroborated with a regional groundwater model [*Thompson, et al.*, 2007]. Therefore, areal discharge flux to the lakes and wetlands of the Tay River watershed is ~2 times lower than estimates from other lakes and wetlands and are consistent with the low estimates of submarine groundwater discharge documented in topographically-subdued areas.

Low-flow groundwater discharge rates from the Tay River watershed can be compared to other watersheds with similar geology and climate by normalizing discharge rate to precipitation rate (unitless) as part of a water budget, although water budgets usually contain significant uncertainties [*Winter*, 1981]. This approach is only reasonable for humid areas where the monthly precipitation rate is relatively constant. For the Tay River watershed the discharge/precipitation ratio (total I_g divided by product of the watershed area and precipitation rate) is 4%. Mirror Lake, New Hampshire is a small, well-characterized watershed also underlain by fractured crystalline rock and variable soil thickness. *Rosenberry and Winter* [1993] estimated a 4% discharge/precipitation ratio for bedrock discharge in the Mirror Lake water budget. WE-38 is a small watershed in Pennsylvania is also underlain by fractured crystalline rock and variable soil thickness. Low flow rates in WE-38 are 34 L/s [*Gburek and Folmar*, 1999b] which equates to a discharge/precipitation ratio of 14%. In contrast, groundwater discharge rates are often estimated to be 15-50% of precipitation rates in porous media watersheds [*Arnold and Allen*, 1996; *Corbett, et al.*, 1997]. Therefore, groundwater discharge from fractured bedrock normalized to precipitation rate may be relatively low compared to porous media watersheds. For some fractured rock watersheds such as the Tay River and Mirror Lake, the rate of bedrock groundwater discharge is a relatively insignificant part of the water budget compared to the residual of the water budget [*Rosenberry and Winter*, 1993].

4.5.3 Groundwater discharge in fractured bedrock watersheds

The small areal discharge flux, low discharge/precipitation ratio and low I_g/I_s ratio (Figure 4.7 and Table 4.2) all suggest that the Tay River watershed is a surface-water dominated system. Yet during low-flow conditions the groundwater discharge rate may be 20- 40% of the Tay River streamflow suggesting that groundwater discharge may be volumetrically supporting streamflow low flow conditions. Figure 4.12 illustrates how surface water influx (I_s) dominates over groundwater discharge (I_g) but that groundwater discharge can be a volumetrically appreciable component of streamflow. This apparent contradiction is due to the importance of surface water storage in the watershed. The Tay River and the flux of groundwater (I_g) to the lakes and wetlands that contribute to Bob's Lake in Figure 4.12 can be viewed as two minor fluxes compared to the reservoir volume or the substantial surface water influx (I_s). The importance of storage to watershed dynamics is underscored by the fact that at low streamflow the Tay River would take 2000-5000 days to drain the volume of the lakes and wetlands, depending on the low-flow rate.

The low rates of groundwater discharge may impact our understanding of fractured bedrock watershed processes. The low groundwater discharge rates suggest that the groundwater and surface water system may be largely decoupled in this watershed compared to watersheds underlain by porous media. The low discharge rate is consistent with the low rate of groundwater recharge to the fractured bedrock aquifer [*Novakowski, et al.*, 2007b]. The low rates of groundwater discharge are consistent with previous studies of small watersheds in the Canadian

Shield that indicate that groundwater discharge is limited where soil is minimal [*Buttle, et al.*, 2004; *Steedman, et al.*, 2004].

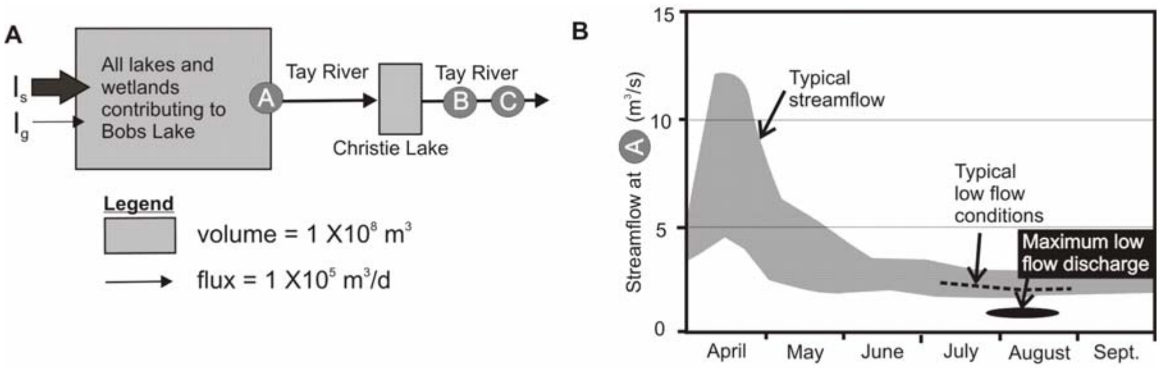

Figure 4.12 (A) Comparison of the streamflow of the Tay River to the contribution of surface water (I_s) and groundwater (I_g) to lakes and wetlands that are the source of the Tay River. The thickness of the line is scaled to the flux and the size of the surface water body is scaled to the volume (Table 4.1). The contribution of groundwater to Christie Lake and the Tay River is not shown because it is insignificant relative to the depicted fluxes. (B) Typical streamflow of the Tay River including low flow conditions, measured at Bolingbroke Dam (compiled from five years of data from the Rideau Valley Conservation Authority). The maximum low flow discharge for the contributing area of Bob's Lake is compiled from Table 4.1. Applying baseflow recession techniques to the Tay River during low flow conditions would grossly overestimate groundwater discharge.

4.5.4 Groundwater discharge methods in a large watershed

Groundwater discharge rates or baseflow is often used as a proxy for groundwater recharge [*Rorabaugh*, 1964; *Rutledge and Daniel*, 1994; *Mau and Winter*, 1997; *Risser, et al.*, 2005; *Risser, et al.*, 2009] but in regulated or lake-dominated watersheds the assumption that low flow streamflow equals recharge can be problematic. Therefore I developed a mixture of novel and standard field methods and calculations to determine discharge patterns and rates in a large watershed independent of baseflow recession. The methodology is transferable to any large watershed even though this chapter focuses on a large, regulated watershed underlain by fractured bedrock. Here I make recommendations that might streamline the design of future research projects. One caveat is that the methods used in this chapter were implemented to constrain groundwater discharge but other study areas may have surface water bodies with sections that are gaining from groundwater discharge while other sections are losing. For example, comparing different streamflow measurements along a reach integrates both discharge and recharge fluxes. In these settings with complex groundwater-surface water interactions, each method must be implemented carefully.

Temperature and specific conductance transects can be a useful and affordable tool to use, especially during reconnaissance, to identify significant groundwater discharge points (*e.g.* Cameron Creek). Similarly, synoptic sampling for stable isotopes and bulk chemistry can identify overall pattern in groundwater discharge versus evaporation or actual groundwater discharge in creeks sampled along their reach (Figure 4.4). Radon activities alone and concurrent with chloride measurement were used in the novel steady-state advective model that was essential to quantifying groundwater and surface water inflow rates. The accuracy of this method is limited by the dependence on well mixed surface water bodies and representative groundwater radon activities. These limitations should be considered when planning future applications of the steady-state model. Manual flow measurements of creeks with a low velocity can be misleading due to the large error (Figure 4.11). Measuring streamflow with acoustic or doppler flow meter or installing a permanent stream gauge could reduce these uncertainties.

4.6 Conclusions and Implications

In this chapter I evaluate the pattern and rate of groundwater discharge in a regulated watershed using methods that are independent of baseflow recession. Natural conservative (δ^2H, $\delta^{18}O$, Cl, and specific conductance), radioactive (^{222}Rn), and thermal tracers are integrated with flow measurements to delimit the discharge locations and quantify the discharge fluxes to lakes, wetlands, creeks and the Tay River. The results improve our understanding of the rate, localization and conceptualization of discharge in a large, fractured rock watershed:

1) The groundwater discharge rate to the Tay River watershed is low. Surface water inflow to lakes and wetlands is up to an order of magnitude larger than groundwater discharge. Groundwater discharge to the Tay River is not geochemically, thermally or hydraulically detectable. A few creeks in the watershed have a groundwater component but the streamflow of these creeks is a minor fraction (<0.1%) the overall watershed budget. The low permeability of the bedrock aquifer likely limits the rate of groundwater discharge.
2) Groundwater discharge is not localized around lineaments or high-density zones of exposed brittle fractures. Instead, groundwater discharge seems to be distributed throughout the watershed except in the case of Cameron Creek which is a zone of localized groundwater discharge that was not predicted from lineament or fracture mapping. Therefore groundwater discharge in the Tay River watershed is best conceptualized as a distributed, minimal flux. Groundwater discharge not being localized at lineament is consistent with a recent re-interpretation of lineaments as watershed-scale hydraulic barriers (Chapter 3).
3) Distributed discharge is difficult to measure with physical methods, therefore geochemical methods that can integrate larger areas are more effective. Multiple complimentary methods are essential, especially in watersheds that are hydraulically complex (*i.e.* multiple surface water body types). A suite of methods are useful for corroborating results and because a single methods does not work for all types of water bodies.
4) This chapter focuses on a large watershed underlain by fractured bedrock although the methodology developed is transferable to any large watershed. This suite of methods can

constrain groundwater discharge rates in regulated or unregulated watersheds which is increasingly important since dams control many of the medium to large rivers in the world [*Nilsson, et al.*, 2005]. The developed steady-state advective model provides important constraints on groundwater discharge and surface water inflows to the lakes and wetlands. The field data are relatively easy to acquire making it a useful screening-level tool.

The low groundwater discharge rates have significant implications for the ecology, sustainability and management of large, crystalline watersheds which are common in North America, northern Europe and tropical shield regions in South America and Africa.
Low flows are integral to sustaining cold-temperature fish species and other aquatic ecology [*Hayashi and Rosenberry*, 2002; *Sophocleous*, 2002]. Low flows also have important socio-economic impacts such as water supply, recreation and reservoir operation [*Burn, et al.*, 2008]. Prediction of low flow conditions in ungauged basins remains a challenge and an important management concern [*Burn, et al.*, 2008; *Spence, et al.*, 2008]. Most attempts to predict low flow conditions in ungauged basins focus on hydrologic, geomorphic, physiographic and geological comparisons of basins. Re-examining basins using the suite of isotopic and geochemical methods described in this chapter may enable better prediction of low flows in ungauged basins [*Soulsby and Tetzlaff*, 2008].

Chapter 5
Discussion and conclusions

The objective of this thesis is to constrain the fundamental hydrogeological processes of a large crystalline fractured rock watershed in the Canadian Shield in order to enable sustainable groundwater management. As introduced in Chapter 1, the fundamental hydrogeological processes in a watershed are groundwater recharge, flow and discharge [*Winter*, 2001]. Chapters 2 to 4 examine each of the fundamental processes individually in order to address the following:

1) How does groundwater recharge the fractured rock aquifer? (Chapter 2)
2) How do lineaments affect groundwater flow in the fractured rock aquifer? (Chapter 3)
3) How does groundwater discharge to surface water bodies from the fractured rock aquifer? (Chapter 4).

This chapter begins by summarizing key conclusions for each fundamental process and estimates a flux at multiple scales for groundwater recharge, flow and discharge. The fluxes are hypothesized to be governed by the representative elementary area (REA) concept proposed for other watersheds in the Canadian Shield [*Sanford, et al.*, 2007]. Proposing the REA concept provides a useful theoretical framework for analyzing the vertical fluxes (recharge and discharge) at different scales (Figure 1.3) but assumes that hydraulic conductivity and gradient are also represented by the REA concept (Chapter 1). The fluxes are examined qualitatively rather than using a formalized scaling theory [*Blöschl and Sivapalan*, 1995] because each flux is relatively poorly constrained (Sections 5.1 and 5.3). Next, the fundamental processes are examined holistically by developing a revised conceptual model for the hydrogeology of crystalline fractured rock watersheds. Finally, I conclude with discussions on sustainable groundwater resources and future research.

5.1 Recharge processes

Event-scale recharge processes examined in Chapter 2 are highly heterogeneous temporally and spatially. The two distinct hydraulic, thermal and isotopic responses observed in wells suggest two different recharge mechanisms are occurring simultaneously in the study area. One recharge process is rapid and localized and the other is slow and widespread. Rapid recharge is a direct but localized and transient connection between the hydrosphere and the shallow geosphere. Event-scale recharge to fractured rock aquifers is localized due to subsurface hydrogeological conditions, specifically the distribution of overlying soils and vertical bedrock fractures. Stable isotopes (*e.g.* δ^2H), temperature and water table fluctuations are robust indicators of actual recharge mass flux during snowmelt. Although recharge is clearly occurring, quantifying the recharge rate or flux is difficult. The event-scale recharge flux is estimated using numerical simulations (Figures 2.6, 2.7, 2.8). The watershed-scale recharge flux is largely unconstrained but hypothesized below. The longer term recharge flux (*i.e.* m/year) is not quantified here but is the focus of ongoing research efforts using ^{3}H/^{3}He age dating and a multi-year record of stable isotopes.

Numerical simulations are useful for understanding the governing physical parameters (Section 2.5.3) as well as estimating recharge fluxes. The simulated recharge flux of the base case with no soil is 5 x 10^{-2} m^3/day which is a vertical recharge flux of 5 x 10^{-4} m/day when normalized by the domain area (Figure 5.1). This recharge flux represents 2% of the applied precipitation which a low percentage but is consistent with independent results using the water table fluctuation method

[*Milloy*, 2007; *Novakowski, et al.*, 2007b]. The thermal, isotopic and hydraulic response of the recharge process is obvious even though the recharge flux is low because of the low specific yield of the aquifer. The maximum simulated recharge flux is $<1 \times 10^{-3}$ m/day (Figure 5.1) for simulations with additional vertical fractures, greater depth of snow water equivalent or smaller horizontal fracture aperture (Figure 2.7). For the simulations with soil, the recharge flux is at least one order of magnitude lower. Although event-based recharge was only examined at the well-scale our improved understanding of the governing processes allows hypothesizing of recharge fluxes at larger scales. Since the localized rapid recharge flux is the maximum flux both spatially and temporally, it can be considered the maximum plausible value of larger scale recharge fluxes (Figure 5.1). A representative elementary area (see Chapter 1) is hypothesized since the two recharge processes (rapid and slow) would be sampled collectively at larger scales.

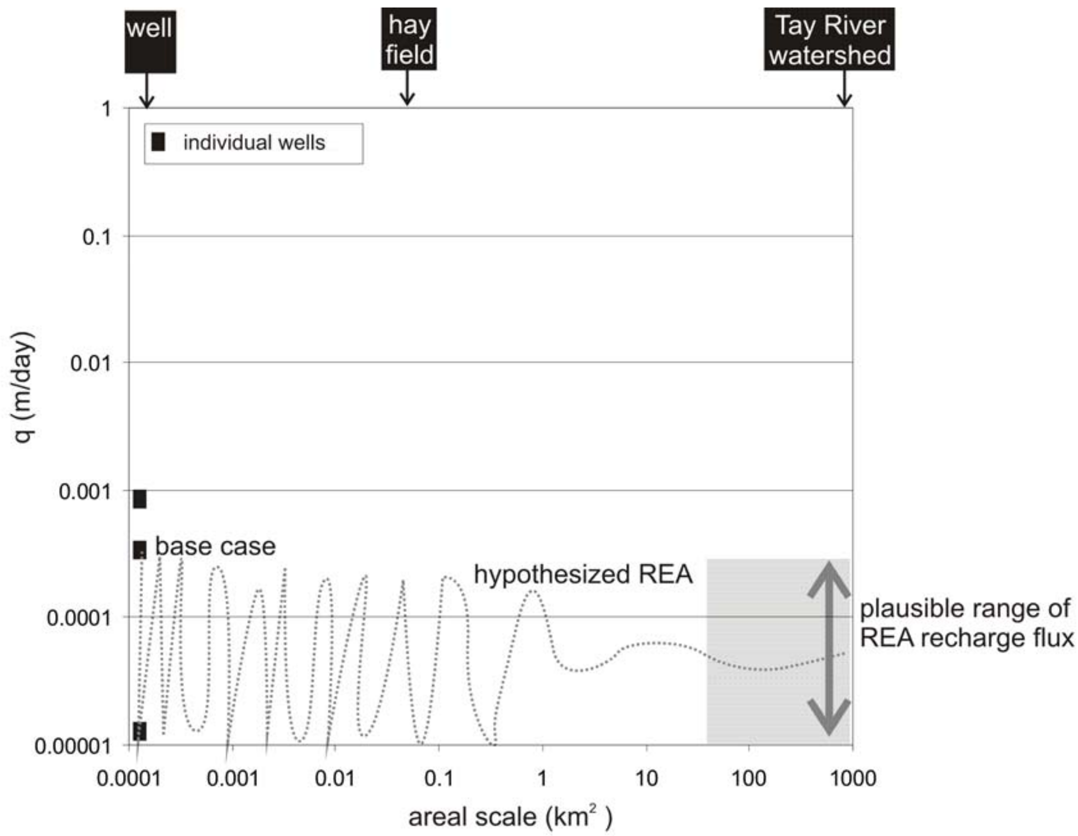

Figure 5.1 Simulated well-scale recharge flux and hypothesized representative elementary area (REA) at larger scales.

5.2 Groundwater flow processes

Lineaments are striking linear discontinuities that are often observed at watershed scales in many landscapes. In Chapter 3, diverse geomatic, geological and hydrogeological data sets and numerical simulations are integrated. Contrary to previous conceptual models, lineaments are re-interpreted as geological structures that could impact watershed-scale flow systems in a low gradient crystalline bedrock aquifer. Fracture and lineament patterns suggest lineaments are structural features, either fault zones or fracture zones with limited displacement. The fractured bedrock underlying lineaments is generally poorly connected, low permeability zones due to fault zone and/or fluid flow processes. Permeability reduction results in lineament areas acting as recharge and flow barriers that compartmentalize lateral flow systems. Faulted lineaments can be more effectively identified by topographic data (*e.g.* DEM) than by tonal imagery (*e.g.* Landsat). Although lineaments have been controversial in the geological and hydrogeological literature, Chapter 3 shows that lineaments are important and useful if identified with a defensible method and analyzed with supplementary geomatic, geologic and hydrogeological data within a well-documented structural geology framework.

5.3 Discharge processes

Discharge rates and patterns were examined at multiple scales in Chapter 4. Natural conservative (δ^2H, δ^{18}O, Cl, and specific conductance), radioactive (^{222}Rn), and thermal tracers were integrated with streamflow measurements to delimit the discharge locations and quantify the discharge fluxes to lakes, wetlands, creeks and the Tay River. The results improve the understanding of the rate, localization and conceptualization of discharge in a large, fractured rock watershed. The groundwater discharge rate to the Tay River watershed is low. Surface water inflow to lakes and wetlands is up to an order of magnitude larger than groundwater discharge. Groundwater discharge to the Tay River is not geochemically, thermally or hydraulically detectable. A few creeks in the watershed have a groundwater component but the streamflow of these creeks is a minor fraction ($<0.1\%$) the overall watershed budget. The low permeability of the bedrock aquifer likely limits the rate of groundwater discharge. Groundwater discharge is not localized around lineaments or high-density zones of exposed brittle fractures. Instead, groundwater discharge seems to be distributed throughout the watershed except in the case of Cameron Creek which is a zone of localized groundwater discharge that was not predicted from lineament or fracture mapping. Therefore groundwater discharge in the Tay River watershed is best conceptualized as a distributed, minimal flux. Groundwater discharge not being localized at lineaments is consistent with the interpretation of lineaments as watershed-scale hydraulic barriers (Chapter 3).

Figure 5.2 illustrates the flux of groundwater discharge at multiple scales in the Tay River watershed based on data derived from the from the steady-state advective model. To examine discharge fluxes at larger scales, water bodies are amalgamated into subwatershed groups [*Rideau Valley Conservation Authority and Mississippi Valley Conservation Authority*, 2006]. The discharge flux is normalized by the area of the water body or the area of examined water bodies within the subwatershed or the Tay River watershed (Figure 5.2). A representative elementary area (REA) is hypothesized based on the consistency of fluxes at larger scales. A REA was proposed for other watersheds within the Canadian Shield at similar scales (>4-6 km^2) also based on low flow data [*Sanford, et al.*, 2007]. The maximum discharge flux measured is 6×10^{-3} m/day and the probable range of REA discharge flux is 8×10^{-4} m/day to 3×10^{-3} m/day.

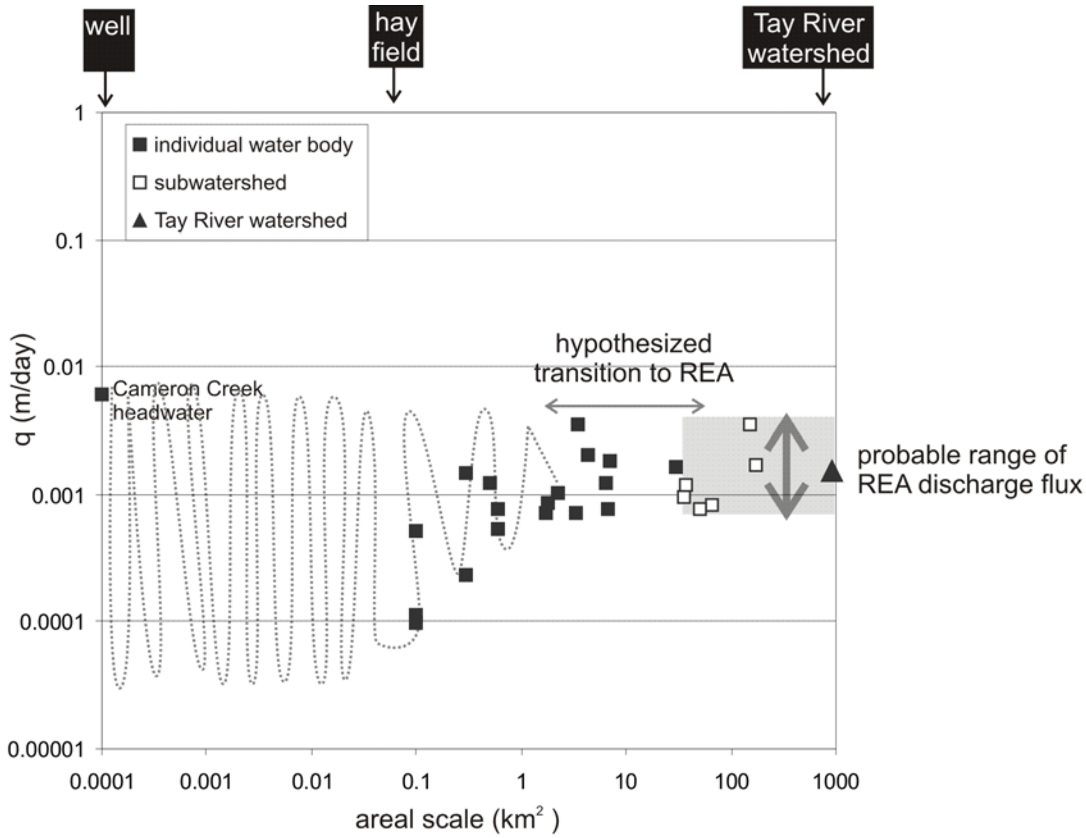

Figure 5.2 Discharge flux at multiple scales from the steady-state advective model. Individual water bodies (data in Table 4.1) are amalgamated into the subwatersheds delineated by the Rideau Valley Conservation Authority. Discharge rate is normalized to the area of the individual water body or area of examined water bodies in each subwatershed or the Tay River watershed. Probable range of discharge flux at scales greater than the hypothesized representative elementary area (REA) is indicated.

5.4 Conceptual model

A conceptual model is a depiction of the defining features of the groundwater flow and transport system as understood at the time of formulation. A key objective of this thesis is to examine the conceptual model for groundwater flow at a watershed scale in crystalline fractured rock terrain. As illustrated in Figure 1.1, groundwater recharge, flow and discharge are the key processes that define the hydrogeological functions of a watershed. Note that the focus here is the fractured rock groundwater system rather than the overlying soil or overall hydrologic function of the watershed although the previous conceptual model is drawn from both hydrologic and hydrogeological literature [*Davison and Kozak*, 1988; *Farvolden, et al.*, 1988; *Stephenson, et al.*, 1992; *Gascoyne, et al.*, 1993; *Rosenberry and Winter*, 1993; *Peters, et al.*, 1995; *Devito, et al.*, 1996; *Branfireun and Roulet*, 1998; *Kotzer, et al.*, 1998; *Gburek and Folmar*, 1999b; *Buttle, et al.*, 2001; *Spence and Woo*, 2003; *Buttle, et al.*, 2004; *Gascoyne*, 2004; *Steedman, et al.*, 2004; *Peters, et al.*, 2006; *Manning and Caine*, 2007; *Winter*, 2007]. Refining the conceptual model for crystalline watersheds is important because this hydrogeomorphic setting is common in Canada, the northeastern United States and northern Europe.

In the previous conceptual model for crystalline watersheds in subdued topography (Figure 5.3), the shallow bedrock aquifer is considered relatively permeable and cross-cut by significant structural discontinuities [*Davison and Kozak*, 1988]. The subdued topography results in low hydraulic gradients and slow groundwater movement but modern groundwater (recharged since 1950) is ubiquitous in the shallow (<100 m) relatively permeable bedrock aquifer [*Stephenson, et al.*, 1992; *Gascoyne, et al.*, 1993; *Kotzer, et al.*, 1998; *Gascoyne*, 2004]. The shallow bedrock is interpreted to function largely as a porous media aquifer with water tables near the surface, groundwater recharging in topographic highs, and discharging in topographically lower surface water features [*Thorne and Gascoyne*, 1993; *Tiedeman, et al.*, 1998]. The hydraulic role of the structural discontinuities is uncertain. *Stephenson et al.* [1992] documented discharge localization around lineaments whereas other studies consider lineaments to be zones of enhanced groundwater recharge and flow [*e.g. Krishnamurthy, et al.*, 2000; *Sener, et al.*, 2005; *Shaban, et al.*, 2006]. Groundwater discharge is limited where soil is minimal (*i.e.* exposed bedrock areas) and perennial streams only develop in drainage areas >0.25-0.5 km^2 [*Buttle, et al.*, 2004;

Steedman, et al., 2004]. In the previous conceptual model, the flux of groundwater recharge and discharge and the role of lineaments was largely uncertain.

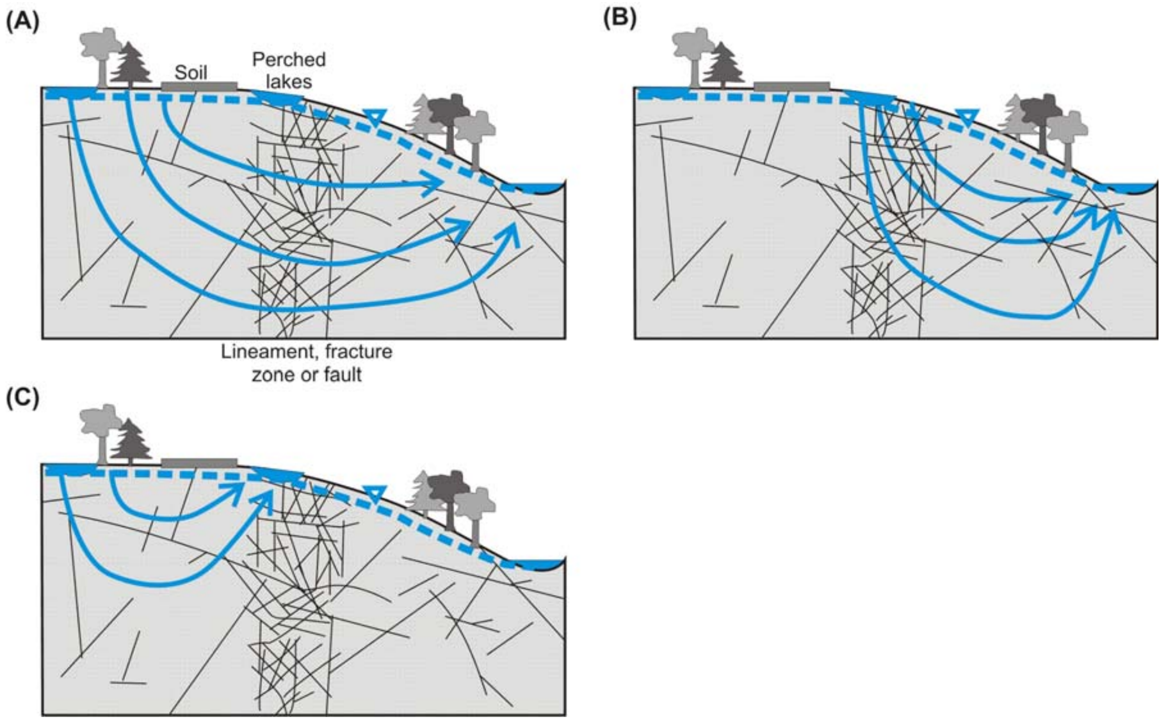

Figure 5.3 Previous conceptual model of groundwater flow in crystalline watersheds. Structural discontinuities such as lineaments, fracture zones or faults are interpreted to (A) have no effect on flow field, (B) localize recharge and flow or (C) localize discharge. The horizontal distance is > 10 km and the vertical height is 10's of meters. The fracture patterns are illustrative because discrete fractures are not visible at this scale.

Figure 5.4 illustrates a revised conceptual model for crystalline watersheds based on the improved understanding of the basic hydrogeological processes in the Tay River watershed. The groundwatershed may not be coincident with the surface watershed. Overall, the water table is near the surface and generally within the fractured bedrock. Groundwater recharges in topographically higher areas and discharges in topographically lower surface water features, like previous conceptual models. Recharge is depicted as two separate processes. Rapid recharge (black arrows in Figure 5.4) is localized around the areas with thin soil whereas slow recharge probably occurs seasonally (spring and fall) in most areas where the water table is not at the surface. The soils may locally act as small reservoirs increasing recharge rates if the water table is within the soils (which is expected to vary spatially and temporally). In the Tay River watershed, Palaeozoic sediments locally outcrop on topographic highs (Figure 3.1) and generally have a higher permeability and storage capacity than the Precambrian units (Section 3.2). On topographic highs with Palaeozoic sediments (not depicted in Figure 5.4), the recharge rate is likely higher than other areas. Lineaments are interpreted to be watershed-scale hydraulic barriers that compartmentalize the groundwater flow system, resulting in high water table gradients between adjacent surface water bodies. As discussed in Chapter 3, lineaments are interpreted as fault or fracture zones with diminished permeability. Groundwater discharge is interpreted to be largely diffuse and not localized around lineaments and discrete fractures. As discussed above the discharge flux is considerably lower than porous media watersheds.

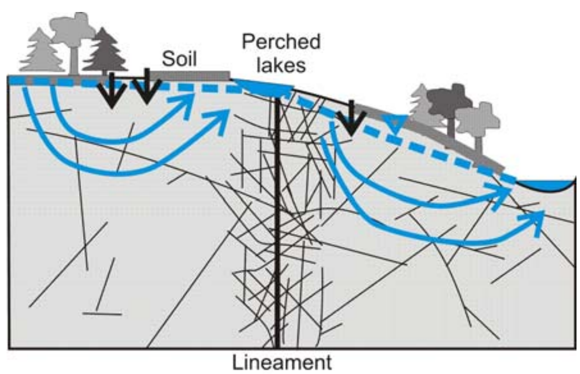

Figure 5.4 A conceptual model for the Tay River watershed. Rapid and slow recharge process are differentiated by black and blue arrows, respectively. Lineaments are considered hydraulic barriers. The horizontal distance is > 10 km and the vertical height is 10's of meters. The fracture patterns are illustrative because discrete fractures are not visible at this scale.

5.5 Sustainable groundwater resources

The sustainability of groundwater in fractured bedrock aquifers is critical to many communities and ecosystems across Canada. As discussed in Chapter 1, this thesis considers groundwater a critical resource and therefore sustaining both groundwater quantity and quality is paramount. Sustainability is discussed qualitatively since watershed-scale fluxes are not well constrained. First, groundwater sustainability is evaluated by examining if groundwater recharge and discharge fluxes are balanced. Second, the watershed-scale discharge rate is examined in the context of water budgets. Third, the impact of recharge processes upon groundwater quality is discussed.

Before groundwater development, aquifers are considered to be in a steady-state dynamic equilibrium where long-term recharge and discharge flux is balanced [*Theis*, 1940]. Groundwater development induces recharge or decreases discharge, which can lead to a new dynamic equilibrium [*Bredehoeft*, 2002]. Therefore, a rudimentary test of groundwater resource sustainability is if the recharge and discharge fluxes are balanced. In Section 5.1 and 5.3, watershed-scale discharge fluxes are hypothesized to be larger than watershed-scale discharge fluxes. It must be emphasized that the uncertainty on these hypothesized estimates is significant and more research is necessary in order to make recommendations for water management. It is noteworthy that watershed-scale recharge and discharge fluxes remain poorly constrained even after a detailed and well-designed study. Additionally, this rudimentary sustainability test of groundwater resources does not explicitly incorporate the impact of groundwater development and storage, climate change, land use change or the potential effect of decreased discharge on surface water bodies and ecology.

Watershed-scale fluxes are critical for watershed budgets and groundwater discharge is the best constrained watershed-scale flux (Figure 5.2). As discussed in Chapter 4, the low-flow groundwater discharge rate normalized to the precipitation rate is 4% for the Tay River watershed. This is generally consistent with other well characterized fractured rock watersheds such as Mirror Lake in New Hampshire and WE-38 in Pennsylvania [*Rosenberry and Winter*, 1993; *Gburek and Folmar*, 1999b]. In contrast, groundwater discharge rates are often estimated to be 15-50% of precipitation rates in porous media watersheds [*Arnold and Allen*, 1996; *Corbett, et al.*, 1997]. Therefore, groundwater discharge from fractured bedrock normalized to precipitation rate may be relatively low compared to porous media watersheds. For some fractured rock watersheds such as the Tay River and Mirror Lake, the rate of bedrock groundwater discharge is a relatively insignificant part of the water budget compared to the residual of the water budget [*Winter*, 1981; *Rosenberry and Winter*, 1993].

Chapter 2 documents rapid pulses of recharge that locally reach greater than 20 m depth within days in a shallow fractured rock with thin soil. Ongoing research in the Tay River watershed supports the interpretation of rapid and localized recharge in this hydrogeomorphic setting. Agricultural contaminants have been documented in numerous wells [*Levison and Novakowski*, 2009]. Long-term water level monitoring reveals that rapid and significant water table fluctuations are locally common but that these result in minimal actual recharge [*Milloy*, 2007; *Novakowski, et al.*, 2007b]. Stable isotope data suggest seasonal, recharge-related isotopic excursions that are highly heterogeneous both with depth and location [*Praamsma, et al.*, 2009b]. An artificial recharge tracer experiment revealed that water ponded at the surface rapidly travels into bedrock piezometers [*Levison and Novakowski*, 2007; *Praamsma, et al.*, 2009a]. This data indicates that recharge processes can affect groundwater quality in this hydrogeomorphic setting and are a potential sustainability concern.

5.6 Future research

This multidisciplinary thesis resulted in significant potential for future research at the intersection of the disciplines of hydrogeology, geochemistry, structural geology and geomatics. This section summarizes potential future research that specifically addresses the primary objective of this thesis: to better understand fundamental hydrogeological processes in a fractured rock watershed.

Rapid recharge processes are localized to areas with soils less than 0.4 m and fractures near the surface (Section 2.6). Since rapid recharge is important for sustaining groundwater quality (Section 5.5), mapping the distribution of soil thickness at the watershed scale using GIS and field ground-truthing is an important future research project. Constraining the long-term recharge flux is critical to quantifying sustainable groundwater resources. Quantifying the long-term recharge flux at the hay field is the focus of ongoing research using a multiple-year stable isotope data set and $^{3}H/^{3}He$ apparent ages. Preliminary results suggest that mean residence time in the shallow, fractured rock aquifer is highly heterogeneous.

Watershed-scale recharge fluxes remain poorly constrained. Upscaling the long-term recharge flux to the watershed scale is difficult and tools for measuring recharge at large scales are scarce. Microgravity surveys have been used to quantify large-scale recharge [*Pool and Eychaner*, 1995] but are unlikely to be useful in the Tay River watershed because surface water features rather than groundwater would dominate the gravity field. The primary tool for examining watershed-scale recharge fluxes is likely numerical simulations using a coupled surface water-groundwater model but non-uniqueness is a significant concern [*Sanford*, 2002]. Key constraints for future simulations include: 1) permeability data (Appendix A); 2) local-scale recharge flux (Chapter 2 and Section 5.1); 3) discharge flux or measured streamflow data (Table 4.1, Figure 4.11, Appendix G); 4) groundwater and surface water elevations; 5) onsite weather data.

Similarly, the hydraulic role of lineaments could be examined in watershed-scale numerical simulations. A key question would be if reduced lineament permeability results in more accurate simulations. Another critical future research project is examining lineaments in other watersheds using the multidisciplinary tools explored in Chapter 3 since the interpretation of lineaments as hydraulic barriers is novel.

Prediction of low flow conditions in ungauged basins remains a challenge and an important management concern [*Burn, et al.*, 2008; *Spence, et al.*, 2008]. Most attempts to predict low flow conditions in ungauged basins focus on hydrologic, geomorphic, physiographic and geological comparisons of basins. Applying the geochemical methods developed in Chapter 4 to other watersheds is an important future research direction that may enable better prediction of low flows in ungauged basins. Another vital future research project is testing the assumptions of the steady-state model developed in Chapter 4.

References

Abbott, M. D., A. Lini, and P. R. Bierman (2000), $\delta^{18}O$, δD and ^{3}H measurements constrain groundwater recharge patterns in an upland fractured bedrock aquifer, Vermont, USA, *Journal of Hydrology*, *228*, 101-112.

Aeschbach-Hertig, W., P. Schlosser, M. Stute, H. J. Simpson, A. Ludin, and J. F. Clark (1998), A $^{3}H/^{3}He$ study of ground water flow in a fractured bedrock aquifer, *Ground Water*, *36*, 661-670.

Ahmed, S., R. Jayakumar, and A. Salih (2007), *Groundwater dynamics in hard rock aquifers: sustainable management and optimal monitoring network design*, Capital Publishing Company, New Delhi. 251 pp.

Alley, W. M., and S. A. Leake (2004), The journey from safe yield to sustainability, *Ground Water*, *42*, 12-16.

Alley, W. M., R. W. Healy, J. W. LaBaugh, and T. E. Reilly (2002), Flow and storage in groundwater systems, *Science*, *296*, 1985-1990.

Allison, G. B. (1988), A review of some of the physical, chemical and isotopic techniques available for estimating groundwater recharge, in *Estimation of natural groundwater recharge*, edited by I. Simmers, pp. 49-72, D.Reidel Publishing, Dordrecht, Netherlands.

Allison, H. J., and A. J. Peck (1989), Hydraulic scaling theory in recharge estimation, in *Groundwater recharge*, edited by M. L. Sharma, pp. 57-66, Balkema, Rotterdam.

American Society for Testing and Materials (2007), Classification of soils for engineering purposes (United Soil Classification System): Annual book of ASTM Standards, D 2487-06, edited by S. J. Bailey, et al., pp. 239-250.

Andjelkovic, D., and A. R. Cruden (1998), Relationships between fractures in Paleozoic cover rocks and structures in the Precambrian basement, south-central Ontario, *Ontario Geological Survey Miscellaneous Paper 169: Summary of fieldwork and other activities 1998*, 275-280.

Arnold, J. G., and P. M. Allen (1996), Estimating hydrologic budgets for three Illinois watersheds, *Journal of Hydrology*, *176*, 57-77.

Banks, D., M. L. Solbjorg, and E. Rohr-Torp (1992), Permeability of fracture zones in a Precambrian granite, *Quarterly Journal of Engineering Geology*, *25*, 377-388.

Bear, J. (1972), *Dynamics of Fluids in Porous Media*, Courier Dover Publications. 784 pp.

Becker, M. W. (2006), Potential for satellite remote sensing of ground water, *Ground Water*, *44*, 306-318.

Becker, M. W., T. Georgian, H. Ambrose, J. Siniscalchi, and K. Fredrick (2004), Estimating flow and flux of ground water discharge using water temperature and velocity, *Journal of Hydrology*, *296*, 221-233.

Bense, V. F., and M. A. Person (2006), Faults as conduit-barrier systems to fluid flow in siliciclastic sedimentary aquifers, *Water Resources Research*, *42*, doi:10.1029/2005WR004480

Bergstrom, S., and L. P. Graham (1998), On the scale problem in hydrological modelling, *Journal of Hydrology*, *211*, 253-265.

Berkowitz, B. (2002), Characterizing flow and transport in fractured geological media: a review, *Advances in Water Resources*, *25*, 861-884.

Blöschl, G., and M. Sivapalan (1995), Scale issues in hydrological modelling: a review, *Hydrological Processes*, *9*, 251-290.

Bockgard, N., A. Rodhe, and K. A. Olsson (2004), Accuracy of CFC groundwater dating in a crystalline bedrock aquifer: Data from a site in southern Sweden, *Hydrogeology Journal*, *12*, 171-183.

Bonnet, E., O. Bour, N. E. Odling, P. Davy, I. Main, P. Cowie, and B. Berkowitz (2001), Scaling of fracture systems in geological media, *Reviews of Geophysics*, *39*, 347-383.

Bouwer, H. M. (1986), Intake rate: cylindrical infiltrometer, in *Methods of soil analysis, part 1. physical and mineralogical methods*, edited, pp. 825-845, Soil Science Society of America, Madison, WI.

Branfireun, B. A., and N. T. Roulet (1998), The baseflow and storm flow hydrology of a precambrian shield headwater peatland, *Hydrological Processes*, *12*, 57-72.

Bredehoeft, J. D. (2002), The water budget myth revisited: why hydrogeologists model, *Ground Water*, *40*, 340-345.

Brooks, R. H., and A. T. Corey (1964), *Hydraulic properties of porous media, Hydrology Paper 3*, University of Colorado, Ft. Collins.

Brunner, P., H. J. H. Franssen, L. Kgotlhang, P. Bauer-Gottwein, and W. Kinzelbach (2007), How can remote sensing contribute in groundwater modeling?, *Hydrogeology Journal*, *V15*, 5-18.

Burn, H. B., J. M. Buttle, D. Caissie, G. MacCulloch, C. Spence, and K. Stahl (2008), The processes, patterns and impacts of low flows across Canada, *Canadian Water Resources Journal*, *32*, 107-124.

Burnett, W. C., G. Kim, and D. Lane-Smith (2001), A continuous monitor for assessment of ^{222}Rn in the coastal ocean, *Journal of Radioanalytical and Nuclear Chemistry*, *249*, 167-172.

Butler, J. J., Jr. (1998), *The design, performance and analysis of slug tests*, CRC Press, Boca Raton, Fl. 245 pp.

Buttle, J. M., P. J. Dillon, and G. R. Eerkes (2004), Hydrologic coupling of slopes, riparian zones and streams: an example from the Canadian Shield, *Journal of Hydrology*, *287*, 161-177.

Buttle, J. M., P. W. Hazlett, C. D. Murray, I. F. Creed, D. S. Jeffries, and R. Semkin (2001), Prediction of groundwater characteristics in forested and harvested basins during spring snowmelt using a topographic index, *Hydrological Processes*, *15*, 3389-3407.

Caine, J. S., and C. B. Forster (1999), Fault zone architecture and fluid flow: insights from field data and numerical modeling, in *Faults and subsurface fluid flow in the shallow crust*, edited by W. C. Haneberg, et al., pp. 101-127, American Geophysical Union.

Caine, J. S., and S. R. A. Tomusiak (2003), Brittle structures and their role in controlling porosity and permeability in a complex Precambrian crystalline-rock aquifer system in the Colorado Rocky Mountain Front Range, *Geological Society of American Bulletin*, *115*, 1410-1424.

Caine, J. S., J. P. Evans, and C. B. Forster (1996), Fault zone architecture and permeability structure, *Geology*, *24*, 1025-1028.

Canadell, J., R. B. Jackson, J. R. Ehleringer, H. A. Mooney, O. E. Sala, and E. D. Schulze (1996), Maximum rooting depth of vegetation types at the global scale, *Oecologia*, *108*, 583-595.

Cey, E., D. Rudolph, and R. Therrien (2006), Simulation of groundwater recharge dynamics in partially saturated fractured soils incorporating spatially variable fracture apertures, *Water Resources Research*, *42*, doi:10.1029/2005WR004589.

Charette, M. A., W. S. Moore, and W. C. Burnett (2008), Chapter 5 Uranium- and thorium-series nuclides as tracers of submarine groundwater discharge, *Radioactivity in the Environment*, *13*, 155-191.

Chester, F. M., J. P. Evans, and R. L. Biegel (1993), Internal structure and weakening mechanisms of the San Andreas fault, *Journal of Geophysical Research*, *98*, 771-786.

Clark, I., and P. Fritz (1997), *Environmental isotopes in hydrogeology*, Lewis Publishers, Florida. 328 pp.

Clark, S. F., Jr., R. B. Moore, E. W. Ferguson, and M. Z. Picard (1996), Criteria and methods for fracture-trace analysis of the New Hampshire bedrock aquifer, 12 pp, United States Geological Survey Open-File Report 96-479.

Clauser, C. (1992), Permeability of crystalline rocks, *EOS, Transactions*, *73*, 233-238.

Conant, B., Jr. (2004), Delineating and quantifying ground water discharge zones using streambed temperatures, *Ground Water*, *42*, 243-257.

Constantz, J. (1998), Interaction between stream temperature, streamflow and groundwater exchanges in alpine streams, *Water Resources Research*, *34*, 1609-1615.

Cook, P. G. (2003), *A guide to regional groundwater flow in fractured rock aquifers*, CSIRO Land and Water, Henley Beach, AU. 108 pp.

Cook, P. G., and N. I. Robinson (2002), Estimating groundwater recharge in fractured rock from environmental ^{3}H and ^{36}Cl, Clare Valley, South Australia, *Water Resources Research*, *38*, doi:10.1029/2001WR000772.

Cook, P. G., A. J. Love, N. I. Robinson, and C. T. Simmons (2005), Groundwater ages in fractured rock aquifers, *Journal of Hydrology*, *308*, 284-301.

Cook, P. G., S. Lamontague, D. Berhane, and J. F. Clark (2006), Quantifying groundwater discharge to Cockburn River, Southeastern Australia, using dissolved gas tracers ^{222}Rr and SF^{6}, *Water Resources Research*, *42*, doi:10.1029/2006WR004921

Cook, P. G., D. K. Solomon, W. E. Sanford, E. Busenberg, L. N. Plummer, and R. J. Poreda (1996), Inferring shallow groundwater flow in saprolite and fractured rock using environmental tracers, *Water Resources Research*, *32*, 1501-1510.

Cook, P. G., C. Wood, T. White, C. T. Simmons, T. Fass, and P. Brunner (2008), Groundwater inflow to a shallow, poorly-mixed wetland estimated from a mass balance of radon, *Journal of Hydrology*, *354*, 213-226.

Cooke, B. E. (2007), Investigation of the effects of biofouling on the hydraulic properties of wells in fractured bedrock aquifers, 146 pp, Unpublished Master's thesis, Queen's University, Kingston.

Corbett, D. R., W. C. Burnett, P. H. Cable, and S. B. Clark (1997), Radon tracing of groundwater input into Par Pond, Savannah River Site, *Journal of Hydrology*, *203*, 209-227.

Cox, M. H., G. W. Su, and J. Constantz (2007), Heat, chloride, and specific conductance as ground water tracers near streams, *Ground Water*, *45*, 187-195.

Culotta, R. C., T. Pratt, and P. J. Oliver (1990), A tale of two sutures: COCORP's deep seismic surveys of the Grenville province in the eastern U.S. midcontinent, *Geology*, *18*, 646-649.

Daniel, C. (1973), One-at-a-time plans, *Journal of American Statistical Association*, *68*, 353-360.

Danielopol, D. L., C. Griebler, A. Gunatilaka, and J. Notenboom (2003), Present state and future prospects for groundwater ecosystems, *Environmental Conservation*, *30*, 104-130.

Danielopol, D. L., J. Gibert, C. Griebler, A. Gunatilaka, H. Jurgen, G. Messana, J. Notenboom, and B. Sket (2004), Incorporating ecological perspectives in European groundwater management policy, *Environmental Conservation*, *31*, 185-189.

Davidson, A., and J. W. F. Ketchum (1993), Observations of the Maberly shear zone, a terrane boundary within the Central Metasedimentary Belt, Grenville Province, Ontario, in *Geological Survey of Canada, Current Research, Paper 93-1C*, edited, pp. 265-269.

Davison, C. C., and E. T. Kozak (1988), Hydrogeological characteristics of major fracture zones in a granite batholith of the Canadian Shield., paper presented at Canadian/American Conference on Hydrogeology 4., National Water Well Association.

Day-Lewis, F. D., P. A. Hsieh, and S. M. Gorelick (2000), Identifying fracture-zone geometry using simulated annealing and hydraulic-connection data, *Water Resources Research*, *36*, 1707-1721.

Denny, S. C., D. M. Allen, and J. M. Journeay (2007), DRASTIC-Fm: a modified vulnerability mapping method for structurally controlled aquifers in the southern Gulf Islands, British Columbia, Canada, *Hydrogeology Journal*, *15*, 483-493.

Desbarats, A., and S. Bachu (1994), Geostatistial analysis of aquifer heterogeneity from the core scale to basin scale: a case study, *Water Resources Research*, *30*, 673-684.

Devito, K. J., A. R. Hill, and N. Roulet (1996), Groundwater-surface water interactions in headwater forested wetlands of the Canadian Shield, *Journal of Hydrology*, *181*, 127-147.

Easton, R. M. (1992), The Grenville Province, in *Geology of Ontario, Ontario Geological Survey, Special Volume 4, Part 2*, edited by P. C. Thurston, et al., pp. 713-904, Toronto.

Easton, R. M. (2001), Precambrian geology, Tichborne area, Ontario Geological Survey Map P.3442.

Edet, A. E., C. S. Okereke, S. C. Teme, and E. O. Esu (1998), Application of remote-sensing data to groundwater exploration: a case study of the Cross River State, southeastern Nigeria, *Hydrogeology Journal*, *6*, 394-404.

Ellins, K. K., A. Roman-Mas, and R. Lee (1990), Using ^{222}Rn to examine groundwater/surface discharge interaction in the Rio Grande de Manati, Puerto Rico, *Journal of Hydrology*, *115*, 319-341.

EPA (2002), Environmental Protection Agency, 40 Code of Federal Regulations (CFR), Part 280, *Chapter 1*, 375.

Evans, J. P. (1988), Deformation mechanisms in granitic rocks at shallow crustal levels, *Journal of Structural Geology*, *10*, 437-443.

Evans, J. P., and F. M. Chester (1995), Fluid-rock interaction in faults of the San Andres system: Inferences from San Gabriel fault rock geochemistry and microstructures, *Journal of Geophysical Research*, *100*, 13007-13020.

Evans, J. P., C. B. Forster, and J. V. Goddard (1997), Permeability of fault-related rocks, and the implications for hydraulic structure of fault zones, *Journal of Structural Geology*, *19*, 1393-1404.

Fairley, J. P., and J. J. Hinds (2004), Rapid transport pathways for geothermal fluids in an active Great Basin fault zone, *Geology*, *32*, 825-828.

Fan, Y., L. Toran, and R. W. Schlische (2007), Groundwater flow and groundwater-stream interaction in fractured and dipping sedimentary rocks: insights from numerical models, *Water Resources Research*, *43*, W01409, doi:01410.01029/02006WR004864.

Farvolden, R. N., O. Pfannkuch, R. Pearson, and P. Fritz (1988), Region 12, Precambrian Shield, in *The Geology of North America Vol. O-2, Hydrogeology*, edited by W. Back, et al., pp. 101-114, Geological Society of America, Boulder.

Ferrill, D. A., D. W. Sims, D. J. Waiting, A. P. Morris, N. M. Franklin, and A. L. Schultz (2004), Structural framework of the Edwards Aquifer recharge zone in south-central Texas, *Geological Society of America Bulletin*, *116*, 407 - 418.

Fetter, C. W. (2001), *Applied hydrogeology*, Prentice-Hall, Upper Saddle River, NJ. 598 pp.

Flint, A. L., L. E. Flint, E. M. Kwicklis, G. S. Bodvarsson, and J. M. Fabryka-Martin (2001), Hydrology of Yucca Mountain, *Reviews of Geophysics*, *39*, 447-470.

Flint, A. L., L. E. Flint, E. M. Kwicklis, J. M. Fabryka-Martin, and G. S. Bodvarsson (2002), Estimating recharge at Yucca Mountain, Nevada, USA: comparison of methods, *Hydrogeology Journal*, *10*, 180-204.

Folger, P. F., E. P. Poeter, R. B. Wanty, D. Frishman, and W. Day (1996), Controls on ^{222}Rn variations in a fractured crystalline rock aquifer evaluated using aquifer tests and geophysical logging, *Ground Water*, *34*, 250-261.

Follin, S., M. Stigsson, and U. Svensson (2005), Regional hydrogeological simulations for Forsmark - numerical modelling using DarcyTools 159 pp, SKB R-05-60.

Forster, C. B., and J. P. Evans (1991), Hydrogeology of thrust faults and crystalline thrust sheets: results from combined field and modeling studies, *Geophysical Research Letters*, *19*, 979-982.

Fredrick, K. C., M. W. Becker, L. S. Matott, A. Daw, K. Bandilla, and D. M. Flewelling (2007), Development of a numerical groundwater flow model using SRTM elevations, *Hydrogeology Journal*, *15*, 171-181.

Freeze, R. A., and P. A. Witherspoon (1967), Theoretical analysis of regional groundwater flow, 2. Effect of water-table configuration and subsurface permeability variation, *Water Resources Research*, *3*, 623-634.

Freeze, R. A., and J. A. Cherry (1979), *Groundwater*, Prentice-Hall Inc., Eaglewood Cliffs, NJ. 604 pp.

French, H., and A. Binley (2004), Snowmelt infiltration: monitoring temporal and spatial variability using time-lapse electrical resistivity, *Journal of Hydrology*, *297*, 174-186.

Gascoyne, M. (2004), Hydrogeochemistry, groundwater ages and sources of salts in a granitic batholith on the Canadian Shield, southeastern Manitoba, *Applied Geochemistry*, *19*, 519-560.

Gascoyne, M., D. M. Wuschke, and E. M. Durrance (1993), Fracture detection and groundwater flow characterization using He and Rn in soil gases, Manitoba, Canada, *Applied Geochemistry*, *8*, 223-233.

Gburek, W. J., and G. J. Folmar (1999a), A ground water recharge field study: site characterization and initial results, *Hydrological processes*, *13*, 2813-2831.

Gburek, W. J., and G. J. Folmar (1999b), Flow and chemical contributions to streamflow in an upland watershed: a baseflow survey, *Journal of Hydrology*, *217*, 1-18.

Genereux, D. P., H. F. Hemond, and P. J. Mulholland (1993), Use of radon-222 and calcium as tracers in a three-end-member mixing model for streamflow generation on the west fork of the Walker Branch Watershed, *Journal of Hydrology*, *142*, 167-211.

Gleeson, T., K. S. Novakowski, J. Levison, and K. Kyser (2007), Groundwater recharge in bedrock aquifers: rapid, localized and limited, paper presented at GSA 2006 Annual Meeting, Denver.

Goddard, J. V., and J. P. Evans (1995), Chemical changes and fluid-rock interaction in faults of crystalline thrust sheets, northwestern Wyoming, U.S.A., *Journal of Structural Geology*, *12*, 869-882.

Golder Associates Ltd. (2003), Renfrew county-Mississippi-Rideau groundwater study, 34 pp, Ottawa.

Gonfiantini, R. (1986), Environmental isotopes in lake studies, in *Handbook of environmental isotope geochemistry: Volume 2, The Terrestrial Environment*, edited by P. Fritz and J. C. Fontes, pp. 113-168, Elsevier, Amsterdam.

Gustafsson, P. (1994), SPOT satellite data for exploration of fractured aquifers in a semi-arid area in southeastern Botswana, *Applied Hydrogeology*, *2*, 9-18.

Harvey, F. E., D. R. Lee, D. L. Rudolph, and S. K. Frape (1997), Locating groundwater discharge in large lakes using bottom sediment electrical conductivity mapping, *Water Resources Research*, *33*, 2609-2615.

Hayashi, M., and D. O. Rosenberry (2002), Effects of ground water exchange on the hydrology and ecology of surface water, *Ground Water*, *40*, 309-316.

Hayashi, M., G. van der Kamp, and R. Schmidt (2003), Focused infiltration of snowmelt water in partially frozen soil under small depressions, *Journal of Hydrology*, *270*, 214-229.

Healy, R., and P. Cook (2002), Using groundwater levels to estimate recharge, *Hydrogeology Journal*, *10*, 91-109.

Heppner, C., J. Nimmo, G. Folmar, W. Gburek, and D. Risser (2007), Multiple-methods investigation of recharge at a humid-region fractured rock site, Pennsylvania, USA, *Hydrogeology Journal*, *15*, 915-927.

Hill, M. C. (2006), The practical use of simplicity in developing ground water models, *Ground Water*, *44*, 775-781.

Hill, M. C., and C. R. Tiedeman (2007), *Effective groundwater model calibration*, Wiley. 455 pp.

Hinton, M. J. (2005), Methodology for measuring the spatial distribution of low streamflow within watersheds, 62 pp, Geological Survey of Canada Open File 4891.

Hiscock, K. M., M. O. Rivett, and R. M. Davison (2002), Sustainable groundwater development, in *Sustainable groundwater development*, edited by K. M. Hiscock, et al., pp. 1-14, Geological Society, London, Special Publications.

Holzhausen, G. R. (1989), Origin of sheet structure, 1. Morphology and boundary conditions, *Engineering Geology*, *27*, 225-278.

Hsieh, P. A. (1998), Scale effects in fluid flow through fractured geologic media, in *Scale dependence and scale independence in hydrology*, edited by G. Sposito, pp. 335-353, Cambridge University Press.

Hsieh, P. A., and A. M. Shapiro (Eds.) (1996), *Hydraulic characteristics of fractured bedrock underlying the FSE well field at the Mirror Lake site, Grafton County, New Hampshire*, 127-130 pp., U.S. Geological Survey Toxic Substances Hydrology Program--Proceedings of the technical meeting, Colorado Springs, Colorado, September 20-24, 1993: U.S. Geological Survey Water-Resources Investigations Report 94-4015, v. 1.

Hvorslev, M. J. (1951), *Time lag and soil permeability in ground-water observations*, U.S. Army Corps of Engineers Waterways Experimental Station Bulletin, no.36. 50 pp.

Isachsen, Y. W. (1976), Fracture analysis of New York state using multi-stage remote sensing data and ground study; possible application to plate tectonic modeling, in *Proceedings of the First International Conference on the New Basement Tectonics*, edited by R. A. Hodgson, et al., pp. 200-217, Utah Geological Association Publication No.5, Salt Lake City.

Jackson, J. A., ed. (1997), *Glossary of Geology* Geological Institute, Alexandria, VA

Kalbus, E., F. Reinstorf, and M. Schirmer (2006), Measuring methods for groundwater- surface water interactions: a review, *Hydrology and Earth System Sciences*, *10*, 873-887.

Karasaki, K., B. Freifeld, A. Cohen, K. Grossenbacher, P. Cook, and D. Vasco (2000), A multidisciplinary fractured rock characterization study at Raymond field site, Raymond, CA, *Journal of Hydrology*, *236*, 17-34.

Kay, G. M. (1942), Ottawa-Bonnechere Graben and Lake Ontario Homocline, *Geological Society of America Bulletin*, *53*, 585-646.

Kennedy, P. L., and A. D. Woodbury (2002), Geostatistics and Bayesian updating from transmissivity estimation in a multiaquifer system in Manitoba, Canada, *Ground Water*, *40*, 273-283.

Kettles, I. M. (1992), *Glacial geology and glacial sediment geochemistry in the Clyde Forks-Westport area of Ontario*, Geological Survey of Canada. 34 pp.

Kluge, T., J. Ilmberger, C. von Rohden, and W. Aeschbach-Hertig (2007), Tracing and quantifying groundwater inflow into lakes using a simple method for radon-222 analysis, *Hydrology and Earth System Sciences*, *11*, 1621-1631.

Konzuk, J. S., and B. H. Kueper (2004), Evaluation of cubic law based models describing single-phase flow through a rough-walled fracture, *Water Resources Research*, *40*, W02402, doi:02410.01029/02003WR002356.

Kotzer, T., M. Gascoyne, M. Mukai, J. Ross, G. Waito, G. Milton, and R. J. Cornett (1998), 36Cl, 129I and noble gas isotope systematics in groundwaters from the Lac du Bonnet batholith, Manitoba, Canada, *Radiochimica Acta*, *82*, 313-318.

Krásný, J., and J. M. Sharp (2007), Hydrogeology of fractured rocks from particular fractures to regional approaches: state-of-the-art and future challenges, in *Groundwater in Fractured Rocks, IAH Selected Paper Series, volume 9*, edited by J. Krásný and J. M. Sharp, pp. 1-32, Taylor and Francis, London.

Krishnamurthy, J., A. Mani, V. Jayaraman, and M. Manivel (2000), Groundwater resources development in hard rock terrain - an approach using remote sensing and GIS techniques, *International Journal of Applied Earth Observation and Geoinformation*, *2*, 204-215.

Kumarapeli, P. S. (1978), The St. Lawrence paleo-rift system: a comparative study, in *Tectonics and Geophysics of Continental Rifts*, edited by I. B. Ramberg and E. R. Neumann, pp. 367-384, D.Reidel Publishing, Dordrecht, Holland.

Kumarapeli, P. S. (1981), Origin and development of the Ottawa graben, in *Abstracts of papers presented at the conference on Processes of Planetary Rifting*, edited, pp. 114-116, Lunar and Planetary Institute, Houston.

La Pointe, P. R., and J. A. Hudson (1985), *Characterization and interpretation of rock mass joint patterns*, Geological Society of America, Boulder, CO. 37 pp.

Lai, J., and L. Ren (2007), Assessing the size dependency of measured hydraulic conductivity using double-ring infiltrometers and numerical simulation, *Soil Science Society of America Journal*, *71*, 1667-1675.

Lattman, L. H., and R. R. Parizek (1964), Relationship between fracture traces and the occurrence of groundwater in carbonate rocks, *Journal of Hydrology*, *2*, 73-91.

Lattman, L. H., and R. H. Matzke (1971), Fracture traces and joints in central Pennsylvania, *AAPG Bulletin*, *55*, 1878-1881.

Lee, D. R. (1977), A device for measuring seepage flux in lakes and estuaries, *Limnology and Oceanography*, *22*, 140-147.

Lee, D. R. (1985), Method for locating sediment anomalies in lakebeds that can be caused by groundwater flow, *Journal of Hydrology*, *79*, 187-193.

Lee, K. S., D. B. Wenner, and I. Lee (1999), Using H- and O-isotopic data for estimating the relative contributions of rainy and dry season precipitation to groundwater: example from Cheju Island, Korea, *Journal of Hydrology*, *222*, 65-74.

Lehr, J., J. Keeley, and J. Lehr (2005), *Water Encyclopedia, Volumes 1-5*, John Wiley & Sons.

Lerner, D. N. (1997), Groundwater recharge, in *Geochemical processes, weathering and groundwater recharge in catchments*, edited by O. M. Saether and P. de Caritat, pp. 109-150, Balkema, Rotterdam.

Lerner, D. N., A. S. Issar, and I. Simmers (1990), *Groundwater recharge: a guide to understanding and estimating natural recharge*, Verlag Heinz Heise, Hanover. 345 pp.

Levison, J., and K. S. Novakowski (2007), A novel tracer experiment conducted from ground surface water to a fractured rock aquifer, paper presented at 2007 US EPA/NGWA Fractured Rock Conference, Portland, Maine.

Levison, J., and K. S. Novakowski (2009), The impact of cattle pasturing on groundwater quality in bedrock aquifers having minimal overburden, *Hydrogeology Journal*, *17*, 559-569.

Li, Q., A. J. A. Unger, E. A. Sudicky, D. Kassenaar, E. J. Wexler, and S. Shikaze (2008), Simulating the multi-seasonal response of a large-scale watershed with a 3D physically-based hydrologic model, *Journal of Hydrology*, *357*, 317-336.

Love, A. J., C. T. Simmons, P. G. Cook, G. A. Harrington, A. L. Herczeg, and T. Halihan (2007), Estimating groundwater flow rates in fractured metasediments: Clare Valley, Australia, in *Groundwater in Fractured Rocks, IAH Selected Paper Series, volume 9*, edited by J. Krásný and J. M. Sharp, pp. 463-477, Taylor and Francis, London.

Lowry, C. S., J. F. Walker, R. J. Hunt, and M. P. Anderson (2007), Identifying spatial variability of groundwater discharge in a wetland system using a distributed temperature sensor, *Water Resources Research*, *43*, doi:10.1029/2007WR006145.

Mabee, S. B. (1999), Factors influencing well productivities in glaciated metamorphic rocks, *Ground Water*, *37*, 88-97.

Mabee, S. B., K. C. Hardcastle, and D. U. Wise (1994), A method of collecting and analyzing lineaments for regional-scale fractured-bedrock aquifer studies, *Ground Water*, *32*, 884-894.

Mabee, S. B., P. J. Curry, and K. C. Hardcastle (2002), Correlation of lineaments to ground water inflows in a bedrock tunnel, *Ground Water*, *40*, 37-43.

Magowe, M., and J. R. Carr (1999), Relationship between lineaments and ground water occurrence in Western Botswana, *Ground Water*, *37*, 282-286.

Manning, A. H., and J. S. Caine (2007), Groundwater noble gas, age, and temperature signatures in an Alpine watershed: Valuable tools in conceptual model development, *Water Resources Research*, *43*, doi:10.1029/2006WR005349.

Marler, J., and S. Ge (2003), The permeability of the Elkhorn fault zone, South Park, Colorado *Ground Water*, *41*, 321-332.

Mau, D. P., and T. C. Winter (1997), Estimating ground-water recharge from streamflow hydrographs for a small mountain watershed in a temperate humid climate, New Hampshire, USA, *Ground Water*, *35*, 291-304.

Mayer, J. R., and J. M. Sharp (1998), Fracture control of regional ground-water flow in a carbonate aquifer in a semi-arid region, *Geological Society of America Bulletin*, *110*, 269-283.

Mayo, A. L., T. H. Morris, S. Peltier, E. C. Petersen, K. Payne, L. S. Holman, D. Tingey, T. Fogel, B. J. Black, and T. D. Gibbs (2003), Active and inactive groundwater flow systems: evidence from a stratified, mountainous terrain, *Geological Society of America Bulletin*, *115*, 1456 - 1472.

McCoy, C. A., D. R. Corbett, B. A. McKee, and Z. Top (2007), An evaluation of submarine groundwater discharge along the continental shelf of Louisiana using a multiple tracer approach, *Journal of Geophysical Research*, *112*, doi:10.1029/2006JC003505.

Milloy, C. A. (2007), Measurement of hydraulic head for the evaluation of groundwater recharge to discrete fracture zones in a crystalline bedrock aquifer, 131 pp, Unpublished MSc. thesis, Queen's University, Kingston, ON.

Minor, S. A., and M. R. Hudson (2006), Regional survey of structural properties and cementation patterns of fault zones in the northern part of the Albuquerque Basin, New Mexico - implications fo ground-water flow, 34 pp, USGS Professional Paper 1719.

MOE (2006), Water well information system database. Ontario Ministry of the Environment. Toronto, ON.

Moore, G. K. (1992), Hydrograph seperation in a fractured rock terrane, *Ground Water*, *30*, 390-395.

Moore, R. B., G. E. Schwarz, S. F. Clark, Jr., G. J. Walsh, and J. R. Degnan (2002), Factors related to well yield in the fractured-bedrock aquifer of New Hampshire 51 pp, U.S. Geological Survey Professional Paper 1660.

Nastev, M., M. M. Savard, P. A. Lapcevic, R. Lefebvre, and R. Martel (2004), Hydraulic properties and scale effects investigation in regional rock aquifers, south-western Quebec, Canada, *Hydrogeology Journal*, *12*, 257-269.

NATChem (2008), Canadian National Atmospheric Chemistry (NATChem) Database, Meteorological Service of Canada, 4905 Dufferin Street, Toronto, Ontario, Canada M3H 5T4. http://www.msc.ec.gc.ca/natchem/index_e.html accessed October 1, 2008.

Neff, B. P., A. R. Piggott, and R. A. Sheets (2005), Estimation of shallow ground-water recharge in the Great Lake basin, 19 pp, U.S. Geological Survey Scientific Investigations Report 2005-5284.

Neuman, S. P. (1987), Stochastic continuum representation of fractured rock permeability as an alternative to the REV and fractured network concepts, in *Rock mechanics: proceedings of the 28th U.S. Symposium*, edited by I. W. Farmer, et al., pp. 533-561, Balkema, Rotterdam.

Neuman, S. P. (1990), Universal scaling of hydraulic conductivities and dispersivities in geologic media *Water Resources Research*, *26*, 1749-1758.

Neuman, S. P. (2005), Trends, prospects and challenges in quantifying flow and transport through fractured rocks, *Hydrogeology Journal*, *13*, 124-147.

Nilsson, C., C. A. Reidy, M. Dynesius, and C. Revenga (2005), Fragmentation and flow regulation of the world's large river systems, *Science*, *308*, 405-408.

Novakowski, K. S., P. A. Lapcevic, and E. A. Sudicky (2007a), Groundwater flow and solute transport in fractured media, in *Handbook of Groundwater Engineering*, edited by J. W. Delleur, pp. 20-21 - 20-43, CRC Press, Boca Ratan, FL.

Novakowski, K. S., G. S. Bickerton, P. A. Lapcevic, J. Voralek, and N. Ross (2006), Measurements of groundwater velocity in discrete rock fractures, *Journal of Contaminant Hydrology*, *82*, 44-60.

Novakowski, K. S., C. A. Milloy, T. Gleeson, T. W. Praamsma, J. Levison, and K. Hall (2007b), Groundwater recharge in a gneissic terrain having minimal overburden, paper presented at IAH Ottawa 2007.

NRC (1996), *Rock fractures and fluid flow: contemporary understanding and applications*, National Academy Press, Washington, DC. 551 pp.

Nyborg, M., J. Berglund, and C.-A. Triumf (2007), Detection of lineaments using airborne laser scanning technology: Laxemar-Simpevarp, Sweden, *Hydrogeology Journal*, *15*, 29-32.

O'Leary, D. W., J. D. Friedman, and H. A. Pohn (1976), Lineament, linear, lineation: some proposed new standards for old terms, *Geological Society of America Bulletin*, *87*, 1463-1469.

Oxtobee, J. P. A., and K. S. Novakowski (2002), A field investigation of groundwater/surface water interaction in a fractured bedrock environment, *Journal of Hydrology*, *269*, 169-193.

Panday, S., and P. S. Huyakorn (2004), A fully coupled physically-based spatially-distributed model for evaluating surface/subsurface flow, *Advances in Water Resources*, *27*, 361-382.

Peters, D. L., J. M. Buttle, C. H. Taylor, and B. D. LaZerte (1995), Runoff production in a forested, shallow soil, Canadian Shield basin, *Water Resources Research*, *31*, 1291-1304.

Peters, N. E., J. B. Shanley, B. T. Aulenbach, R. M. Webb, D. H. Campbell, R. Hunt, M. C. Larsen, R. F. Stallard, J. Troester, and J. F. Walker (2006), Water and solute mass balance of five small, relatively undisturbed watersheds in the U.S, *Science of The Total Environment*, *358*, 221-242.

Pool, D. R., and J. H. Eychaner (1995), Measurements of aquifer-storage change and specific yield using gravity surveys, *Ground Water*, *33*, 425-432.

Praamsma, T. W. (2006), Complex groundwater-surface water interaction in a gneissic terrain, 115 pp, Unpublished MSc. thesis, Queen's University, Kingston.

Praamsma, T. W., S. Trimper, and K. S. Novakowski (2009a), Surface to fracture transport of e. coli-sized microspheres and a conservative tracer in a fractured rock aquifer, Perth, Ontario, paper presented at First International Conference on Microbial Transport and Survival in Porous Media, Niagara-on-the-Lake, ON.

Praamsma, T. W., K. S. Novakowski, T. K. Kyser, and K. Hall (2009b), Using stable isotope and hydraulic head data to investigate groundwater recharge and discharge in a fractured rock aquifer, *Journal of Hydrology*, *366*, 35-45.

Prost, G. L. (1994), *Remote sensing for geologists: a guide to image interpretation*, Gordon and Breach Science Amsterdam. 326 pp.

Randall, J. E. (2005), The analysis of seasonally varying flow in a crystalline rock watershed using an integrated surface water and groundwater model, 88 pp, Unpublished MSc. thesis, University of Waterloo.

Rawling, G. C., L. B. Goodwin, and J. L. Wilson (2001), Internal architecture, permeability and hydrologic significance of contrasting fault-zone types, *Geology*, *29*, 43-46.

Rayne, T., K. Bradbury, and M. Muldoon (2001), Delineation of capture zones for municipal wells in fractured dolomite, Sturgeon Bay, Wisconsin, USA, *Hydrogeology Journal*, *9*, 432-450.

Redclift, M. (1987), *Sustainable development: exploring the contradictions*, Methuen, London. 221 pp.

Reitsma, S., and B. H. Kueper (1994), Laboratory measurement of capillary pressure-saturation relationships in a rock fracture, *Water Resources Research*, *30*, 865-878.

Reynolds, W. D. (1993), Saturated hydraulic conductivity: field measurement, in *Soil sampling and methods of analysis*, edited by M. R. Carter, pp. 599-613, Canadian Society of Soil Science.

Rideau Valley Conservation Authority and Mississippi Valley Conservation Authority (2006), Conceptual understanding of the water budget, Interm report, 66 pp, Manotick, ON.

Rimando, R. E., and K. Benn (2005), Evolution of faulting and paleo-stress field within the Ottawa graben, Canada, *Journal of Geodynamics*, *39*, 337-360.

Risser, D., W. Gburek, and G. Folmar (2009), Comparison of recharge estimates at a small watershed in east-central Pennsylvania, USA, *Hydrogeology Journal*, *17*, 287-298; doi: 210.1007/s10040-10008-10406-y.

Risser, D. W., W. J. Gburek, and G. J. Folmar (2005), Comparision of methods for estimating ground-water recharge and base flow at a small watershed underlain by fractured bedrock in the eastern United States, 31 pp, USGS Scientific Investigations Report 2005-5038.

Rodhe, A. (1998), Snowmelt-dominated systems, in *Isotope tracers in catchment hydrology*, edited by C. Kendall and J. J. McDonnell, pp. 391-434, Elsevier.

Rodhe, A., and N. Bockgard (2006), Groundwater recharge in a hard rock aquifer: a conceptual model including surface-loading effects, *Journal of Hydrology*, *330*, 389-401.

Rogers, A. S. (1958), Physical behavior and geologic control of radon in mountain streams, 187-207 pp, US Geological Survey Bulletin 1052-E.

Rorabaugh, M. I. (1964), Estimating changes in bank storage and groundwater contribution to stream flow, in *International Association of Scientific Hydrology Publication 63*, edited, pp. 432-441.

Rosenberry, D. O., and T. C. Winter (1993), The significance of fracture flow to the water balance of a lake in fractured crystalline rock terrane., in *Hydrogeology of Hard Rocks, Memoirs of the XXIVth Congress of the International Association of Hydrogeologists*, edited by S. Banks and D. Banks, pp. 967-977, Oslo, Norway.

Rutledge, A. T., and C. C. I. Daniel (1994), Testing an automated method to estimate ground-water recharge from streamflow records, *Ground Water*, *32*, 180-189.

Saltelli, A., K. Chan, and E. M. Scott (Eds.) (2000), *Sensitivity analysis*, 465 pp., Wiley.

Sander, P. (2007), Lineaments in groundwater exploration: a review of applications and limitations, *Hydrogeology Journal*, *15*, 71-74.

Sander, P., T. B. Minor, and M. M. Chesley (1997), Ground-water exploration based on lineament analysis and reproducibility tests, *Ground Water*, *35*, 888-894.

Sanford, S. E., I. F. Creed, C. L. Tague, F. D. Beall, and J. M. Buttle (2007), Scale-dependence of natural variability of flow regimes in a forested landscape, *Water Resources Research*, *43*, W08414, doi:08410.01029/02006WR005299.

Sanford, W. (2002), Recharge and groundwater models: an overview, *Hydrogeology Journal*, *10*, 110-120.

Scanlon, B., R. Healy, and P. Cook (2002), Choosing appropriate techniques for quantifying groundwater recharge, *Hydrogeology Journal*, *10*, 18-39.

Schroeder, P. R., T. S. Dozier, P. A. Zappi, B. M. McEnroe, J. W. Sjostrom, and R. L. Payton (1997), The Hydrologic Evaluation of Landfill Performance (HELP) Model, Engineering Documentation for Version 3. U.S. Army Corps of Engineers, Vicksburg, MS., 84 pp.

Schulz, S. E., and J. P. Evans (2000), Mesoscopic structure of Punchbowl Fault, Southern California and the geological and geophysical structure of active strike-slip faults, *Journal of Structural Geology*, *22*, 913-930.

Schulze-Makuch, D., D. A. Carlson, D. S. Cherkauer, and P. Malik (1999), Scale dependency of hydraulic conductivity in heterogeneous media, *Ground Water*, *37*, 904-919.

Scurlock, J. M. O., G. P. Asner, and S. T. Gower. (2001), Worldwide historical estimates and bibliography of leaf area index, 1932-2000. Oak Ridge National Laboratory Technical Memorandum TM-2001/268. Oak Ridge, Tennessee, U.S.A., 40 pp.

Seaton, W. J., and T. J. Burbey (2005), Influence of ancient thrust faults on the hydrogeology of the Blue Ridge province, *Ground Water*, *43*, 301-313.

Sener, E., A. Davraz, and M. Ozcelik (2005), An integration of GIS and remote sensing in groundwater investigations: a case study in Burdur, Turkey, *Hydrogeology Journal*, *13*, 826-834.

Shaban, A., M. Khawlie, and C. Abdallah (2006), Use of remote sensing and GIS to determine recharge potential zones: the case of Occidental Lebanon, *Hydrogeology Journal*, *14*, 433-443.

Shapiro, A. M. (2001), Effective matrix diffusion in kilometer-scale transport in fractured crystalline rock, *Water Resources Research*, *37*, 507-522.

Sharma, M. L., G. A. Gander, and C. G. Hunt (1980), Spatial variability of infiltration in a watershed, *Journal of Hydrology*, *45*, 101-122.

Siddiqui, S. H., and R. R. Parizek (1971), Hydrogeological factors affecting well-yields in folded and faulted carbonate rocks in central Pennsylvania, *Water Resources Research*, *7*, 85-97.

Singer, S. N., C. K. Cheng, and M. G. Scafe (2003), Hydrogeology of Southern Ontario, 200 pp, Ontario Ministry of the Environment.

Singhal, B. B. S., and R. P. Gupta (1999), *Applied hydrogeology of fractured rocks*, Kluwer, Dordrecht. 399 pp.

Smakhtin, V. U. (2001), Low flow hydrology: a review, *Journal of Hydrology*, *240*, 147-186.

Solomon, D. K., S. L. Schiff, R. J. Poreda, and W. B. Clarke (1993), A validation of the $^3H/^3He$ method for determining groundwater recharge, *Water Resources Research*, *29*, 2951-2962.

Solomon, S., and F. Quiel (2006), Groundwater study using remote sensing and geographic information systems (GIS) in the central highlands of Eritrea, *Hydrogeology Journal*, *14*, 729-741.

Sophocleous, M. (1992), Groundwater recharge estimation and regionalization: the Great Bend Prairie of central Kansas and its recharge statistics, *Journal of Hydrology*, *137*, 113-140.

Sophocleous, M. (1997), Managing water resources systems: why "safe yield" is not sustainable, *Ground Water*, *35*, 561.

Sophocleous, M. (2000), From safe yield to sustainable development of water resources - the Kansas experience, *Journal of Hydrology*, *235*, 27-43.

Sophocleous, M. (2002), Interactions between groundwater and surface water: the state of the science, *Hydrogeology Journal*, *10*, 52-67.

Soulsby, C., and D. Tetzlaff (2008), Towards simple approaches for mean residence time estimation in ungauged basins using tracers and soil distributions, *Journal of Hydrology*, *363*, 60-74.

Spence, C., and M.-k. Woo (2003), Hydrology of subarctic Canadian shield: soil-filled valleys, *Journal of Hydrology*, *279*, 151-166.

Spence, C., P. H. Whitfield, and T. B. M. J. Ouarda (2008), Introduction to the special issue on low-flow prediction in ungauged basins (PUB) in Canada, *Canadian Water Resources Journal*, *33*, 103-106.

Spitzer, R. (1981), Landsat and Seasat data for lineament and lithologic mapping in southeastern Ontario, 190 pp, Unpublished MSc. McMaster University.

Steedman, R. J., C. J. Allen, R. L. France, and R. S. Kushneriuk (2004), Land, water, and human activity on boreal watersheds, in *Boreal shield watersheds: lake trout ecosystems in a changing environment*, edited by J. M. Gunn, et al., pp. 59-85, Lewis Publishers, Boca Raton, FL.

Stellato, L., E. Petrella, F. Terrasi, P. Belloni, M. Belli, U. Sansone, and F. Celico (2008), Some limitations in using ^{222}Rn to assess river–groundwater interactions: the case of Castel di Sangro alluvial plain (central Italy), *Hydrogeology Journal*, *16*, 701-712.

Stephenson, M., W. J. Schwartz, L. D. Evenden, and G. A. Bird (1992), Identification of deep groundwater discharge areas in the Boggy Creek catchment, southeastern Manitoba, using excess aqueous helium, *Canadian Journal of Earth Science*, *29*, 2640-2652.

Sukhija, B. S., D. V. Reddy, P. Nagabhushanam, S. K. Bhattacharya, R. A. Jani, and K. Devender (2006), Characterisation of recharge processes and groundwater flow mechanisms in weathered-fractured granites of Hyderabad (India) using isotopes, *Hydrogeology Journal*, *14*, 663-674.

Surrette, M. J. (2006), Quantifying heterogeneity in variability fractured rock using a hydrostructural domain approach, Gulf Islands, British Columbia, Simon Fraser University Unpublished MSc. thesis.

Sykes, J. F., S. D. Normani, and E. A. Sudicky (2003), Regional scale groundwater flow in a Canadian Shield setting, 46 pp, Ontario Power Generation 06819-REP-01200-10114-R00.

Tam, V. T., F. De Smedt, O. Batelaan, and A. Dassargues (2004), Study on the relationship between lineaments and borehole specific capacity in a fractured and karstified limestone area in Vietnam, *Hydrogeology Journal*, *12*, 662-673.

Taniguchi, M., W. C. Burnett, J. E. Cable, and J. V. Turner (2002), Investigation of submarine groundwater discharge, *Hydrological Processes*, *16*, 2115-2129.

Tetzlaff, D., and C. Soulsby (2008), Sources of baseflow in larger catchments - using tracers to develop a holistic understanding of runoff generation, *Journal of Hydrology*, *359*, 287-302.

Theis, C. V. (1940), The source of water derived from wells, *Civil Engineering*, *10*, 277-280.

Therrien, R., and E. A. Sudicky (1996), Three-dimensional analysis of variably-saturated flow and solute transport in discretely-fractured porous media, *Journal of Contaminant Hydrology*, *23*, 1-44.

Therrien, R., R. G. McLaren, E. A. Sudicky, and S. M. Panday (2006), *HydroGeoSphere: a three-dimensional numerical model describing fully-integrated subsurface and surface flow and solute transport.*, Unpublished User Manual. Groundwater Simulations Group, Waterloo, ON. 349 pp.

Thompson, C., L. Smith, and R. Maji (2007), Hydrogeological modeling of submarine groundwater discharge on the continental shelf of Louisiana, *Journal of Geophysical Research*, *112*, doi:10.1029/2006JC003557.

Thorne, G. A., and M. Gascoyne (1993), Groundwater recharge and discharge characteristics in granitic terranes of the Canadian Shield, in *Hydrogeology of Hard Rocks: Memoires of the XXIVth Congress of the International Association of Hydrogeologists*, edited by S. Banks and D. Banks, pp. 368-374, Geological Survey of Norway, Oslo.

Tiedeman, C. R., D. J. Goode, and P. A. Hsieh (1998), Characterizing a ground water basin in a New England mountain and valley terrain, *Ground Water*, *36*, 611-620.

Tóth, J. (1962), A theory of groundwater motion in small drainage basins in Central Alberta, Canada, *Journal of Geophysical Research*, *67*, 4375-4387.

Veeger, A. I., and N. C. Ruderman (1998), Hydrogeologic controls on radon-222 in a buried valley-fractured bedrock aquifer system, *Ground Water*, *36*, 596-604.

Wanninkhof, R., P. J. Mulholland, and J. W. Elwood (1990), Gas exchange rates for a first-order stream determined with deliberate and natural tracers, *Water Resources Research*, *26*, 1621-1630.

Waters, P., D. Greenbaum, P. L. Smart, and H. Osmaston (1990), Applications of remote sensing to groundwater hydrology, *Remote Sensing Reviews*, *4*, 223-264.

Weeks, E. P. (2002), The Lisse effect revisited, *Ground Water*, *40*, 652-656.

Wellman, T. P., and E. P. Poeter (2005), Estimating spatially variable representative elementary scales in fractured architecture using hydraulic head observations, *Water Resources Research*, *41*, doi:10.1029/2004WR003287.

Wellman, T. P., and E. P. Poeter (2006), Evaluating uncertainty in predicting spatially variable representative elementary scales in fractured aquifers, with application to Turkey Creek Basin, Colorado, *Water Resources Research*, *42*, doi:10.1029/2005WR004431.

Wilson, M. E. (1961), Geology, Perth, Lanark and Leeds Counties, Ontario, Geological Survey of Canada, Map 1089A.

Winter, T. C. (1978), Numerical simulation of steady-state three-dimensional groundwater flow near lakes, *Water Resources Research*, *14*, 245-254.

Winter, T. C. (1981), Uncertainties in estimating the water balance of lakes, *Journal of the American Water Resources Association*, *17*, 82-115.

Winter, T. C. (1999), Relation of streams, lakes, and wetlands to groundwater flow systems, *Hydrogeology Journal*, *7*, 28-45.

Winter, T. C. (2001), The concept of hydrologic landscapes, *Journal of the American Water Resources Association*, *37*, 335-349.

Winter, T. C. (2007), The role of ground water in generating streamflow in headwater areas and in maintaining base blow, *Journal of the American Water Resources Association*, *43*, 15-25.

Wise, D. U. (1982), Linesmanship and the practice of linear geo-art, *Geological Society of America Bulletin*, *93*, 886-888.

Wise, D. U., R. Funiciello, M. Parotto, and F. Salvini (1985), Topographic lineament swarms: clues to their origin from domain analysis in Italy, *Geological Society of America Bulletin*, *96*, 952-967.

Wood, E. F., M. Sivapalan, K. Beven, and L. Band (1988), Effects of spatial variability and scale with implications to hydrologic modeling, *Journal of Hydrology*, *102*, 29-47.

Wood, W. W., T. F. Kraemer, and A. Shapiro (2004), Radon (^{222}Rn) in ground water of fractured rocks: a diffusion/ion exchange model, *Ground Water*, *42*, 552-567.

Woods, R., M. Sivapalan, and M. Duncan (1995), Investigating the representative elementary area concept: An approach based on field data, *Hydrological Processes*, *9*, 291-312.

Yeh, T.-C. J., C.-H. Lee, K.-C. Hsu, W. A. Illman, W. Barrash, X. Cai, J. Daniels, E. Sudicky, L. Wan, G. Li, and C. L. Winter (2008), A view toward the future of subsurface characterization: CAT scanning groundwater basins, *Water Resources Research*, *44*.

Zanini, L., K. S. Novakowski, P. A. Lapcevic, G. S. Bickerton, J. Voralek, and C. Talbot (2000), Ground water flow in a fractured carbonate aquifer inferred from combined hydrogeological and geochemical measurements, *Ground Water*, *38*, 350-360.

Appendix A: Well data

Appendix A compiles well data for the five wells (TW12-16) drilled and tested using the methodology outlined in Chapter 2. Additionally, transmissivity data for wells TW3-16 is compiled in Table A.1. The wells are located in Figure 2.1. For wells TW12-16, the geology, fracture patterns and static water levels from field notes is summarized on the left. In the center is the transmissivity of discrete intervals from slug testing. The well completion of piezometers and open intervals is summarized on the right. For TW14, the drawdown of piezometers during development is also included. The limited drawdown in adjacent piezometers suggests the connection between the wells is due to vertical fractures rather than well completion. *Milloy* [2007], *Praamsma et al.* [2009b] and *Levison and Novakowski* [2009] compile well data for TW1-11.

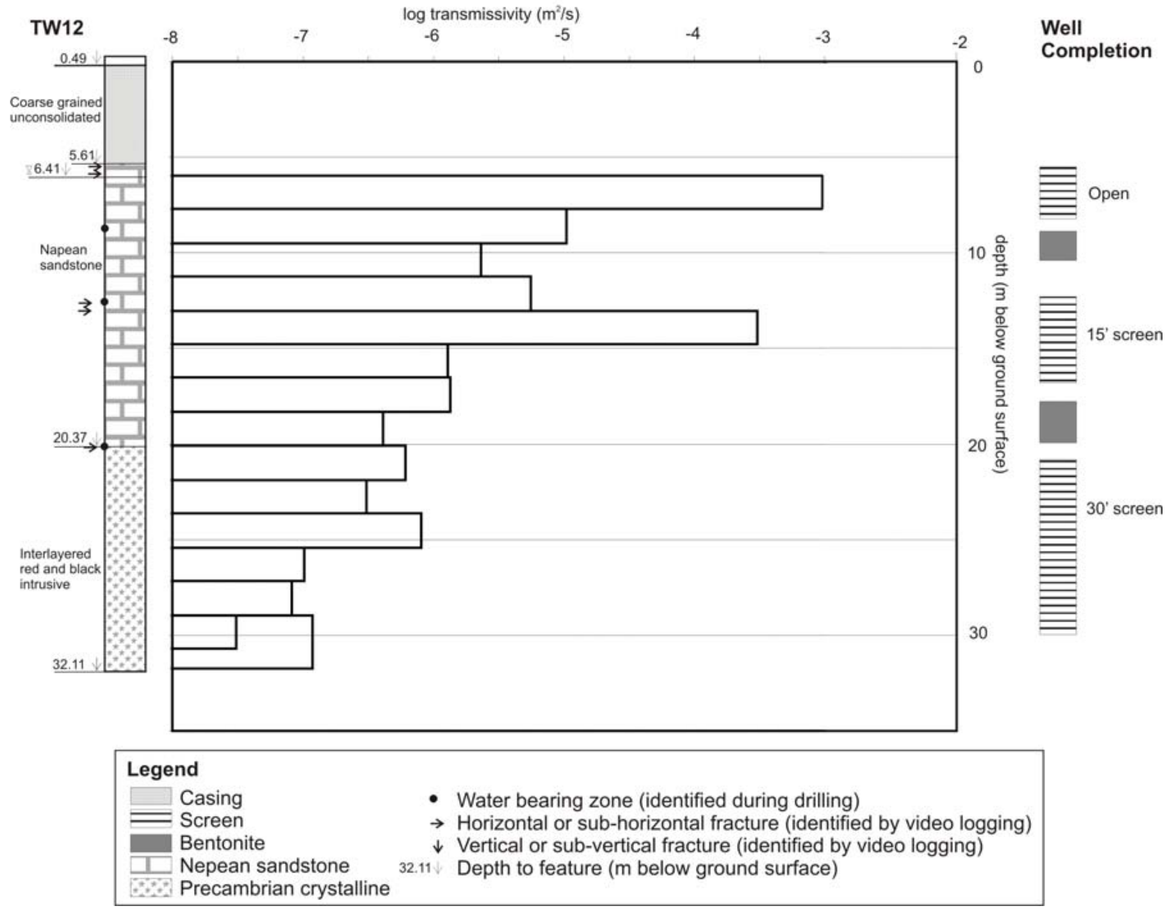
TW12
log transmissivity (m²/s)
-8
-7
-6
-5
-4
-3
-2
0
10
20
30
depth (m below ground surface)
Well Completion
0.49
Coarse grained unconsolidated
5.61
6.41
Napean sandstone
20.37
Interlayered red and black intrusive
32.11
Open
15' screen
30' screen
Legend
Casing
Screen
Bentonite
Nepean sandstone
Precambrian crystalline
Water bearing zone (identified during drilling)
Horizontal or sub-horizontal fracture (identified by video logging)
Vertical or sub-vertical fracture (identified by video logging)
32.11
Depth to feature (m below ground surface)

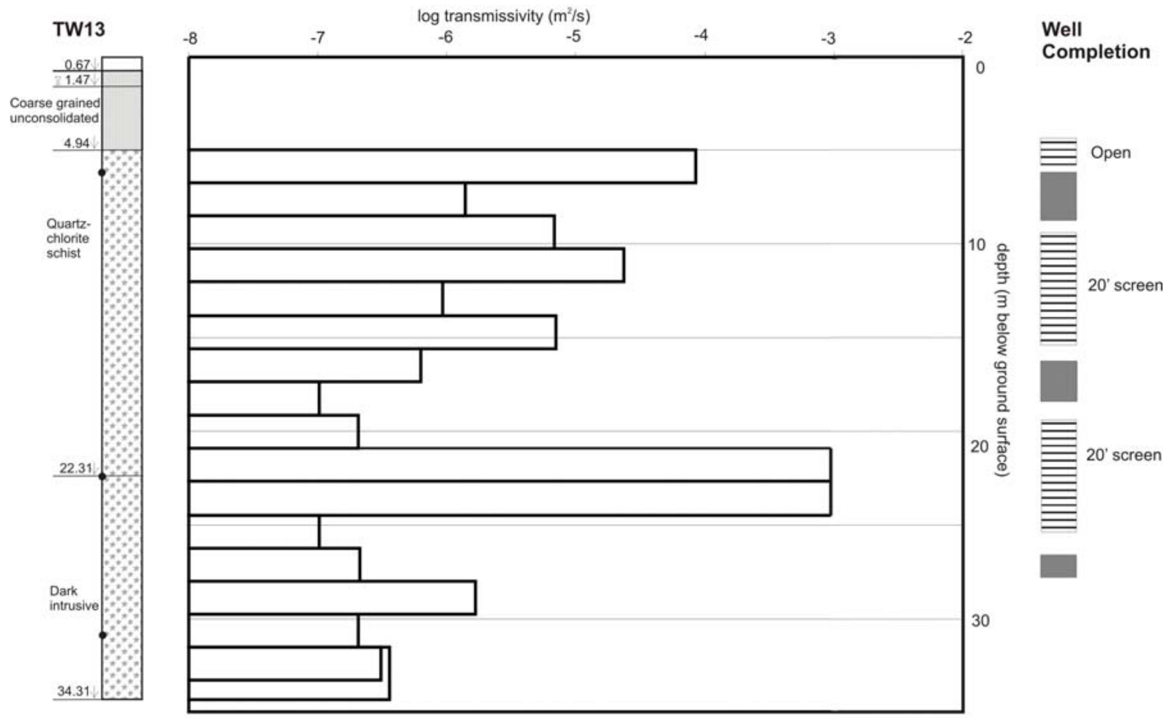
TW13
log transmissivity (m²/s)
-8
-7
-6
-5
-4
-3
-2
0
10
20
30
depth (m below ground surface)
0.67
1.47
Coarse grained unconsolidated
4.94
Quartz-chlorite schist
22.31
Dark intrusive
34.31
Well Completion
Open
20' screen
20' screen

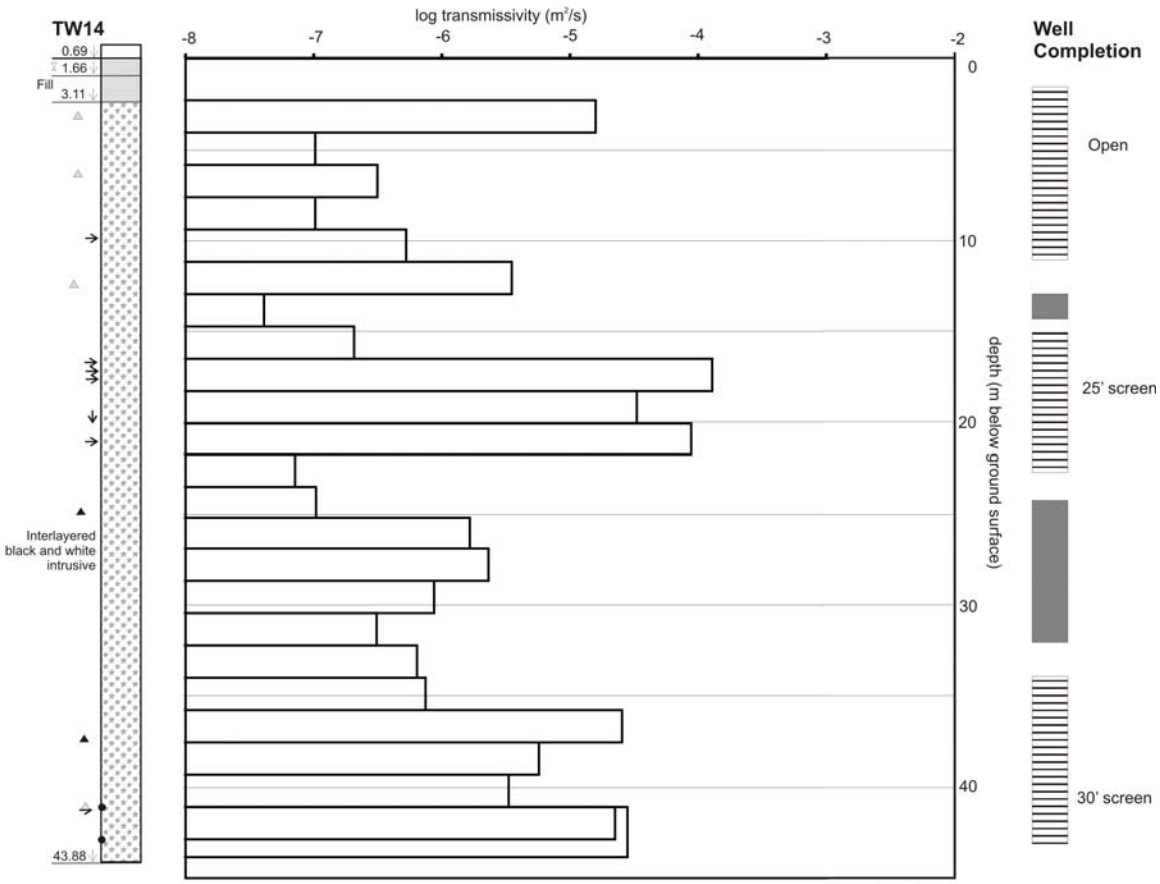

TW14
0.69
1.66
Fill
3.11
Interlayered black and white intrusive
43.88
log transmissivity (m²/s)
-8
-7
-6
-5
-4
-3
-2
0
10
20
30
40
depth (m below ground surface)
Well Completion
Open
25' screen
30' screen

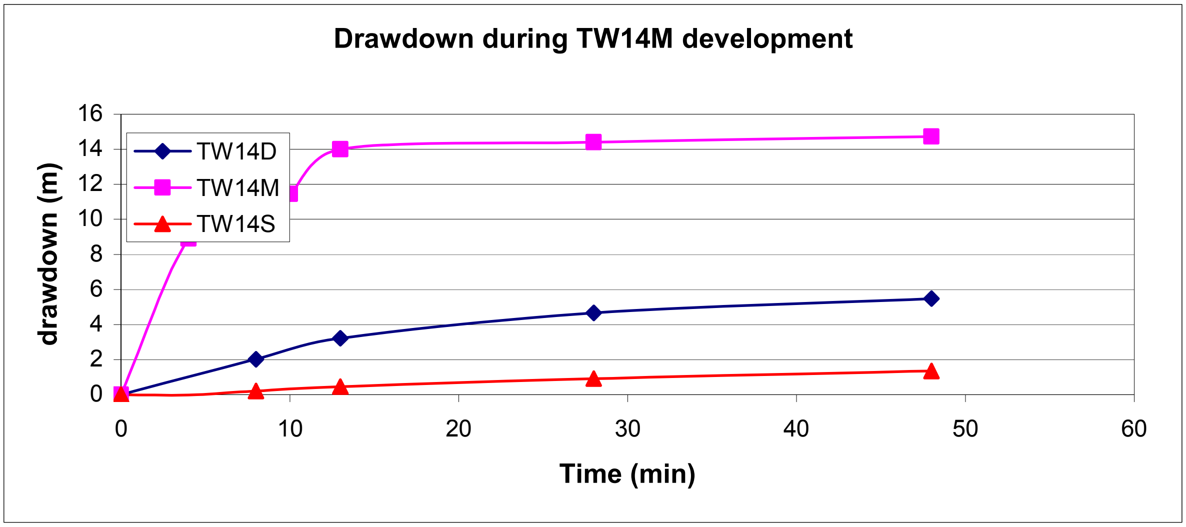

Drawdown during TW14M development
TW14D
TW14M
TW14S
drawdown (m)
Time (min)
0
2
4
6
8
10
12
14
16
0
10
20
30
40
50
60

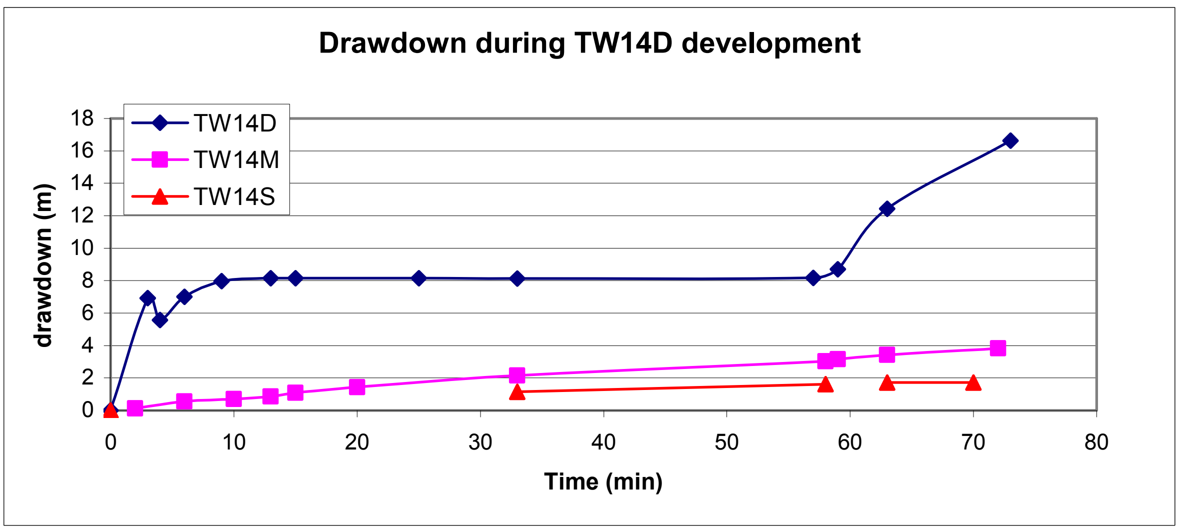

Drawdown during TW14D development
TW14D
TW14M
TW14S
drawdown (m)
Time (min)
0
2
4
6
8
10
12
14
16
18
0
10
20
30
40
50
60
70
80

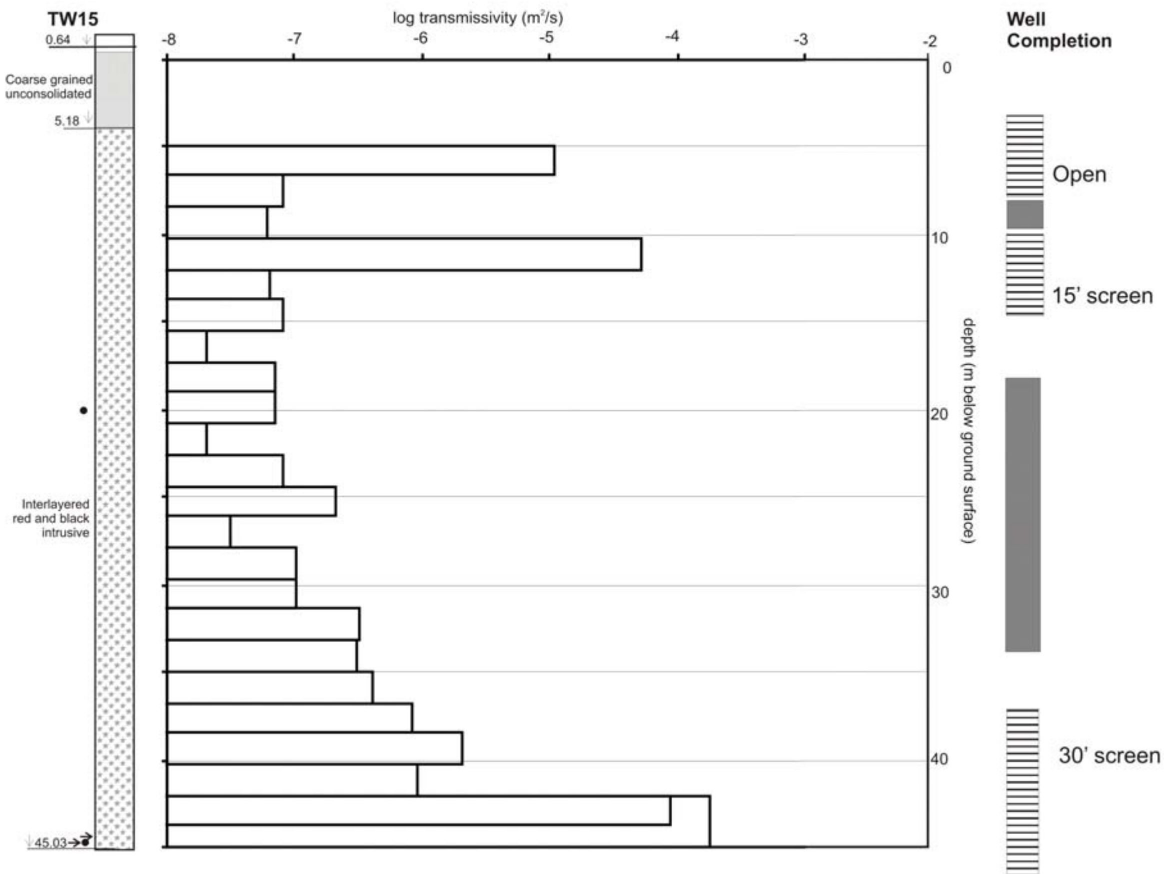

TW15
0.64
Coarse grained unconsolidated
5.18
Interlayered red and black intrusive
45.03
log transmissivity (m²/s)
-8
-7
-6
-5
-4
-3
-2
0
10
20
30
40
depth (m below ground surface)
Well Completion
Open
15' screen
30' screen

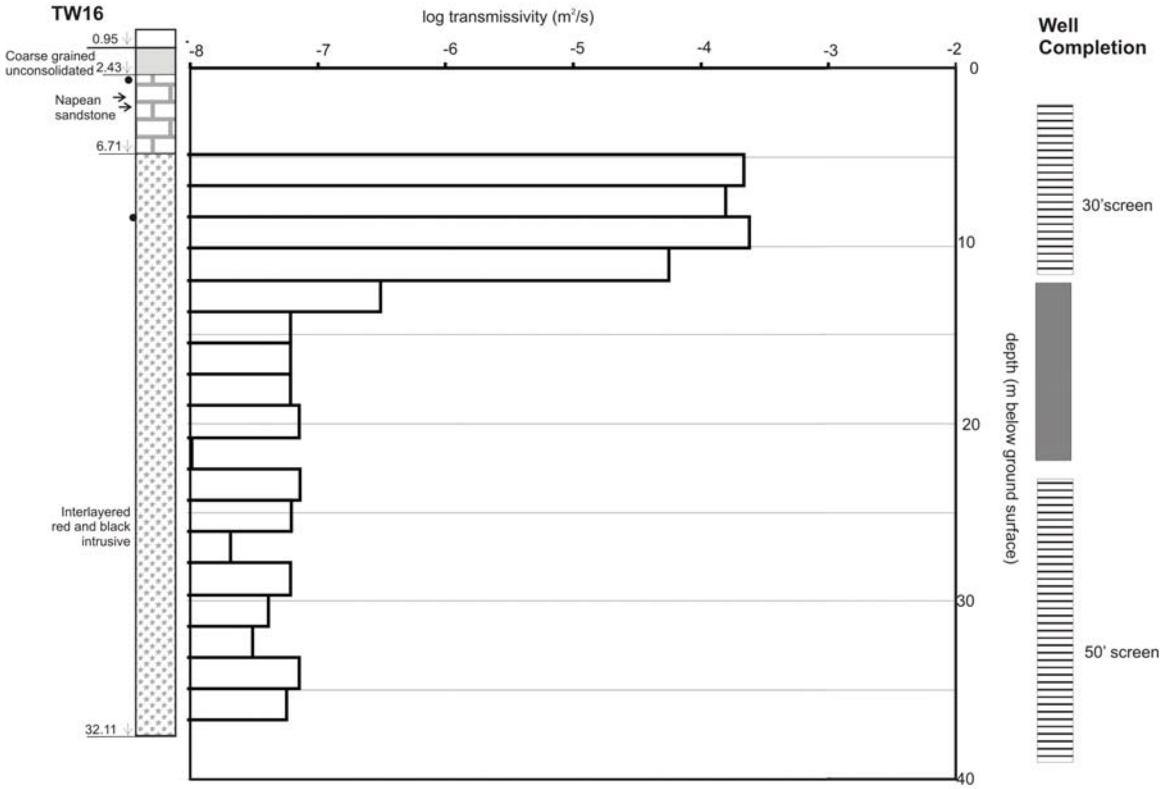
TW16
log transmissivity (m^2/s)
Well Completion
0.95
Coarse grained unconsolidated
2.43
Napean sandstone
6.71
Interlayered red and black intrusive
32.11
-8
-7
-6
-5
-4
-3
-2
0
10
20
30
40
depth (m below ground surface)
30'screen
50' screen

Table A.1 Compiled transmissivity (log T, m^2/s) data sorted into 5 m intervals with depth, d (m). Mean (μ) and standard deviation (1σ) for each 5 m interval also indicated.

TW3		TW4		TW5		TW6		TW7		TW8		TW9		TW10		TW11		TW12		TW13		TW14			
d	log T	d	log T	d	log T	d	log T	d	log T	d	log T	d	log T	d	log T	d	log T	d	log T	d	log T	d	log T	μ	σ
				54.2	-5.7																			-6.0	0.4
				52.4	-6.3																				
				50.7	-6.4	48.0	-4.4																	-5.4	1.1
				48.9	-5.5	46.2	-4.3																		
				47.1	-6.4																				
				45.4	-6.6	44.5	-3.9	44.2	-5.3	41.2	-5.6			42.6	-4.9									-5.3	1.2
				43.6	-6.3	42.7	-4.4	42.4	-3.1					42.6	-6.4										
				41.8	-6.4																				
				40.1	-5.9	40.9	-4.5	40.6	-4.8	39.5	-5.8			40.8	-6.1							41.1	-4.7	-5.6	0.8
				38.3	-7.0	39.2	-4.6	38.9	-5.1	37.7	-6.9			39.0	-6.5							39.3	-5.5		
				36.5	-6.5	37.4	-4.7	37.1	-5.5					37.3	-5.9							37.6	-5.2		
				34.7	-6.1	35.6	-4.7	35.3	-1.4	35.9	-2.8	34.3	-6.1	35.5	-6.1	34.0	-6.5			31.5	-6.4	35.8	-4.6	-5.3	1.4
				33.0	-6.3	33.9	-4.7	33.6	-5.2	34.1	-2.7	34.3	-5.6	33.7	-6.2	34.0	-6.4			31.5	-6.5	34.0	-6.1		
				31.2	-6.3	32.1	-4.4	31.8	-5.0	32.4	-3.2	32.6	-5.6	32.0	-6.4	32.0	-6.1					32.2	-6.2		
29.0	-5.5	28.8	-4.7	29.4	-6.5	30.3	-4.1	30.0	-5.5	30.6	-6.3	30.8	-5.4	30.2	-6.1	30.2	-7.3	28.9	-7.2	29.8	-6.7	30.5	-6.5	-5.8	1.1
27.0	-5.5	27.4	-4.6	27.7	-6.1	28.5	-4.7	28.2	-3.7	28.8	-5.5	29.0	-5.5	28.4	-6.4	28.5	-7.7	28.9	-7.3	28.0	-5.8	28.7	-6.1		
		26.1	-4.7			26.8	-3.9	26.5	-2.7	27.1	-5.9	27.3	-5.6	26.7	-6.5	26.7	-6.3	27.2	-7.7	26.2	-6.7	26.9	-5.6		
25.0	-5.3	24.7	-4.5	25.9	-5.9	25.0	-4.4	24.7	-2.7	25.3	-2.4	25.5	-5.6	24.9	-6.4	24.9	-6.7	25.4	-7.3	24.4	-7.0	25.2	-5.8	-5.5	1.3
23.0	-5.5	23.4	-4.6	24.1	-5.9	23.2	-4.9	22.9	-3.9	23.5	-4.3	23.7	-5.7	23.1	-6.4	23.2	-6.6	23.6	-6.3	22.7	-3.0	23.6	-7.0		
21.0	-6.5	22.0	-4.8	22.4	-5.8	21.5	-4.9	21.2	-3.9	22.3	-4.3	21.9	-5.6	21.3	-6.3	21.4	-6.8	21.8	-7.0			21.8	-7.1		
										22.3	-6.3														
19.0	-6.0	20.6	-4.8	20.6	-6.2	19.7	-3.8	19.4	-4.4	20.6	-6.1	20.2	-5.7	19.6	-6.6	19.6	-6.7	20.1	-6.4	20.9	-3.0	20.0	-4.1	-5.7	1.2
17.0	-8.0	19.3	-4.7	18.8	-6.7	17.9	-5.2	17.6	-4.8	18.8	-6.8	18.4	-5.6	17.8	-6.4	17.8	-7.2	18.3	-6.2	19.1	-6.7	18.2	-4.5		

		19.9 16.6	-3.4 -3.4	17.0	-4.9	16.2	-5.3			17.0	-6.2	16.6	-5.7	16.0	-7.3	16.1	-7.1	16.5	-5.9	17.4	-7.0	16.5	-3.9		
15.0 13.0 11.0	-8.0 -5.6 -8.0	15.2 13.8 12.5 11.1	-5.1 -5.0 -5.2 -5.4	15.3 13.5 11.7	-5.7 -5.9 -5.5	14.4 12.6	-4.2 -3.6	15.9 14.1 12.3	-5.7 -5.0 -6.3	15.2 13.5 11.7	-5.6 -6.3 -6.5	14.9 13.1 11.3	-5.7 -6.2 -6.9	14.3 12.5	-6.2 -4.3	14.3 12.5 10.8	-7.1 -7.3 -3.9	14.8 13.0 11.2	-6.1 -3.5 -5.3	15.6 13.8 12.1	-6.2 -5.2 -6.0	14.7 12.9 11.2	-6.7 -7.4 -5.5	-5.8	1.1
9.0 7.0	-4.1 -4.7	9.8 8.4 7.0	-5.8 -5.9 -5.8	10.0 8.2 6.4	-3.8 -4.0 -4.2	10.8 9.1 7.3	-4.5 -5.4 -5.4	10.5 8.8 7.0	-6.2 -2.2 -2.9	9.9 8.2 6.4	-3.6 -5.6 -6.3	9.6 7.8 6.0	-6.0 -6.8 -6.8	10.7 8.9 7.2	-4.0 -3.6 -3.4	9.0 7.2 6.3	-3.8 -3.9 -4.3	9.5 7.7 5.9	-5.6 -5.0 -7.5	10.3 8.5 6.7	-4.6 -5.2 -5.9	9.4 7.6	-6.3 -7.0	-5.0	1.3
		5.7 4.3	-5.7 -3.3			5.5	-2.9					4.2 2.5	-4.2 -4.1	5.4 3.6 2.7	-4.3 -3.9 -4.3					5.0	-4.1	5.9 4.1 2.3	-6.5 -7.0 -4.8	-4.6	1.2

Appendix B: Soil data

Appendix B compiles soil data for the 27 transects completed using the methodology outlined in Chapter 2. Individual holes are located ZZ meters from the start of each transect in the station signifier MH08-XX-ZZ, where XX is the transect number. Transects are located on Figure B.1 with arrows indicating direction of observation. For each hole the refusal depth (or 'no refusal') and soil type at different depths is noted. No data was recorded for Transect 1.

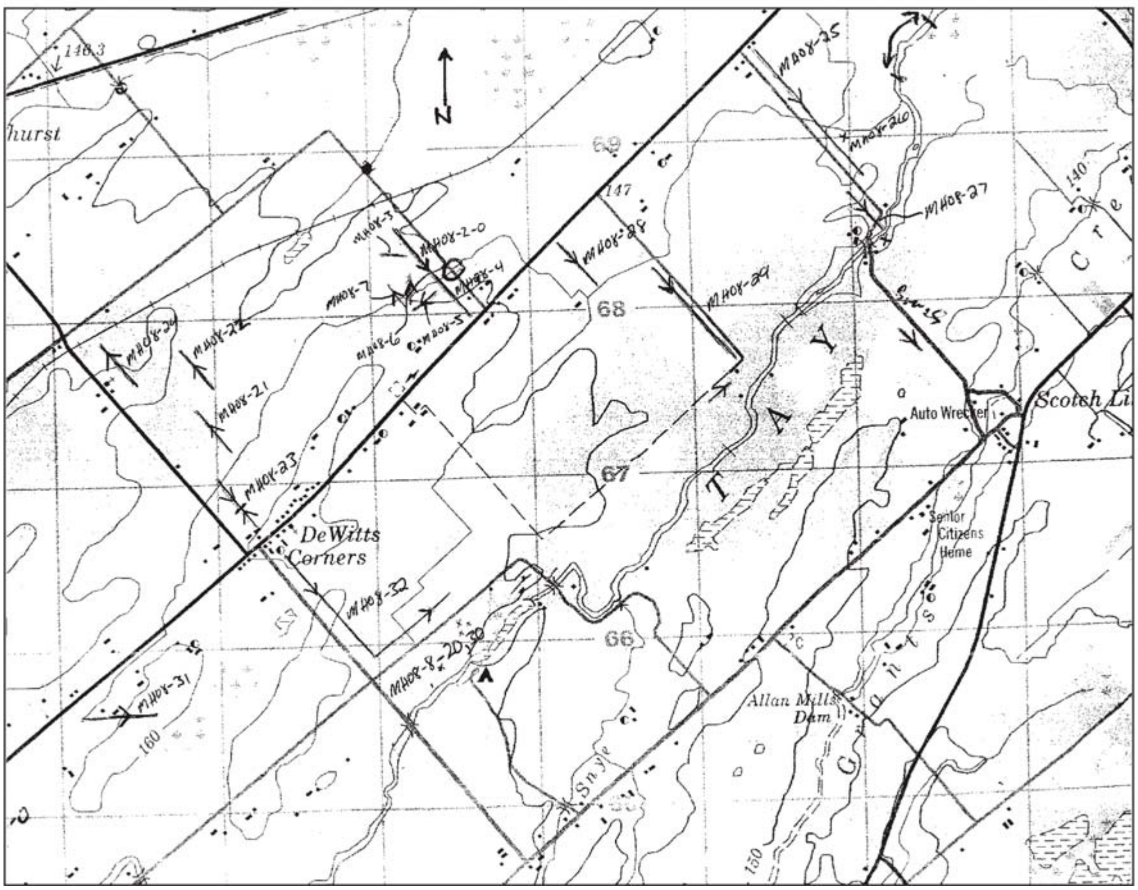

Figure B. 1 Location of transects.

TRANSECT 2

Date: 06/10/08 **Weather: Sun** **Time started: 3:30pm**

Site description: **Badour field near cattle barn, parallel with Perkins Rd. Near TW18**

Hole	Refusal Depth (cm)	Auger Intervals (cm)
MH08-2-0	39	0-40 silty clay, brown, organic 40-50 grey, clay, some orange oxidized patches
MH08-2-20	67	
MH08-2-40	74	
MH08-2-60	108 no refusal	0-45 very fine sand and clay, roots 45-104 very dense, malleable grey clay with some oxidized patches

TRANSECT 3

Date: 06/11/08 **Weather: Sun** **Time started: 2:00pm**

Site description: **Perkins Rd field with creek in it near house on left side of road**

Hole	Refusal Depth (cm)	Auger Intervals (cm)
MH08-3-0	135 no refusal	0-28 black, malleable organicl, silty clay, roots 28-87 clay, varves-poorly defined?, oxidized patches 87-101 sandt clay with some gravel
MH08-3-20	121	
MH08-3-40	132 no refusal	
MH08-3-60	118	0-32 brown, organic, silty clay 32-80 tan/grey, dry clay, malleable 80-91 sand and clay mix with some gravel

TRANSECT 4

Date: 06/11/08 **Weather: Sun** **Time started: 2:00pm**

Site description: **Perkins Rd field with creek in it near house on left side of road**

Hole	Refusal Depth (cm)	Auger Intervals (cm)
MH08-4-0	36	0-28 malleable, black, oraganic silty clay
MH08-4-20	39	
MH08-4-40	79	
MH08-4-60	105	0-18 black, organic, silty clay 18-75 tan/grey clay, some oxidized patches, dry 75-82 very wet sand and clay mix - water fills hole

TRANSECT 5

Date: 06/12/08 **Weather: Sun** **Time started: 10:30am**

Site description: **Perkins Rd field with creek in it near house moving uphill**

Hole	Refusal Depth (cm)	Auger Intervals (cm)
MH08-5-0	134	0-88 very fine, brown, medium sand and some gravel/boulders
MH08-5-20	89	
MH08-5-40	138 no refusal	
MH08-5-60	104 boulder?	0-26 very fine - medium brown sand and gravel

TRANSECT 6

Date: 06/12/08 **Weather: Sun** **Time started: 3:00pm**

Site description: **Perkins Rd field with creek in it near far west fence line**

Hole	Refusal Depth (cm)	Auger Intervals (cm)
MH08-6-0	142 no refusal	0-45 brown, coarse sand, very gravelly
MH08-6-20	130	
MH08-6-40	120	
MH08-6-60	86	0-23 sily clay, organic muck, malleable 23-80 tan clay with oxidized patches, dry, dense 80-87 wet, saturated, sandy clay with some gravel hole filled with water

TRANSECT 7

Date: 06/12/08 **Weather: Sun** **Time started: 3:00pm**

Site description: Perkins Rd field with creek in it near far west fence line

Hole	Refusal Depth (cm)	Auger Intervals (cm)
MH08-7-0	79	0-45 brown, sandy, organic muck 45-54 sandy clay, brown organics 54-62 brown/tan wet sandy clay hole fills with water
MH08-7-20	91	
MH08-7-40	148 no refusal	
MH08-7-60	144 no refusal	0-18 brown, silty, organic, malleable muck 18-52 tan, oxidized clay, dry, dense 52-103 wet, tan, medium/coarse sandy clay hole filled with water

TRANSECT 8

Date: 06/16/08 **Weather: Sun** **Time started: 9:00am**

Site description: Hay field from weather station towards Tay

Hole	Refusal Depth (cm)	Auger Intervals (cm)
MH08-8-0	29	0-27 dark, brown, organic, fine to coarse sand and silt
MH08-8-20	40	
MH08-8-40	142 no refusal	
MH08-8-60	133 no refusal	0-23 dark brown, organic, fine to coarse sand and silt

TRANSECT 9

Date: 06/16/08 **Weather: Sun** **Time started: 10:30am**

Site description: Hay field from weather station east towards TW13

Hole	Refusal Depth (cm)	Auger Intervals (cm)
MH08-9-0	46	0-20 brown, organic sand and silt 20-39 above soil turns more orange-brown Refusal at 39
MH08-9-20	25	
MH08-9-40	28	
MH08-9-60	93	0-21 brown, organic sand and silt 21-72 orange brown sand and silt, gravel Refusal at 72

TRANSECT 10

Date: 06/16/08 **Weather: Sun** **Time started: 12:30am**

Site description: **Hay field from weather station west towards TW1**

Hole	Refusal Depth (cm)	Auger Intervals (cm)
MH08-10-0	90	0-65 brown, black organic sand and silt 65-87 slight clay and clay clasts-grey
MH08-10-20	140 no refusal	
MH08-10-40	120	
MH08-10-60		on outcrop at TW1

TRANSECT 11

Date: 06/17/08 **Weather: Sun** **Time started: 10:00am**

Site description: **Hay field from TW1 towards Tay**

Hole	Refusal Depth (cm)	Auger Intervals (cm)
MH08-11-0	135 no refusal	0-79 brown, organic, fine-medium sand and gravel
MH08-11-20	140 no refusal	
MH08-11-40	90	
MH08-11-60	182-39 no refusal	0-23 brown-orange medium sand and gravel

TRANSECT 12

Date: 06/17/08 **Weather: Sun** **Time started: 3:00pm**

Site description: **Hay field east along south treeline**

Hole	Refusal Depth (cm)	Auger Intervals (cm)
MH08-12-0		0-23 brown, medium to fine sand and gravel
MH08-12-20	134 no refusal	
MH08-12-40	109	
MH08-12-60		0-15 fine to medium, brown, sand and gravel

TRANSECT 13

Date: 06/17/08 **Weather: Cloud** **Time started: 4:00pm**

Site description: **Hay field south from TW3**

Hole	Refusal Depth (cm)	Auger Intervals (cm)
MH08-13-0	89	0-89 medium to fine sand and silt, brown, gravel
MH08-13-20	132 no refusal	
MH08-13-40	139 no refusal	
MH08-13-60	97	0-22 as above

TRANSECT 14

Date: 06/18/08 **Weather: Rain** **Time started: 11:00am**

Site description: **Hay field east from TW3**

Hole	Refusal Depth (cm)	Auger Intervals (cm)
MH08-14-0	182-48 no refusal	0-44 brown, organic, sand and silt, more orange-brown with depth
MH08-14-20	136 no refusal	
MH08-14-40	138 no refusal	
MH08-14-60		0-94 as above

TRANSECT 15

Date: 06/18/08 **Weather: Rain** **Time started: 1:00pm**

Site description: **Hay field along treeline from TW5 towards TW5**

Hole	Refusal Depth (cm)	Auger Intervals (cm)
MH08-15-0	182-46 no refusal	0-62 brown, organic, sand and silt, more orange-brown with depth
MH08-15-20	132 no refusal	
MH08-15-40	133 no refusal	
MH08-15-60	134 no refusal	0-40 brown, organic, sand and silt, more orange-brown with depth, gravel

TRANSECT 16

Date: 06/18/08 **Weather: Rain** **Time started: 3:00pm**

Site description: **Hay field east from TW8 along treeline**

Hole	Refusal Depth (cm)	Auger Intervals (cm)
MH08-16-0	20	0-16 brown, organic, sand and silt
MH08-16-20	60	
MH08-16-40	79	
MH08-16-60	132 no refusal	0-40 brown, organic, sand and silt, more orange-brown with depth, gravel

TRANSECT 17

Date: 06/19/08 **Weather: Rain** **Time started: 10:30pm**

Site description: **Hay field east from TW8 towards TW3**

Hole	Refusal Depth (cm)	Auger Intervals (cm)
MH08-17-0	37	
MH08-17-20	50	
MH08-17-40	133 no refusal	
MH08-17-60	136 no refusal	

TRANSECT 18

Date: 06/19/08 **Weather: Rain** **Time started: 11:00am**

Site description: **Hay field along north treeline near TW3**

Hole	Refusal Depth (cm)	Auger Intervals (cm)
MH08-18-0	130	
MH08-18-20	131 no refusal	
MH08-18-40	128 no refusal	
MH08-18-60	132 no refusal	

TRANSECT 19

Date: 06/19/08 **Weather: Rain** **Time started: 3:30pm**

Site description: **Hay field from TW4 to TW2**

Hole	Refusal Depth (cm)	Auger Intervals (cm)
MH08-19-0	82	
MH08-19-20	88	
MH08-19-40	132 no refusal	
MH08-19-60	outcrop	

TRANSECT 20

Date: 06/19/08 **Weather: Rain** **Time started: 4:00pm**

Site description: **Hay field from TW2 along boundary**

Hole	Refusal Depth (cm)	Auger Intervals (cm)
MH08-20-0	134 no refusal	
MH08-20-20	69	
MH08-20-40	135 no refusal	
MH08-20-60	118	

TRANSECT 21

Date: 06/24/08 **Weather: Cloud** **Time started: 10:15pm**

Site description: **Mitchell field just north of creek towards tracks**

Hole	Refusal Depth (cm)	Auger Intervals (cm)
MH08-21-0	73	
MH08-21-60	84	0-15 organic 15-46 sandy, grey, clay rich, wet water fills hole
MH08-21-120	120	
MH08-21-180	182-50 no refusal	
MH08-21-240	132 no refusal	

TRANSECT 22

Date: 06/24/08 **Weather: Cloud** **Time started: 11:30pm**

Site description: **Mittchell field just north of tower towards tracks**

Hole	Refusal Depth (cm)	Auger Intervals (cm)
MH08-22-0	66	
MH08-22-60	133 no refusal	0-15 organic 15-46 sandy, grey, clay rich, wet water fills hole
MH08-22-120	132 no refusal	
MH08-22-180	132 no refusal	
MH08-22-240	93	
MH08-22-300	62	0-20 black, wet organics 20-61 tan/orange clay, continuous, varved?
MH08-22-360	132 no refusal	

TRANSECT 23

Date: 06/25/08 **Weather: Sun** **Time started: 11:30am**

Site description: **Kerr field near CR#6 heading towards creek**

Hole	Refusal Depth (cm)	Auger Intervals (cm)
MH08-23-0	53	0-15 brown organic 15-53 orange-tan clay, some sand increasing with depth and stating to dominate gradually
MH08-23-60	132 no refusal	
MH08-23-120	132 no refusal	
MH08-23-180	132 no refusal	
MH08-23-240	93	
MH08-23-300	99 2m from creek	

TRANSECT 24

Date: 06/26/08 **Weather: Cloud** **Time started: 10:30pm**

Site description: **Kerr field near church/TW12, towards tracks**

Hole	Refusal Depth (cm)	Auger Intervals (cm)
MH08-24-0	115 50m from quarry	0-15 gravelly, organic
MH08-24-60	85	
MH08-24-120	132 no refusal	
MH08-24-180	132 no refusal	
MH08-24-240	132 no refusal	
MH08-24-300	132 no refusal	

TRANSECT 25

Date: 06/27/08 **Weather: Cloud** **Time started: 12:00pm**

Site description: **Bowes hay and corn field near CR#6, towards Tay**

Hole	Refusal Depth (cm)	Auger Intervals (cm)
MH08-25-0	109	grey to dun clay, loam, minor silt hole filled with water
MH08-25-60	132 no refusal some water in bottom 10cm	organic clay turning to compact grey clay and silt silt content increases with depth
MH08-25-120	132 no refusal	dark brown clay loam, sandy, disintregrated and intact Nepean cobbles, moist to saturated
MH08-25-180	132 no refusal	
MH08-25-240	102 no refusal	gradational contact of sand and clay filled with water 25m from creek at Bowes Rd.
MH08-25-300	67	sand and minor silt and clay with intact and diaggreagated Nepean cobbles, dry
MH08-25-360	117 no refusal outcrop at MH08-25-340	brown, silt with minor sand and abundant cobbles
MH08-25-420	132 no refusal sample	grey, dun, brown sand with greay clay and occasional Nepean cobbles
MH08-25-480	sample	black-brown sand with brown clay, cobbles with dissagregated black nodules (bt,hb?) and varves

TRANSECT 26

Date: 07/3/08 **Weather: Rain** **Time started: 1:00pm**

Site description: **Bowes clover field towards Tay**

Hole	Refusal Depth (cm)	Auger Intervals (cm)
MH08-26-0	100	0-15 back, oraganic clay
		15-45 brown, sandy clay, Nepean cobbles and grit
	sample	45-70 mica mud, pure biotite grains up to 2mm, moist
MH08-26-60	132	0-0 black, organic clay
	no refusal	10-91 tan clay with oxidized patches, dry, dense, varved?
	20m from outcrop	
MH08-26-120	132	0-60 dry, orange-brown sand and clay
	no refusal	

TRANSECT 27

Date: 07/4/08 **Weather: Sun** **Time started: 1:30pm**

Site description: **Bowes field on west side near south treeline on ridge opposite clover field**

Hole	Refusal Depth (cm)	Auger Intervals (cm)
MH08-27-0	132	0-78 quartz medium to very fine sandy loam and intact and disaggreagated Nepean cobbles
	no refusal	
MH08-27-60	107	
	5m from small creek	
MH08-27-120	132	
	no refusal	
	near well at Bowes house	

TRANSECT 28

Date: 07/8/08 **Weather: Sun** **Time started: 10:30am**

Site description: **Conboy hay field on Leonard from CR#6 towards well**

Hole	Refusal Depth (cm)	Auger Intervals (cm)
MH08-28-0	134 no refusal	0-10 clay rich organic 10-35 greay clay, oxidized, few Nepean cobbles 35-60 clay rich sand with numerous cobbles
MH08-28-60	134 no refusal	
MH08-28-120	93	
MH08-28-180	134 no refusal	
MH08-28-240	134 no refusal	0-7 clay rich organic 7-110 brown-tan clay, dry, dense hole filled with water
MH08-28-300	134 no refusal	
MH08-28-360	134 no refusal	
MH08-28-420	134 no refusal	
MH08-28-480	134 no refusal	

Appendix C: Infiltrometer data

Appendix C compiles data from the seven double-ring infiltrometer experiments completed using the methodology outlined in Chapter 2. The experiments are located on Figure 2.1. **Penet.** is the penetration depth of the inner ring (**I.R.**) and outer ring (**O.R.**) ring. $\mathbf{H_0}$ is the initial water depth in the rings. Each 60 minute experiment is divided into trials with a beginning ($\mathbf{t_o}$), end ($\mathbf{t_1}$), and duration ($\Delta\mathbf{t_o}$). The volume (**V**) and flow rate (**Q**) was measured during each trial and in each ring. The infiltration rate after 60 minutes ($\boldsymbol{i_{60}}$) and the saturated hydraulic conductivity ($\boldsymbol{K_s}$) are calculated following *Sharma et al.* [1980].

Double-ring infiltrometer test

Station: 1 — Location: Hay field near TW8

Date: July 23/08

Ground T (°C)

Water T (°C)

Notes/Problems:

	Penet. (cm)	Area (m^2):	Ho (cm)	Vo (m^3)
I.R.	3.5"	0.292	3"	
O.R.	3.5"	0.83	3"	

				Inner Ring					Outer Ring				
Trial	t_0 (min)	t_1 (min)	Δt	V_0 (cc)	V_1 (cc)	ΔV (cc)	V_{tot}	Q (cc/min)	V_0 (cc)	V_1 (cc)	ΔV (cc)	V_{tot}	Q (cc/min)
1	0.0	9.5	10	0	2150	2150	2150	226.3	0	7000	7000	7000	736.84
2	9.5	15.5	6	0	600	600	2750	100	0	3100	3100	10100	516.67
3	15.5	25.5	10	0	1450	1450	4200	145	0	4000	4000	14100	400
4	25.5	40.5	15	0	2050	2050	6250	136.7	0	5500	5500	19600	366.67
5	40.5	60	20	0	2300	2300	8550	117.9	0	5300	5300	24900	271.79

V_{tot} = infiltrated sum

$Q = \Delta V/\Delta t$ (cc/min)

Interpretation

	I.R.	O.R.	
i_{60}=	142.5	415	cc/min
K_s	3E-06	3.E-06	m/s

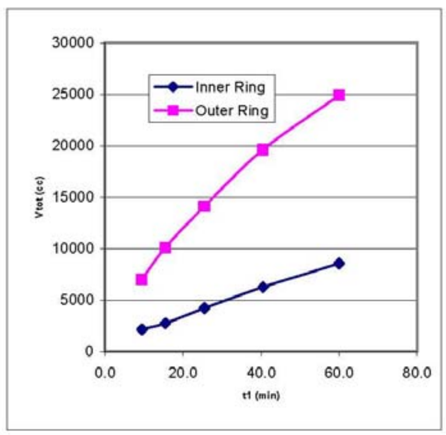

Double-ring infiltrometer test

Station: 2

Location: Hay field in tracer pit near TW7

Date: July 23/08

Ground T (°C)

Water T (°C)

Notes/Problems:

	Penet. (cm)	Area (m^2):	Ho (cm)	Vo (m^3)
I.R.	2.5"	0.292	5"	
O.R.	4.5"	0.83	5"	

				Inner Ring					Outer Ring				
Trial	t_0 (min)	t_1 (min)	Δt	V_0 (cc)	V_1 (cc)	ΔV (cc)	V_{tot}	Q (cc/min)	V_0 (cc)	V_1 (cc)	ΔV (cc)	V_{tot}	Q (cc/min)
1	0.0	6.2	6	0	500	500	500	81.3	0	1200	1200	1200	195.12
2	6.2	17.5	11	0	800	800	1300	70.8	0	2700	2700	3900	238.94
3	18	32.5	15	0	900	900	2200	62.07	0	3200	3200	7100	220.69
4	33	49.5	17	0	1100	1100	3300	66.67	0	3400	3400	####	206.06
5	50	60	10	0	550	550	3850	55	0	2000	2000	####	200

V_{tot} = infiltrated sum

$Q = \Delta V/\Delta t$ (cc/min)

Interpretation

	I.R.	O.R.	
i_{60}=	64.17	208.3	cc/min
K_s	1.E-06	1.E-06	m/s

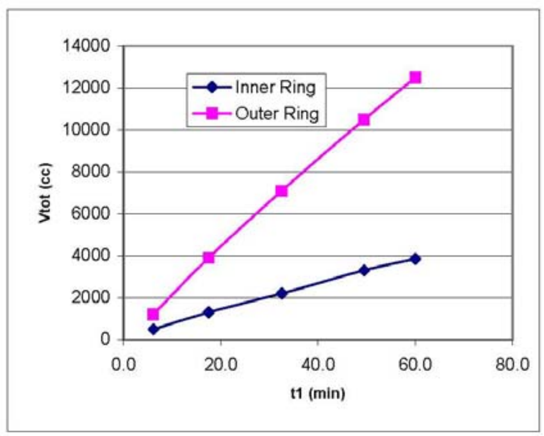

Double-ring infiltrometer test

Station: 3

Location: Hay field in tracer pit near TW7

Date: July 24/08

Ground T (°C)

Water T (°C)

Notes/Problems:

	Penet. (cm)	Area (m^2):	Ho (cm)	Vo (m^3)
I.R.	4"	0.292	3.5"	
O.R.	4"	0.83	3.5"	

				Inner Ring					Outer Ring				
Trial	t_0 (min)	t_1 (min)	Δt	V_0 (cc)	V_1 (cc)	ΔV (cc)	V_{tot}	Q (cc/min)	V_0 (cc)	V_1 (cc)	ΔV (cc)	V_{tot}	Q (cc/min)
1	0.0	5.0	5	0	350	350	350	70	0	200	200	200	40
2	5	15	10	0	600	600	950	60	0	800	800	1000	80
3	15	30	15	0	900	900	1850	60	0	1500	1500	2500	100
4	30	50	20	0	1150	1150	3000	57.5	0	1600	1600	4100	80
5	50	60	10	0	350	350	3350	35	0	200	200	4300	20

V_{tot} = infiltrated sum

$Q = \Delta V/\Delta t$ (cc/min)

Interpretation

	I.R.	O.R.	
i_{60}=	55.83	71.67	cc/min
K_s	1E-06	5.E-07	m/s

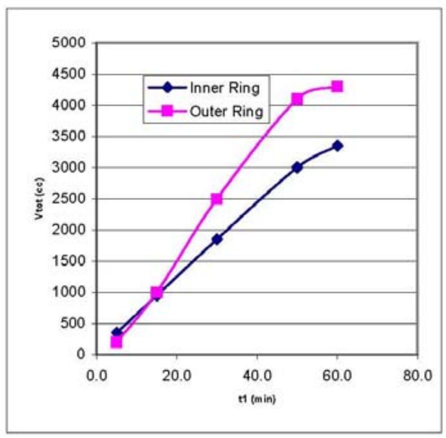

Double-ring infiltrometer test

Station: 4

Location: Hay field near TW3

Date: July 28/08

Ground T (°C)

Water T (°C)

Notes/Problems:

	Penet. (cm)	Area (m^2):	Ho (cm)	Vo (m^3)
I.R.	3"	0.292	4"	
O.R.	3.5"	0.83	3.5"	

				Inner Ring					Outer Ring				
Trial	t_0 (min)	t_1 (min)	Δt	V_0 (cc)	V_1 (cc)	ΔV (cc)	V_{tot}	Q (cc/min)	V_0 (cc)	V_1 (cc)	ΔV (cc)	V_{tot}	Q (cc/min)
1	0.0	5.0	5	0	300	300	300	60	0	2900	2900	2900	580
2	5	15	10	0	400	400	700	40	0	3300	3300	6200	330
3	15	30	15	0	200	200	900	13	0	5000	5000	11200	333.33
4	30	40	10	0	350	350	1250	35	0	3400	3400	14600	340
5	40	60	20	0	1000	1000	2250	50	0	7500	7500	22100	375

V_{tot} = infiltrated sum

Q = ΔV/Δt (cc/min)

Interpretation

	I.R.	O.R.	
i_{60}=	37.5	368.3	cc/min
K_s	7E-07	2.E-06	m/s

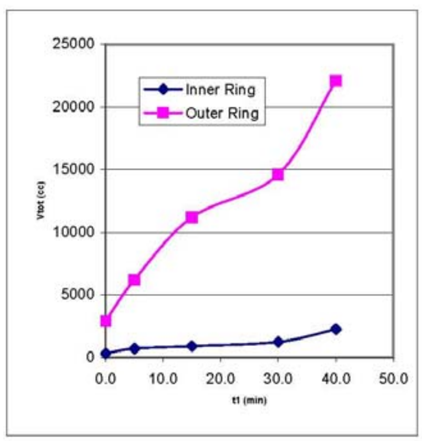

Double-ring infiltrometer test

Station: 5

Location: Hay field near TW22

Date: July 28/08

Ground T (°C)

Water T (°C)

	Penet. (cm)	Area (m^2):	Ho (cm)	Vo (m^3)
I.R.	3.5"	0.292	4"	
O.R.	3.5"	0.83	4"	

Notes/Probler trouble with outer ring float

				Inner Ring					Outer Ring				
Trial	t_0 (min)	t_1 (min)	Δt	V_0 (cc)	V_1 (cc)	ΔV (cc)	V_{tot}	Q (cc/min)	V_0 (cc)	V_1 (cc)	ΔV (cc)	V_{tot}	Q (cc/min)
1	0.0	5.0	5	0	1400	1400	1400	280	0	7100	7100	7100	1420
2	5	15	10	0	1350	1350	2750	135	0	10100	10100	17200	1010
3	15	30	15	0	1500	1500	4250	100	0	5300	5300	22500	353.33
4	30	50	20	0	1900	1900	6150	95	0	6900	6900	29400	345
5	50	60	10	0	600	600	6750	60	0	3300	3300	32700	330

V_{tot} = infiltrated sum

Q = ΔV/Δt (cc/min)

Interpretation

	I.R.	O.R.	
i_{60}=	112.5	545	cc/min
K_s	2E-06	4.E-06	m/s

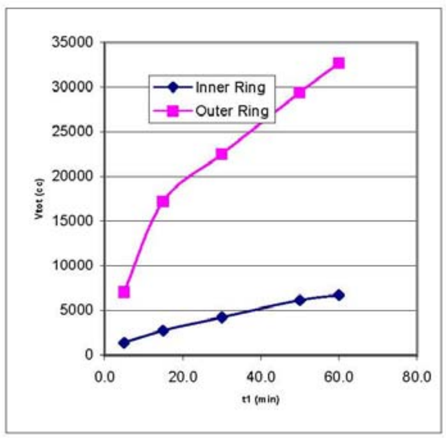

Double-ring infiltrometer test

Station: 6 | Location: Hay field near TW10

Date: July 28/08

	Penet. (cm)	Area (m^2):	Ho (cm)	Vo (m^3)
Ground T (°C) I.R.	3.5"	0.292	4"	
Water T (°C) O.R.	3.5"	0.83	4"	

Notes/Probler trouble with outer ring float

				Inner Ring					Outer Ring				
Trial	t_0 (min)	t_1 (min)	Δt	V_0 (cc)	V_1 (cc)	ΔV (cc)	V_{tot}	Q (cc/min)	V_0 (cc)	V_1 (cc)	ΔV (cc)	V_{tot}	Q (cc/min)
1	0.0	5.0	5	0	2400	2400	2400	480	0	6100	2400	2400	480
2	5	15	10	0	3800	3800	6200	380	0	100	1300	3700	130
3	15	30	15	0	4950	4950	11150	330	0	50	1900	5600	126.67
4	30	50	20	0	4800	4800	15950	240	0	0	2300	7900	115
5	50	60	10	0	2300	2300	18250	230	0	0	1100	9000	110

V_{tot} = infiltrated sum

Q = ΔV/Δt (cc/min)

Interpretation

	I.R.	O.R.	
i_{60}=	304.2	150	cc/min
K_s	6E-06	1.E-06	m/s

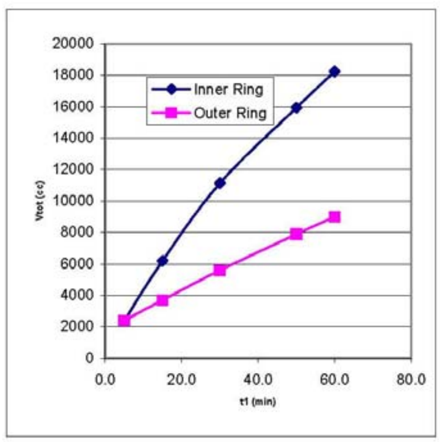

Double-ring infiltrometer test

Station: 7 Location: Near TW12 on Cameron Side Road

Date: July 28/08

Ground T (°C)

Water T (°C)

Notes/Probler trouble with outer ring float

	Penet. (cm)	Area (m^2):	Ho (cm)	Vo (m^3)
I.R.	3.5"	0.292	4"	
O.R.	3.5"	0.83	4"	

1"=2.54 cm

1'=0.3048 m

1 cm/min = 1.66e-4 m/s

1' squared = 0.0929 m2

				Inner Ring					Outer Ring				
Trial	t_0 (min)	t_1 (min)	Δt	V_0 (cc)	V_1 (cc)	ΔV (cc)	V_{tot}	Q (cc/min)	V_0 (cc)	V_1 (cc)	ΔV (cc)	V_{tot}	Q (cc/min)
1	0.0	5.0	5	0	2300	2300	2300	460	0	4100	4100	4100	820
2	5	15	10	10	3300	3290	5590	329	0	7000	7000	11100	700
3	15	30	15	0	4750	4750	10340	316.7	0	8400	8400	19500	560
4	30	50	20	500	4250	3750	14090	187.5	0	15000	15000	34500	750
5	50	60	10	0		0	16908	0	0		0	41400	0

V_{tot} = infiltrated sum

Q = ΔV/Δt (cc/min)

Interpretation

	I.R.	O.R.	
i_{60}=	281.8	690	cc/min
K_s	5E-06	5.E-06	m/s

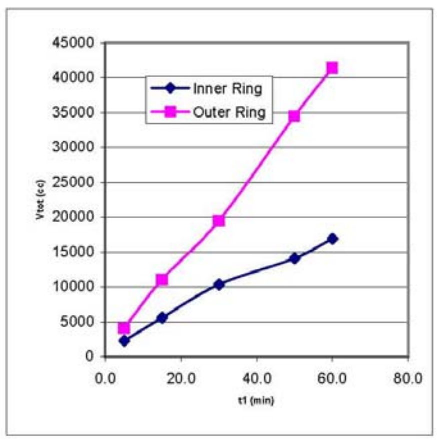

Appendix D: Simulation input files

Appendix D compiles simulation input files for three representative simulations: RR6.0 (base case from Chapter 2), RR7.0 (simulation with soil from Chapter 2), and LIN (lineament simulation from Chapter 3 with two vertical fractures). The simulations are described in detail in Sections 2.5 and 3.4.4 and the parameter values are summarized in Tables 2.4 and 3.1. All simulations were completed in *HydroGeoSphere* [*Therrien, et al.*, 2006]. For each simulation four files are included: XX.grok (general input file), XX.mprops (matrix parameters), XX.fprops (fracture parameters) and XX.oprops (overland flow parameters) where XX is the simulation name (*e.g.* RR6.0).

RR6.0.grok

```
!-------------------------  Grid generation
Generate blocks interactive
grade x
0.0 1.0 0.1 1 0.1
grade y
50.0 0.0 0.001 5 0.5
grade y
50.0 100.0 0.001 5 0.5
grade z
2.5 0.0 0.002 5 0.25
grade z
2.5 9.5 0.002 5 0.25
grade z
10.0 9.50 0.005 2 0.025
end generate blocks intereactive
end grid generation
mesh to tecplot
gridadoodle.dat
```

```
!-------------------------  General simulation parameters
units: kilogram-metre-day
unsaturated
finite difference mode
remove negative coefficients
compute underrelaxation factor
!compute fd cross terms
no nodal flow check
!echo to output
do transport
transient flow

!-------------------------  Porous media properties
use zone type
porous media
properties file
rr.mprops

!-------rest of the domain
clear chosen elements
choose elements block
0.0, 1.0
0.0, 100.0
0.0, 10.0

new zone
2
clear chosen zones
choose zone number
2

read properties
```

layer2

!------------top layer (just around fracture)
clear chosen elements
choose elements block
0.0, 1.0
49.995, 50.005
9.99, 10.0

new zone
1
clear chosen zones
choose zone number
1
read properties
layer1

!------------------------- Porous media flow
clear chosen nodes
choose nodes all
initial head
5.05

clear chosen nodes
choose nodes block
0.0, 1.0,
0.0, 0.0
0.0, 7.00
specified head
1
0.0, 5.5

clear chosen nodes

```
choose nodes block
0.0, 1.0,
100.0, 100.0
0.0, 7.00
specified head
1
0.0, 4.5

!------------------------- Solute Transport
Solute
name
precip

free-solution diffusion coefficient
1.74d-4     ! (m2/d)
End solute
Solute
name
matrix
free-solution diffusion coefficient
1.74d-4     ! (m2/d)
End solute

clear chosen nodes
choose nodes all
initial concentration
0.0  !precip
1.0  !matrix

clear chosen nodes
choose nodes top
specified concentration
1                    ! number of time panels
```

```
0.0,  10.0, 1.0, 0.0    ! timeon, time off, species 1, 2, 3 concentration

clear chosen nodes
clear chosen faces
choose nodes y plane
0.0
1.e-5

specified concentration
1                    ! number of time panels
0.0,  10.0, 0.0, 1.0    ! timeon, time off, species 1, 2, 3 concentration

!-------------------------  Fracture media properties
use zone type
fracture
properties file
rr.fprops

!----Vertical Fracture...when fracture only goes to bottom of high K pm layer
!clear chosen faces
!choose faces block
!0.0, 1.0
!0.5, 0.5
!0.0, 2.5

!-----Vertical Fracture...when fracture goes all the way to the top
clear chosen faces
choose faces y plane
50.0
1.e-5

new zone
1
```

clear chosen zones
choose zone number
1
read properties
vfracture

!....horizontal fracture
clear chosen faces
choose faces z plane
2.5
1.e-5
new zone
2
clear chosen zones
choose zone number
2
read properties
hfracture

!------------------------- Surface flow media properties
dual nodes for surface flow
use zone type
surface
properties file
rr.oprops

clear chosen faces
choose faces top
new zone
1
clear chosen zones
choose zone number
1

```
read properties
overland flow

clear chosen nodes
choose nodes top
initial water depth
1.D-6

clear chosen faces
choose faces top
specified rainfall
3
 0.0, 0.0
 1, 0.025
 2.0, 0.0

critical depth boundary all around
!------------------------------ Output
make observation point
5.0m_from_frac
0.5  55  2.5
initial timestep
1e-7
maximum timestep
1.0
output times
0.5
1
1.5
2
3
4
5
```

10

20

30

end

newton iteration control

10

Newton maximum iterations

12

Jacobian epsilon

1.0d-6

Newton absolute convergence criteria

1.0d-4

Newton residual convergence criteria

1.0d-4

flow solver convergence criteria

1e-8

RR6.0.mprops

! Porous medium property set

layer1

k isotropic

1.0D-0

specific storage

1.0D-5

porosity

0.01

longitudinal dispersivity

0.05

transverse dispersivity

0.005

vertical transverse dispersivity

0.005

tortuosity

```
0.1
bulk density
2000.0
unsaturated tables
pressure-saturation
-1000   0.22532178  ! pressure, Saturation
-200    0.25661515
-100    0.28004868
-50     0.31313708
-20     0.37839157
-10     0.45060625
-7.0    0.49739729
-5.0    0.54802657
-4.0    0.58496215
-3.4    0.61336611
-3.0    0.63597157
-2.7    0.65539787
-2.3    0.68544939
-2.0    0.71186889
-1.7    0.74246249
-1.4    0.77817876
-1.2    0.80535621
-1.0    0.83555850
-0.8    0.86890602
-0.65   0.89582405
-0.5    0.92389193
-0.4    0.94276352
-0.3    0.96115858
-0.2    0.97821106
-0.1    0.99248653
-0.06   0.99686866
-0.03   0.99937138
-0.02   1.00000000
```

```
0.   1.
end p-s table
saturation-relative k
0.22532178  2.680690E-11    ! saturation, Relative Permeability
0.25661515  5.008289E-09
0.28004868  4.760099E-08
0.31313708  4.516213E-07
0.37839157  8.763402E-06
0.45060625  8.090113E-05
0.49739729  2.496616E-04
0.54802657  7.088787E-04
0.58496215  1.394431E-03
0.61336611  2.258633E-03
0.63597157  3.250622E-03
0.65539787  4.391261E-03
0.68544939  6.861189E-03
0.71186889  9.994493E-03
0.74246249  0.01521536
0.77817876  0.02446315
0.80535621  0.03484376
0.83555850  0.05144394
0.86890602  0.07927722
0.89582405  0.11338976
0.92389193  0.16789906
0.94276352  0.22326156
0.96115858  0.30396440
0.97821106  0.42754706
0.99248653  0.63711289
0.99686866  0.77405567
0.99937138  0.92735098
1.       1.0
end s-k table
end tables
```

```
end material
!------------------------
! Porous medium property set
layer2
k isotropic
1.0D-5
specific storage
1.0D-5
porosity
0.01

longitudinal dispersivity
0.05
transverse dispersivity
0.005
vertical transverse dispersivity
0.005
tortuosity
0.1
bulk density
2000.0
unsaturated tables
pressure-saturation
-1000   0.22532178  ! pressure, Saturation
-200    0.25661515
-100    0.28004868
-50     0.31313708
-20     0.37839157
-10     0.45060625
-7.0    0.49739729
-5.0    0.54802657
-4.0    0.58496215
-3.4    0.61336611
```

-3.0 0.63597157

-2.7 0.65539787

-2.3 0.68544939

-2.0 0.71186889

-1.7 0.74246249

-1.4 0.77817876

-1.2 0.80535621

-1.0 0.83555850

-0.8 0.86890602

-0.65 0.89582405

-0.5 0.92389193

-0.4 0.94276352

-0.3 0.96115858

-0.2 0.97821106

-0.1 0.99248653

-0.06 0.99686866

-0.03 0.99937138

-0.02 1.00000000

0. 1.

end p-s table

saturation-relative k

0.22532178 2.680690E-11 ! saturation, Relative Permeability

0.25661515 5.008289E-09

0.28004868 4.760099E-08

0.31313708 4.516213E-07

0.37839157 8.763402E-06

0.45060625 8.090113E-05

0.49739729 2.496616E-04

0.54802657 7.088787E-04

0.58496215 1.394431E-03

0.61336611 2.258633E-03

0.63597157 3.250622E-03

0.65539787 4.391261E-03

0.68544939 6.861189E-03
0.71186889 9.994493E-03
0.74246249 0.01521536
0.77817876 0.02446315
0.80535621 0.03484376
0.83555850 0.05144394
0.86890602 0.07927722
0.89582405 0.11338976
0.92389193 0.16789906
0.94276352 0.22326156
0.96115858 0.30396440
0.97821106 0.42754706
0.99248653 0.63711289
0.99686866 0.77405567
0.99937138 0.92735098
1.   1.0
end s-k table
end tables
end material

RR6.0.fprops
vfracture
specific storage
4.4e-6
aperture
250.e-6
unsaturated brooks-corey functions
beta
2.5
pore connectivity
1.
air entry pressure
-0.14

generate tables from unsaturated functions

end

end material

!-------------------------

hfracture

specific storage

4.4e-6

aperture

125.e-6

end material

!-------------------------

RR6.0.oprops

overland flow

x friction

3.5D-6

y friction

3.5D-6

rill storage height

0.002 3.75d-3

!obstruction storage height

!0.25

coupling length

1.e-4

end material

RR7.0.grok

!-------------------------- Grid generation

Generate blocks interactive

grade x

0.0 1.0 0.1 1 0.1

grade y

50.0 0.0 0.002 5 1.0

grade y

```
50.0 100.0 0.002 5 1.0
grade z
2.5 0.0 0.002 5 0.25
grade z
2.5 9.5 0.002 5 0.25
grade z
10.0 9.90 0.002 1 0.002
grade z
9.90 9.50 0.002 10 0.01
end generate blocks intereactive
end grid generation
mesh to tecplot
gridadoodle.dat

!-------------------------  General simulation parameters
units: kilogram-metre-day
unsaturated
finite difference mode
remove negative coefficients
compute underrelaxation factor
no nodal flow check
do transport
transient flow

!-------------------------  Porous media properties
use zone type
porous media
properties file
rr.mprops

!-------rest of the domain
clear chosen elements
choose elements block
```

0.0, 1.0
0.0, 100.0
0.0, 10.0

new zone
2
clear chosen zones
choose zone number
2

read properties
layer2

!------------top layer (just around fracture)
clear chosen elements
choose elements block
0.0, 1.0
49.995, 50.005
9.89, 9.91
choose elements block
0.0, 1.0
0.0, 100.0
9.9, 10.0

new zone
1
clear chosen zones
choose zone number
1

read properties
layer1

```
!---soil
clear chosen elements
choose elements block
0.0, 1.0
0.0, 100.0
9.9, 10.0

new zone
3
clear chosen zones
choose zone number
3

read properties
soil

!-------------------------  Porous media flow

clear chosen nodes
choose nodes all
initial head
5.05

clear chosen nodes
choose nodes block
0.0, 1.0,
0.0, 0.0
0.0, 7.00
specified head
1
0.0, 5.5

clear chosen nodes
```

```
choose nodes block
0.0, 1.0,
100.0, 100.0
0.0, 7.00
specified head
1
0.0, 4.5

!------------------------- Solute Transport
Solute
name
precip

free-solution diffusion coefficient
1.74d-4
End solute

Solute
name
matrix
free-solution diffusion coefficient
1.74d-4     ! (m2/d)
End solute

clear chosen nodes
choose nodes all
initial concentration
0.0  !precip
1.0  !matrix

clear chosen nodes
choose nodes top
specified concentration
```

```
1                    ! number of time panels
0.0,  10.0, 1.0, 0.0    ! timeon, time off, species 1, 2, 3 concentration

clear chosen nodes
clear chosen faces
choose nodes y plane
0.0
1.e-5

specified concentration
1                    ! number of time panels
0.0,  30.0, 0.0, 1.0    ! timeon, time off, species 1, 2, 3 concentration

!-------------------------  Fracture media properties
use zone type
fracture
properties file
rr.fprops

!----Vertical Fracture...when fracture only goes to bottom of high K pm layer
clear chosen faces
choose faces block
0.0, 1.0
50.0, 50.0
0.0, 9.9

!-----Vertical Fracture...when fracture goes all the way to the top
!clear chosen faces
!choose faces y plane
!50.0
!1.e-5

new zone
```

```
1

clear chosen zones
choose zone number
1
read properties
vfracture

!....horizontal fracture
clear chosen faces
choose faces z plane
2.5
1.e-5

new zone
2

clear chosen zones
choose zone number
2
read properties
hfracture

!------------------------- Surface flow media properties
dual nodes for surface flow
use zone type
surface
properties file
rr.oprops
clear chosen faces
choose faces top
new zone
1
```

clear chosen zones
choose zone number
1

read properties
overland flow
clear chosen nodes
choose nodes top
initial water depth
1.D-6

clear chosen faces
choose faces top
specified rainfall
3
 0.0, 0.0
 1, 0.025
 2.0, 0.0

critical depth boundary all around
!------------------------------ Output
make observation point
5.0m_from_frac
0.5 55 2.5

initial timestep
1e-7
maximum timestep
1.0
output times
0.5
1

1.5
2
3
4
5
10
20
30
end

newton iteration control
7
Newton maximum iterations
12
Jacobian epsilon
1.0d-6
Newton absolute convergence criteria
1.0d-3
Newton residual convergence criteria
1.0d-3
flow solver convergence criteria
1e-8

RR7.0.mprops

! Porous medium property set
soil
k isotropic
1.0D-1
specific storage
1.0D-5
porosity
0.2
longitudinal dispersivity

0.05

transverse dispersivity

0.005

vertical transverse dispersivity

0.005

tortuosity

0.1

bulk density

2000.0

unsaturated tables

pressure-saturation

```
-1000   0.22532178  ! pressure, Saturation
-200    0.25661515
-100    0.28004868
-50     0.31313708
-20     0.37839157
-10     0.45060625
-7.0    0.49739729
-5.0    0.54802657
-4.0    0.58496215
-3.4    0.61336611
-3.0    0.63597157
-2.7    0.65539787
-2.3    0.68544939
-2.0    0.71186889
-1.7    0.74246249
-1.4    0.77817876
-1.2    0.80535621
-1.0    0.83555850
-0.8    0.86890602
-0.65   0.89582405
-0.5    0.92389193
-0.4    0.94276352
```

-0.3   0.96115858
-0.2   0.97821106
-0.1   0.99248653
-0.06   0.99686866
-0.03   0.99937138
-0.02   1.00000000
0.   1.
end p-s table

saturation-relative k
0.22532178 2.680690E-11   ! saturation, Relative Permeability
0.25661515 5.008289E-09
0.28004868 4.760099E-08
0.31313708 4.516213E-07
0.37839157 8.763402E-06
0.45060625 8.090113E-05
0.49739729 2.496616E-04
0.54802657 7.088787E-04
0.58496215 1.394431E-03
0.61336611 2.258633E-03
0.63597157 3.250622E-03
0.65539787 4.391261E-03
0.68544939 6.861189E-03
0.71186889 9.994493E-03
0.74246249 0.01521536
0.77817876 0.02446315
0.80535621 0.03484376
0.83555850 0.05144394
0.86890602 0.07927722
0.89582405 0.11338976
0.92389193 0.16789906
0.94276352 0.22326156
0.96115858 0.30396440

```
0.97821106  0.42754706
0.99248653  0.63711289
0.99686866  0.77405567
0.99937138  0.92735098
1.      1.0
end s-k table
end tables
end material
!-------------------------
! Porous medium property set
layer1
k isotropic
1.0D-1
specific storage
1.0D-5
porosity
0.01
longitudinal dispersivity
0.05
transverse dispersivity
0.005
vertical transverse dispersivity
0.005
tortuosity
0.1

bulk density
2000.0
unsaturated tables
pressure-saturation
-1000   0.22532178  ! pressure, Saturation
-200    0.25661515
-100    0.28004868
```

-50 0.31313708
-20 0.37839157
-10 0.45060625
-7.0 0.49739729
-5.0 0.54802657
-4.0 0.58496215
-3.4 0.61336611
-3.0 0.63597157
-2.7 0.65539787
-2.3 0.68544939
-2.0 0.71186889
-1.7 0.74246249
-1.4 0.77817876
-1.2 0.80535621
-1.0 0.83555850
-0.8 0.86890602
-0.65 0.89582405
-0.5 0.92389193
-0.4 0.94276352
-0.3 0.96115858
-0.2 0.97821106
-0.1 0.99248653
-0.06 0.99686866
-0.03 0.99937138
-0.02 1.00000000
0. 1.
end p-s table

saturation-relative k
0.22532178 2.680690E-11 ! saturation, Relative Permeability
0.25661515 5.008289E-09
0.28004868 4.760099E-08
0.31313708 4.516213E-07

```
0.37839157  8.763402E-06
0.45060625  8.090113E-05
0.49739729  2.496616E-04
0.54802657  7.088787E-04
0.58496215  1.394431E-03
0.61336611  2.258633E-03
0.63597157  3.250622E-03
0.65539787  4.391261E-03
0.68544939  6.861189E-03
0.71186889  9.994493E-03
0.74246249  0.01521536
0.77817876  0.02446315
0.80535621  0.03484376
0.83555850  0.05144394
0.86890602  0.07927722
0.89582405  0.11338976
0.92389193  0.16789906
0.94276352  0.22326156
0.96115858  0.30396440
0.97821106  0.42754706
0.99248653  0.63711289
0.99686866  0.77405567
0.99937138  0.92735098
1.      1.0
end s-k table
end tables
end material

!-------------------------
! Porous medium property set
layer2
k isotropic
1.0D-5
```

specific storage

1.0D-5

porosity

0.01

longitudinal dispersivity

0.05

transverse dispersivity

0.005

vertical transverse dispersivity

0.005

tortuosity

0.1

bulk density

2000.0

unsaturated tables

pressure-saturation

```
-1000   0.22532178  ! pressure, Saturation
-200    0.25661515
-100    0.28004868
-50     0.31313708
-20     0.37839157
-10     0.45060625
-7.0    0.49739729
-5.0    0.54802657
-4.0    0.58496215
-3.4    0.61336611
-3.0    0.63597157
-2.7    0.65539787
-2.3    0.68544939
-2.0    0.71186889
-1.7    0.74246249
-1.4    0.77817876
-1.2    0.80535621
```

-1.0 0.83555850
-0.8 0.86890602
-0.65 0.89582405
-0.5 0.92389193
-0.4 0.94276352
-0.3 0.96115858
-0.2 0.97821106
-0.1 0.99248653
-0.06 0.99686866
-0.03 0.99937138
-0.02 1.00000000
0. 1.
end p-s table

saturation-relative k
0.22532178 2.680690E-11 ! saturation, Relative Permeability
0.25661515 5.008289E-09
0.28004868 4.760099E-08
0.31313708 4.516213E-07
0.37839157 8.763402E-06
0.45060625 8.090113E-05
0.49739729 2.496616E-04
0.54802657 7.088787E-04
0.58496215 1.394431E-03
0.61336611 2.258633E-03
0.63597157 3.250622E-03
0.65539787 4.391261E-03
0.68544939 6.861189E-03
0.71186889 9.994493E-03
0.74246249 0.01521536
0.77817876 0.02446315
0.80535621 0.03484376
0.83555850 0.05144394

```
0.86890602  0.07927722
0.89582405  0.11338976
0.92389193  0.16789906
0.94276352  0.22326156
0.96115858  0.30396440
0.97821106  0.42754706
0.99248653  0.63711289
0.99686866  0.77405567
0.99937138  0.92735098
1.      1.0
end s-k table
end tables
end material
```

RR7.0.fprops

```
vfracture
specific storage
4.4e-6
aperture
250.e-6
unsaturated brooks-corey functions
beta
2.5
pore connectivity
1.
air entry pressure
-0.14
generate tables from unsaturated functions
end
end material
!------------------------
hfracture
specific storage
```

4.4e-6

aperture

125.e-6

end material

!-------------------------

RR7.0.oprops

overland flow

x friction

3.5D-6

y friction

3.5D-6

rill storage height

0.002 3.75d-3

!obstruction storage height

!0.25

coupling length

1.e-4

end material

LIN.grok

! ----------- Grid Generation

Read gb 2d grid

.\lingrid1m\lin50

Generate layers from gb 2d grid

.false.

.true.

0.0

2

Base Layer

65

.true.

65.0

```
Surface Layer
15
.false.
.\lingrid1m\lin50.nprop.50

end Grid Generation

mesh to tecplot
lingridcheck.dat

!-------------General simulation parameters
unsaturated
transient flow
no nodal flow check

! ------------Porous media properties
use zone type
porous media

properties file
lin.mprops

clear chosen zones
choose zones all
read properties
Sand, Borden unsat props

!------------Porous media flow
clear chosen nodes
choose nodes all
initial Head surface elevation

!-------------------------  Fracture media properties
```

```
use zone type
fracture
properties file
lin.fprops

!----------------150 um horizontal fractures
clear chosen faces
clear chosen nodes

!horizontal fracture in hill
choose faces block by layer
0.0, 20.0
0.0, 1.0
65.0,75.0
72, 72

choose faces block
0.0,50.0
0.0, 1.0
30.0, 32.0

choose faces block
0.0,50.0
0.0, 1.0
42.0, 44.0

choose faces block
0.0,50.0
0.0, 1.0
58.0, 58.0

new zone
1
```

clear chosen zones
choose zone number
1

read properties
hfracture150

!----------------300 um horizontal fractures
clear chosen faces
choose faces block
0.0,50.0
0.0, 1.0
28.0, 28.0
choose faces block
0.0,50.0
0.0, 1.0
33.0, 33.0
choose faces block
0.0,50.0
0.0, 1.0
50.0, 50.0
choose faces block
0.0,50.0
0.0, 1.0
65.0, 65.0
new zone
2
clear chosen zones
choose zone number
2
read properties
hfracture300

```
!----------------500 um horizontal fractures
clear chosen faces
choose faces block
0.0,50.0
0.0, 1.0
49.0, 49.0

choose faces block
0.0,50.0
0.0, 1.0
52.0, 52.0

new zone
3
clear chosen zones
choose zone number
3

read properties
hfracture500

!----------------vertical fractures
clear chosen faces
choose faces x plane
3.0
0.5
choose faces x plane
4.0
0.5
choose faces x plane
41.0
0.5
choose faces x plane
```

```
42.0
0.5
new zone
4
clear chosen zones
choose zone number
4

read properties
vfracture200

!-------------------------  Surface flow media properties

dual nodes for surface flow

use zone type
surface

properties file
lin.oprops

clear chosen faces
choose faces top

new zone
1

clear chosen zones
choose zone number
1

read properties
overland flow
```

```
clear chosen nodes
choose nodes top
initial water depth
1.e-4

clear chosen faces
choose faces top
uniform rainfall
2.9D-8  !0.9 m/year

!------------------------  Surface flow parameters

clear chosen nodes
choose node
50,0,69.5
choose node
50,1,69.5
write chosen nodes
thenodesare.txt

critical depth boundary
.false.        ! grid builder numbering
7937
7938
end

!-------------Output

output times
1.
10.
100.
```

1E3

1E5

1E7

1E9

end

make observation point

upper_swamp_ob_pt

4,0.5,78

make observation point

lower_swamp_ob_pt

42,0.5,68

!--------------Numerical parameters

newton iteration control

10

Newton maximum iterations

15

Newton absolute convergence criteria

1.0d-3

Newton residual convergence criteria

1.0d-4

LIN.mprops

Sand, Borden unsat props

k isotropic

1.0e-7

porosity

0.35

unsaturated tables

pressure-saturation

! drying table

```
-1000.0        1.800000000e-01
  -5.000000D+00 1.800105973D-01
  -4.900000D+00 1.800117237D-01
  -4.800000D+00 1.800129968D-01
  -4.700000D+00 1.800144396D-01
  -4.600000D+00 1.800160788D-01
  -4.500000D+00 1.800179466D-01
  -4.400000D+00 1.800200808D-01
  -4.300000D+00 1.800225269D-01
  -4.200000D+00 1.800253394D-01
  -4.100000D+00 1.800285841D-01
  -4.000000D+00 1.800323402D-01
  -3.900000D+00 1.800367046D-01
  -3.800000D+00 1.800417950D-01
  -3.700000D+00 1.800477566D-01
  -3.600000D+00 1.800547683D-01
  -3.500000D+00 1.800630523D-01
  -3.400000D+00 1.800728863D-01
  -3.300000D+00 1.800846194D-01
  -3.200000D+00 1.800986935D-01
  -3.100000D+00 1.801156721D-01
  -3.000000D+00 1.801362790D-01
  -2.900000D+00 1.801614518D-01
  -2.800000D+00 1.801924153D-01
  -2.700000D+00 1.802307847D-01
  -2.600000D+00 1.802787110D-01
  -2.500000D+00 1.803390894D-01
  -2.400000D+00 1.804158621D-01
  -2.300000D+00 1.805144636D-01
  -2.200000D+00 1.806424873D-01
  -2.100000D+00 1.808106990D-01
  -2.000000D+00 1.810346076D-01
```

-1.900000D+00 1.813369475D-01
-1.800000D+00 1.817516898D-01
-1.700000D+00 1.823306801D-01
-1.600000D+00 1.831549152D-01
-1.516621D+00 1.841212434D-01
-1.454555D+00 1.850767205D-01
-1.404231D+00 1.860513249D-01
-1.362548D+00 1.870321195D-01
-1.327140D+00 1.880178341D-01
-1.296499D+00 1.890067482D-01
-1.269582D+00 1.899979273D-01
-1.245641D+00 1.909907523D-01
-1.224129D+00 1.919848088D-01
-1.204630D+00 1.929798091D-01
-1.186826D+00 1.939755476D-01
-1.170464D+00 1.949718739D-01
-1.155344D+00 1.959686756D-01
-1.141303D+00 1.969658671D-01
-1.128208D+00 1.979633817D-01
-1.115948D+00 1.989611675D-01
-1.104429D+00 1.999591827D-01
-1.093573D+00 2.009573939D-01
-1.083312D+00 2.019557737D-01
-1.073052D+00 2.030111066D-01
-1.063052D+00 2.040980402D-01
-1.053052D+00 2.052463626D-01
-1.043052D+00 2.064600684D-01
-1.033052D+00 2.077434411D-01
-1.023052D+00 2.091010757D-01
-1.013052D+00 2.105379025D-01
-1.003052D+00 2.120592129D-01
-9.930521D-01 2.136706875D-01
-9.830521D-01 2.153784255D-01

-9.730521D-01	2.171889769D-01
-9.630521D-01	2.191093765D-01
-9.530521D-01	2.211471809D-01
-9.430521D-01	2.233105069D-01
-9.330521D-01	2.256080731D-01
-9.230521D-01	2.280492439D-01
-9.130521D-01	2.306440754D-01
-9.030521D-01	2.334033645D-01
-8.930521D-01	2.363386990D-01
-8.830521D-01	2.394625109D-01
-8.730521D-01	2.427881303D-01
-8.630521D-01	2.463298408D-01
-8.530521D-01	2.501029348D-01
-8.430521D-01	2.541237691D-01
-8.330521D-01	2.584098175D-01
-8.230521D-01	2.629797215D-01
-8.130521D-01	2.678533350D-01
-8.030521D-01	2.730517619D-01
-7.930521D-01	2.785973835D-01
-7.830521D-01	2.845138719D-01
-7.730521D-01	2.908261864D-01
-7.630521D-01	2.975605459D-01
-7.530521D-01	3.047443739D-01
-7.430521D-01	3.124062077D-01
-7.330521D-01	3.205755645D-01
-7.230521D-01	3.292827562D-01
-7.130521D-01	3.385586425D-01
-7.030521D-01	3.484343130D-01
-6.930521D-01	3.589406855D-01
-6.830521D-01	3.701080119D-01
-6.730521D-01	3.819652788D-01
-6.630521D-01	3.945394950D-01
-6.530521D-01	4.078548593D-01

-6.430521D-01	4.219318038D-01
-6.330521D-01	4.367859181D-01
-6.230521D-01	4.524267619D-01
-6.130521D-01	4.688565875D-01
-6.030521D-01	4.860690018D-01
-5.930521D-01	5.040476139D-01
-5.830521D-01	5.227647261D-01
-5.730521D-01	5.421801425D-01
-5.630521D-01	5.622401805D-01
-5.530521D-01	5.828769834D-01
-5.430521D-01	6.040082311D-01
-5.330521D-01	6.255373462D-01
-5.230521D-01	6.473542759D-01
-5.130521D-01	6.693369047D-01
-5.030521D-01	6.913531167D-01
-4.930521D-01	7.132634796D-01
-4.830521D-01	7.349244702D-01
-4.730521D-01	7.561921115D-01
-4.630521D-01	7.769258427D-01
-4.530521D-01	7.969924138D-01
-4.430521D-01	8.162695787D-01
-4.330521D-01	8.346493723D-01
-4.230521D-01	8.520407811D-01
-4.130521D-01	8.683716669D-01
-4.030521D-01	8.835898627D-01
-3.930521D-01	8.976634244D-01
-3.830521D-01	9.105800835D-01
-3.730521D-01	9.223460002D-01
-3.630521D-01	9.329839522D-01
-3.530521D-01	9.425311174D-01
-3.430521D-01	9.510366113D-01
-3.330521D-01	9.585589328D-01
-3.230521D-01	9.651634513D-01

```
  -3.130521D-01 9.709200398D-01
  -3.030521D-01 9.759009330D-01
  -2.930521D-01 9.801788595D-01
  -2.830521D-01 9.838254706D-01
  -2.730521D-01 9.869100712D-01
  -2.630521D-01 9.894986385D-01
  -2.530521D-01 9.916531063D-01
  -2.430521D-01 9.934308830D-01
  -2.330521D-01 9.948845715D-01
  -2.230521D-01 9.960618561D-01
  -2.130521D-01 9.970055245D-01
  -2.030521D-01 9.977535953D-01
  -1.930521D-01 9.983395246D-01
  -1.830521D-01 9.987924701D-01
  -1.730521D-01 9.991375933D-01
  -1.630521D-01 9.993963848D-01
  -1.530521D-01 9.995870014D-01
  -1.430521D-01 9.997246035D-01
  -1.312358D-01 9.998358001D-01
  -1.087065D-01 9.999469535D-01
  -4.592805D-02 9.999996982D-01
   0.000000D+00 1.000000000D+00
end  ! drying
saturation-relative k
  1.800105973D-01 4.4549345538D-04
  1.800117237D-01 4.4550599991D-04
  1.800129968D-01 4.4552017931D-04
  1.800144396D-01 4.4553624767D-04
  1.800160788D-01 4.4555450525D-04
  1.800179466D-01 4.4557530809D-04
  1.800200808D-01 4.4559908001D-04
  1.800225269D-01 4.4562632744D-04
  1.800253394D-01 4.4565765803D-04
```

1.800285841D-01	4.4569380394D-04
1.800323402D-01	4.4573565137D-04
1.800367046D-01	4.4578427795D-04
1.800417950D-01	4.4584100062D-04
1.800477566D-01	4.4590743715D-04
1.800547683D-01	4.4598558573D-04
1.800630523D-01	4.4607792874D-04
1.800728863D-01	4.4618756896D-04
1.800846194D-01	4.4631840982D-04
1.800986935D-01	4.4647539581D-04
1.801156721D-01	4.4666483605D-04
1.801362790D-01	4.4689484378D-04
1.801614518D-01	4.4717593946D-04
1.801924153D-01	4.4752188707D-04
1.802307847D-01	4.4795086747D-04
1.802787110D-01	4.4848714515D-04
1.803390894D-01	4.4916346825D-04
1.804158621D-01	4.5002457562D-04
1.805144636D-01	4.5113240530D-04
1.806424873D-01	4.5257396940D-04
1.808106990D-01	4.5447349924D-04
1.810346076D-01	4.5701159952D-04
1.813369475D-01	4.6045623081D-04
1.817516898D-01	4.6521430296D-04
1.823306801D-01	4.7192054431D-04
1.831549152D-01	4.8159681033D-04
1.841212434D-01	4.9313695138D-04
1.850767205D-01	5.0475784737D-04
1.860513249D-01	5.1682968789D-04
1.870321195D-01	5.2920371018D-04
1.880178341D-01	5.4187074558D-04
1.890067482D-01	5.5481462030D-04
1.899979273D-01	5.6802818405D-04

1.909907523D-01	5.8150777724D-04
1.919848088D-01	5.9525204449D-04
1.929798091D-01	6.0926106629D-04
1.939755476D-01	6.2353586674D-04
1.949718739D-01	6.3807811112D-04
1.959686756D-01	6.5288991471D-04
1.969658671D-01	6.6797371824D-04
1.979633817D-01	6.8333220465D-04
1.989611675D-01	6.9896824192D-04
1.999591827D-01	7.1488484320D-04
2.009573939D-01	7.3108513829D-04
2.019557737D-01	7.4757235298D-04
2.030111066D-01	7.6531300583D-04
2.040980402D-01	7.8392543534D-04
2.052463626D-01	8.0396957172D-04
2.064600684D-01	8.2558596457D-04
2.077434411D-01	8.4893207950D-04
2.091010757D-01	8.7418470106D-04
2.105379025D-01	9.0154272607D-04
2.120592129D-01	9.3123041827D-04
2.136706875D-01	9.6350120895D-04
2.153784255D-01	9.9864214557D-04
2.171889769D-01	1.0369791109D-03
2.191093765D-01	1.0788829611D-03
2.211471809D-01	1.1247767600D-03
2.233105069D-01	1.1751443273D-03
2.256080731D-01	1.2305403630D-03
2.280492439D-01	1.2916024647D-03
2.306440754D-01	1.3590654287D-03
2.334033645D-01	1.4337783043D-03
2.363386990D-01	1.5167247806D-03
2.394625109D-01	1.6090476098D-03
2.427881303D-01	1.7120779289D-03

2.463298408D-01	1.8273705357D-03
2.501029348D-01	1.9567464126D-03
2.541237691D-01	2.1023440799D-03
2.584098175D-01	2.2666817196D-03
2.629797215D-01	2.4527324414D-03
2.678533350D-01	2.6640155893D-03
2.730517619D-01	2.9047076276D-03
2.785973835D-01	3.1797769025D-03
2.845138719D-01	3.4951474917D-03
2.908261864D-01	3.8578984193D-03
2.975605459D-01	4.2765057549D-03
3.047443739D-01	4.7611365245D-03
3.124062077D-01	5.3240049165D-03
3.205755645D-01	5.9798029200D-03
3.292827562D-01	6.7462191842D-03
3.385586425D-01	7.6445613662D-03
3.484343130D-01	8.7004982804D-03
3.589406855D-01	9.9449383647D-03
3.701080119D-01	1.1415059772D-02
3.819652788D-01	1.3155503977D-02
3.945394950D-01	1.5219738126D-02
4.078548593D-01	1.7671580136D-02
4.219318038D-01	2.0586863278D-02
4.367859181D-01	2.4055191998D-02
4.524267619D-01	2.8181706582D-02
4.688565875D-01	3.3088730143D-02
4.860690018D-01	3.8917117464D-02
5.040476139D-01	4.5827064020D-02
5.227647261D-01	5.3998070355D-02
5.421801425D-01	6.3627701242D-02
5.622401805D-01	7.4928744697D-02
5.828769834D-01	8.8124380815D-02
6.040082311D-01	1.0344103486D-01

6.255373462D-01	1.2109873181D-01
6.473542759D-01	1.4129900198D-01
6.693369047D-01	1.6421070653D-01
6.913531167D-01	1.8995453347D-01
7.132634796D-01	2.1858731009D-01
7.349244702D-01	2.5008761564D-01
7.561921115D-01	2.8434437509D-01
7.769258427D-01	3.2115009442D-01
7.969924138D-01	3.6020011246D-01
8.162695787D-01	4.0109869638D-01
8.346493723D-01	4.4337205836D-01
8.520407811D-01	4.8648753647D-01
8.683716669D-01	5.2987740681D-01
8.835898627D-01	5.7296522094D-01
8.976634244D-01	6.1519229214D-01
9.105800835D-01	6.5604202701D-01
9.223460002D-01	6.9506018153D-01
9.329839522D-01	7.3186972446D-01
9.425311174D-01	7.6617969392D-01
9.510366113D-01	7.9778811440D-01
9.585589328D-01	8.2657960330D-01
9.651634513D-01	8.5251868209D-01
9.709200398D-01	8.7564000061D-01
9.759009330D-01	8.9603670340D-01
9.801788595D-01	9.1384805426D-01
9.838254706D-01	9.2924723811D-01
9.869100712D-01	9.4243002512D-01
9.894986385D-01	9.5360474747D-01
9.916531063D-01	9.6298383045D-01
9.934308830D-01	9.7077695012D-01
9.948845715D-01	9.7718576495D-01
9.960618561D-01	9.8240008546D-01
9.970055245D-01	9.8659529863D-01

```
  9.977535953D-01 9.8993084456D-01
  9.983395246D-01 9.9254954370D-01
  9.987924701D-01 9.9457758693D-01
  9.991375933D-01 9.9612502270D-01
  9.993963848D-01 9.9728659971D-01
  9.995870014D-01 9.9814284907D-01
  9.997246035D-01 9.9876131293D-01
  9.998358001D-01 9.9926131293D-01
  9.999469535D-01 9.9976131293D-01
  9.999996982D-01 9.9999864220D-01
  1.000000000D+00 1.0000000000D+00
end ! sat-krw
end ! unsat tables
end  ! material
```

LIN.fprops

```
hfracture150
specific storage
4.4e-6
aperture
150.0e-6
unsaturated tables
pressure-saturation
-1.5        0.29
-0.225    0.29
-0.15   0.3
0.0 1.0
end  ! p-sat
saturation-relative k
  0.0 0.0
  0.2399   0.0
  0.24   0.0017
  0.33  0.0251
```

```
  1.0  1.0
end ! sat-krw
end ! unsat tables
end  ! material

!------------------------
hfracture300
specific storage
4.4e-6
aperture
300.e-6

unsaturated tables
pressure-saturation
-1.5         0.29
-0.225    0.29
-0.15   0.3
0.0 1.0
end  ! p-sat
saturation-relative k
  0.0 0.0
  0.2399   0.0
  0.24   0.0017
  0.33  0.0251
  1.0  1.0
end ! sat-krw
end ! unsat tables
end  ! material

!------------------------
hfracture500
specific storage
4.4e-6
```

```
aperture
500.e-6
unsaturated tables
pressure-saturation
-1.5        0.29
-0.225    0.29
-0.15   0.3
0.0 1.0
end  ! p-sat
saturation-relative k
  0.0 0.0
  0.2399   0.0
  0.24   0.0017
  0.33  0.0251
  1.0  1.0
end ! sat-krw
end ! unsat tables
end  ! material

!-----------------------
vfracture200
specific storage
4.4e-6
aperture
100.e-6
unsaturated tables
pressure-saturation
-1.5        0.29
-0.225    0.29
-0.15   0.3
0.0 1.0
end  ! p-sat
saturation-relative k
```

```
  0.0 0.0
  0.2399   0.0
  0.24   0.0017
  0.33  0.0251
  1.0  1.0
end ! sat-krw
end ! unsat tables
end  ! material
end material
!------------------------
```

LIN .oprops

```
overland flow
x friction
0.3
y friction
0.3
rill storage height
0.002  3.75d-3
!obstruction storage height
!0.25
coupling length
1.e-4
end material
```

Appendix E: Lineament identification methodology and data

Multiple data types highlight different lineament characteristics resulting in a defensible lineament identification method [*Mabee, et al.*, 1994; *Clark, et al.*, 1996; *Sander, et al.*, 1997]. Landsat imagery highlights tonal differences; a digital elevation model (DEM) reveals topographic differences; and aerial photographs show detailed geomorphology. To conduct this study a multispectral Landsat 5 Thematic Mapper image with 30 m resolution was acquired at 15:34:50 on Sept. 26, 2004 from orbit 109424. The center of the frame is 44.61N. False color composites of bands 742, 754 and 432 were examined, but false color composite 754 was the most useful, as found by *Andjelkovic and Cruden* [1998]. The DEM was developed by the Ontario Ministry of Natural Resources and is accurate to ± 5 m vertically and ± 10 m horizontally, with a raster resolution of 10 m. Surface water elevations are considered representative ± 5 m because elevations were corrected to provincial time-series flow data. For lineament identification, the DEM was hillshade enhanced to accentuate features in the subdued landscape. Aerial photographs of selected areas at 1:5,000 to 1:12,000 scales were examined to further characterize the geomorphology and hydrology of lineaments during ground truthing.

Lineaments were identified on DEM and the False Color Composite Landsat images, at scales of 1:250,000, 1:100,000 and 1:50,000. The scale observed is considered an important lineament characteristic for classifying the spatial significance of the lineament. Lineament attributes (azimuth, scale observed, date observed, and curvilinear form) were compiled during identification. All lineaments were identified manually because attempts at automated lineament detection primarily identified anthropomorphic features. Lineaments were observed during multiple trials separated by a week to test reproducibility [*Mabee, et al.*, 1994]. All lineaments not repeatedly identified at the same scale, as well as all anthropomorphic lineaments (roads, electrical lines, *etc.*), were removed from the database. In addition, lineaments derived from Landsat imagery were compared to lineaments derived from the same area using a different Landsat image by *Andjelkovic and Cruden* [1998]. Lineaments were not explicitly correlated to nearby fracture patterns, as recommended *Mabee et al.* [1994], in order to keep the lineament and fracture data bases independent for subsequent structural analysis. Lineament orientation was plotted as rose diagrams with a 10 degree smoothing function and the linear directional mean was calculated.

As discussed in Section 3.4.1, the specific capacity of water wells was interpolated using kriging and inverse weighted distance functions. For kriging, two different experimental variograms were created (Table E.1). Variogram 1 (67 m lag distance) was generated automatically in ArcGIS (Figure E.1). Whereas the lag distance of variogram 2 (500 m) is more representative of the average distance between water wells in the study area (Figure E.2). At both lag distances there was limited anisotropy in the experimental variogram. Figure E.3 illustrates kriged maps for the two different lag distances and indicates that the lineament distribution is not coincident with the areas of high well specific capacity. Figure 3.4 illustrates the interpolation using the inverse weighted distance function.

Table E.1 Variogram characteristics from geostatistical analysis of well specific capacity.

Parameter	Variogram 1 (Figure E.1A)	Variogram 2 (Figure E.1B)
Lag distance (m)	67	500
Number of lags	12	12
Range (m)	800	911
Sill $(L/min/m)^2$	350	180
Nugget $(L/min/m)^2$	5.4	113

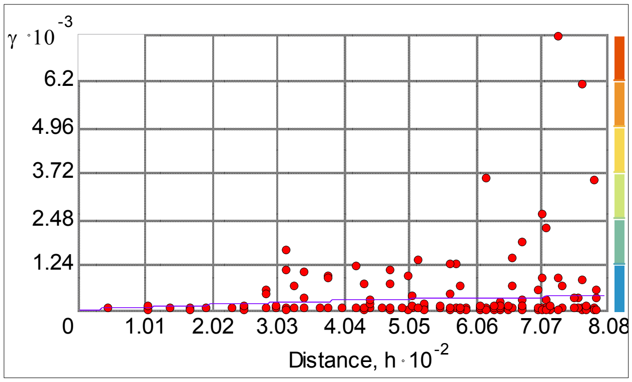

Figure E.1 Experimental and model variogram 1 with a lag distance of 67 m.

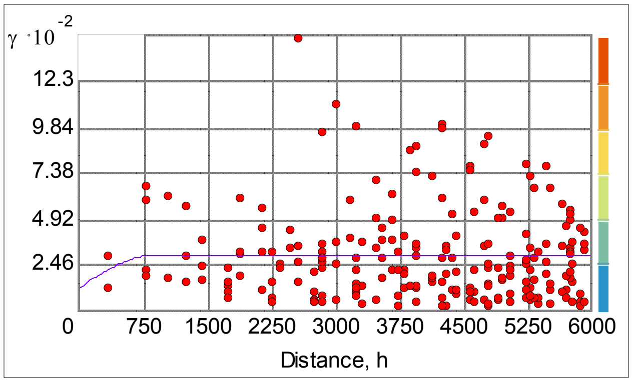

Figure E.2 Experimental and model variogram 2 with a lag distance of 500 m.

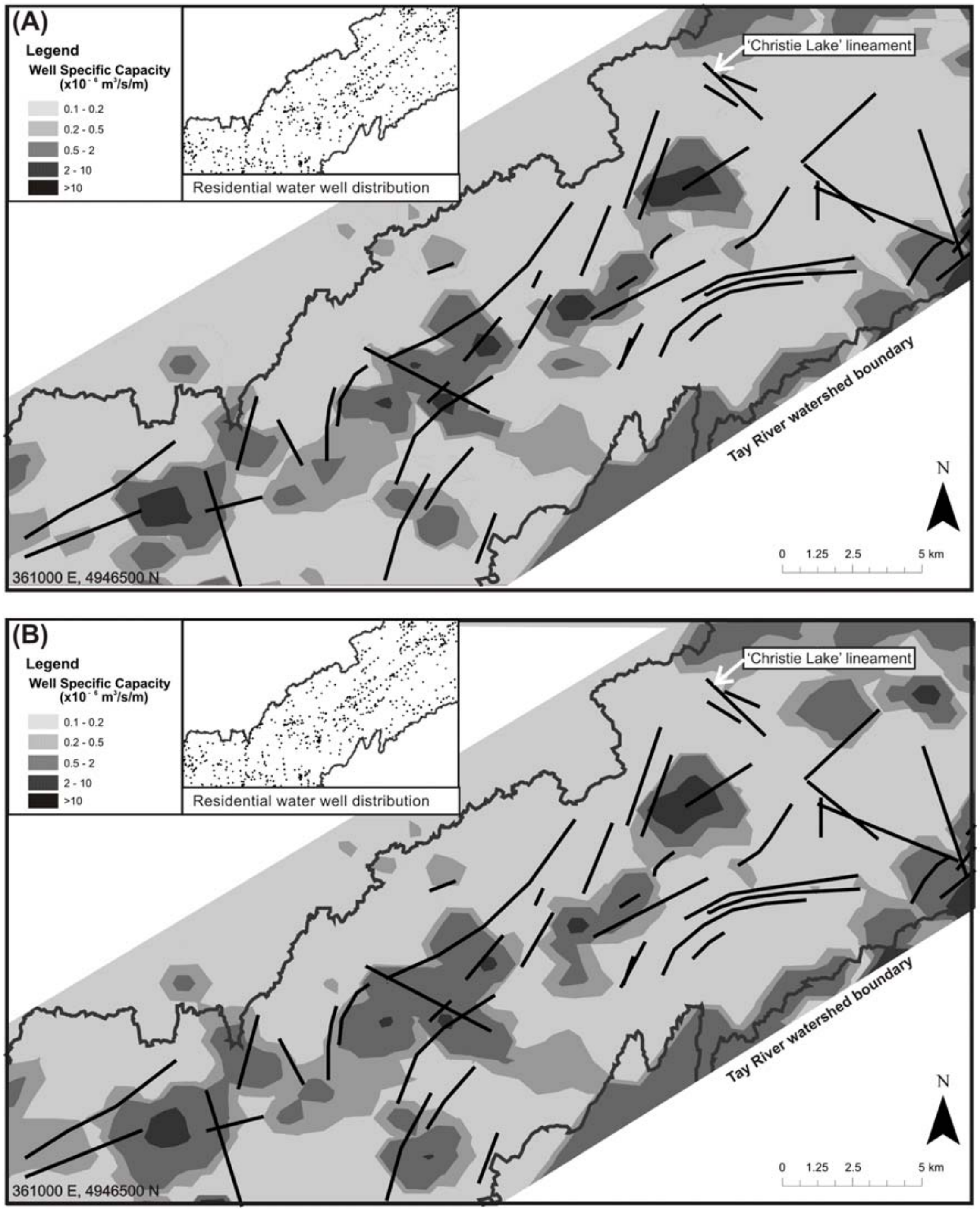

Figure E.3 The distribution of DEM-derived lineaments comparted to the kriged well specific capacity with a lag distance of (A) 67 m and (B) 500 m.

Table E.2. Lineaments identified using digital elevation model (DEM)

Scale observed (1:XXX,000)	Curvilinear (1=yes; 0=no)	Lakeshore (1=yes; 0=no)
50	0	0
50	0	0
50	0	0
50	0	0
50	1	0
50	1	1
50	0	0
50	1	1
50	0	0
50	0	0
50	0	0
50	0	0
50	0	0
50	1	0
50	0	1
50	0	0
50	0	0
50	0	0
100	0	0
100	0	0
100	0	0
100	0	0
100	0	0
100	0	0
100	0	0
100	0	1
100	0	0
100	0	0
100	0	0
100	1	0

100	0	1
100	0	1
100	1	0
100	1	1
100	0	1
100	0	0
100	0	0
100	0	0
250	0	0
250	0	0
250	1	1
250	0	0
250	0	0
250	0	0
250	1	0
250	1	0
250	1	0
250	1	1
250	0	1
250	0	0
250	0	0
250	0	1
250	1	0
250	1	1
250	0	0
250	0	0
250	1	1
250	1	1
250	1	0
250	0	0

Table E.3 Lineaments identified using Landsat imagery

Scale observed (1:XXX,000)	Curvilinear (1=yes; 0=no)	Lakeshore (1=yes; 0=no)
50	0	0
50	0	0
50	0	0
50	0	0
50	0	0
50	0	1
50	0	0
50	0	0
50	0	0
50	0	0
50	0	0
50	0	0
50	0	0
50	0	1
50	0	0
50	0	0
50	0	0
50	0	1
50	0	0
50	0	0
50	0	0
50	0	1
50	0	1
50	0	0
50	0	0
50	0	0
50	0	1
50	0	0
50	0	1
50	0	1

50	0	0
50	0	0
50	0	0
50	0	1
50	0	0
50	0	1
50	0	1
50	0	1
50	0	1
50	0	0
50	0	0
50	0	0
50	0	0
50	0	0
50	0	0
50	0	0
50	0	0
50	0	1
50	0	0
50	0	0
50	1	0
50	1	0
50	1	0
100	0	0
100	0	0
100	0	1
100	0	0
100	0	1
100	0	0
100	0	0
100	0	1
100	0	0
100	0	0

100	0	0
100	0	1
100	0	0
100	0	1
100	0	0
100	0	0
100	0	0
100	0	0
100	0	0
100	0	0
100	0	1
100	0	0
100	0	0
100	0	0
100	0	0
100	0	1
100	0	1
100	0	1
100	0	0
100	0	0
100	0	0
100	0	0
100	0	0
100	0	0
100	0	0
100	0	0
100	0	0
100	0	0
100	0	0
100	0	0
100	0	0
100	1	0
100	1	1

100	1	1
100	1	1
100	1	1
100	1	0
250	0	0
250	0	1
250	0	1
250	0	1
250	0	0
250	0	0
250	0	1
250	0	0
250	0	1
250	0	1
250	1	1
250	1	1

Appendix F: Structural data

Appendix F compiles structural data from the Tay River watershed that was collected using the methodology outlined in Chapter 3. Station names and locations in UTM coordinates are listed in Table 3. Table 4 compiles the strike and dip (XXX/YY) using the right-hand rule of discrete fractures (S_f) and foliation (S_1). For discrete fractures at select stations, the fracture termination style (A = abutting; B = blind; X = cross-cutting), fracture length and distance along outcrop are also recorded.

Table F.1 Station location

Station	Easting	Northing
TG06-01	383730	4956800
TG06-02	386441	4957213
TG06-03	395319	4965421
TG06-04	395238	4964172
TG06-05	394834	4964565
TG06-06	375580	4955973
TG06-07	385069	4962408
TG06-08	385183	4962687
TG06-09	377141	4956313
TG06-10	378110	4956577
TG06-11	387600	4960035
TG06-12	388167	4959963
TG06-13	389953	4956400
TG06-20	384710	4962955
TG06-21	384670	4962817
TG06-22	393495	4968266
TG06-23	380710	4959617

Table F.2 Structural data

Station (TG06-)	S_1/S_f	Strike	Dip	Dipping	Length (m)	Termination 1 (A,B,X)	Termination 2 (A,B,X)	Distance along outcrop (m)
TG06-01	S_f	83	37	S				
TG06-01	S_f	70	49	S				
TG06-01	S_1	60	36	S				
TG06-03	S_f	241	80					
TG06-03	S_f	135	85					
TG06-03	S_f	140	90					
TG06-03	S_1	25	?					
TG06-05	S_f	142	87					
TG06-05	S_1	200	?					
TG06-06	S_f	347	11	NE				
TG06-06	S_f	2	15	E				
TG06-06	S_f	347	23	E				
TG06-06	S_f	344	25	NE				
TG06-06	S_f	4	31	E				
TG06-06	S_f	353	35	E				
TG06-06	S_f	323	35	NE				
TG06-06	S_f	140	54					
TG06-06	S_f	46	85					
TG06-06	S_f	150	87					
TG06-06	S_f	325	87					
TG06-06	S_f	123	89					
TG06-06	S_f	136	90					
TG06-06	S_f	133	90					
TG06-06	S_f	125	90					
TG06-06	S_f	43	90					
TG06-06	S_f	49	90					
TG06-06	S_f	50	90					
TG06-06	S_1	16	81	E				
TG06-06	S_1	35	85	SE				
TG06-07	S_f	141	3	S	5	A	A	39-44

TG06-07	S_f	190	5					
TG06-07	S_f	45	8					131
TG06-07	S_f	270	9		4	-	A	27-31
TG06-07	S_f	36	13	SE	14	A	X	53-67
TG06-07	S_f	81	14	S		A	A	0-4.3
TG06-07	S_f	76	14	S	10	A	-	6.6-17
TG06-07	S_f	65	14		6	A	-	17-24.5
TG06-07	S_f	220	15	NW	3	A	A	165-168
TG06-07	S_f	100	16	S		A	A	0-4.3
TG06-07	S_f	150	17	W		-	-	24
TG06-07	S_f	8	19	S	4	-	A	31
TG06-07	S_f	105	26	S	2	A	A	6-8.5
TG06-07	S_f	246	27					
TG06-07	S_f	225	30	NW				
TG06-07	S_f	230	32					
TG06-07	S_f	225	33		11	A	A	71-82
TG06-07	S_f	260	34		7	-	A	86-93
TG06-07	S_f	230	40	NW				
TG06-07	S_f	270	44					
TG06-07	S_f	175	45	S	6	A	A	45-51
TG06-07	S_f	176	46	W	1.5	A	-	7
TG06-07	S_f	230	47	NW	7	A	-	113
TG06-07	S_f	306	49	N	1	A	B	32
TG06-07	S_f	302	53	N	4	-	A	111
TG06-07	S_f	205	53	NE	8	A	A	134-142
TG06-07	S_f	222	55	NW	2	-	-	96
TG06-07	S_f	264	56	N	4	-	A	10
TG06-07	S_f	242	57	N	20	-	-	57
TG06-07	S_f	220	57		19	-	A	160
TG06-07	S_f	56	58	S	4	-	A	33
TG06-07	S_f	324	59		1.5	A	A	33
TG06-07	S_f	332	60	NE	2	-	A	84
TG06-07	S_f	40	62					

TG06-07	S_f	53	63	S	15	-	A	42
TG06-07	S_f	266	64	NE	5	B	A	63
TG06-07	S_f	312	67	NE	7	A	-	47
TG06-07	S_f	132	67	SW	5	-	A	105
TG06-07	S_f	54	67	SE	8	-	A	164
TG06-07	S_f	306	68	NE				
TG06-07	S_f	208	68					
TG06-07	S_f	1	68	E	3	-	A	11.5-15
TG06-07	S_f	306	68	NE	7	A	A	55
TG06-07	S_f	95	69	S				31
TG06-07	S_f	244	71	NW	15	-	-	31
TG06-07	S_f	305	72	NE	3	A	A	44
TG06-07	S_f	303	73	NE	6	-	-	46
TG06-07	S_f	250	73		7	A	-	142
TG06-07	S_f	324	74	NE				
TG06-07	S_f	270	74	N				
TG06-07	S_f	86	74		5	-	A	15.6
TG06-07	S_f	308	74	NE	6	-	B	103
TG06-07	S_f	141	74	SW	4	-	A	112
TG06-07	S_f	296	75	NE	5	A	A	55
TG06-07	S_f	251	76					
TG06-07	S_f	272	76	N	2.5	A	-	3
TG06-07	S_f	300	76		3	A	A	24
TG06-07	S_f	184	76	W		-	-	32
TG06-07	S_f	269	79	N	4	-	A	4.3
TG06-07	S_f	265	80	N				
TG06-07	S_f	136	81	SW	1	A	-	100
TG06-07	S_f	303	82	NE	7	A	A	72
TG06-07	S_f	252	82	N	15	-	-	131
TG06-07	S_f	275	83		15	A	A	77
TG06-07	S_f	272	83	N	8	-	A	81
TG06-07	S_f	306	84	NE	5	A	-	2.7
TG06-07	S_f	306	84	NE	7	-	A	59

TG06-07	S_f	303	84		20	-	-	74
TG06-07	S_f	261	84		8	-	-	88
TG06-07	S_f	51	86					
TG06-07	S_f	286	86	N	12	-	-	40
TG06-07	S_f	304	87	NE	7	-	A	67
TG06-07	S_f	141	87		20	-	A	142
TG06-07	S_f	306	88	NE				
TG06-07	S_f	70	89		3	A	A	23
TG06-07	S_f	290	90					
TG06-07	S_f	142	90					
TG06-07	S_f	254	90					
TG06-07	S_f	265	90					
TG06-07	S_f	270	90					
TG06-07	S_1	231	46					
TG06-07	S_1	242	52					
TG06-07	S_1	69	79					
TG06-08	S_f	60	65					
TG06-08	S_f	104	87					
TG06-08	S_f	120	90					
TG06-08	S_1	60	65					
TG06-9	S_f	32	60					
TG06-9	S_f	40	60					
TG06-9	S_f	325	60					
TG06-9	S_f	44	61					
TG06-9	S_f	38	61					
TG06-9	S_f	40	62					
TG06-9	S_f	42	64					
TG06-9	S_f	32	65					
TG06-9	S_f	42	68					
TG06-9	S_f	44	68					
TG06-9	S_f	44	68					
TG06-9	S_f	39	69					
TG06-9	S_f	36	70					

TG06-9	S_f	45	70					
TG06-9	S_f	34	72					
TG06-9	S_f	44	72					
TG06-9	S_f	36	74					
TG06-9	S_f	36	74					
TG06-9	S_f	38	74					
TG06-9	S_f	40	74					
TG06-9	S_f	44	74					
TG06-9	S_f	36	76					
TG06-9	S_f	309	80					
TG06-9	S_f	44	81					
TG06-9	S_f	272	82					
TG06-9	S_f	45	84					
TG06-9	S_f	36	84					
TG06-9	S_f	306	85					
TG06-9	S_f	306	85					
TG06-9	S_f	292	88					
TG06-9	S_f	294	90					
TG06-9	S_f	310	90					
TG06-9	S_f	306	90					
TG06-9	S_f	308	90					
TG06-09	S_f	330	11					
TG06-09	S_f	6	19					
TG06-09	S_f	348	25					
TG06-09	S_f	344	30					
TG06-09	S_f	324	66					
TG06-09	S_f	36	66	SE				
TG06-09	S_f	34	71					
TG06-09	S_f	275	73					
TG06-09	S_f	32	74					
TG06-09	S_f	279	75					
TG06-09	S_f	283	79					
TG06-09	S_f	34	79					

TG06-09	S_f	311	83					
TG06-09	S_f	286	84					
TG06-09	S_f	308	85					
TG06-09	S_f	120	86					
TG06-09	S_f	295	87					
TG06-09	S_1	36	66	SE				
TG06-09	S_1	34	71					
TG06-09	S_1	32	74					
TG06-09	S_1	34	79					
TG06-10	S_f	8	21					
TG06-10	S_f	330	21					
TG06-10	S_f	300	25					
TG06-10	S_f	2	28					
TG06-10	S_f	148	44					
TG06-10	S_f	126	62					
TG06-10	S_f	22	64					
TG06-10	S_f	310	71					
TG06-10	S_f	306	72	N				
TG06-10	S_f	36	76					
TG06-10	S_f	301	80					
TG06-10	S_f	293	81					
TG06-10	S_f	40	84					
TG06-10	S_f	34	84					
TG06-10	S_f	33	88					
TG06-10	S_f	298	88					
TG06-10	S_f	260	90					
TG06-10	S_1	51	75	SE				
TG06-10	S_1	59	79					
TG06-10	S_1	46	81	SE				
TG06-11	S_f	295	86					
TG06-12	S_f	340	?					
TG06-12	S_f	261	?					
TG06-13	S_f	276	11					

TG06-13	S_f	281	12					
TG06-13	S_f	12	12	E				
TG06-13	S_f	254	15					
TG06-13	S_f	279	15					
TG06-13	S_f	355	21					
TG06-13	S_f	2	21					
TG06-13	S_f	338	23					
TG06-13	S_f	10	25					
TG06-13	S_f	345	26	E				
TG06-13	S_f	346	27					
TG06-13	S_f	15	27					
TG06-13	S_f	20	27					
TG06-13	S_f	19	39					
TG06-13	S_f	40	40					
TG06-13	S_f	224	54					
TG06-13	S_f	226	60					
TG06-13	S_f	70	60					
TG06-13	S_f	4	68					
TG06-13	S_f	350	68					
TG06-13	S_f	346	70					
TG06-13	S_f	308	70					
TG06-13	S_f	306	75					
TG06-13	S_f	351	75					
TG06-13	S_f	340	75					
TG06-13	S_f	356	78					
TG06-13	S_f	309	79					
TG06-13	S_f	311	79					
TG06-13	S_f	310	82					
TG06-13	S_f	330	82					
TG06-13	S_f	312	82					
TG06-13	S_f	309	84					
TG06-13	S_f	306	86	NE				
TG06-13	S_f	301	86					

TG06-13	S_f	312	86					
TG06-13	S_f	348	88					
TG06-13	S_f	328	88					
TG06-13	S_f	309	89					
TG06-13	S_f	316	90					
TG06-13	S_1	235	46					
TG06-13	S_1	237	54					
TG06-13	S_1	224	54					
TG06-13	S_1	246	59					
TG06-13	S_1	226	60					
TG06-13	S_1	246	64					
TG06-20	S_f	46	55					
TG06-20	S_f	43	55					
TG06-20	S_f	44	56					
TG06-20	S_f	44	56					
TG06-20	S_f	40	56					
TG06-20	S_f	42	56					
TG06-20	S_f	42	58					
TG06-20	S_f	44	58					
TG06-20	S_f	45	58					
TG06-20	S_f	28	58					
TG06-20	S_f	58	60					
TG06-20	S_f	44	60					
TG06-20	S_f	38	60					
TG06-20	S_f	45	62					
TG06-20	S_f	20	62					
TG06-20	S_f	40	64					
TG06-20	S_f	28	66					
TG06-20	S_f	36	68					
TG06-20	S_f	45	68					
TG06-20	S_f	35	70					
TG06-20	S_f	310	72					
TG06-20	S_f	38	75					

TG06-20	S_f	32	75					
TG06-20	S_f	295	78					
TG06-20	S_f	318	80					
TG06-20	S_f	306	80					
TG06-20	S_f	304	80					
TG06-20	S_f	42	80					
TG06-20	S_f	54	84					
TG06-20	S_f	42	84					
TG06-20	S_f	28	85					
TG06-20	S_f	315	85					
TG06-20	S_f	321	85					
TG06-20	S_f	306	85					
TG06-20	S_f	318	87					
TG06-20	S_f	316	88					
TG06-20	S_f	308	88					
TG06-20	S_f	314	88					
TG06-21	S_f	28	44					
TG06-21	S_f	315	48					
TG06-21	S_f	36	60					
TG06-21	S_f	48	64					
TG06-21	S_f	32	66					
TG06-21	S_f	30	68					
TG06-21	S_f	30	70					
TG06-21	S_f	15	74					
TG06-21	S_f	36	74					
TG06-21	S_f	42	76					
TG06-21	S_f	35	76					
TG06-21	S_f	320	76					
TG06-21	S_f	246	78					
TG06-21	S_f	44	78					
TG06-21	S_f	34	80					
TG06-21	S_f	36	82					
TG06-21	S_f	60	82					

TG06-21	S_f	54	82					
TG06-21	S_f	20	82					
TG06-21	S_f	50	82					
TG06-21	S_f	302	82					
TG06-21	S_f	292	84					
TG06-21	S_f	306	84					
TG06-21	S_f	38	85					
TG06-21	S_f	246	86					
TG06-21	S_f	44	86					
TG06-21	S_f	46	86					
TG06-21	S_f	50	86					
TG06-21	S_f	36	86					
TG06-21	S_f	44	86					
TG06-21	S_f	31	86					
TG06-21	S_f	40	86					
TG06-21	S_f	44	86					
TG06-21	S_f	322	86					
TG06-21	S_f	301	86					
TG06-21	S_f	304	86					
TG06-21	S_f	48	88					
TG06-21	S_f	312	88					
TG06-21	S_f	302	88					
TG06-21	S_f	37	89					
TG06-21	S_f	28	90					
TG06-21	S_f	310	90					
TG06-21	S_f	310	90					
TG06-21	S_f	298	90					
TG06-22	S_f	76	56					
TG06-22	S_f	60	56					
TG06-22	S_f	34	68					
TG06-22	S_f	83	74					
TG06-22	S_f	38	78					
TG06-22	S_f	310	85					

TG06-22	S_f	314	86					
TG06-22	S_f	20	90					
TG06-23	S_f	36	53					
TG06-23	S_f	68	58					
TG06-23	S_f	60	60					
TG06-23	S_f	56	64					
TG06-23	S_f	56	64					
TG06-23	S_f	56	76					
TG06-23	S_f	313	76					
TG06-23	S_f	316	76					
TG06-23	S_f	285	77					
TG06-23	S_f	306	80					
TG06-23	S_f	320	80					
TG06-23	S_f	62	80					
TG06-23	S_f	300	82					
TG06-23	S_f	298	84					
TG06-23	S_f	312	86					
TG06-23	S_f	296	88					
TG06-23	S_1	36	53					
TG06-23	S_1	56	76					

Appendix G: Streamflow measurements

Appendix G compiles streamflow measurements completed using the methodology outlined in Chapter 4. The uncertainty (X_Q) of the measured flow rate (Q) is calculated following *Hinton* [2005].

Table G.1 Streamflow measurements

Site Name	Date	GPS		Q (L/s)	Q uncertainty	
		Easting	Northing		X_Q (%)	X_Q (L/s)
Cameron Creek @ Perkins Rd.	28-Aug-07	393239	4968004	1.6	0.32	0.5
Rudsdale Creek @ Cty. Rd. #6	16/08/2007	395865	4970087	7.9	0.48	3.8
Rudsdale Creek @ Hwy. #7	27/08/2007	386475	4967907	3.7	0.35	1.3
Eagle Lake Dam @ Cty. Rd. #38	27/08/2007	367405	4947897	126.4	0.42	53.5
Eagle Lake Dam @ Bobs Lake Rd.	27/08/2007	368781	4946473	219.7	0.26	56.2
Vens Creek @ McLean Rd.	27/08/2007	356155	4952384	3.7	0.46	1.7
Vens Creek @ Babcock Rd.	27/08/2007	356536	4949640	2.7	0.57	1.6
Grants Creek @ Pike L. Dam off Cty. Rd. #10	28/08/2007	394971	4962937	150.0	0.41	70.0
Grants Creek @ Upper Scotch Line	28/08/2007	397079	4966916	292.7	0.46	134.9
Grants Creek @ Glen Tay	28/08/2007	397916	4969025	266.9	0.33	88.2